K.E.M. Benders

Osteochondral defect repair: back to nature's template

Osteochondral defect repair: back to nature's template

K.E.M. Benders, MD, MSc

Osteochondral defect repair: back to nature's template
Kim Eva Maria Benders

PhD thesis, Utrecht University, University Medical Center Utrecht, Utrecht, The Netherlands

The research in this thesis was financially supported by: Alexandre Suerman Stipendium, University Medical Center Utrecht, Utrecht, The Netherlands.

Layout and printing: Optima Grafische Communicatie, Rotterdam, The Netherlands

Osteochondral defect repair: back to nature's template

Herstel van osteochondrale defecten: terug naar de natuurlijke template
(met een samenvatting in het Nederlands)

Proefschrift

ter verkrijging van de graad van doctor aan de Universiteit Utrecht op gezag van de rector magnificus, prof.dr. G.J. van der Zwaan, ingevolge het besluit van het college voor promoties in het openbaar te verdedigen op donderdag 8 juni 2017 des avonds te 06.00 uur

door

Kim Eva Maria Benders
geboren op 12 oktober 1984
te Nieuwegein

Promotoren: Prof. dr. J. Malda
Prof. dr. D.B.F. Saris

Dit proefschrift werd (mede) mogelijk gemaakt met financiële steun van:
Chipsoft
Anna Fonds
Nederlandse Orthopaedische Vereniging
Spronken Orthopedie N.V.
iMove Medical
Bauerfeind
George In der Maur orthopedische schoentechniek
Eemland Orthopedie Techniek

Voor mijn ouders

TABLE OF CONTENTS

THIS THESIS IS BASED ON THE FOLLOWING PUBLICATIONS

Comparative study of depth-dependent characteristics of equine and human osteochondral tissue from the medial and lateral femoral condyles. Malda J, Benders KE, Klein TJ, de Grauw JC, Kik MJ, Hutmacher DW, Saris DB, van Weeren PR, Dhert WJ. Osteoarthritis Cartilage. 2012 Oct;20(10):1147-51.

Of mice, men and elephants: the relation between articular cartilage thickness and body mass Malda J, de Grauw JC, Benders KE, Kik MJ, van de Lest CH, Creemers LB, Dhert WJ, van Weeren PR.PLoS One. 2013;8(2):e57683.

Formalin fixation affects equilibrium partitioning of an ionic contrast agent-microcomputed tomography (EPIC-μCT) imaging of osteochondral samples. Benders KE, Malda J, Saris DB, Dhert WJ, Steck R, Hutmacher DW, Klein TJ. Osteoarthritis Cartilage. 2010 Dec;18(12):1586-91.

Extracellular matrix scaffolds for cartilage and bone regeneration. Benders KE, van Weeren PR, Badylak SF, Saris DB, Dhert WJ, Malda J. Trends Biotechnol. 2013 Mar;31(3):169-76.

Multipotent Stromal Cells Outperform Chondrocytes on Cartilage-Derived Matrix Scaffolds. Benders KE, Boot W, Cokelaere SM, Van Weeren PR, Gawlitta D, Bergman HJ, Saris DB, Dhert WJ, Malda J. Cartilage. 2014 Oct;5(4):221-30.

Decellularized cartilage-derived matrix as substrate for endochondral bone regeneration. Gawlitta D*, Benders KE*, Visser J, van der Sar AS, Kempen DH, Theyse LF, Malda J, Dhert WJ. Tissue Eng Part A. 2015 Feb;21(3-4):694-703. doi: 10.1089/ten.TEA.2014.0117.

Fabrication of decellularized cartilage-derived matrix scaffolds. Benders KE, Levato R, Malda J. *Submitted to Journal of Visual Experiments*

Varying particle sizes has no influence on cartilage matrix production on decellularized cartilage-derived matrix scaffolds. Benders KE, Haut Donahue TL, Boot W, Saris DB, van Weeren PR, Malda J. *Submitted to Cartilage*

Chapter 1

General background and outline of the thesis

CARTILAGE DEFECTS: A CLINICAL CHALLENGE

Within the field of orthopedic surgery one of the major clinical challenges is the treatment of (osteo-)chondral defects. Traumatic cartilage defects often occur in the active population, burdening patients with painful joints and decreased mobility[1-4]. These patients are often relatively young and still participating actively to society and the working population. Their immobility due to joint problems not only greatly burdens them, but also puts a significant strain on health care systems[5]. Moreover, from a biological perspective, untreated cartilage damage will inevitably progress towards osteoarthritis. Unfortunately, the only treatment for this condition is the salvage therapy of joint replacement surgery.

The treatment modalities for cartilage or osteochondral defects can generally be classified based on the size and depth of the defect. Relatively small defects are often treated by microfracture. This involves penetration of the subchondral bone plate to release bone marrow that in turn will lead to coverage of the defect with often fibrocartilagenous tissue[6-8]. Larger cartilage defects are currently successfully treated with autologous chondrocyte implantation (ACI)[9, 10]. This technique involves regenerative tissue engineering strategies in which autologous chondrocytes are harvested and expanded *ex vivo* and later reimplanted into the cartilage defect on a carrier material. This technique has been extensively studied and has a scientifically proven large patient benefit[11]. Unfortunately, it is relatively expensive[12] and worldwide application is hampered by legislative issues and profit-driven incentives. Moreover, a recent publication questions the superiority of ACI over microfracture in larger defects when comparing failure rate and the progression towards osteoarthritis[13]. Deeper defects can be treated by using osteochondral autograft transfer (OAT). In these cases osteochondral plugs are harvested from a non-weight bearing area in the knee and transferred to the site of the defect[14, 15]. However, as these osteochondral plugs are harvested from the same knee as the defect, this will undoubtedly influence joint homeostasis, and create donor site morbidity, which will obviously affect the cartilage tissue repair[16]. This technique can also be performed using allografts rather than autografts. However, healthy osteochondral plugs from young deceased humans are relatively scarce.

The disadvantages to the before-mentioned techniques, which include fibro-cartilagenous repair tissue, high costs[12, 17], and the creation of additional defects within the already injured joint drives researchers to develop innovative strategies to safely, and fully repair cartilage defects at relatively low cost. One of the general beliefs is that ultimate cartilage tissue engineering involves the optimal combination of a scaffold material, biologicals and cells[18]. However, thorough knowledge of the characteristics of cartilage tissue of both our patients (humans) and the pre-clinical testing subjects (animals) is required before such a combined approach can be successfully applied.

CARTILAGE CHARACTERISTICS, NOT AS SIMPLE AS IT MAY SEEM

Articular cartilage may at first present itself as a relatively simple tissue for tissue engineering. It does not require the regeneration of different structures, such as a vascular system in bone tissue engineering. Moreover, the articular cartilage is composed of a dense extracellular matrix (ECM) with only a few cells dispersed throughout this matrix[19]. However, this low cell content, as well as the lack of a continuous nutrient supply through a vascular system hampers natural tissue repair and makes tissue regeneration more challenging. Therefore, potential tissue-engineering strategies to address cartilage damage will have to initiate a great chondrogenic impulse to drive repair or regeneration.

Cartilage tissue might thus be considered a homogenous tissue that can be regenerated as a whole. However, when taking a closer look at the tissue, three distinctive layers have been identified in the non-calcified cartilage. The superficial (top 10-20%), middle (the next 40-50%), and deep zone (the last 30-40%) of cartilage differ in cell number, collagen fiber orientation and the proteoglycan content[20, 21]. The presence of these different layers allows for differentiated functions throughout the tissue, which make it possible to deal with the challenging biomechanical environment of the joint. The resilience against sheer forces is the highest within the top layer where joint surfaces move over one another. The ability to transmit loading forces towards the underlying bone is most abundant in the deepest layer. Ultimately, tissue-engineering approaches would involve recreating these different layers in the repair tissue. However, it remains unclear whether this is a definite requirement in the early stages of repair. Perhaps, the development of these different layers can be considered a process of maturation that is mainly driven by biomechanical cues to which the tissue is exposed[21].

Nevertheless, the underlying subchondral bone, which is an additional layer in osteochondral tissue that should be taken into account, must be addressed in regenerative strategies. As stated before, cartilage defects may in some instances involve a deep defect that also affects this underlying bony layer. Biomechanically this is an important part of the joint as the daily impacts on the articular surfaces are being transferred and absorbed in this area. Loss of bone underneath the cartilage will lead to an increase in impact forces on the cartilage surface and the margins of the defect. These increases make it more prone to further injury and degeneration. Also, injury to the subchondral bone is thought to enhance the catabolic cascade in damaged cartilage tissue, thus enhancing the general degenerative process through altered joint homeostasis[22, 23].

The benefit of considering the subchondral bone as an essential component of the tissue that must be repaired is that the subchondral bone, in contrast to cartilage tissue, is rich in resident cell populations within the bone marrow. It also has a vast nutrient reservoir through the presence of a vascular system, which will naturally provide the required nutrients. One of the cell populations within the bone marrow is the multipotent stromal cell

(MSC). These cells are known to have the ability to differentiate towards the adipogenic, osteogenic, but also the chondrogenic lineage. This makes them a potential cell source to aid in cartilage regeneration[24]. In osteochondral defects, the presence of MSCs might make *ex vivo* chondrocyte expansion prior to implantation redundant, as is required in various current ACI therapies. Anchoring the scaffolds in an environment that will allow for homing of autologous cells onto the scaffold would greatly simplify the treatment of cartilage defects as no *ex vivo* cell expansion is required.

The challenges in using the osteochondral approach to drive joint repair involve the regeneration of two different tissue types, ensuring that the bone and cartilage components remain two separate layers and that no endochondral ossification takes place in the cartilage layer[23].

THE EQUINE MODEL FOR (OSTEO-)CHONDRAL REPAIR STRATEGIES

The use of a relevant animal model to evaluate laboratory findings on cartilage repair in an *in vivo* setting is of the utmost importance. One of the main benefits of using small animal models, such as rats and rabbits, is that they are relatively easy and cheap to house. Therefore, these animals may still play an important role in performing the first preliminary tests of repair strategies in the initial phases of *in vivo* testing. However, conclusions that are drawn based on the results of novel regenerative strategies that have only been tested in these small animal models may not be readily extrapolated to the human situation[25]. An important aspect underlying this limited translational potential is that smaller animals tend to have subchondral growth plates that remain open throughout their lifespan[26]. Open growth plates include a large reservoir of progenitor cells that are constantly supplied with nutrients through the available vascularization[27]. This leads to an increased intrinsic repair capacity in skeletally immature mammals. Moreover, the articular cartilage of smaller animals tends to have relatively high numbers of cells when compared to the cartilage of larger animals. This may be advantageous for the reparative response as the natural hypocellularity of cartilage leads to a lack of a sufficient cell source for regeneration[28].

Currently, large animal models that are used to study the outcomes of cartilage-engineered constructs are the canine, porcine, caprine and equine models. Although these animals resemble the human application more closely in terms of size and the maturity of the tissue, some differences should be taken into account. Dogs are known to have an anatomically different knee joint from humans with the presence of a digital extensor tendon originating within the knee joint[25, 29]. This may be of influence on the biomechanical strain that occurs in these joints. Goats are relatively easy to handle and have a sufficiently large joint to adequately perform articular surgery. However, articular cartilage in goats is relatively thin when compared to humans. This in turn makes cartilage repair less challenging due to less

constraints regarding nutrient supply through diffusion[29]. Pigs or mini-pigs, are slightly harder to house than goats, but appear a widely accepted animal model as long as skeletally mature animals are used.

In the past decades, the equine model has gained a stronger foothold as a pre-clinical model for joint regeneration. It may prove to be beneficial over the slightly smaller large animal models. First of all, equine stifle (knee) joints are larger in size than human knees. Hence, allowing for the creation of larger defects and the possibility to study larger histological and biochemical samples. Also, the surgical approach may be easier in larger joints. The option of repetitive synovial fluid sampling is also available in the stifle joint as it is relatively easy to access and contains enough synovial fluid due to its size. This may be beneficial in studying new drug therapy approaches or responses in joint homeostasis.

Obviously, the biomechanical forces that come to play in horses and humans differ. Horses are much larger mammals that walk, and gallop on four feet instead of our bipedal stance and walking position. Also, the anatomically different position of the stifle joint in horses leads to a difference in biomechanical loading. Nonetheless, the shape and function of the knee joint in these two mammals is similar. Moreover, if a scaffold would survive and lead to cartilage repair in such a challenging environment such as the stifle joint in the horse, human application might not be too far away.

Like humans, the equine population suffers from the development of cartilage defects. These are either the result of traumatic events or due to congenital disorders (osteochondrosis)[30]. Especially in professional equestrian sports, the development of cartilage defects greatly impacts both the rider and the horse. This similarity between the human and equine clinical incidence of cartilage defects makes this animal an excellent pre-clinical model for human practice, as well as a clinically relevant target animal.

USING NATURE AS A TEMPLATE – EXTRACELLULAR MATRIX SCAFFOLDS

To drive regeneration, cells, nutrients and bioactive cues are required. Scaffolds may aid in the delivery of cells to the cartilage defect or induce homing of cells to the appropriate site. These scaffolds can be considered resorbable delivery vehicles for cells and an anchoring site for their subsequently produced matrix. Moreover, scaffolds can also play a role in carrying biologically active cues to drive extracellular matrix (ECM) production, and provide a platform for cells to deposit this matrix in an orderly fashion[31, 32]. Several scaffold materials have been used over the years, ranging from natural scaffolds, such as collagen[33, 34], hyaluronic acid[35] or gelatin[36], to synthetic scaffolds, such as PCL[37], PLLA[38], or PEG[39]. Scaffold structures can be generated through a wide range of production technologies. For example through casting the scaffold material into a mold, bioprinting technologies or electrospinning. Each of these techniques results in a specific

scaffold architecture that stimulates cell attachment, drives cell proliferation and differentiation, enhances ECM deposition and is eventually fully replaced by the regenerated tissue. The main advantages of using synthetic materials are their relatively good biomechanical properties, and the possibility of functionalizing the material using biological components, such as hyaluronic acid (HA), or functional peptides[37]. Moreover, synthetic polymers can be laid down in 3D constructs[40, 41] while controlling pore-size and architectural build-up. Their major downside is their restricted biodegradability and limited bioactivity. The slow degradation rate and acid byproducts of degrading synthetic materials, such as PLA, interferes with tissue integration and new tissue formation[42]. Natural materials that can be used for scaffold production, such as collagen, HA or gelatin, bypass the issues of bioactivity and biodegradability. However, their relative simplicity is in sharp contrast to the complex build-up of the native cartilaginous tissues.

Approaches addressing the regeneration of tissue types other than cartilage and bone have focused on using ECM as a scaffold material. ECM scaffolds are already used to regenerate skin, tendons, cardiovascular structures and *in vitro* visceral organ systems[43-45]. Extracellular matrix in itself is a natural biomaterial. It should, however, be considered a natural biomaterial *plus* as it consists of multiple components, rather than just one selected protein such as collagen. Extracellular matrix scaffolds are based on allogeneic and sometimes xenogeneic matrix that have undergone a decellularization process to remove all residing cells to prevent adverse immune responses[46]. Decellularization does, however, preserve the multiple components and bioactive cues that allow ECM scaffolds to be more like the naturally complex ECM[47]. The retention of all these functional components aids in tissue regeneration. The limited regenerative capacity of cartilaginous tissues makes the use of ECM scaffolds a new field of interest in cartilage tissue engineering. Currently, cartilage ECM scaffolds can be made from *in vitro* grown tissues[48] or from allogeneic and xenogeneic cartilage particles[49]. However, their true value for (osteo-)chondral repair has yet to be determined.

AIMS AND OUTLINE OF THIS THESIS

The overall aim of this thesis is to evaluate a new approach to osteochondral repair by using natural cartilage ECM to promote cartilage tissue regeneration. To this extent this thesis consists of two parts. Part A aims at the characterization of articular cartilage, and to evaluate the morphological differences in both human and equine articular cartilage throughout the different layers. These studies were performed to underscore the rationale for choosing the equine model to further evaluate osteochondral repair. The aim of part B of this thesis is to investigate natural ECM scaffolds as a platform for (osteo-)chondral tissue engineering both *in vitro* and *in vivo* in equine experimental subjects.

Part I:

In **Chapter 2** we characterized and compared the zonal characteristics of articular cartilage of both equine and human origin. Next, in **Chapter 3** we draw a correlation between cartilage thickness and body mass across different species ranging from mice to elephants, putting the strong resemblance between equine and human cartilage in a broader perspective. In **Chapter 4** we studied a new technique to non-destructively analyze the depth-dependent proteoglycan distribution in *ex vivo* samples.

Part II:

The second part of this thesis focuses on using natural cartilage ECM to promote cartilage tissue regeneration. In **Chapter 5** an overview is given of the literature regarding ECM scaffolds for osteochondral repair. **Chapter 6** then describes the differences in response of multipotent stromal cells and chondrocytes to a decellularized cartilage-derived scaffold. Subsequently, **Chapter 7** describes the protocol to develop these cartilage-derived matrix scaffolds in more detail. To illustrate the versatility of cartilage-derived matrix scaffolds, we describe the use of these scaffolds to drive endochondral bone regeneration i*n vivo* in **Chapter 8**. In **Chapter 9** we describe that varying the particle size in the production of decellularized cartilage-derived matrix scaffolds has no effect on their capacity to form cartilage-like tissue. Lastly, **Chapter 10** describes the first equine pilot study in which cartilage-derived matrix scaffolds are evaluated for osteochondral repair as a first step towards a larger animal study in the future. Final thoughts and points of discussion regarding the architectural make-up of cartilage tissue and the use of ECM scaffolds in cartilage tissue engineering are addressed in **Chapter 11.**

REFERENCES

1. Fitzpatrick K, Tokish JM. A military perspective to articular cartilage defects. J Knee Surg; 24: 159-166.
2. Flanigan DC, Harris JD, Trinh TQ, Siston RA, Brophy RH. Prevalence of chondral defects in athletes' knees: a systematic review. Med Sci Sports Exerc; 42: 1795-1801.
3. Hjelle K, Solheim E, Strand T, Muri R, Brittberg M. Articular cartilage defects in 1,000 knee arthroscopies. Arthroscopy 2002; 18: 730-734.
4. Widuchowski W, Widuchowski J, Trzaska T. Articular cartilage defects: study of 25,124 knee arthroscopies. Knee 2007; 14: 177-182.
5. Dunlop DD, Semanik P, Song J, Manheim LM, Shih V, Chang RW. Risk factors for functional decline in older adults with arthritis. Arthritis Rheum 2005; 52: 1274-1282.
6. McAdams TR, Mithoefer K, Scopp JM, Mandelbaum BR. Articular Cartilage Injury in Athletes. Cartilage; 1: 165-179.
7. Steadman JR, Briggs KK, Matheny LM, Guillet A, Hanson CM, Willimon SC. Outcomes following microfracture of full-thickness articular cartilage lesions of the knee in adolescent patients. J Knee Surg; 28: 145-150.
8. Steadman JR, Hanson CM, Briggs KK, Matheny LM, James EW, Guillet A. Outcomes after knee microfracture of chondral defects in alpine ski racers. J Knee Surg; 27: 407-410.
9. Brittberg M. Autologous chondrocyte implantation--technique and long-term follow-up. Injury 2008; 39 Suppl 1: S40-49.
10. Peterson L, Vasiliadis HS, Brittberg M, Lindahl A. Autologous chondrocyte implantation: a long-term follow-up. Am J Sports Med; 38: 1117-1124.
11. Brittberg M. Autologous chondrocyte implantation--technique and long-term follow-up. Injury 2008; 39: S40-49.
12. Elvidge J, Bullement A, Hatswell AJ. Cost Effectiveness of Characterised Chondrocyte Implantation for Treatment of Cartilage Defects of the Knee in the UK. Pharmacoeconomics; 34: 1145-1159.
13. Knutsen G, Drogset JO, Engebretsen L, Grontvedt T, Ludvigsen TC, Loken S, et al. A Randomized Multicenter Trial Comparing Autologous Chondrocyte Implantation with Microfracture: Long-Term Follow-up at 14 to 15 Years. J Bone Joint Surg Am; 98: 1332-1339.
14. Easley ME, Scranton PE, Jr. Osteochondral autologous transfer system. Foot Ankle Clin 2003; 8: 275-290.
15. Lynch TS, Patel RM, Benedick A, Amin NH, Jones MH, Miniaci A. Systematic review of autogenous osteochondral transplant outcomes. Arthroscopy; 31: 746-754.
16. Reddy S, Pedowitz DI, Parekh SG, Sennett BJ, Okereke E. The morbidity associated with osteochondral harvest from asymptomatic knees for the treatment of osteochondral lesions of the talus. Am J Sports Med 2007; 35: 80-85.
17. Clar C, Cummins E, McIntyre L, Thomas S, Lamb J, Bain L, et al. Clinical and cost-effectiveness of autologous chondrocyte implantation for cartilage defects in knee joints: systematic review and economic evaluation. Health Technol Assess 2005; 9: iii-iv, ix-x, 1-82.
18. Vinatier C, Bouffi C, Merceron C, Gordeladze J, Brondello JM, Jorgensen C, et al. Cartilage tissue engineering: towards a biomaterial-assisted mesenchymal stem cell therapy. Curr Stem Cell Res Ther 2009; 4: 318-329.
19. Martel-Pelletier J, Boileau C, Pelletier JP, Roughley PJ. Cartilage in normal and osteoarthritis conditions. Best Pract Res Clin Rheumatol 2008; 22: 351-384.

20. Klein TJ, Rizzi SC, Reichert JC, Georgi N, Malda J, Schuurman W, et al. Strategies for zonal cartilage repair using hydrogels. Macromol Biosci 2009; 9: 1049-1058.
21. Schuurman W, Klein, T.J., Dhert, W.J., van Weeren, P.R., Hutmacher, D.W., Malda, J. Cartilage regeneration using zonal chondrocyte subpopulations: a promising approach or an overcomplicated strategy? J Tissue Eng Regen Med 20015; 9: 669-678.
22. Findlay DM, Kuliwaba JS. Bone-cartilage crosstalk: a conversation for understanding osteoarthritis. Bone Res; 4: 16028.
23. Li X, Ding J, Wang J, Zhuang X, Chen X. Biomimetic biphasic scaffolds for osteochondral defect repair. Regen Biomater; 2: 221-228.
24. Arthur A, Zannettino A, Gronthos S. The therapeutic applications of multipotential mesenchymal/stromal stem cells in skeletal tissue repair. J Cell Physiol 2009; 218: 237-245.
25. Chu CR, Szczodry M, Bruno S. Animal models for cartilage regeneration and repair. Tissue Eng Part B Rev; 16: 105-115.
26. Kilborn SH, Trudel G, Uhthoff H. Review of growth plate closure compared with age at sexual maturity and lifespan in laboratory animals. Contemp Top Lab Anim Sci 2002; 41: 21-26.
27. Kember NF, Sissons HA. Quantitative histology of the human growth plate. J Bone Joint Surg Br 1976; 58-B: 426-435.
28. Stockwell RA. The interrelationship of cell density and cartilage thickness in mammalian articular cartilage. J Anat 1971; 109: 411-421.
29. Moran CJ, Ramesh A, Brama PA, O'Byrne JM, O'Brien FJ, Levingstone TJ. The benefits and limitations of animal models for translational research in cartilage repair. J Exp Orthop; 3: 1.
30. Olstad K, Ekman S, Carlson CS. An Update on the Pathogenesis of Osteochondrosis. Vet Pathol; 52: 785-802.
31. Steele JA, McCullen SD, Callanan A, Autefage H, Accardi MA, Dini D, et al. Combinatorial scaffold morphologies for zonal articular cartilage engineering. Acta Biomater; 10: 2065-2075.
32. Woodfield TB, Van Blitterswijk CA, De Wijn J, Sims TJ, Hollander AP, Riesle J. Polymer scaffolds fabricated with pore-size gradients as a model for studying the zonal organization within tissue-engineered cartilage constructs. Tissue Eng 2005; 11: 1297-1311.
33. Levingstone TJ, Ramesh A, Brady RT, Brama PA, Kearney C, Gleeson JP, et al. Cell-free multi-layered collagen-based scaffolds demonstrate layer specific regeneration of functional osteochondral tissue in caprine joints. Biomaterials; 87: 69-81.
34. Levingstone TJ, Thompson E, Matsiko A, Schepens A, Gleeson JP, O'Brien FJ. Multi-layered collagen-based scaffolds for osteochondral defect repair in rabbits. Acta Biomater; 32: 149-160.
35. Levett PA, Hutmacher DW, Malda J, Klein TJ. Hyaluronic acid enhances the mechanical properties of tissue-engineered cartilage constructs. PLoS One; 9: e113216.
36. Schuurman W, Levett PA, Pot MW, van Weeren PR, Dhert WJ, Hutmacher DW, et al. Gelatin-methacrylamide hydrogels as potential biomaterials for fabrication of tissue-engineered cartilage constructs. Macromol Biosci; 13: 551-561.
37. Lee CH, Cook JL, Mendelson A, Moioli EK, Yao H, Mao JJ. Regeneration of the articular surface of the rabbit synovial joint by cell homing: a proof of concept study. Lancet; 376: 440-448.
38. Childs A, Hemraz UD, Castro NJ, Fenniri H, Zhang LG. Novel biologically-inspired rosette nanotube PLLA scaffolds for improving human mesenchymal stem cell chondrogenic differentiation. Biomed Mater; 8: 065003.
39. Zhang W, Lian Q, Li D, Wang K, Hao D, Bian W, et al. Cartilage repair and subchondral bone migration using 3D printing osteochondral composites: a one-year-period study in rabbit trochlea. Biomed Res Int; 2014: 746138.

40. Levato R, Visser J, Planell JA, Engel E, Malda J, Mateos-Timoneda MA. Biofabrication of tissue constructs by 3D bioprinting of cell-laden microcarriers. Biofabrication; 6: 035020.
41. Nowicki MA, Castro NJ, Plesniak MW, Zhang LG. 3D printing of novel osteochondral scaffolds with graded microstructure. Nanotechnology; 27: 414001.
42. Patel JM, Merriam AR, Kohn J, Gatt CJ, Jr., Dunn MG. Negative Outcomes of Poly(l-Lactic Acid) Fiber-Reinforced Scaffolds in an Ovine Total Meniscus Replacement Model. Tissue Eng Part A; 22: 1116-1125.
43. Faulk DM, Wildemann JD, Badylak SF. Decellularization and cell seeding of whole liver biologic scaffolds composed of extracellular matrix. J Clin Exp Hepatol; 5: 69-80.
44. Londono R, Badylak SF. Biologic scaffolds for regenerative medicine: mechanisms of in vivo remodeling. Ann Biomed Eng; 43: 577-592.
45. Swinehart IT, Badylak SF. Extracellular matrix bioscaffolds in tissue remodeling and morphogenesis. Dev Dyn; 245: 351-360.
46. Crapo PM, Gilbert TW, Badylak SF. An overview of tissue and whole organ decellularization processes. Biomaterials; 32: 3233-3243.
47. Chun SY, Lim GJ, Kwon TG, Kwak EK, Kim BW, Atala A, et al. Identification and characterization of bioactive factors in bladder submucosa matrix. Biomaterials 2007; 28: 4251-4256.
48. Jin CZ, Choi BH, Park SR, Min BH. Cartilage engineering using cell-derived extracellular matrix scaffold in vitro. J Biomed Mater Res A; 92: 1567-1577.
49. Rowland CR, Colucci LA, Guilak F. Fabrication of anatomically-shaped cartilage constructs using decellularized cartilage-derived matrix scaffolds. Biomaterials; 91: 57-72.

Chapter 2

Comparative study of depth-dependent characteristics of equine and human osteochondral tissue from the medial and lateral femoral condyles

J. Malda
K.E.M. Benders
T.J. Klein
J.C. de Grauw
M.J.L. Kik
D.W. Hutmacher
D.B.F. Saris
P.R. van Weeren
W.J.A. Dhert

Osteoarthritis Cartilage. 2012 Oct;20(10):1147-51.

ABSTRACT

Articular cartilage defects are common after joint injuries. When left untreated, the biomechanical protective function of cartilage is gradually lost, making the joint more susceptible to further damage, causing progressive loss of joint function[1] and eventually osteoarthritis (OA). In the process of translating promising tissue-engineering cartilage repair approaches from bench to bedside, pre-clinical animal models including mice, rabbits, goats, and horses, are widely used[2]. The equine species is becoming an increasingly popular model for the *in vivo* evaluation of regenerative orthopedic approaches[3]. As there is also an increasing body of evidence suggesting that successful lasting tissue reconstruction requires an implant that mimics natural tissue organization, it is imperative that depth-dependent characteristics of equine osteochondral tissue are known, to assess to what extent they resemble those in humans. Therefore, osteochondral cores (4-8mm) were obtained from the medial and lateral femoral condyles of equine and human donors. Cores were processed for histology and for biochemical quantification of DNA, glycosaminoglycan (GAG) and collagen content. Equine and human osteochondral tissues possess similar geometrical (thickness) and organizational (GAG, collagen and DNA distribution with depth) features. These comparable trends further underscore the validity of the equine model for the evaluation of regenerative approaches for articular cartilage.

BRIEF REPORT

Osteochondral cores (4-8mm) were taken from the central sites of both medial and lateral femoral condyles of cadaveric horses (n=15 for cartilage thickness, n=14 for biochemical analysis, mean age: 10.5 years) and humans (n=7 for biochemical analysis, n=23 for cartilage thickness, mean age: 74.4 years). Donor horses had been euthanized for reasons unrelated to their femorotibial joints. Human material was obtained from human cadavers. After harvest, osteochondral cores were either fixed in 10% formalin (for histology) or frozen at -20˚C for biochemical analyses.

Osteochondral samples for histology were decalcified using Luthra solution (3.2% 11M HCl, 10% formic acid in distilled water). After decalcification, samples were dehydrated, cleared in xylene and embedded in paraffin. Subsequently, the samples were sectioned (5µm) and stained with hematoxylin and eosin for cells or with hematoxylin, fast green and Safranin-O for proteoglycan distribution. The sections were examined using a light microscope (Olympus, BX51, USA) and scored according to the histological and histochemical grading system (HHGS) as described by Mankin *et al.*[4].

The cartilage of the frozen osteochondral plugs was sectioned in the tangential plane, *i.e.* parallel to the joint surface, to yield 50µm slices using a cryotome (Cryocut 1800, Leica, Germany). Four consecutive sections were stored together as 200µm aliquots (approximately 15mg tissue) at -20˚C until further use. After thawing, samples were digested overnight in 20ml papain solution (0.01M cysteine, 250mg/ml papain, 0.2M NaH_2PO_4 and 0.01M EDTA) per mg cartilage tissue at 60˚C. The cartilage digests were used for glycosaminoglycan (GAG), DNA and collagen analysis. GAG content was determined spectrophotometrically after reaction with dimethylmethylene blue (DMMB, Sigma-Aldrich, USA) as previously described[5]. DNA content was determined using the Picogreen DNA assay (Invitrogen, P7589) in accordance with the manufacturer's instructions. Collagen content and cross-links were analyzed by HPLC-MS/MS using multiple reaction monitoring (MRM). Cartilage samples were hydrolyzed (110˚C, 18–20h) in 6M HCl. Homo-arginine was added to the hydrolyzed samples as an internal standard, after which they were vacuum-dried and dissolved in 30% methanol containing 0.2% heptafluor buteric acid (HFBA). The supernatants were subjected to HPLC-MS/MS analysis, using an API3000 mass-spectrometer (Applied Biosystems/MDS Sciex, Foster City, CA) at a source temperature of 300˚C and a spray voltage of 4.5kV. Amino acids were separated on a Synergi MAX-RP 80A (250 x 3mm, 4µm) column (Phenomenex Inc., Torrance, CA) at a flow rate of 400µl/min, using a gradient from MilliQwater (Millipore, Billerica, MA) containing 0.2% HFBA to methanol. Amino acids and collagen were analysed in MRM mode using the mass transitions 189.2/143.7 for homo-arginine, 131.8/67.8 for hydroxyproline (Hyp). Data were analysed by reference to the corresponding calibration curves and corrected for the recovery of internal standard. Collagen content was calculated as follows: µg collagen (pmol Hyp/300)*0.3 (300 is the

number of Hyp residues in one collagen triple helix, 0.3 is the molecular weight of collagen, 300,000Da).

To measure cartilage thickness, digital images of hematoxylin and eosin-stained sections were analysed using cell^F software (Olympus, USA). Average thickness of the articular cartilage of each sample was determined by averaging 4 measurements per image at different locations.

Statistical comparisons of Mankin scores and cartilage thickness were conducted using a paired two-tailed Student's *t*-test. For comparison of the GAG, DNA, and, collagen content at each of the different depths a repeated measurement analysis (one-way ANOVA) was performed, followed by a Bonferroni post-hoc test. Significance level was set at a *p*-value smaller than 0.05. All data are represented as mean ± standard deviation.

Cartilage from both the lateral and medial femoral equine condyles was macroscopically healthy, as confirmed by relatively low average Mankin scores (0.9±0.9, Figure 1A). Mankin scores for human osteochondral tissues were higher (3.7±1.8, Figure 1B), illustrated by early signs of OA with increasing age in these samples, such as decreased staining for proteoglycans (Figure 1A and 1B) and hypercellularity.

Equine cartilage thickness ranged from 0.96-3.13mm, closely resembling cartilage thickness observed in the human samples (0.65-3.52mm). The equine cartilage at the centre of the medial femoral condyle was significantly thicker than on the lateral side (2.19±0.80mm vs. 1.35±0.31mm, p=0.003) (Figure 1C). Cartilage thickness on the human femoral condyles did not show a statistically significant difference between the medial and the lateral side (2.01±0.75mm vs.1.96±0.45mm, p=0.95).

The GAG content significantly increased over the first 600mm from the surface in both the lateral and medial equine samples (lateral p=0.001 and medial p=0.0002, Figure 2A), beyond this depth, GAG levels stayed constant until the bone-cartilage interface. The same trend was observed for human cartilage tissue from both the lateral and medial condyles with only a significant difference between 400μm and 600μm on the lateral condyle (p=0.041) (Figure 2B).

DNA content in samples derived from both the medial and the lateral equine femoral condyle decreased with depth up to approximately 1000mm, whereafter a relatively constant level was reached (Figure 2C). Both lateral and medial equine condyles showed significant differences between subsequent 200μm sections (lateral respectively, p=0.002, p=0.0004, p<0.0001, p<0.0001 and medial respectively, p=0.002, p<0.0001, p<0.0001, p<0.0001). When comparing the lateral and medial equine condyles, no significant differences in DNA content were observed in the first 200μm sections. However, the deeper layers had a significantly lower DNA content in the medial equine condyle (p=0.002). A similar decreasing trend in DNA content was observed in human cartilage, although no significant differences were found between the subsequent 200μm sections (Figure 2D).

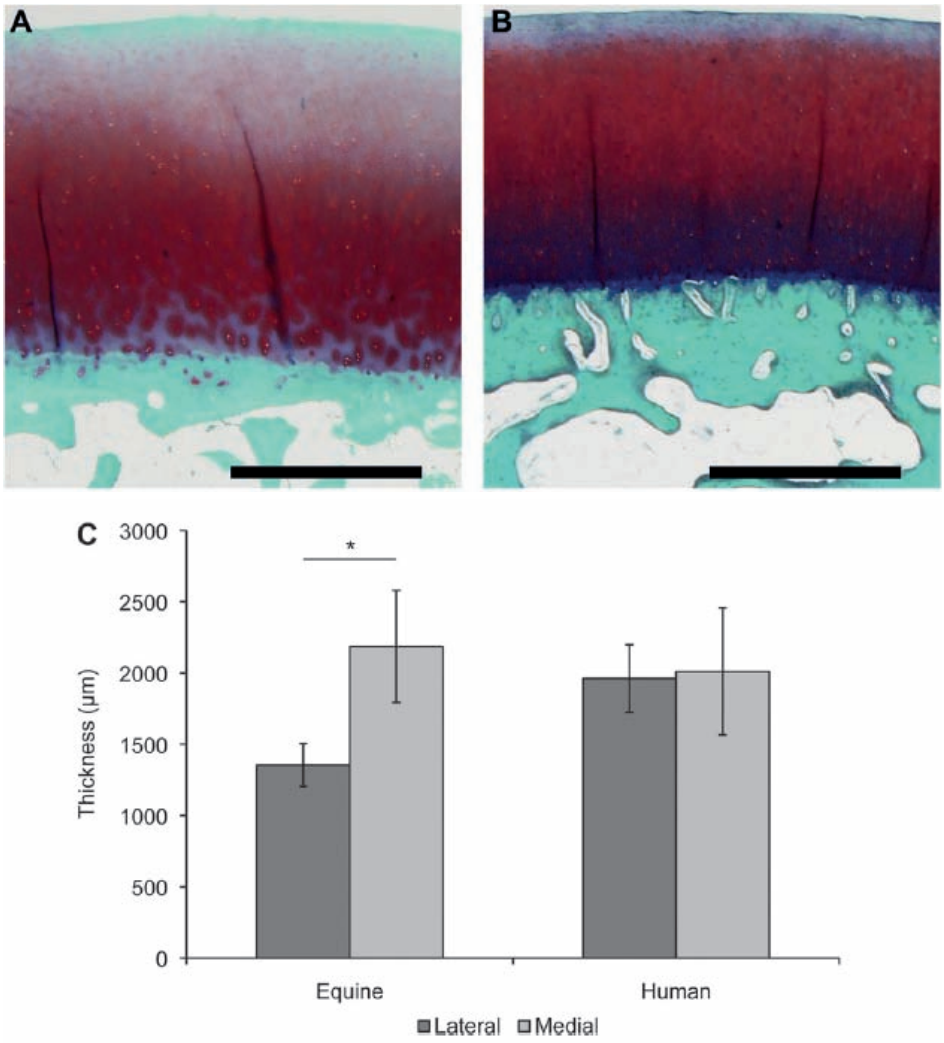

Figure 1: Safranin-O staining of equine (A) and human (B) articular cartilage from the central sites of the femoral condyles. Average thickness of equine and human cartilage from the central sites of the femoral condyles (C). A significant difference was observed between the lateral and medial condyle of equine samples ($p<0.01$).

No significant differences in hydroxyproline, as a measure of collagen content, were observed with depth or location (lateral and medial) in equine and human articular cartilage (Figure 2E and 2F).

The *in vivo* evaluation of cartilage tissue engineering applications is inevitable when aiming at the implementation of new regenerative techniques. Over the past few years, the equine model has gained popularity for this purpose[2, 3], but more insight is required in the histological and biochemical characteristics of equine cartilage and how these relate to the human situation to better appreciate the value of this model.

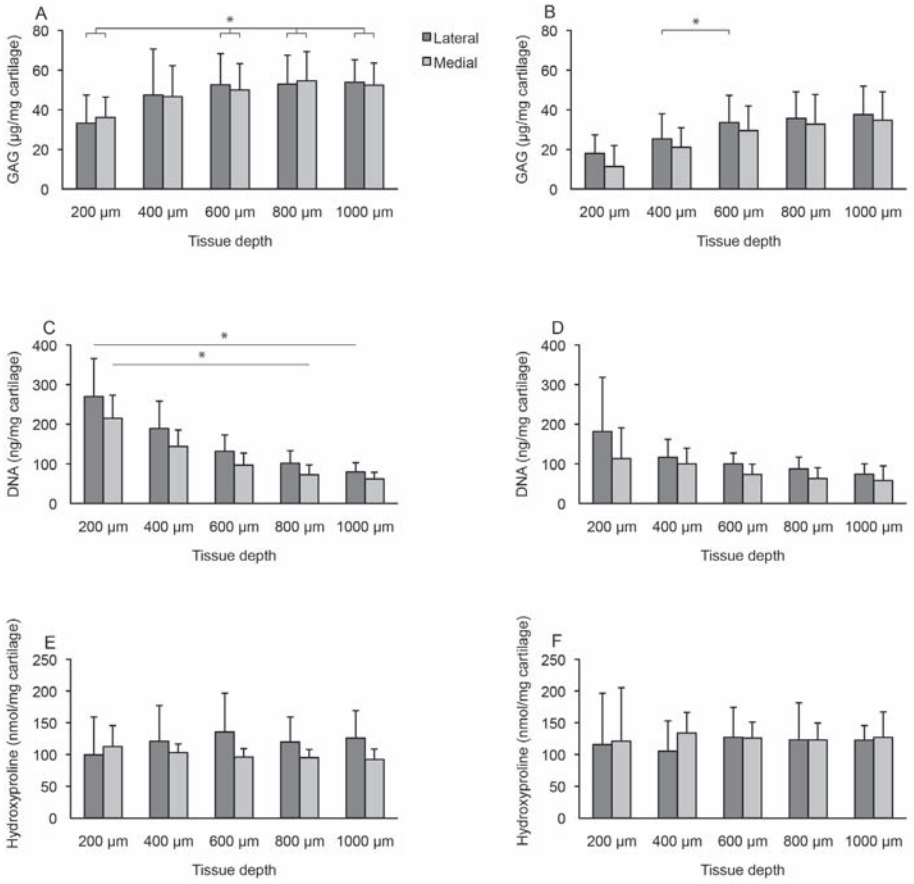

Figure 2: Depth-dependent biochemical content of equine GAG (A), DNA (C), and hydroxyproline (E) and human GAG (B), DNA (D) and hydroxyproline (F). Statistical differences ($p<0.05$) are indicated by *.

Cartilage thickness allows for the accommodation of the stresses and strains that are exerted on the cartilage matrix[6] during daily movement and is thus an important factor when choosing a suitable animal model. Cartilage thickness of the equine and human knee joints was found to be within the same range and in line with earlier reports[7, 8]. This is of relevance when studying the healing capacity of the tissue after creating a full-thickness critical size defect. It is known that in smaller animal species, such as rabbits, average osteochondral defects are smaller due to the thinner cartilage in these animals[7]. Thinner cartilage often leads to cartilage defects that protrude into the subchondral bone or growth plate, thereby stimulating spontaneous repair. Results obtained from small animal studies are therefore more difficult to extrapolate to the human situation.

The significant difference in cartilage thickness between the lateral and medial condyle in equine tissue might be attributed to the larger loading that the medial condyle experiences.

Indeed, it has been suggested that cartilage thickness is area-specific and proportional to local loading[7]. Joint congruency plays a role too with thinner cartilage in a more congruent joint, as the stresses can more easily be distributed over a larger surface area[8]. A higher degree of congruence of the lateral equine condyle may explain the difference with the human knee joints, where we did not observe a significant difference in cartilage thickness between the lateral and medial condyle (n=23), which is in line with earlier reports[8]. This may be a gradual difference, however, as Hall and Wyshak[9] investigated cartilage thickness on arthrograms (n=370) of young (average age 34.7 years) patients and found a small but significant difference, suggesting that differences in thickness between the medial and lateral femoral condyle are not non-existent in humans, but less evident than in horses.

GAGs are important extracellular matrix components in articular cartilage; they attract water molecules and thereby aid in shock absorbance[10]. This is the first time that depth-dependent GAG concentrations were biochemically quantified in the equine femorotibial joint. Previous research has only focused on the metacarpophalangeal joint and showed depth-dependent distributions, similar to our findings[11].

Collagen is another key building block of articular cartilage, providing structural integrity and tensile strength[10]. Throughout the different layers of articular cartilage, the orientation of the collagen fibrils changes, from parallel in the superficial zone to perpendicular in the deep zone[12]. This contributes to the different mechanical properties of each of the three zones. In the present study, no distinct significant differences were found in collagen content throughout the different cartilage layers in either equine or human samples. This suggests that although the alignment of the fibers changes throughout the tissue, the collagen content remains stable.

DNA content showed a clear depth-dependent distribution in both equine and human tissue with declining cell numbers with increasing distance to the surface, in line with previous reports[13]. No substantial differences were observed in DNA content between equine and human tissue, which is noteworthy, as cellularity of the cartilage tissue is known to be higher in smaller animals[14]. The increased cell number may relate to the more naturally occuring spontaneous cartilage repair in smaller animals, which again brings about extrapolation issues towards the human situation.

The comparable trends in GAG, collagen and DNA distributions throughout the different layers in both human and equine articular cartilage underscore the translational value of the equine model. However, there are additional advantages to using this model. First, naturally occuring cartilage defects due to osteochondrosis or trauma are not uncommon in equine veterinary medicine. Hence, performing pre-clinical testing of regenerative cartilage repair applications in the horse may be of direct clinical benefit to the species itself. Furthermore, the size of the equine femorotibial joint allows for second-look arthroscopies to evaluate the ongoing repair process *in vivo* and allows for monitoring by means of biomarker analysis of serially sampled synovial fluid[15]. Moreover, long-term follow-up studies are impossible

in small rodents, but pivotal in evaluating functional performance of cartilage regenerative techniques. Lastly, the high degree of mechanical loading in the equine knee joint is advantageous for pre-clinical evaluation of new therapies, as novel cartilage regenerative applications that are successful in horses are much more likely to survive the less biomechanically challenging environment of the human knee joint.

In conclusion, these findings add to the knowledge base on comparative equine and human osteochondral biology and may provide valuable information for researchers who consider using the equine model for pre-clinical animal testing of new cartilage tissue engineering applications.

REFERENCES

1. Buckwalter JA, Mankin HJ. Articular cartilage: degeneration and osteoarthritis, repair, regeneration, and transplantation. Instr Course Lect 1998; 47: 487-504.
2. Chu CR, Szczodry M, Bruno S. Animal models for cartilage regeneration and repair. Tissue Eng Part B Rev 2010; 16: 105-115.
3. McIlwraith CW, Fortier LA, Frisbie DD, Nixon AJ. Equine models of articular cartilage repair. Cartilage 2011.
4. Mankin HJ, Dorfman H, Lippiello L, Zarins A. Biochemical and metabolic abnormalities in articular cartilage from osteo-arthritic human hips. II. Correlation of morphology with biochemical and metabolic data. J Bone Joint Surg Am 1971; 53: 523-537.
5. Farndale RW, Buttle DJ, Barrett AJ. Improved quantitation and discrimination of sulphated glycosaminoglycans by use of dimethylmethylene blue. Biochim Biophys Acta 1986; 883: 173-177.
6. Simon WH. Scale effects in animal joints. I. Articular cartilage thickness and compressive stress. Arthritis Rheum 1970; 13: 244-256.
7. Frisbie DD, Cross MW, McIlwraith CW. A comparative study of articular cartilage thickness in the stifle of animal species used in human pre-clinical studies compared to articular cartilage thickness in the human knee. Vet Comp Orthop Traumatol 2006; 19: 142-146.
8. Shepherd DE, Seedhom BB. Thickness of human articular cartilage in joints of the lower limb. Ann Rheum Dis 1999; 58: 27-34.
9. Hall FM, Wyshak G. Thickness of articular cartilage in the normal knee. J Bone Joint Surg Am 1980; 62: 408-413.
10. Martel-Pelletier J, Boileau C, Pelletier JP, Roughley PJ. Cartilage in normal and osteoarthritis conditions. Best Pract Res Clin Rheumatol 2008; 22: 351-384.
11. Brama PA, Holopainen J, van Weeren PR, Firth EC, Helminen HJ, Hyttinen MM. Influence of exercise and joint topography on depth-related spatial distribution of proteoglycan and collagen content in immature equine articular cartilage. Equine Vet J 2009; 41: 557-563.
12. Herzog W, Federico S. Considerations on joint and articular cartilage mechanics. Biomech Model Mechanobiol 2006; 5: 64-81.
13. Klein TJ, Malda J, Sah RL, Hutmacher DW. Tissue engineering of articular cartilage with biomimetic zones. Tissue Eng Part B Rev 2009; 15: 143-157.
14. Stockwell RA. The interrelationship of cell density and cartilage thickness in mammalian articular cartilage. J Anat 1971; 109: 411-421.
15. De Grauw JC, van de Lest CHA, van Weeren PR. Inflammatory mediators and cartilage biomarkers in synovial fluid after a single inflammatory insult: a longitudinal experimental study. Arthritis Res Ther 2009; 11: R35.

Chapter 3

Of mice, men, and elephants: the relation between articular cartilage thickness and body mass

J. Malda
J.C. de Grauw
K.E.M. Benders
M.J.L. Kik
C.H.A. van de Lest
L.B. Creemers
W.J.A. Dhert
P.R. van Weeren

PLoS One. 2013;8(2):e57683

ABSTRACT

Mammalian articular cartilage serves diverse functions, including shock absorption, force transmission and enabling low-friction joint motion. These challenging requirements are met by the tissue's thickness combined with its highly specific extracellular matrix, consisting of a glycosaminoglycan-interspersed collagen fiber network that provides a unique combination of resilience and high compressive and shear resistance. It is unknown how this critical tissue deals with the challenges posed by increases in body mass.

For this study, osteochondral cores were harvested post-mortem from the central sites of both medial and lateral femoral condyles of 58 different mammalian species ranging from 25g (mouse) to 4000kg (African elephant). Joint size and cartilage thickness were measured and biochemical composition (glycosaminoclycan, collagen and DNA content) and collagen cross-links densities were analyzed.

Here, we show that cartilage thickness at the femoral condyle in the mammalian species investigated varies between 90μm and 3000μm and bears a negative allometric relationship to body mass, unlike the isometric scaling of the skeleton. Cellular density (as determined by DNA content) decreases with increasing body mass, but gross biochemical composition is remarkably constant. This however need not affect life-long performance of the tissue in heavier mammals, due to relatively constant static compressive stresses, the zonal organization of the tissue and additional compensation by joint congruence, posture and activity pattern of larger mammals.

These findings provide insight in the scaling of articular cartilage thickness with body weight, as well as in cartilage biochemical composition and cellularity across mammalian species. They underscore the need for the use of appropriate *in vivo* models in translational research aiming at human applications.

INTRODUCTION

Articular cartilage is a heavily challenged tissue, as its main functions (shock absorption, force transmission and enabling low-friction movement of joints) require a combination of both great resilience and high compressive and shear resistance[1]. These demands are difficult to reconcile, but the tissue succeeds in doing so by the specific characteristics of its extracellular matrix (ECM) that consists of a glycosaminoglycan-interspersed collagen fiber network[2]. As articular cartilage is aneural, avascular and of low cellularity, its ECM is of relatively homogeneous composition. The downside, however, is that this constitution is thought to be the underlying cause of the very limited regenerative capacity of the tissue[3].

There is a huge difference in adult body mass amongst the currently living mammalian species. A mouse may weigh as little as 25 grams, whereas an African elephant easily reaches 4 tons, which represents 150,000-fold increase in body mass. The cube square law[4] stipulates that with increasing volume of a body, total mass increases with the third power of unit length, while the cross-sections of the supporting structures only increase with the second power, thus resulting in a linear increase in potential load (force per unit area) on these structures. The mammalian skeleton (y) generally scales proportionally[5] (isometrically; $y = bx^a$; $a = 0.33$) with body mass (x), and to compensate for the relatively higher loading of specific supporting structures, bone mass increases at certain sites[5,6,7,8] and thus scales with positive allometry ($a>0.33$). However, the basic biological requirement for bone is to provide rigidity, which is more straightforward than the specific demands cartilage has to meet. Thus far, little is known about how articular cartilage deals with the challenges posed by increases in body mass[9]. The biochemical composition of the cartilage varies significantly over different topographical locations of the joint surface[10,11,12], and glycosaminoglycan (GAG) content appears to be dependent on local tissue loading[10,13,14]. While some significant differences in cartilage biochemical composition have been demonstrated between species[15], it is not known to what extent a similar mechanism would be necessary and may indeed exist to accommodate for the much larger differences in loading generated by the size differences between species.

Increases in thickness are likely to be limited by the avascular nature of cartilage. Previous studies in small groups of mammals, however, demonstrated that cartilage thickness does increase with increasing body mass[16,17,18]. Simon[16] found that cartilage thickness in 5 species of quadrupeds (mouse, rat, dog sheep, and cow) generally increased with body mass although marked variations were noted. Interestingly, Simon did not observe a consistent relationship between tissue thickness and the estimated compressive stress on the joint[16]. Stockwell[17] also showed that overall articular cartilage thickness is proportional to body mass in 8 mammalian species (mouse, rat, cat, rabbit, dog, sheep, man, and cow), although human cartilage was found to be relatively thicker. While these studies are helpful, they unfortunately comprised only a few species, were not fully conclusive, and failed to find

evidence of a mechanism that may compensate for the more than proportional increase in potential loading that follows from the cube-square law.

We investigated the thickness and composition of the articular cartilage at the femoral condyle in 58 mammalian species with a wide variation in body mass. The hypotheses to be tested were that, (1) due to diffusional constraints[19,20], cartilage thickness, unlike the dimensions of bones, cannot scale isometrically with increasing body mass and hence will be relatively thinner in larger animals; (2) a high cellularity of the articular cartilage could only be sustained in mammals with a low body mass; and (3) dramatic changes in extracellular matrix composition would not be required in view of the previously reported similar static compressive stresses in the articular cartilage of various species[16]. The results indeed show that cartilage thickness scales with negative allometry with body mass and that collagen and glycosaminoglycan content remain relatively constant over a wide body mass range.

MATERIALS AND METHODS

Tissue harvest

Osteochondral cores were harvested post-mortem from the central sites of both the medial and lateral femoral condyles of different-sized mammals sent in for autopsy at the Department of Pathobiology, Faculty of Veterinary Medicine, Utrecht University, The Netherlands. Prior to harvest, animal species, age and body mass were recorded and macroscopic photographs of the joints were taken. Joints demonstrating macroscopic signs of cartilage degeneration, a microscopic Mankin score above 7 (see histology) or originating from skeletally immature animals were excluded. Human tissue samples were obtained from the Department of Pathology, University Medical Center Utrecht, The Netherlands, with approval of the local ethics committee and in line with the Dutch code of conduct "Proper Secondary Use of Human Tissue" as installed by the Federation of Biomedical Scientific Societies. In total, tissue was harvested (121 samples for histological and 84 for biochemical analysis) from mammals belonging to 58 different species (Table 1).

Histology

Osteochondral tissue samples for histology were decalcified using Luthra solution (3.2% 11M HCl, 10% formic acid in distilled water), dehydrated, cleared in xylene, embedded in paraffin and cut to yield 5μm sections. Sections were either stained with hematoxylin and eosin for image analysis or with hematoxylin, fast green and Safranin-O for measurement of cartilage thickness from the surface down to the chondro-osseous junction and for osteoarthritic grading using the Mankin score[21]. Digital images were analyzed using cell^F

Table 1: Number of animals per species included in this study.

	Species	***Average body mass (kg)***	***Histology (n)***	***Biochemistry (n)***
1	Mouse (*Mus Musculus*)	0.025	5	
2	Pygmy marmoset (*Callithrix pygmaea*)	0.13	1	
3	Common marmoset (*Callithrix jacchus*)	0.3	1	1
4	Rat (*Rattus sp.)*	0.3	5	4
5	Cotton-top or Pinché tamarin *(Saguinus oedipus)*	0.34	1	1
6	Eurasian Red squirrel (*Sciurus vulgaris*)	0.4		1
7	Cape Ground squirrel (*Xerus inauris*)	0.65		1
8	Guineapig *(Cavia porcellus)*	0.78	3	3
9	Potto (*Perodicticus potto*)	0.99	1	1
10	Ferret (*Mustela putorius furo*)	1.3	1	2
11	White-faced saki (*Pithecia pithecia*)	2	1	1
12	Ring-tailed lemur *(Lemur catta)*	2.2	1	2
13	Opossum (*Didelphis sp.*)	2.4	1	1
14	Oriental small-clawed otter (*Aonyx cinerea*)	2.81		1
15	Hare (*Lepus sp.*)	3.1	2	4
16	Rabbit *(Oryctolagus cuniculus)*	3.7	6	7
17	South American coati (*Nasua Nasua)*	5.1	2	1
18	European otter (*Lutra lutra*)	6.5	1	1
19	Linnaeus's two-toed sloth (*Choloepus didactylus*)	6.5	1	1
20	Black Mangabey (*Lophocebus albigena*)	7	1	1
21	Vervet monkey *(Chlorocebus pygerythrus)*	7.7	2	1
22	Southern or Chilean Pudú (*Pudu puda*)	7.8	2	2
23	Woolly Monkey *(Lagothrix lagotricha)*	8.4	1	1
24	Barbary macaque (*Macaca sylvanus*)	8.5	2	2
25	Badger (*Meles meles*)	10	2	2
26	Dikdik (*Madoqua kirkii*)	10	1	
27	Beagle dog (*Canis sp.*)	12	4	2
28	Tammar wallaby (*Macropus eugenii*)	12.5	2	1
29	Hamadryas baboon (*Papio hamadryas*)	15.8	3	3
30	Indian crested porcupine (*Hystrix indica*)	16	1	1
31	Thomson's gazelle (*Eudorcas thomsoni*)	18	4	1
32	Roe deer (*Capreolus capreolus*)	19.2	5	2
33	Capybara *(Hydrochoerus hydrochaeris)*	22	1	1
34	Dutch milk goat (*Capri hircus*)	25	1	
35	West African dwarf goat (*Capri sp.*)	29	1	1
36	Cheetah (*Acinonyx jubatus*)	39.5	4	1
37	Impala (*Aepyceros melampus*)	41	2	2
38	Red Kangaroo (*Macropus rufus*)	52.5	2	1

Table 1: Number of animals per species included in this study. (continued)

	Species	*Average body mass (kg)*	*Histology (n)*	*Biochemistry (n)*
39	Human (*Homo Sapiens*)	68.3	10	2
40	Fallow deer (*Dama dama*)	70	1	1
41	Gorilla (*Troglodytes gorilla*)	74		1
42	Siberian tiger (*Panthera tigris*)	80	1	1
43	Reindeer (*Rangifer tarandus*)	125	1	
44	Lion *(Panthera leo))*	148	1	
45	Horse (mini-shetland) (*Equus sp.*)	150	1	
46	Kudu (*Tragelaphus strepsiceros*)	150	1	
47	Llama (*Lama Glama*)	160	1	
48	Polar bear (*Ursus Maritimus*)	175	1	1
49	South American tapir (*Tapirus terrestris*)	250	1	1
50	European moose (*Alces alces alces*)	343	1	1
51	Watoessi (*Bos Taurus Taurus watussi*)	350	1	
52	Dairy cow (*Bovinae*)	450	2	
53	Giraffe (*Giraffa camelopardalis*)	555	3	1
54	Horse (*Equus ferus caballus*)	557	15	13
55	Banteng (*Bos javanicus*)	600	1	1
56	White rhinoceros (*Ceratotherium simum*)	1550	2	2
57	Asian elephant (*Elaphus maximus*)	3350	2	1
58	African Elephant *(Loxodonta africanus)*	4000	1	
	Total		**121**	**84**

software (Olympus, USA). The average thickness of the articular cartilage of each sample was determined by averaging 4 measurements per image at different locations.

Glycosaminoglycan and DNA content

Cartilage samples for biochemical analyses were digested overnight at 60°C in 20µL papain solution (0.01M cysteine, 250µg/ml papain, 0.2M NaH_2PO_4 and 0.01M EDTA.$2H_2O$) per mg cartilage tissue. Glycosaminoglycan (GAG) content of the digests was determined spectrophotometrically after reaction with dimethylmethylene blue reagent (DMMB, Sigma-Aldrich, USA)[22]. DNA content was determined using the Picogreen DNA assay[23] (Invitrogen, P7589) in accordance with the manufacturer's instructions.

Collagen content

Hydroxyproline content (as a measure of collagen content) and collagen cross-links were analyzed by HPLC-MS/MS using multiple reaction monitoring (MRM) as previously described[24]. Briefly, aliquots of digested cartilage samples were hydrolyzed (110°C, 18–20h)

in 6M HCl. Homo-arginine was added to the hydrolyzed samples as an internal standard. Samples were vacuum-dried and dissolved in 30% methanol containing 0.2% heptafluor buteric acid (HFBA). After centrifugation at 13,000*g* for 10 min, the supernatants were analyzed with HPLC-MS/MS, using an API3000 mass-spectrometer (Applied Biosystems/MDS Sciex, Foster City, CA) at a source temperature of 300°C and a spray voltage of 4.5kV. Amino acids were separated on a Synergi MAX-RP 80A (250 x 3mm, 4µm) column (Phenomenex Inc., Torrance, CA) at a flow rate of 400µL/min, using a gradient from 0.2% HFBA in MilliQwater (Millipore, Billerica, MA) to 100% methanol (Biosolve, Valkenswaard, The Netherlands).

Statistics

Statistical comparison of the medial and lateral cartilage thicknesses was conducted using a paired one-sample Student's t-test on the ratios. For correlations between body mass and cartilage thickness, a regression analysis using a power curve fit was performed. Statistical comparison of the obtained power coefficient with the theoretical coefficient of 0.33 (isometric scaling) was performed using a one-sample T-test. Significance of both tests was assumed at $p<0.05$.

RESULTS

The total width of the lateral and medial condyles was analyzed (Figure 1) as a measure of joint size in the 58 different species of mammals evaluated (Table 1). We found an increase in total condyle size with body mass that scaled according to an isometric relation (a=0.337, Figure 1), in line with previous observations on the scaling of the mammalian skeleton. Histological analysis revealed a relatively higher bone density of the subchondral bone in larger species in our study (Figure 2).

Within the cartilage tissue of all species, a decreased intensity of Safranin-O staining was observed within the superficial layers compared to the deeper layers, indicative of lower glycosaminoglycan content in the upper tissue regions (Figure 2).

We found that the thickness of the calcified plus non-calcified cartilage layer on the summits of the lateral and medial femoral condyles varied widely between species (Figure 3), ranging from about 90µm in the mouse to 2,000µm in humans and approximately 3,000µm in the Asian elephant (Figure 3, Table 2). Moreover, cartilage thickness was (on average per species) significantly greater at the medial than at the lateral condyle (15%, p=0.004).

There was a direct relationship between cartilage thickness and body mass, but our data reveal that cartilage thickness increased less than would be expected based on isometric scaling of the skeleton (as illustrated in Figure 1), and consequently bore a negative allometric relationship to body mass over the range 25g (mouse) – 4,000kg (African elephant)

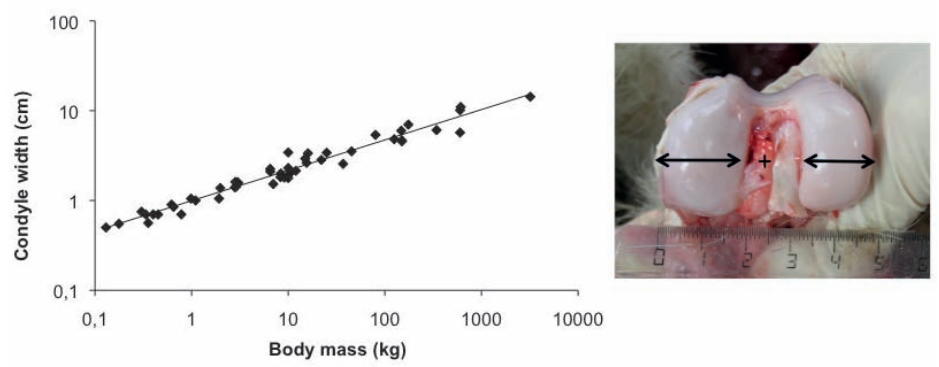

Figure 1: Scaling of the knee joint. The total average width of the articulating lateral and medial condyles per species follows an isometric relationship with body mass (a=0.337, R^2=0.96), illustrating the isometric scaling of the entire skeleton. Image shows the lateral and medial condyles of a cheetah.

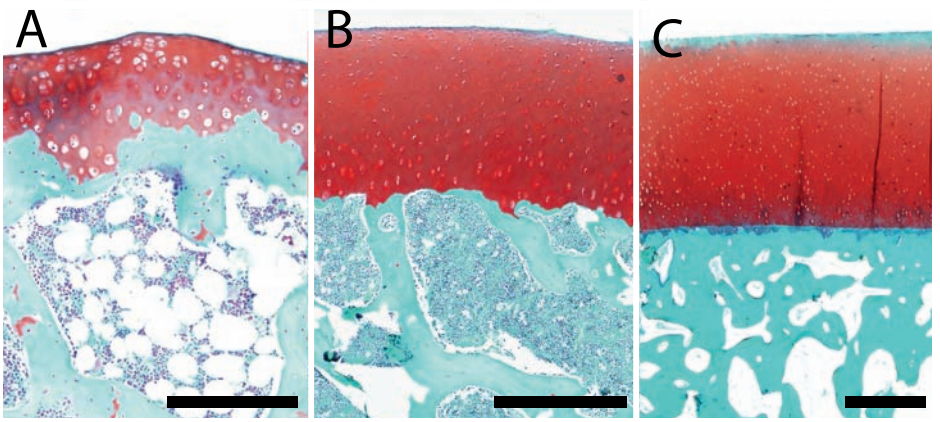

Figure 2: Safranin-O staining (stains GAGs red) of osteochondral tissue of the (A) rat, (B) barbary macaque and (C) white rhinoceros. Scale bars indicate (A) 200µm, (B) 400µm, and (C) 1000µm.

for both the lateral (a=0.262; R^2=0.80, p<0.001) and medial (a=0.280; R^2=0.79, p<0.001) condyles (Figure 3). The obtained power coefficients (a) were significantly different from the theoretical coefficient of 0.33 for both lateral (p<0.001) and medial (p=0.01) sites.

The average overall GAG content across species (lateral: 47±14µg per mg, medial: 49±15µg per mg cartilage) appeared not to be related to body mass (Figure 4A). In addition, hydroxyproline content, as a measure of collagen content, (lateral: 350±154nmol hydroxyproline per mg, medial: 419±180nmol hydroxyproline per mg) was also independent of body mass across different species (Figure 4B). In contrast, an inverse relationship between DNA content and body mass was observed (lateral: R^2=0.50 and medial: R^2=0.51) (Figure 4C), resulting in a rapid decrease in DNA content with increasing body mass, particularly in the 25g-10kg range.

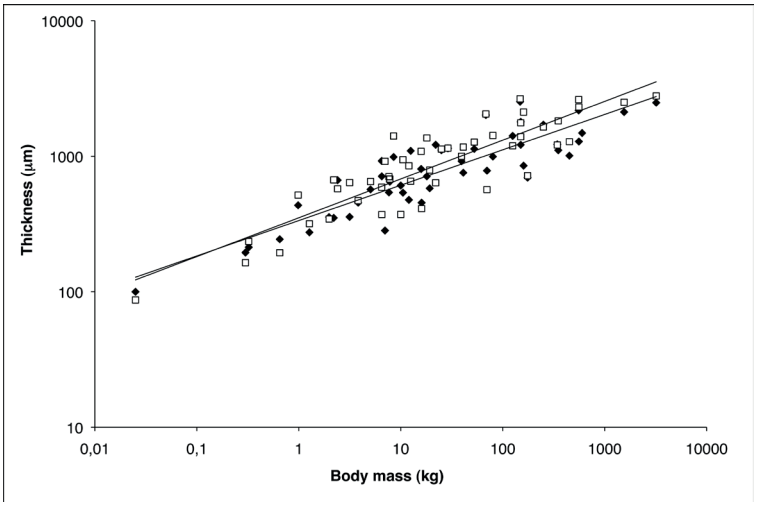

Figure 3: Average mammalian articular cartilage thickness per species at the center of lateral (black diamonds) and medial (open squares) condyles varies allometrically with body mass (a=0.262 and a=0.280, respectively).

Table 2: Cartilage thickness at the lateral en femoral condyles of selected species. *=only one sample was available.

Species	***(n)***	***Thickness Lateral*** ±SD ***(µm)***	***Thickness Medial*** ±SD ***(µm)***
Mouse (*Mus Musculus*)	5	99±32	87±13
Rat (*Rattus sp.)*	5	213±29	235±46
Rabbit *(Oryctolagus cuniculus)*	6	455±119	470±139
Vervet monkey *(Chlorocebus pygerythrus)*	2	540±142	707±48
Beagle dog (*Canis sp.*)	4	476±146	849±184
Hamadryas baboon (*Papio hamadryas*)	3	805±85	1087±145
Cheetah (*Acinonyx jubatus*)	4	919±152	999±297
Human (*Homo Sapiens*)	10	2014±512	2050±780
Horse (*Equus ferus caballus*)	15	1283±205	2309±726
White rhinoceros (*Ceratotherium simum*)	2	2119*	2502±192
Asian elephant (*Elaphus maximus*)	2	2413±101	3021±335

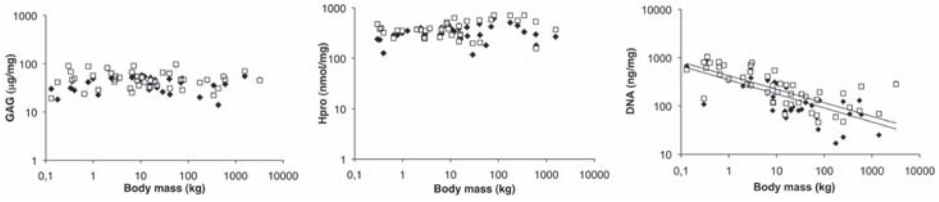

Figure 4: Average (A) glycosaminoglycan (GAG) and (B) hydroxyproline (Hpro) content of the articular cartilage per species is independent of body mass, whilst an inverse relation was observed for (C) DNA at the lateral (black diamonds, a=-0.327) and medial (open squares, a=-0.282) condyles.

Since structural features of the collagen network might also influence the mechanical properties of the tissue, collagen cross-links were analyzed as well. However, no significant correlation between lysyl-pyridinoline (LP) or hydroxylsyl-pyridinoline (HP) cross-link density and body mass was found (Figure 5).

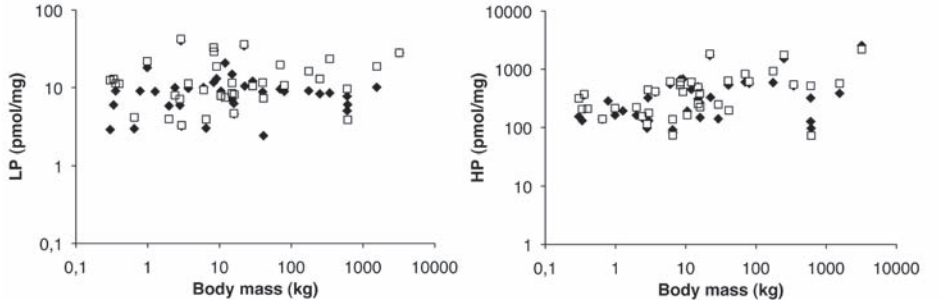

Figure 5: Average collagen cross-link content as a function of body mass. (A) Lysyl-pyridinoline (LP) and (B) hydroxylsyl-pyridinoline (HP) cross-links are independent of body mass at the lateral (black diamonds) and medial (open squares) condyles.

DISCUSSION

The present study shows for the first time that cartilage thickness at the femoral condyle bears a negative allometric relationship body mass, unlike the size of the mammalian skeleton that generally scales proportionally (isometrically) with body mass[5,6,7,8]. In addition, we show that cellular density (as determined by DNA content) decreases with increasing body mass particularly in the lower end of the mass spectrum, but that gross biochemical composition is remarkably constant over a wide range of mammalian body mass.

The condylar cartilage thicknesses reported here are in line with the outcomes of earlier studies investigating cartilage thicknesses in small groups of animals of different species[16,17,18]. Moreover, the average greater thickness of the medial compared to the lateral condyle is also in line with previous reports on a number of different species including the horse[25], cow[26], sheep[27] and rabbit[28]. Cartilage thickness scaled according to a negative allometric relationship with body mass; *i.e.*, based on the thickness observed in small mammals and assuming proportional scaling, one would have expected a considerably greater tissue thickness (approximately 4,500-6,000μm) than the actual observed value (3,000μm) for the African elephant. This lower-than-expected increase in tissue thickness may be related to diffusional constraints, as adult articular cartilage lacks vascularization[20,29]. Interestingly, recent research on fossilized material of the largest land creatures that ever lived, the dinosaurs, revealed traces of vascularization to potentially sustain the substantially thicker articular cartilage[30]. In contrast to our findings, previous investiga-

tions[16,17,26] have suggested a positive allometric relationship between articular cartilage thickness and body mass. These studies were however performed on only a small number (5-8) of mammalian species of less than 300kg, analyzed the maximum cartilage thickness in the joint and included skeletally immature animals[16,17,26]. These factors likely explain the overestimation of cartilage thickness in the larger species in these studies.

Besides variation in thickness, the mechanical characteristics of articular cartilage are determined by the interplay of its three main biochemical constituents: collagen, proteoglycans and water. Although some species differences in biochemical composition of the articular cartilage have previously been demonstrated[15], we found that gross biochemical composition is remarkably constant. It should be noted however that the DMMB assay[22] we employed is a rather crude technique for GAG quantification that for example does not discriminate between keratan sulphate and chondrotin sulphate[31]. The ratio of these components in the cartilage may significantly affect the overall fixed charge density[31], which in turn will affect the mechanical characteristics of the tissue[32]. Nevertheless, our results indicate a certain immutability of cartilage ECM with respect to gross composition, as both collagen content and the abundance of pyridinoline cross-links that heavily influence mechanical properties, were likewise found to be relatively stable over a wide range of mammalian body mass.

Cartilage DNA content, as a measure of cellular density, decreases with increasing body mass. This observation is consistent with the finding that cell density in thinner cartilages is considerably higher[17], although in the current study potential species-specific differences in DNA content per cell were not taken into account. The relatively high DNA content in mouse and rat cartilage is not a specific feature of rodent cartilage, as the cartilage of the Capybara (the largest extant rodent in the world), showed considerably lower DNA content, which is in the range of other similarly-sized mammals. The high DNA content of the thinner cartilages could also be related to the high cell content in the superficial zone of the tissue[17,25,33,34], which likely contributes relatively more to total tissue thickness in thin cartilage than in thicker cartilage. Regardless, the relatively high DNA content in the lighter species is indicative of a higher cellularity of thinner cartilage (as supported by histological evaluation of tissue cell density). This may impact (positively) on the regenerative capacity of cartilage in these smaller animals and underscores the need for the use of appropriate *in vivo* models[35,36], which approximate the human situation, when evaluating experimental approaches for cartilage repair.

An increase in mammalian body mass will require adaptations of the musculoskeletal system to accommodate for higher loading. Alterations in tissue dimensions and/or composition constitute a logical response to such changes. Indeed, articular cartilage biochemical composition (and with it biomechanical characteristics) have been shown to be both location and age dependent[37,38,39], which may explain the higher variation of the biochemical data in comparison to the joint sized in our study.

When gross ECM composition is remarkably stable over a large range of species and body mass, differences may exist at a more detailed (structural/molecular) level. These may explain previously reported interspecies differences in mechanical properties[32]. Although cartilage is a relatively homogeneous tissue, distinct zones, each with their own specific compressive properties, biochemical composition and structural organization, can be distinguished from the articular surface down to the cartilage-bone interface. For example, the superficial zone is known to exhibit larger strain[40] and to have lower GAG content[25] compared to deeper zones (in line with our histological Safranin-O stainings). Moreover, the superficial zone contains a number of specific extracellular matrix components, including lubricin (proteoglycan-4)[41] and clusterin[42] that are not found in the deeper zones. In addition, the chondroitin sulphate sulphation motifs and the ratio of chondroitin sulphate to keratan sulphate also vary with depth[31,43]. Collagen content is relatively stable throughout the depth of the tissue[25], but collagen fibril orientation is notably depth-dependent[44]. These depth-dependent differences clearly have implications for the overall mechanical characteristics of tissue with a specific thickness and may hence contribute to the adaptation to higher loads. Consequently, the potential variation in depth-dependent biochemical properties of the cartilage over a range of species and body masses warrants further investigation.

The limited increase in thickness of cartilage and its biochemical constancy are probably largely compensated for, as supported by the fact that static compressive stresses in the joint cartilage among various species are within one order of magnitude and are unrelated to cartilage thickness[16]. Moreover, compression of the tissue is radially confined and shear forces are further resisted by bonding with the subchondral bone and periarticular structures. This, together with the increase in joint surface area in the larger species and accompanying changes in joint alignment, posture and activity pattern (which are related to body mass[9]), might be sufficient to compensate for the additional loading. However, whether the less-than-proportional increase of articular cartilage thickness in larger mammals contributes to a greater susceptibility to degenerative joint disorders in these animals remains unclear and could be an interesting area of future investigation.

CONCLUSION

Articular cartilage thickness scales according to negative allometry, and, as a result, cartilage is relatively thinner in larger animals. This is potentially due to diffusional constraints, as is illustrated by the presence of high cell densities only in thin cartilages. However, gross biochemical composition is remarkably constant over a wide range of body mass, which, together with the negative allometric scaling of thickness, theoretically leads to a decrease in biomechanical resistance with increasing body weight. However, an isometric increase in

thickness may not be required for life-long performance, in light of relatively constant static compressive stresses on the tissue perhaps facilitated by additional compensatory factors like congruence, posture and activity pattern of the animal.

REFERENCES

1. Grodzinsky AJ, Levenston ME, Jin M, Frank EH (2000) Cartilage tissue remodeling in response to mechanical forces. Annu Rev Biomed Eng 2: 691-713.
2. Buckwalter J, Mankin H (1997) Articular Cartilage. Part I: Tissue Design and Chondrocyte-Matrix Interactions. J Bone Joint Surg Am 79: 600-611.
3. Steinert AF, Ghivizzani SC, Rethwilm A, Tuan RS, Evans CH, et al. (2007) Major biological obstacles for persistent cell-based regeneration of articular cartilage. Arthritis Res Ther 9: 213.
4. Galilei Linceo G (1683) Discorzsi e demostrazioni matematiche, intorno à duo nuoue scienze. Leiden: Elsevier.
5. Schmidt-Nielsen K (1984) Scaling; Why is animals size so important? Cambridge: University of Cambridge.
6. Christiansen P (2002) Mass allometry of the appendicular skeleton in terrestrial mammals. Journal of Morphology 251: 195-209.
7. Doube M, Klosowski MM, Wiktorowicz-Conroy AM, Hutchinson JR, Shefelbine SJ (2011) Trabecular bone scales allometrically in mammals and birds. Proc Biol Sci.
8. Reynolds WW (1977) Skeleton weight allometry in aquatic and terrestrial vertebrates. Hydrobiology 56: 35–37.
9. Biewener AA (2005) Biomechanical consequences of scaling. Journal of Experimental Biology 208: 1665-1676.
10. Brama PA, Tekoppele JM, Bank RA, Karssenberg D, Barneveld A, et al. (2000) Topographical mapping of biochemical properties of articular cartilage in the equine fetlock joint. Equine Vet J 32: 19-26.
11. Rogers BA, Murphy CL, Cannon SR, Briggs TW (2006) Topographical variation in glycosaminoglycan content in human articular cartilage. J Bone Joint Surg Br 88: 1670-1674.
12. Esquisatto MA, Pimentel ER, Gomes L (1997) Extracellular matrix composition of different regions of the knee joint cartilage in cattle. Ann Anat 179: 433-437.
13. Kiviranta I, Jurvelin J, Tammi M, Saamanen AM, Helminen HJ (1987) Weight bearing controls glycosaminoglycan concentration and articular cartilage thickness in the knee joints of young beagle dogs. Arthritis Rheum 30: 801-809.
14. Kempson GE, Muir H, Swanson SA, Freeman MA (1970) Correlations between stiffness and the chemical constituents of cartilage on the human femoral head. Biochim Biophys Acta 215: 70-77.
15. Buckwalter JA, Pedrini-Mille A, Dobrowolski AM, Olmstead M, Grood E (1989) Differences in articular cartilage matrices of humans monkeys and rabbits. Trans Orthop Res Soc 14: 155.
16. Simon WH (1970) Scale effects in animal joints. I. Articular cartilage thickness and compressive stress. Arthritis Rheum 13: 244-256.
17. Stockwell RA (1971) The interrelationship of cell density and cartilage thickness in mammalian articular cartilage. J Anat 109: 411-421.
18. Frisbie DD, Cross MW, McIlwraith CW (2006) A comparative study of articular cartilage thickness in the stifle of animal species used in human pre-clinical studies compared to articular cartilage thickness in the human knee. Vet Comp Orthop Traumatol 19: 142-146.
19. Brighton C, Heppenstall R (1971) Oxygen tension in zones of the epiphyseal plate, the metaphysis and diaphysis. An in vitro and in vivo study in rats and rabbits. J Bone Joint Surg Am 53: 719-728.
20. Malda J, Rouwkema J, Martens DE, Le Comte EP, Kooy FK, et al. (2004) Oxygen gradients in tissue-engineered Pegt/Pbt cartilaginous constructs: Measurement and modeling. Biotechnol Bioeng 86: 9-18.

21. Mankin HJ, Dorfman H, Lippiello L, Zarins A (1971) Biochemical and metabolic abnormalities in articular cartilage from osteo-arthritic human hips. II. Correlation of morphology with biochemical and metabolic data. J Bone Joint Surg Am 53: 523-537.
22. Farndale R, Buttle D, Barrett A (1986) Improved quantitation and discrimination of sulphated glycosaminoglycans by use of dimethylmethylene blue. Biochim Biophys Acta 883: 173-177.
23. McGowan KB, Kurtis MS, Lottman LM, Watson D, Sah RL (2002) Biochemical quantification of DNA in human articular and septal cartilage using PicoGreen and Hoechst 33258. Osteoarthritis Cartilage 10: 580-587.
24. Souza MV, van Weeren PR, van Schie HT, van de Lest CH (2010) Regional differences in biochemical, biomechanical and histomorphological characteristics of the equine suspensory ligament. Equine Vet J 42: 611-620.
25. Malda J, Benders KE, Klein TJ, de Grauw JC, Kik MJ, et al. (2012) Comparative study of depth-dependent characteristics of equine and human osteochondral tissue from the medial and lateral femoral condyles. Osteoarthritis Cartilage 20: 1147-1151.
26. McLure SW, Fisher J, Conaghan PG, Williams S (2012) Regional cartilage properties of three quadruped tibiofemoral joints used in musculoskeletal research studies. Proceedings of the Institution of Mechanical Engineers, Part H 226: 652-656.
27. Armstrong SJ, Read RA, Price R (1995) Topographical variation within the articular cartilage and subchondral bone of the normal ovine knee joint: a histological approach. Osteoarthritis Cartilage 3: 25-33.
28. Rasanen T, Messner K (1996) Regional variations of indentation stiffness and thickness of normal rabbit knee articular cartilage. J Biomed Mater Res 31: 519-524.
29. Silver IA (1975) Measurement of pH and ionic composition of pericellular sites. Philos Trans R Soc Lond B Biol Sci 271: 261-272.
30. Holliday CM, Ridgely RC, Sedlmayr JC, Witmer LM (2010) Cartilaginous Epiphyses in Extant Archosaurs and Their Implications for Reconstructing Limb Function in Dinosaurs. PLoS One 5.
31. Han E, Chen SS, Klisch SM, Sah RL (2011) Contribution of proteoglycan osmotic swelling pressure to the compressive properties of articular cartilage. Biophys J 101: 916-924.
32. Athanasiou KA, Rosenwasser MP, Buckwalter JA, Malinin TI, Mow VC (1991) Interspecies comparisons of in situ intrinsic mechanical properties of distal femoral cartilage. J Orthop Res 9: 330-340.
33. Hunziker EB, Quinn TM, Hauselmann HJ (2002) Quantitative structural organization of normal adult human articular cartilage. Osteoarthritis Cartilage 10: 564-572.
34. Schuurman W, Gawlitta D, Klein TJ, ten Hoope W, van Rijen MH, et al. (2009) Zonal chondrocyte subpopulations reacquire zone-specific characteristics during in vitro redifferentiation. Am J Sports Med 37 Suppl 1: 97S-104S.
35. McIlwraith CW, Fortier LA, Frisbie D, Nixon AJ (2011) Equine Models of Articular Cartilage Repair. Cartilage 2: 317-326.
36. Chu CR, Szczodry M, Bruno S (2010) Animal models for cartilage regeneration and repair. Tissue Eng Part B Rev 16: 105-115.
37. Brama PA, Holopainen J, van Weeren PR, Firth EC, Helminen HJ, et al. (2009) Influence of exercise and joint topography on depth-related spatial distribution of proteoglycan and collagen content in immature equine articular cartilage. Equine Vet J 41: 557-563.
38. Brama PAJ, TeKoppele JM, Bank RA, van Weeren PR, Barneveld A (1999) Influence of site and age on biochemical characteristics of the collagen network of equine articular cartilage. American Journal of Veterinary Research 60: 341-345.

39. Brommer H, Brama PA, Laasanen MS, Helminen HJ, van Weeren PR, et al. (2005) Functional adaptation of articular cartilage from birth to maturity under the influence of loading: a biomechanical analysis. Equine Vet J 37: 148-154.
40. Schinagl RM, Ting MK, Price JH, Sah RL (1996) Video microscopy to quantitate the inhomogeneous equilibrium strain within articular cartilage during confined compression. Ann Biomed Eng 24: 500-512.
41. Schumacher BL, Block JA, Schmid TM, Aydelotte MB, Kuettner KE (1994) A novel proteoglycan synthesized and secreted by chondrocytes of the superficial zone of articular cartilage. Arch Biochem Biophys 311: 144-152.
42. Malda J, ten Hoope W, Schuurman W, van Osch GJ, van Weeren PR, et al. (2010) Localization of the potential zonal marker clusterin in native cartilage and in tissue-engineered constructs. Tissue Eng Part A 16: 897-904.
43. Hayes AJ, Hall A, Brown L, Tubo R, Caterson B (2007) Macromolecular organization and in vitro growth characteristics of scaffold-free neocartilage grafts. Journal of Histochemistry and Cytochemistry 55: 853-866.
44. Benninghoff A (1925) Form und Bau der Gelenkknorpel in Ihren Beziehungen zur Funktion. Z Zellforsch 2: 783-862.

Chapter 4

Formalin fixation affects equilibrium partitioning of an ionic contrast agent-microcomputed tomography (EPIC-μCT) imaging of osteochondral samples

K.E.M. Benders
J. Malda
D.B.F. Saris
W.J.A. Dhert
R. Steck
D.W. Hutmacher
T.J. Klein

Osteoarthritis Cartilage. 2010 Dec;18(12):1586-91

ABSTRACT

Objective: Equilibrium Partitioning of an Ionic Contrast agent with microcomputed tomography (EPICμCT) is a non-invasive technique to quantify and visualize the three-dimensional distribution of glycosaminoglycans (GAGs) in fresh cartilage tissue. However, it is unclear whether this technique isapplicable to already fixed tissues. Therefore, this study aimed at investigating whether formalin fixation of bovine cartilage affects X-ray attenuation, and thus the interpretation of EPIC-μCT data.

Design: Osteochondral samples (n=24) were incubated with ioxaglate, an ionic contrast agent, for 22h prior to μCT scanning. The samples were scanned in both formalin-fixed and fresh conditions. GAG content was measured using a biochemical assay and normalized to wet weight, dry weight, and water content to determine potential reasons for differences in X-ray attenuation.

Results: The expected zonal distribution of contrast agent/GAGs was observed for both fixed and fresh cartilage specimens. However, despite no significant differences in GAG concentrations or physical properties between fixed and fresh samples, the average attenuation levels of formalin-fixed cartilage were 14.3% lower than in fresh samples.

Conclusions: EPIC-μCT is useful for three-dimensional visualization of GAGs in formalin-fixed cartilage. However, a significant reduction in X-ray attenuation for fixed (compared to fresh) cartilage must be taken into account and adjusted for accordingly when quantifying GAG concentrations using EPIC-μCT.

INTRODUCTION

Glycosaminoglycans (GAGs) are one of the most important constituents of articular cartilage. They provide a net negative charge and aid the cartilage in resisting the large compressive loads to which it is exposed on a daily basis[1]. GAGs vary in concentration throughout the depth of articular cartilage, with low concentration in the superficial zone and increasing concentrations in the middle and deep zones[2]. These variations are functionally important, as they allow for compliant articular surfaces, and a relatively smooth transition to the stiffer calcified cartilage and subchondral bone[3]. GAG levels are known to decrease in early osteoarthritis (OA)[1, 4] and are an early indicator of degradation of cartilage tissue and loss of joint function. Further, the GAG content and distribution in *in vitro* cultured tissues may be a key to developing successful tissue engineered cartilage constructs to replace damaged or degenerated cartilage[5]. Thus, knowledge of GAG concentration and distribution in native and tissue-engineered cartilage is fundamentally important to understand the onset and progression of cartilage disease and to develop successful regenerative treatment strategies.

GAG content and distribution in cartilaginous tissues has most commonly been monitored using destructive methods. Typically, small cartilage biopsies are taken, sectioned and mounted on glass slides, after which GAG content is visualized using histological stains, such as Safranin-O[6], Alcian blue[7], or Toluidine blue[8]. These techniques are invasive, creating a defect in clinical situations, and only give two-dimensional information on a relatively small section of the tissue, which may not be representative of the whole tissue. While there have been efforts to make some of the histological methods quantitative using image processing techniques[9], they are generally qualitative in nature. For quantification of the GAG content, pieces of cartilage are commonly digested using an enzyme (*e.g.,* papain or proteinase K), and analysed using a spectrophotometric method with a specific dye (typically dimethylmethylene blue)[10]. This method is the gold standard for quantification, but the distribution of GAGs throughout the depth of the tissue is difficult to obtain.

In the past decade, non-invasive means to quantify GAG content have been developed to overcome the limitations of destructive tests. For example, magnetic resonance imaging (MRI) in combination with a gadolinium contrast, a technique referred to as delayed Gadolinium-Enhanced MRI of Cartilage (dGEMRIC) has been shown to be effective in measuring GAG content of articular cartilage[11-13]. However, MR imaging is a costly process and often does not provide a high enough resolution when looking at thinner layers of cartilage in smaller animals such as rats or mice[14]. This also poses a problem when imaging thin layers of *in vitro* cultured cartilage constructs. GAG content and zonal variations can also be studied by means of microcomputed tomography (μCT) combined with the contrast agent ioxaglate (Hexabrix®). This method, termed Equilibrium Partitioning of an Ionic Contrast agent (EPIC) μCT[14-17] is based on the distribution of the contrast

agent, which is inversely related to the amount of GAGs in the cartilage. It can hence be used to quantify GAG content even in thin cartilage samples[18]. In particular, a strong correlation between EPIC-μCT attenuation levels and GAG content measured in digested tissues was observed[15]. Further, EPIC-μCT has been used to monitor the decrease of GAG content of bovine cartilage explants after treatment with Interleukin-1 (IL-1)[15], as well as age-related differences in GAG content in the articular cartilage of rats[17]. The latter study demonstrated that the GAG differences can be detected by EPIC-μCT, not only in thick cartilage layers, but also in thin cartilage layers *e.g.*, present in smaller animal models.

Thus far, GAG content has only been quantified by EPIC-μCT using freshly harvested specimens, rather than formalin-fixed ones[14, 15, 17, 19]. For EPIC-μCT, fresh samples must be scanned immediately after excision, limiting the settings in which this technology can be used. The ability to use formalin-fixed samples would offer the opportunity of non-invasive GAG quantification of multiple samples over more extensive periods of time. Moreover, degradation of the proteoglycan network would be prevented, facilitating easier sample handling. Further, pre-fixed archival samples could be analysed to determine three-dimensional (3D) GAG concentration and distribution. Thus, extension of EPIC-μCT to formalin-fixed samples would have significant impact on the high-resolution quantification of GAG content and distribution in a broad range of small and large cartilage samples. Therefore, we evaluated the effect of formalin fixation on EPIC-μCT imaging in bovine cartilage samples.

MATERIALS AND METHODS

Design and tissue harvest

Adult bovine osteochondral tissue was obtained from a local abattoir. Twenty-four osteochondral fragments of approximately 3mm x 5mm were obtained from the trochlear groove using a hacksaw, with phosphate buffered saline (PBS) irrigation. The fragments were stored overnight at 4°C in PBS with protease inhibitors (2mM Na_2-EDTA, 1mM PMSF, 5mM Benz-HCl, 10mM NEM) (all Sigma-Aldrich, St. Louis, MO, USA) to prevent degradation. The osteochondral samples were divided into three groups (group I, group II, group IIIa and group IIIb). All samples were incubated in 1mL of an ionic contrast agent solution (1mL 40% ioxaglate (Hexabrix®, Mallingckrodt, Hazelwood, MO)/60% PBS with protease inhibitors) for 22 hours at 37°C with continuous shaking immediately prior to imaging. This time was shown previously to be sufficient for reaching equilibrium[15], and was verified by pilot studies. Group I was incubated directly with ioxaglate and scanned immediately afterwards. Group II was first fixed in 10% neutral buffered formalin for 48 hours, then incubated in ioxaglate and then scanned. Group III was incubated immediately with ioxaglate (like group I) and scanned (group IIIa). Subsequently, the samples were incubated in PBS at 4°C for

48 hours to allow for ioxaglate desorption. Then, the samples were fixed in 10% neutral buffered formalin for 48 hours, incubated in ioxaglate for a second time and scanned (group IIIb) (Figure 1). This allowed us to study the intra-group variation of attenuation levels before and after formalin fixation.

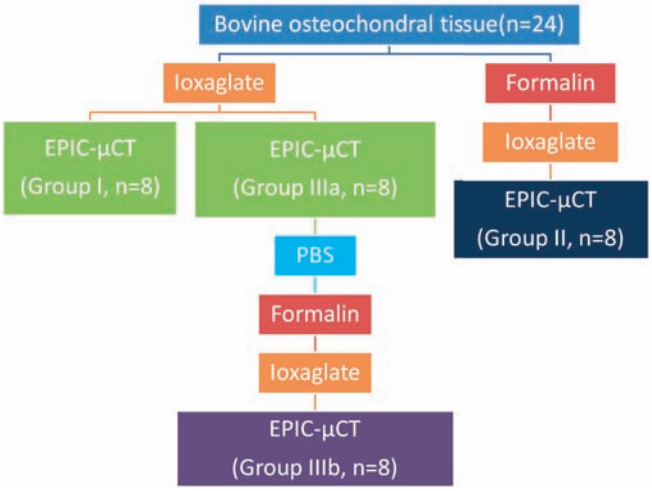

Figure 1: Diagram of experimental protocol for EPIC-uCT imaging of the three experimental groups. Samples in Group I were scanned directly after incubation with ioxaglate. Samples in Group II were fixed prior to ioxaglate incubation and scanning. Samples in Group III were first imaged as samples in Group I, then washed in PBS, fixed, incubated with ioxaglate and imaged again.

From each of the groups, five samples were randomly selected for biochemical GAG analysis. The three remaining samples from group II were used for Safranin-O staining. The remnants of the proteinase K digestion of the fixed samples were also used for Safranin-O staining.

MicroCT

MicroCT scanning was performed at standard resolution in the μCT40 (Scanco Medical, Brüttisellen, Switzerland) at 45kVp, 177μA, resulting in 12μm isotropic voxel size. Scanco μCT software (Scanco Medical, Brüttisellen, Switzerland) was used for the analysis of the osteochondral cores. A cubic volume of interest (2mm x 2mm x cartilage thickness) was defined, and threshold values were determined visually for segmenting the cartilage from the osteochondral bone, using a Gaussian filter with sigma of 1.2 and a support of 2.

Attenuation levels (presented in Hounsfield Units (HU)), which are proportional to the concentration of ioxaglate, and inversely related to the GAG concentration, were calculated using the Scanco software. Three-dimensional images of the osteochondral fragments were generated using the Scanco software for visual inspection of the zonal distribution of GAG

concentration. Additionally, attenuation levels from 2mm x 2mm x 0.012mm slices from the top 20% (superficial zone), next 40% (middle zone), and bottom 40% (deep zone) were averaged for a representative sample from Group III before and after fixation to further investigate zonal differences in attenuation. The cartilage thickness before and after fixation was calculated using a direct distance transformation algorithm. Further, the change of thickness was also evaluated by a shell-to-shell comparison of a single sample from Group III. A difference map showing the deviations of the cartilage surfaces was created by aligning and comparing STL files of a 1mm cross-section, scanned before and after fixation, using Rapidform 2006 (INUS Technology Inc., Seoul Korea).

Histology

Samples from group II and group III were used for Safranin-O staining. Samples were decalcified in EDTA (Sigma-Aldrich) before they were dehydrated through a graded ethanol series, cleared in xylene and embedded in paraffin. Embedded samples were sectioned to yield 5μm sections, which were stained using a triple stain of haematoxylin, fast green FCF (0.001% *w/v*) and Safranin-O (0.1% *w/v*) (all from Sigma-Aldrich). The sections were examined using a light microscope (Olympus, BX51, United States) and photomicrographs taken with a Olympus DP70 camera (United States).

Wet weight/dry weight

For the determination of the wet and dry weight, articular cartilage samples were separated from all the visible subchondral bone using a scalpel (n=5 per group), and weighed (wet weight). Subsequently, samples were snap frozen in liquid nitrogen, lyophilized (Martin-Christ, Germany), and weighed (dry weight).

Glycosaminoglycan assay

Lyophilized cartilage samples were digested with 0.5mg/mL proteinase K (Invitrogen, Carlsbad, USA) at 60°C overnight. Absorbance was measured at 525nm in a microplate reader (Biorad, Philadelphia, USA) after reaction with dimethylmethylene blue (Sigma-Aldrich), and GAG content was calculated using a standard of chondroitin sulphate C (Sigma-Aldrich) [10].

Statistical analysis

Statistical comparisons were made using a 2-tailed Student's *t*-test with significance determined by a *p*-value smaller than 0.05. For comparisons of samples scanned before and after fixation (Group III), paired *t*-tests were used. All data are represented as mean and 95% confidence interval (lower limit, upper limit). Analysis of variance (ANOVA) was used to compare Group I, Group II and Group III with significance determined by a *p*-value smaller than 0.05.

RESULTS

The presence and zonal distribution of GAGs throughout the bovine articular cartilage tissue samples was confirmed by means of Safranin-O staining (Figure 2A), which is directly proportional to the GAG content [9]. The intensity of the staining in the cartilage tissue increased from the superficial layer towards the deeper layers.

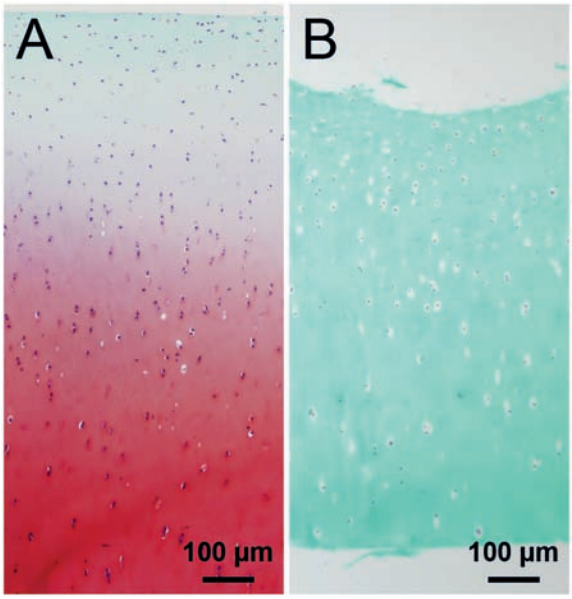

Figure 2: Safranin O staining of (A) fixed bovine osteochondral explant and (B) fixed bovine articular cartilage following overnight digestion with proteinase K. Safranin-O stains GAG red, Fast Green FCF stains proteins green and haematoxylin stains nuclei blue. GAG staining was depth-dependent in (A) fixed bovine cartilage but not observed in (B) proteinase K digested bovine cartilage.

The average attenuation, as an indirect measure of overall GAG content of the unfixed samples, did not significantly differ between Group I and Group IIIa (n=8, 3667.3 (3357.6-3977.0) HU vs. 3618.1 (3248.0-3988.1) HU, p=0.66. However, fixation prior to EPIC-μCT imaging (Group II) resulted in a significant decrease of the attenuation by 14.3% compared to that of unfixed samples (Group I) (n=8, 3142.2 (2812.8-3471.5) HU vs. 3667.3 HU, (3357.6-3977.0) HU, p<0.001). In line, the average attenuation of Group III decreased significantly after fixation (n=8, 3618.1 (3248.0-3988.1) HU vs. 3317.6 (2953.2-3682.1) HU, p<0.05).

A zonal distribution of GAGs was observed in fresh and fixed cartilage using EPIC-μCT imaging (Figure 3). However, as a result of the differences in overall cartilage attenuation between the fixed and unfixed samples, the output ranges needed to be adjusted for optimal visualization of the 3D zonal distribution of GAGs. Output ranges of 1748-4851 HU for freshly scanned samples (Figure 3A) and 1748-3871 HU for fixed samples (Figure 3D) resulted in similar images of the zonal GAG distribution (Figure 3 A,D). The difference

in attenuation between the superficial (top 20%), and middle (20-60% of depth) zones of a representative sample from Group III was 12% (14% after fixation), and 28% (28% after fixation) between the superficial and deep (bottom 40%) zones (Figure 3E). The attenuation level was consistently lower throughout the depth of cartilage after fixation, as demonstrated by similar reductions of attenuation in the superficial (top 20%), middle (20-60%) and deep (bottom 40%) zones (Figure 3E).

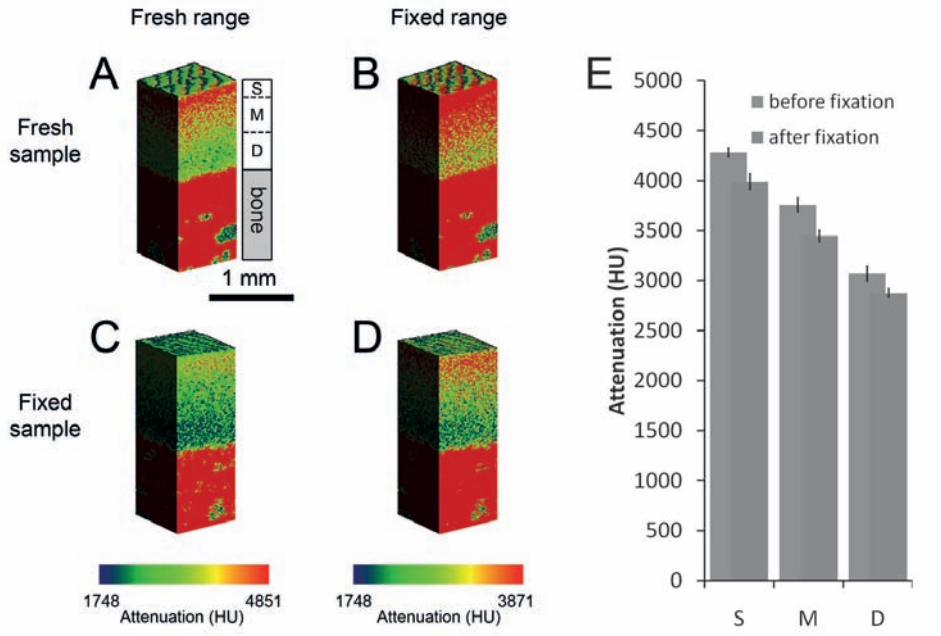

Figure 3: Two-dimensional representations of three-dimensional attenuation values present in (A, B) fresh and (C, D) fixed osteochondral samples. Different attenuation value ranges were chosen to show the greatest range from superficial to deep zones in (A) fresh and (D) fixed tissues. Clear differences in attenuation values can be seen when (B) fresh samples are displayed in the fixed range, and (C) fixed samples are displayed in the fresh range. After adjusting the attenatuation value ranges, images (A) fresh and (D) fixed show the optimal representation of GAG distribution in both fresh and fixed cartilage tissue. Low attenuation (blue) indicates high GAG concentration, high attenuation (red) indicates low GAG concentration. (E) Attenuation values in different zones (mean with 95% CI, n=20 slices for superficial (S), 40 slices for middle (M), and 40 slices for deep (D) zones) for a representative sample from group III before and after fixation.

Moreover, biochemical quantification of GAGs (Table 1) revealed similar levels in fresh (Group I) and fixed tissues (Group II and Group IIIb), whilst Safranin-O staining of fixed and subsequently digested samples confirmed the absence of residual GAGs (Figure 2B). Further, no significant differences in the average amount of GAG per dry weight could be determined between the groups (Table 1).

Table 1: Biochemically quantified GAG content of bovine samples. GAG content of Group 1 (n=5), Group II (n=5) and Group IIIb (n=5) bovine samples shown as mean and 95% confidence interval of the GAG content per wet weight (ww), dry weight (dw), and water. No significant differences were found between the experimental groups using unpaired *t*-tests, with *P*-values comparing respective groups listed below the mean and confidence interval.

	Group I	**Group II**	**Group IIIb**
GAG/ww (μg/mg)	32.9 (30.5, 35.3) $p = 0.28, 0.50$	35.6 (31.8, 39.4) $p = 0.28, 0.83$	36.9 (26.2, 47.6) $p = 0.50, 0.83$
GAG/dw (μg/mg)	165.3 (151.7, 178.8) $p = 0.99, 0.88$	165.3 (141.8, 188.9) $p = 0.99, 0.89$	168.9 (126.8, 211.0) $p = 0.89, 0.88$
GAG/H_2O (μg/mg)	41.2 (37.7, 44.7) $p = 0.19, 0.44$	45.4 (40.8, 50.0) $p = 0.19, 0.81$	47.2 (33.0, 61.5) $p = 0.44, 0.81$

DISCUSSION

We have shown that the non-destructive imaging technique, EPIC-μCT, can be used to detect zonal differences in GAG content in both fresh and formalin-fixed articular cartilage explants. Previous studies have shown that EPIC-μCT is a valuable 3D tool for quantification of GAG levels in the different zones of fresh articular cartilage[14, 15, 17]. However, there are multiple benefits to using formalin-fixed tissue, including prevention of matrix degradation, simplification and standardization of sample processing, and allowing for analysis of GAG content and distribution in already-fixed or archival samples. Thus, this work extends the realm of applications for EPIC-μCT.

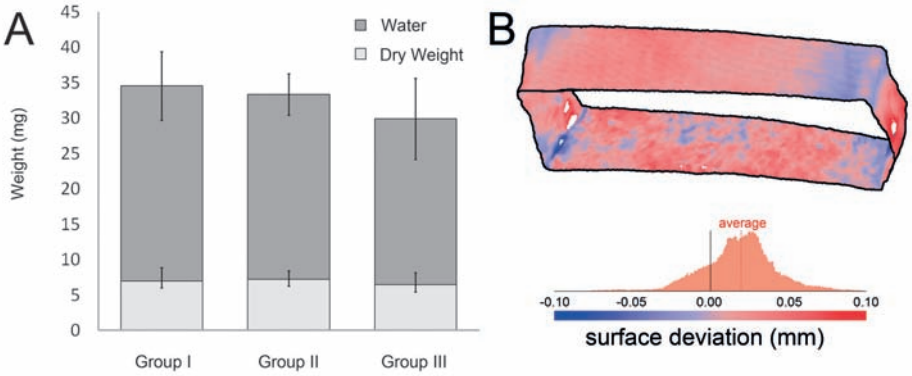

Figure 4: Weights of water and dry cartilage content in Group I (n=5), Group II (n=5), and Group III (n=5) (A). No significant differences were found using an unpaired *t*-test. Error bars represent 95% CI. Comparison of cartilage μCT surfaces of a representative sample from Group III (B). A 1mm thick section is shown, with articular surface on top, cut surfaces on the sides, and cartilage-bone boundary on the bottom. Color intensity represents the variation between surfaces of the fresh and fixed scans. The distribution of differences between scans shows an average difference of 0.02mm, corresponding to a change in thickness of 0.04mm.

One major finding of our study is that formalin fixation decreases X-ray attenuation levels in ioxaglate-stained cartilage. This was apparent in both the average attenuation values (Figure 3) and depth-dependent attenuation values (Figure 4). As the amount of ioxaglate is inversely related to the amount of GAGs[15], one could reach the conclusion that fixed tissues contain a higher concentration of GAGs than fresh tissues. While this could potentially be the case, the samples in Group III, which were both scanned fresh and after fixation, showed lower attenuation levels after fixation, indicating that this phenomenon is probably due to fixation rather than sample variation between experimental groups.

To gain further insight into the potential causes for the observed differences in attenuation between the fresh and fixed samples, several potential explanations for the differences were studied. The first possible explanation is that the GAG content was higher in the fixed tissues, potentially caused by GAG loss in the fresh tissues. Therefore, we quantified the amount of GAGs in the samples by means of a biochemical assay following proteinase K digestion of the tissues. To the best of our knowledge there are no data on the degradation of fixed cartilage tissue by proteinase K. However, other tissues such as lung tissue have successfully been released after fixation using proteinase K[20]. Safranin-O staining revealed that proteinase K digestion of the fixed cartilage tissue was adequate since positive staining for GAGs was absent in the residual tissue after digestion (Figure 1). The total GAG content of the tissue (relative to dry weight, wet weight, or water) did not significantly vary between the fresh and fixed samples and differences in attenuation levels can, therefore, most likely not be explained by differences in GAG content.

A second possible explanation for the observed differences in attenuation could be a variation in water content between the experimental groups. Ioxaglate accumulates in the water compartment of cartilage during incubation. Thus, if the water content in fresh samples is higher than in fixed samples, the amount of ioxaglate in the fixed samples could be lower. No significant differences in cartilage thickness, determined by μCT, were observed within Group III before and after fixation, but small observed differences in volume (~5%) may account for some of the differences in attenuation. Our results also show that there is no significant difference between the water content of fresh samples (Group I, n=5) and the fixed samples (Group II and Group III, n=10). Thus, changes in water content and geometry are not likely to be the sole cause for the observed differences in attenuation levels.

An alternative explanation for the lower attenuation in fixed tissues is that the diffusion of ioxaglate is hindered in fixed tissues due to a tighter extracellular matrix network, and thus a longer incubation is needed to reach equilibrium. EPIC-μCT relies on the principle of equilibrium of the ionic contrast agent[15, 17] and thus it is important to reach equilibrium when using this technique. However, attenuation levels of fixed tissues stained for 72 hours remained unchanged from those stained for 22 hours, and lower than the fresh tissues (data not shown). Formalin fixation has been shown to form strong and stable methylene cross-links with amino, amide and guanidyl groups as well as aromatic amino acids. This

means that formalin would cross-link the NH-groups that are present on the chondroitin and keratan sulfate on GAGs[21]. It is possible that the extensive cross-linking that occurs during formalin fixation[21] leads to a decrease in the maximal possible ioxaglate diffusion because of the tighter extracellular matrix of the osteochondral tissue. This explanation could relate to our results of lower attenuation levels in fixed tissue despite the similar GAG contents in fresh and fixed samples. However, this issue will have to be addressed in future research.

One final possible explanation for the differences in attenuation is that residual formalin interacts with ioxaglate, leading to a lower concentration of the contrast agent in the fixed tissue. There was no precipitate formed in the incubation tubes (both fresh and fixed samples), thus at least a precipitation reaction can be ruled out. Additionally, pilot studies showed that attenuation levels for fixed tissues remained lower than fresh tissues following a 24 hour PBS wash after fixation (to remove any residual formalin) and before a second scan (data not shown). Thus, residual formalin does not likely explain the differences we have measured.

This research has focused on bovine cartilage explants, which could have implications for EPIC-μCT studies on cartilage from different species. Bovine cartilage is a relatively thick tissue when compared to cartilage from smaller animal models, thus zonal variations are more easily discerned than in small animal models. However, previous research has shown that the zonal GAG distribution can be studied in thin cartilage samples from small animals using EPIC-μCT[14,15,17]. Changes to staining protocols, such as shortening ioxaglate incubation time, can be made for thin cartilage specimens, since less time is required for equilibration of the contrast agent. Given that histological staining protocols, such as Safranin-O, work well on fixed tissues irrespective of cartilage thickness, it is likely that fixed thin cartilage tissue will behave similarly to those tissues studied here when using EPIC-μCT. Nonetheless, further research is required to confirm this assumption.

Besides EPIC-μCT, the MRI-based technique, dGEMRIC has also been used to non-destructively quantify GAG content in fresh and fixed articular cartilage[22]. dGEMRIC and EPIC-μCT are both based on the principle of a contrast agent that is distributed throughout the cartilage in an inverse relationship to the concentration of GAGs[13, 15]. One of the main differences between dGEMRIC and EPIC-μCT is their application in research settings. dGEMRIC has already been succesfully used *in vivo*[23, 24], whereas EPIC-μCT has only been used *ex vivo* as there are concerns using this technique regarding the radiation exposure and the high amounts of contrast that will have to be administered[12, 14, 15, 17]. Therefore it seems less likely for EPIC-μCT to be implemented in clinical diagnostics. However, EPIC-μCT in *ex vivo* cartilage imaging of small samples is possibly more relevant than dGEMRIC due to the lower resolution of MRI-generated images when scanning small samples *ex vivo*, unavoidably this leads to unclear images of small cartilage samples. Another difference is that fixation of cartilage appears not to affect GAG quantification

in dGEMRIC[22] whereas our results demonstrate a significant reduction of the average attenuation using EPIC-μCT imaging. Dugar *et al.* performed dGEMRIC imaging on fixed bovine and human tissue. They reported that fixation "had a very modest, if any, effect" on dGEMRIC imaging of bovine and human cartilage tissue[22]. The results of our study however show a significant difference in cartilage attenuation after formalin fixation of bovine cartilage when using EPIC-μCT imaging. This will inevitably influence the quantification of GAGs in the tissue.

Despite the differences between attenuation levels of fresh and fixed tissue, the use of EPIC-μCT to non-destructively determine the local distribution of GAG content in cartilage samples remains a valid and promising technique. As we have shown, there is no change in GAG content after fixation; therefore we believe that the correlation between X-ray attenuation and GAG content is different for fresh and fixed samples. This should be taken into account and adjusted accordingly when quantifying GAG concentrations of both fresh and fixed cartilage samples using EPIC-μCT imaging.

REFERENCES

1. Martel-Pelletier J, Boileau C, Pelletier JP, Roughley PJ. Cartilage in normal and osteoarthritis conditions. Best Pract Res Clin Rheumatol 2008;22(2):351-84.
2. Bhosale AM, and Richardson JB. Articular cartilage: structure, injuries and review of management. Br Med Bull 2008;87:77-95.
3. Rieppo J, Töyräs J, Nieminen MT, Kovanen V, Hyttinen MM, Korhonen RK, et al. Structure-function relationships in enzymatically modified articular cartilage. Cells Tissues Organs 2003;175(3):121-32.
4. Silvast TS, Jurvelin JS, Lammi MJ, Töyräs J. pQCT study on diffusion and equilibrium distribution of iodinated anionic contrast agent in human articular cartilage--associations to matrix composition and integrity. Osteoarthritis Cartilage 2009;17(1):26-32.
5. Klein TJ, Rizzi SC, Reichert JC, Georgi N, Malda J, Schuurman W, et al. Strategies for zonal cartilage repair using hydrogels. Macromol Biosci 2009;9(11):1049-58.
6. Lillie RD, Histopathologic Technic and Practical Histochemistry. New York: Blakiston Division, McGraw-Hill 1965:506-507.
7. Ruggeri A, Dell'orbo C, and Quacci D. Electron microscopic visualization of proteoglycans with Alcian Blue. Histochem J 1975;7(2):187-97.
8. Shepard N, and MitchellN, Simultaneous localization of proteoglycan by light and electron microscopy using toluidine blue O. A study of epiphyseal cartilage. J Histochem Cytochem 1976;24(5):621-9.
9. Martin I, Obradovic B, Freed LE, Vunjak-Novakovic G. Method for quantitative analysis of glycosaminoglycan distribution in cultured natural and engineered cartilage. Ann Biomed Eng 1999;27(5):656-62.
10. Farndale RW, Buttle DJ, and Barrett AJ. Improved quantitation and discrimination of sulphated glycosaminoglycans by use of dimethylmethylene blue. Biochim Biophys Acta 1986;883(2):173-7.
11. Burstein D, Gray M, Mosher T, Dardzinski. Measures of molecular composition and structure in osteoarthritis. Radiol Clin North Am 2009;47(4):675-86.
12. Taylor C, Carballido-Garnio J, Majumdar S, Li X. Comparison of quantitative imaging of cartilage for osteoarthritis: T2, T1rho, dGEMRIC and contrast.
13. Bashir A, Gray ML, Hartke J, Burstein D. Nondestructive imaging of human cartilage glycosaminoglycan concentration by MRI. Magn Reson Med 1999;41(5):857-65.
14. Xie L, Lin AS, Levenston ME, Guldberg RE. Quantitative assessment of articular cartilage morphology via EPIC-microCT. Osteoarthritis Cartilage 2009;17(3):313-20.
15. Palmer AW, Guldberg RE, and Levenston ME. Analysis of cartilage matrix fixed charge density and three-dimensional morphology via contrast-enhanced microcomputed tomography. Proc Natl Acad Sci U S A 2006;103(51):19255-60.
16. Guldberg RE, Duvall CL, Peister A, Oest ME, Lin AS, Palmer AW, et al. 3D imaging of tissue integration with porous biomaterials. Biomaterials 2008;29(28):3757-61.
17. Xie L, Lin AS, Guldberg RE, Levenston ME. Nondestructive assessment of sGAG content and distribution in normal and degraded rat articular cartilage via EPIC-muCT. Osteoarthritis Cartilage 2010;18(1):65-72.
18. Jiang Y, Zhao J, Liao EY, Dai RC, Wu XP, Genant HK. Application of micro-CT assessment of 3-D bone microstructure in preclinical and clinical studies. J Bone Miner Metab 2005;23Suppl:122-31.
19. Aula AS, Jurvelin JS, Töyräs J. Simultaneous computed tomography of articular cartilage and subchondral bone. Osteoarthritis Cartilage 2009; 23 Suppl:1583-8.

20. Takeichi T, Kitamura O. Detection of diatom in formalin-fixed tissue by proteinase K digestion. Forensic Sci Int 2009;190(1-3):19-23.
21. Puchtler H, Meloan SN. On the chemistry of formaldehyde fixation and its effects on immunohistochemical reactions. Histochemistry 1985;82(3):201-4.
22. Dugar A, Farley ML, Wang AL, Goldring MB, Goldring SR, Swaim BH, et al. The effect of paraformaldehyde fixation on the delayed gadolinium-enhanced MRI of cartilage (dGEMRIC) measurement. J Orthop Res 2009;27(4):536-9.
23. Mayerhoefer ME, Welsch GH, Mamisch TC, Kainberger F, Weber M, Nemec S, et al. The in vivo effects of unloading and compression on T1-Gd (dGEMRIC) relaxation times in healthy articular knee cartilage at 3.0 Tesla. Eur Radiol 2009;20(2):443-9.
24. Welsch GH, Mamisch TC, Hughes T, Zilkens C, Quirbach S, Scheffler K, et al. In vivo biochemical 7.0 Tesla magnetic resonance: preliminary results of dGEMRIC, zonal T2, and T2* mapping of articular cartilage. Invest Radiol 2008;43(9):619-26.

Chapter 5

Extracellular matrix scaffolds for cartilage and bone regeneration

K.E.M. Benders
P.R. van Weeren
S.F. Badylak
D.B.F. Saris
W.J.A. Dhert
J. Malda

Trends Biotechnol. 2013 Mar;31(3):169-76.

ABSTRACT

Regenerative medicine approaches based on decellularized extracellular matrix (ECM) scaffolds and tissues rapidly expand. The rationale for using ECM as a natural biomaterial is the presence of bioactive molecules that drive tissue homeostasis and regeneration. Moreover, appropriately prepared ECM is biodegradable and does not elicit adverse immune responses.

Successful clinical application of decellularized tissues has been reported in cardiovascular, gastrointestinal and breast reconstructive surgery. At present, the use of ECM for osteochondral tissue engineering is gaining interest. Recent data underscore the great promise for future application of decellularized ECM for osteochondral repair.

This review describes the rationale for using ECM-based approaches for different regenerative purposes and goes into detail on the application of ECM for cartilage or osteochondral repair.

THE NEED FOR IMPROVED REPAIR OF OSTEOCHONDRAL DEFECTS

Joint injuries are common in the young and active population and often result in cartilage or osteochondral lesions. If untreated, these defects lead to joint swelling, pain and serious restrictions in daily activities and can eventually progress towards osteoarthritis (OA), of which the only end-stage, salvaging therapy is artificial joint replacement. Over 151 million people suffer from OA worldwide[1], implying a huge clinical and socio-economic burden. Established OA is notoriously difficult to treat, but prevention through successful treatment of cartilage lesions will significantly reduce this socio-economic impact.

Natural wound healing in full-thickness cartilage defects leads to the formation of so-called fibrocartilage that is functionally and biomechanically inferior to the original hyaline cartilage. This makes the tissue more prone to further deterioration, thus inciting a vicious cycle.

Currently, many different cartilage repair-enhancing treatments are applied in patients with (osteo-)chondral defects. These techniques are either based on cell therapy, like autologous chondrocyte implantation (ACI)[2] or matrix-induced chondrocyte implantation (MACI)[3], on the replacement of the damaged tissue within the joint, e.g. by mosaicplasty[4] or osteochondral allografting[5, 6], or on the recruitment of mesenchymal stromal cells (MSCs) through, for example, microfracture[7]. All of these techniques provide fairly acceptable clinical results, but neither result in the restoration of fully functional hyaline cartilage, making long-term prognosis uncertain.

In an attempt to optimize the functional restoration of cartilage, tissue engineering has been suggested as a good basis for new regenerative therapies. The key to successful engineering of cartilage with optimal restoration of function lies in finding the optimal combination between biomaterials, biofactors, and cells[8]. Currently applied biomaterials within the field of cartilage tissue engineering can be grossly divided into two groups, the natural biomaterials like collagen[9], gelatin[10], and fibrin[11], and synthetic biomaterials such as polycaprolactone (PCL)[12], and polylactic acid (PLA)[13]. The synthetic materials often have good biomechanical strength and by changing the polymer composition their specific properties can be tailored. However, the major challenge for these materials, which are foreign to the body, is to achieve satisfactory tissue integration and tissue differentiation. A natural biomaterial may surpass this, as these are biocompatible and biodegradable.

Despite the great advances that have been made within the field of material sciences in mimicking the natural tissue environment in order to drive cell proliferation and differentiation, oversimplified biomaterials for (cartilage) tissue regeneration are still being used. In fact, all tissues in the body are composed of a complex mixture of different biomaterials and this situation is not different for cartilage, notwithstanding its seemingly homogeneous and straightforward appearance. In reality, the extracellular matrix (ECM) of cartilage is a structurally complex three-dimensional (3D) environment composed of various types of

collagens and proteoglycans in which multiple bioactive factors, for instance growth factors, integrins and functional peptides are incorporated. Even highly sophisticated, newly developed biomaterials will probably never reach this complexity.

The abovementioned circumstances and considerations have driven the tissue-engineering field towards increased use of biomaterials or scaffolds based on (processed) natural extracellular matrices, an approach that might be a very valid option for cartilage repair as well.

EXTRACELLULAR MATRIX-BASED REGENERATIVE MEDICINE

All tissues are composed of cells surrounded by ECM that consists of a unique and tissue-specific 3D environment of structural and functional molecules and is secreted by the resident cells[14]. There is reciprocal interaction between cells and ECM; cellular products, including proteinases modify the ECM, while ECM-incorporated growth factors and cytokines act as functional cues, steering the metabolic and secretory activity of cells. This situation becomes even more complex, as the intricate interplay of cells and ECM in a given microenvironment is not static, but rather a dynamic event that will respond to external influences, such as biomechanical triggers or hormonal actions[15]. It is the eventual outcome of these dynamic processes that determine tissue homeostasis and possible aberrations thereof. Given the high complexity of these processes and the multiple roles of the ECM, it can be supposed that constructs based on natural ECM sources are better prepared to produce a tissue with optimal functionality than those built from merely artificial compounds.

Extracellular matrix-based tissue engineering strategies are already successfully being used clinically for the regeneration of a range of different tissues, including heart valves[16], trachea[17], muscle[18], tendon[19] and abdominal walls[20], with bladder and small intestinal submucosa[21] derived matrices as most widely used implants. The main advantage of ECM as a scaffolding material is that it allows for so-called 'constructive remodeling'[22], *i.e.* it supports and encourages specific tissue formation at the implantation site rather than forming inferior and less functional scar tissue. However, the functional outcome of ECM-derived scaffolds depends on several aspects, including the retention of growth factors within the ECM, its surface topology, modulation of the immune response (Box 1), and the micro-environmental cues that are exerted upon the cells, such as biomechanical loading (Box 2)[23].

The exact underlying working mechanisms are still not fully understood, but several potential explanations are possible for the positive outcomes obtained with ECM-derived scaffolds. First, the above explained process of "dynamic reciprocity"[24], which is vital to proper functioning of the tissues, is more likely to be effective in a natural tissue that con-

Box 1: The immune response to decellularized matrix

Several decellularized products for different regenerative purposes are available for clinical use. However, the amount of cellular material that remains after decellularization is quite variable[38]. There are no clear-cut guidelines for the degree of decellularization that needs to be achieved, as cell remnants in devitalized tissue do not always hinder tissue regeneration[43, 69].

The immune response that may occur in response to the implantation of foreign cellular material is partially macrophage-mediated[38]. A macrophage response to implantation of a scaffold is a necessary event, as macrophages are involved in scaffold degradation. However, macrophages release several soluble factors upon activation that can be both beneficial and detrimental to neo-tissue formation depending on macrophage phenotype. The activation of M1 macrophages leads to adverse remodeling through the release of catabolic cytokines, whereas the activation of M2 macrophages leads to constructive remodeling through anabolic cytokines[38]. For example, M1 macrophages release IL-1b and IL-6, which are upregulated in patients with damaged knee cartilage. The balance between M1 and M2 macrophages after implantation tends to shift to M2 macrophages if decellularization is more successful[38].

The avascular nature of cartilage is one of the major challenges in initiating intrinsic repair but may also be advantageous, as the tissue is to a large extent immunopriviliged, which opens up many more options in choosing the ECM source, including allogeneic and xenogeneic sources, without rejection issues[70]. Additionally, the dense nature of cartilage ECM may further contribute to the weakly immunogenic, or even non-immunogenic, status, as it physically protects the chondrocytes from T and NK cells that are released in graft rejection processes[70]. The application of xenogeneic products for cartilage repair is still in its infancy but should be explored further, as it overcomes the limited availability of human tissue or cells. The question remains, however, which tissue components may lead to an inappropriate immune response, the cells or the ECM.

tains bioactive cues, like growth factors, polysaccharides or functional peptides, than in an artificial tissue that does not. In the same line, incorporating a certain cell type in a scaffold made from the target ECM will more easily drive the cell towards the appropriate terminal differentiation[25-27]. Second, naturally occurring ECM is the product of the resident cells and has a 3D structure that may guide cell behavior, attachment and migration[28], but incorporated growth factors or other functional proteins are often also associated with the alignment of the collagen fibers that mostly make up the 3D structure of a tissue, and which give a tissue its biomechanical strength and resilience[29]. The biomechanical environment of the cell, which is largely dictated by the biomaterial, can be of great influence on cell differentiation. For example, MSCs are known to commit to the osteogenic lineage in stiff biomaterials, but to the neuronal lineage in more flexible biomaterials[30].

The mechanism behind the successful use of ECM-based scaffolds seems to be to a certain extent generic and not exclusively tissue-specific, as ECM scaffolds originating from other tissues than the target tissue have been used with success. For example, small intestinal submucosa ECM (SIS-ECM) has been used as a scaffold for the repair of the musculotendinous junction between the gastrocnemicus muscle and the Achilles tendon in dogs[31, 32]. The scaffold was re-cellularised by progenitor cells from its surroundings and was ultimately completely replaced by functional contractile muscle and tendon including one of the most challenging types of tissue to regenerate: the neurovascular bed[31]. Extracellular matrix-

Box 2: Biomechanical properties of decellularized matrix

The biomechanical characteristics of articular cartilage in terms of resilience and stiffness are crucial to proper functioning of the tissue in a strictly mechanical sense, but also with respect to tissue homeostasis, as biomechanical cues steer chondrocyte behaviour to a large extent via mechanotransduction pathways[71]. In this context, biomechanical properties influence the growth factor reservoir within the ECM and matrix stiffness may for instance mediate TGFb driven processes through which this reservoir is continuously replenished and emptied[27].

The processes of harvesting, decellularization and sterilization of ECM scaffolds affect the hydration status and 3D configuration and hence strongly influence biomechanical behaviour. Washing steps using SDS or other processes that lead to removal of GAGs entail loss of water and produce a more loosely packed collagen network and hence loss of viscoelastic properties[22, 72]. Freeze-thaw cycles may result in the disruption of the collagen network through crystal formation.

The biomechanical behaviour of ECM scaffolds *in vivo* will depend on the way the scaffold was processed, on the properties and the geometry of the surrounding tissue, the pattern and magnitude of forces exerted on the scaffold, its degradation rate and the extent to which new ECM is formed[73]. The biomechanical properties of any ECM–based scaffold will almost invariably be inferior to those of the original tissue. The extent and rate to which neo-tissue is formed and takes on more physiologic biomechanical characteristics depends mainly on the capacity of the scaffolds (and/or the cells seeded therein, if any) to properly respond in an anabolic way to the cues elicited by joint loading and motion.

based scaffolds can even be of xenogeneic origin[31, 33, 34], after successful decellularization to remove cellular antigens.

Decellularization of tissues can be accomplished using various methods or combinations thereof (Table 1). Physical treatments, such as thermal shock, freeze-thaw cycles and mechanical crushing of the tissue will lead to cell lysis and tissue break-down, allowing for easier infiltration of the chemical and enzymatic treatments that often follow[24]. Treatments with detergents or other chemicals, including SDS and Triton X-100, are used to break down cellular and nuclear membranes[35], which can then be removed in subsequent washing steps. Enzymatic treatments depend on the tissue type, but often trypsin, and nuclease solutions are used to break down peptides, DNA, and RNA[35].

Decellularization should ideally remove all cells and cellular antigens while retaining the bioactive cues that reside in the ECM. The decellularization of bladder submucosa matrix using several washing steps with enzymatic agents and detergents led to full decellularization but also ensured that important growth factors, like VEGF, TGFb1, bFGF, and EGF, typically remain present within the decellularized tissue[36]. In the case of cartilage, preservation of proteoglycans, one of the main ECM components, may be important. Especially as proteoglycans do not only contribute to the mechanical characteristics of the tissue through the attraction of water by variations in fixed charge density[37], but are also thought to be a reservoir of several growth factors at times when these are not readily produced and released by the resident cells[36].

Single tissues, but also whole organs can be decellularized, providing a biological scaffold of resident ECM with the complex geometry of an organ and an intact vascular network

Table 1: Possible decellularization techniques for (osteo-)chondral repair

CARTILAGE TISSUE		
Decellularization method	*Tissue type*	*Described by*
1. Rinsing in PBS 2. Lyophilization 3. Tissue grinding 4. Trypsin treatment 5. Rinsing in PBS 6. Nuclease treatment 7. Hypotonic Tris-HCl treatment 8. Incubation in Triton X-100 9. Rinsing in PBS 10. Lyophilization 11. Crosslinking with UV 12. Sterilization by ethylene oxide	Bovine cartilage	Yang, 2010[46]
1. Rinsing in PBS 2. Shattering of the tissue in PBS 3. Differential centrifuging 4. Incubation in Triton X-100 5. Hypotonic Tris-HCl treatment 6. Nuclease treatment 7. Rinsing in PBS 8. Tris-HCl treatment 9. Rinsing in PBS 10. Lyophilization 11. Dehydrothermal treatment 12. Crosslinking with carbodiimide 13. Rinsing in PBS 14. Sterilization by cobalt g-irradiation	Human cartilage	Yang, 2008[45]
1. Rinsing in distilled water 2. NaOH treatment 3. Rinsing in PBS 4. Defattening in ethanol 5. GndHCl and NaOAc treatment 6. Rinsing in PBS 7. H_2O_2 treatment 8. Rinsing in PBS	Human nasal cartilage Porcine nasal cartilage Porcine meniscus	Schwarz, 2012[47]
1. Rinsing in PBS 2. Freeze and thaw cycles 3. Hypotonic Tris-HCl treatment 4. SDS-EDTA treatment 5. Rinsing in PBS 6. Nuclease treatment 7. Rinsing in PBS 8. Peracetic acid treatment 9. Rinsing in PBS	Porcine cartilage	Kheir, 2011[71]
1. SDS treatment 2. Rinsing in water 3. Lyophilization	Cartilage ECM sheets of 10μm	Gong, 2010[50]

Table 1: Possible decellularization techniques for (osteo-)chondral repair (continued)

BONE TISSUE		
Decellularization method	*Tissue type*	*Described by*
1. Rinsing in demiwater 2. NaN_3 treatment 3. Chloroform and methanol treatment 4. Incubation in Triton X-100 5. SDS treatment 6. Rinse in PBS	Human cancellous bone	Yang, 2011[55]
1. Defattening in acetone 2. Rinsing in saline 3. Trypsin treatment 4. Rinsing in saline 5. Rinsing in acetone 6. Crosslinking with hexamethyldiisocyanate 7. Rinsing in acetone 8. Rinsing in saline 9. Sterilization by g-irradiation	Porcine trabecular bone	Gerhardt, 2012[54]
CULTURED CELL MATRICES		
Decellularization method	*Tissue type*	*Described by*
1. Incubation in Triton X-100 with NH_4OH	Human MSC matrix	Pei, 2011[26]
1. Rinsing in PBS 2. Rinsing in double distilled water 3. Freeze and thaw cycles 4. NH_4OH treatment 5. Rinsing in double distilled water 6. Na_3PO_4 treatment 7. Rinsing in double distilled water	Human MSC matrix, normal human articular chondrocyte matrix, and normal human dermal fibroblast matrix cultured on PLGA meshes	Lu, 2011[49]
1. SDS with nuclease and EDTA treatment 2. Rinsing in PBS 3. Culturing for 4 weeks 4. SDS with nuclease and EDTA treatment 5. PBS rinsing	Immature bovine chondrocyte matrix cultured in agarose wells	Elder, 2009[44]
1. Freeze and thaw cycles 2. Rinsing in PBS 3. Rinsing in double distilled water 4. Perfusion based washing in bioreactor	Human MSC bone matrix cultured on polyesterurethane	Sadr, 2011[56]
1. Freeze and thaw cycles 2. Rinsing in distilled water 3. Lyophilization	Human MSC bone matrix cultured on tissue plastic	Kang, 2011[57]

that will enhance nutrient supply, benefitting regeneration and recellularization[24]. In case of organ decellularization it is imperative that the process does not disrupt the natural integrity of the tissue; in case of tissue decellularization the process can be more rigorous.

Certain criteria have been proposed for successful decellularization, or perhaps better denuclearization: 1) absence of nuclei on histological evaluation (hematoxylin/eosin or DAPI), 2) DNA quantification <50ng/mg dry tissue and 3) DNA fragments <200bp[24].

However, these criteria were based on the decellularization of loosely organized tissues (SIS and urinary bladder matrix (UBM)) and may not apply to more dense tissues like cartilage. Rigorous decellularization enhances loss of structural integrity of the ECM and of certain ECM compounds. However, whether absolute decellularization is necessary is still under discussion as ineffectively decellularized ECM still induced similar host remodeling as effectively decellularized material[38].

In addition to decellularization, artificial cross-linking of ECM scaffolds is often applied to enhance the biomechanical strength of the scaffold in the initial stages after implantation. However, this practice unequivocally affects ECM properties. Artificial, and more specifically, chemical crosslinking will ultimately decrease the degradation rates and thereby the controlled release of bioactive factors[39]; chemical crosslinking may also physically hamper tissue remodeling as it elicits an adverse recipient immune response[40].

The successful application and encouraging results from *in vitro* and *in vivo* work using ECM scaffolds in several different fields hold great promise for this approach in attempts to regenerate (osteo-)chondral tissue.

APPLICATION OF ECM BASED SCAFFOLDS FOR THE TREATMENT OF OSTEOCHONDRAL DEFECTS

Mosaicplasty and allogeneic osteochondral grafting can theoretically be considered ECM-based strategies, as they imply the direct implantation of cartilage and bone matrix (Figure 1). However, the use of seeded or unseeded ECM-based scaffolds is a new and emerging approach within the field of cartilage tissue engineering, supported by a slowly increasing body of evidence of success.

One of the major advantages of using the ECM as a scaffolding material is its potential to retain the growth factors that the tissue is naturally inclined to respond to. For cartilage, some of the most important growth factors are transforming growth factor beta (TGF-beta), fibroblast growth factors (FGF), and insulin-like growth factor (IGF)[8]. The retention of bioactive molecules will be especially beneficial in regenerating cartilage, as this tissue naturally lacks appropriate growth factor and nutrient supply due to its avascular nature.

Bioactive ECM for (osteo-)chondral repair can be applied in many different ways that fall in three general categories (Figure 1). First, non-decellularized cartilage particles[41] have been combined with a degradable biomaterial, showing initial clinical results at least matching the outcomes of microfracture. Even ECM particles from osteoarthritic patients can be used for this purpose[42]. When combining OA cartilage particles that had undergone freeze-thaw cycles (devitalization) with MSCs in fibrin glue and implanting these in subcutaneous pockets in mice the procedure led to better shape fidelity; further glycosaminoglycan (GAG) content and chondrogenic gene expression were also enhanced compared

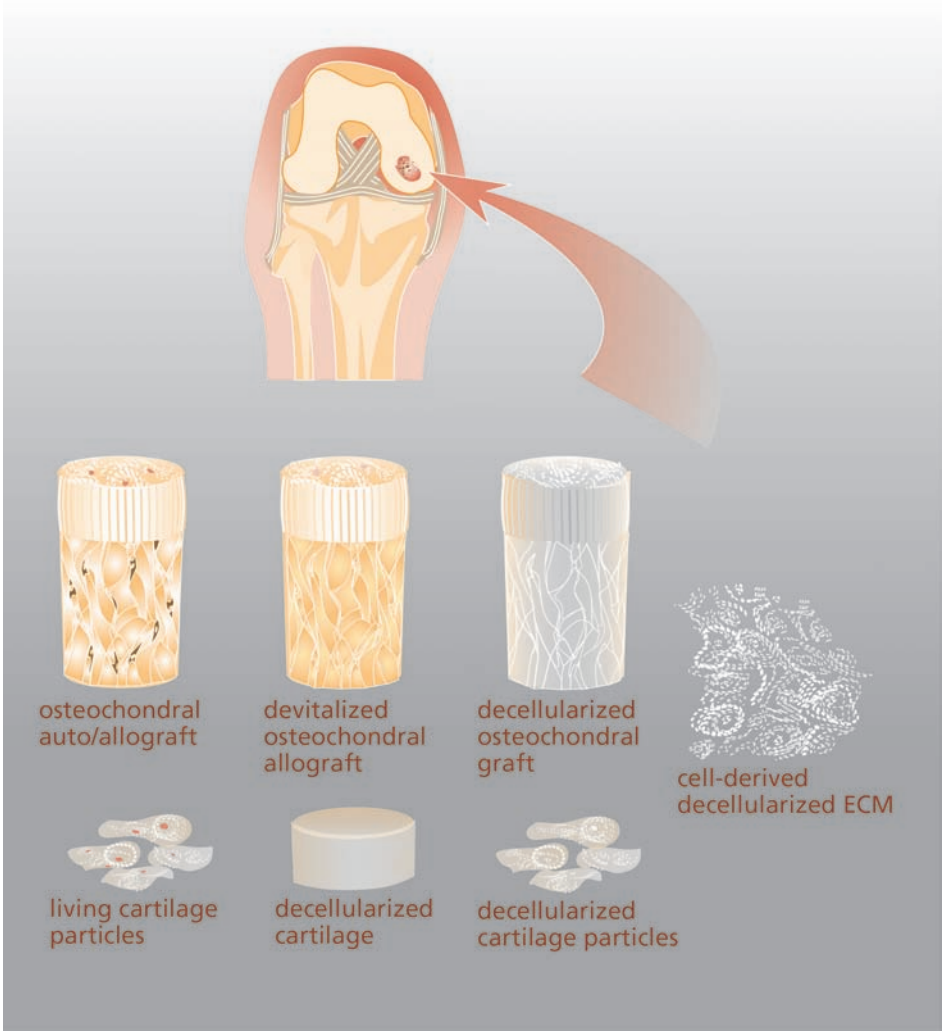

Figure 1: Various possibilities of matrix-based approaches to (osteo-)chondral repair.

to non-supplemented glue[42]. Cartilage tissue can also be processed into cartilage microparticles[43] that may be used as an additive to enhance current cell-centered techniques (ACI or MACI) by mixing it with the cell suspension or biomaterial that fills the defect. The addition of microparticles to pellet cultures leads to an upregulation of chondrogenic gene profiles, and moderately decreases hypertrophic gene expression[43].

Second, cartilage matrix can be harvested from allogeneic or even xenogeneic sources and then used in a scaffold form. The pre-clinical results underscore the benefits of devitalized or decellularized tissue over implantation of living cartilage, as formation of neocartilage of the latter tends to lag behind[44]. Decellularized cartilage matrix can be obtained from

different sources and through different decellularization processes. Due to the dense nature of cartilage ECM in which the cells are embedded, more vigorous protocols are required to decellularize cartilage than in many other tissues. This inevitably leads to more destruction of the ECM components; especially GAGs will be affected[45]. Moreover, cartilage thickness decreases and the tissue loses some of its biomechanical resilience[45]. The effect of GAG loss on the final concentrations of bioactive cues, such as growth factors still needs to be evaluated for different decellularization protocols. Decellularized cartilage ECM can also be rebuild into a scaffold through lyophilization[46-48]. In rabbits, this type of scaffold resulted in the regeneration of hyaline cartilage, when combined with rabbit MSCs[47].

Lastly, the ECM to produce a scaffold for cartilage repair can be harvested from cultured cells to create so-called cell-derived ECM scaffolds[27, 28, 49, 50]. Cell-derived ECM overcomes the issues of possible exogenous pathogen transfer and allows for the use of ECM produced by the patient's own cells. Moreover, different cell types can be mixed to create the appropriate ECM for more complex tissues, and using thin ECM sheets allows for much easier decellularization and recellularization[49]. Extracellular matrix sheets seeded with MSCs or chondrocytes show superior chondrogenesis compared to pellet cultures[49, 51]. The main challenge in using cell-derived ECM is finding a way to upscale the process in such a way that it can be clinically applied for human regenerative therapies. One way to accomplish this is to stack several different decellularized cartilage sheets to create a layered construct[51, 52].

The process of decellularization paves the way for the use of xenogeneic material, the major advantages of which are cost-effectiveness and the relatively limitless availability of ECM. With a xenogeneic matrix, the age of the source animal should be taken into account. Young individuals heal better than adults, and the tissues may be morphologically different. ECM derived from submucosa of the small intestine, for example, is thinner in older animals and has lost its elastic properties, as well as some of the proteoglycans and growth factors[23]. Therefore, the use of tissue from younger donors may be advantageous[23]. For a tissue such as cartilage, that is metabolically stable in mature individuals, it is the question up to which age this is true. Products of the process of non-enzymatic glycation such as pentosidine cross-links are known to start to accumulate linearly in cartilage from approximately the age of 15 onwards[53]. This might be an indication of the cut-off age after which ECM from young individuals can be supposed to have acquired a mature metabolic rate. Xenogeneic use of cartilage has already been successful when implanting human cartilage-derived scaffolds seeded with canine MSCs in nude mice[46]. Cells showed good viability and the neocartilage contained both GAGs and collagen type II[46].

An important feature of the ultimate ECM scaffold is its biomechanical behavior. This is an especially challenging topic when considering the mechanical forces that are exerted daily upon the cartilage and the underlying bone in a human joint. Combining ECM with a stronger synthetic or ceramic material could potentially enhance the biomechanical

properties of an ECM scaffold, an approach that may be especially attractive for the repair of osteochondral defects. Alternatively, Jia *et al.*[54] have tried to use a novel lyophilization method to control the orientation of collagen fibers within a fabricated scaffold. This approach ultimately led to a Young's modulus that was almost three times higher than in non-oriented scaffolds[54]. Moreover, the chondrocytes that were seeded upon these scaffolds tended to align along these fibers, proliferated more rapidly and produced similar amounts of GAG- and collagen-rich neotissue compared to scaffolds without collagen fiber alignment[54].

The repair of cartilage defects penetrating into the subchondral bone (osteochondral defects) poses additional challenges. First, bone regeneration should not extend beyond the osseous phase of the defect, so there may be a need for different biomaterials for the cartilaginous and the osseous phases. Second, the integration between cartilage and bone is challenging and depends on simultaneous maturation of both tissues, which is influenced by the biomaterials chosen for both tissue types. Similar to decellularized cartilage, decellularized bone has also been shown to promote tissue growth upon subcutaneous implantation, even outperforming the bioactivity of established biomaterials such as bioactive glasses[55]. Attempts have been made to combine decellularized cartilage and decellularized bone to create biphasic constructs for osteochondral defect repair[56]. Pre-culturing a biphasic construct with MSCs for 4 days before implantation into an osteochondral defect in canine knees led to full regeneration after 6 months with near-hyaline cartilage repair[56]. Also in the case of bone regeneration, decellularized tissue-engineered ECM can be used to enhance the biological interaction of synthetic or ceramic biomaterials with cells[57-59], and may even aid in the controlled release of incorporated and normally rapidly released growth factors like BMP-2[58].

Current work from our group focuses on the use of decellularized equine cartilage matrix for osteochondral repair. To this extent we performed an equine pilot study in which a critical size osteochondral defect (11mm Æ x 10mm) was created in the stifle (knee) joint

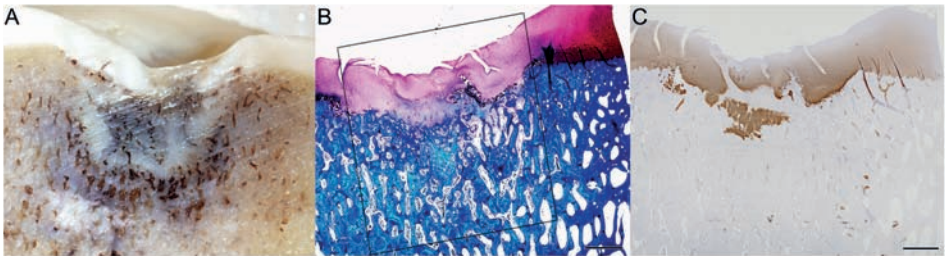

Figure 2: Osteochondral repair in a horse using decellularized cartilage:
Macroscopic overview of osteochondral repair tissue after 8 weeks of implantation (A). Both GAG-rich (B, Safranin-O, Fast Green) and collagen type II (C) rich neo-tissue was found after 8 weeks with a clear distinction between the cartilage and bone phase. Scale bars represent 2mm; the box approximates the created osteochondral defect.

of a horse. This defect was treated using a decellularized cartilage matrix scaffold and after 8 weeks clear regeneration of both the bone and cartilage phase was present (Figure 2). The two tissues could clearly be distinguished and the integration between the two was satisfactory[60]. This might imply that a biphasic construct may not be a biological necessity for osteochondral regeneration, but may only serve as a biomechanical stabiliser during the initial phases of tissue repair in a challenging environment such as the joint. An item that needs attention is assessment of the possible long-term ossification of the neo-cartilage tissue *in vivo* in long-term studies.

FUTURE PERSPECTIVES OF ECM-BASED SCAFFOLDS FOR OSTEOCHONDRAL REPAIR

The use of decellularized extracellular matrix is gaining ground within the field of cartilage tissue engineering and may prove to be of great potential as it allows for multifactorial mimicry that has not yet been achieved by human-made biomaterials. The approach is still relatively underexplored and extensive research is required to understand the biologic response to ECM scaffolds within the joint environment and to optimize the decellularization techniques and ultimately the final repair tissue. There are several items that need to be addressed.

A first topic is that cartilage naturally consists of different zonal layers that exert different functions due to differences in matrix composition and chondrocyte phenotype[29, 61, 62]. The approach of using ECM sheets may offer the possibility to represent this natural microenvironment by stacking ECM sheets produced by the different zonal cell types. Recreation of the zonal structure can be further stimulated through the use of bioprinted 3D porous constructs to deposit zone-specific matrices[63], combining hydrogels and strong synthetic polymers, which permits tailoring of the mechanical properties[64]. The synthetic materials or hydrogels that are ideal for bioprinting are often suboptimal in stimulating cell differentiation[65] and could be functionalized using ECM particles to optimize the cell response to the biomaterial.

A second point is that current decellularization approaches have focused on decellularizing cartilage tissue[47, 56] or ECM produced by either stem cells or chondrocytes[49, 51, 52]. However, the need to use cartilage-specific matrix may be questioned and more readily available tissues, *e.g.* small intestine submucosa or bladder matrices may have similar effects. For example, SIS-ECM has been used successfully to regenerate other tissue types, such as cardiac and vaginal tissues[66, 67]. The use of non-cartilage-specific matrix would have many advantages, as the scaffolds can be produced through standardized protocols that have already been established, the tissue is more easily accessible and available in larger

volumes; and the use of for example SIS-ECM has already been evaluated both *in vitro* and *in vivo* and is currently applied clinically.

A last point is that the repair of osteochondral defects remains a huge orthopedic challenge due to the complex combination of cartilage and bone, which frequently leads to an overgrowth of bone. Osteoinductive materials such as tricalcium phosphate (TCP) or biphasic calcium phosphate (BCP) are already available and successful in the regeneration of critical size bone defects[68]. Therefore, it seems not more than logical to create a biphasic construct of such an already successful ceramic and combine it with bioactive decellularized cartilage, which on its own seems to also drive tissue regeneration *in vivo*. The use of extracellular matrix scaffolds may even allow for a non-cell laden approach to osteochondral repair as they can attract cells from the implant site that will then differentiate into the appropriate cell type and elicit endogenous repair. Eventually, this may lead to natural off-the-shelf products that can be applied for a wide range of cartilage or osteochondral defects.

CONCLUDING REMARKS

Extracellular matrix scaffolds have shown great promise within the field of tissue engineering and are now being developed specifically for cartilage repair. Decellularized ECM-based scaffolds may solve many problems associated with the currently used matrix-based approaches to the repair of cartilage or osteochondral defects, like osteochondral allografting or mosaicplasty. This approach may lead to the development of the "ideal" cartilage or osteochondral scaffold, providing the injured site with the right bioactive cues that stimulate the regeneration of functional tissue that resembles the healthy situation.

REFERENCES:

1. Orthoworld. The Orthopaedic Industry Annual Report. In: 2009-2010.
2. Brittberg M. Autologous chondrocyte implantation--technique and long-term follow-up. Injury 2008; 39 Suppl 1: S40-49.
3. Zheng MH, Willers C, Kirilak L, Yates P, Xu J, Wood D, et al. Matrix-induced autologous chondrocyte implantation (MACI): biological and histological assessment. Tissue Eng 2007; 13: 737-746.
4. Hangody L, Kish G, Karpati Z, Udvarhelyi I, Szigeti I, Bely M. Mosaicplasty for the treatment of articular cartilage defects: application in clinical practice. Orthopedics 1998; 21: 751-756.
5. Bugbee W, Cavallo M, Giannini S. Osteochondral allograft transplantation in the knee. J Knee Surg 2012; 25: 109-116.
6. Bugbee WD, Convery FR. Osteochondral allograft transplantation. Clin Sports Med 1999; 18: 67-75.
7. Steadman JR, Rodkey WG, Briggs KK. Microfracture to treat full-thickness chondral defects: surgical technique, rehabilitation, and outcomes. J Knee Surg 2002; 15: 170-176.
8. Vinatier C, Mrugala D, Jorgensen C, Guicheux J, Noel D. Cartilage engineering: a crucial combination of cells, biomaterials and biofactors. Trends Biotechnol 2009; 27: 307-314.
9. Tohyama H, Yasuda K, Minami A, Majima T, Iwasaki N, Muneta T, et al. Atelocollagen-associated autologous chondrocyte implantation for the repair of chondral defects of the knee: a prospective multicenter clinical trial in Japan. J Orthop Sci 2009; 14: 579-588.
10. Shin H, Olsen BD, Khademhosseini A. The mechanical properties and cytotoxicity of cell-laden double-network hydrogels based on photocrosslinkable gelatin and gellan gum biomacromolecules. Biomaterials 2012; 33: 3143-3152.
11. Ahmed TA, Giulivi A, Griffith M, Hincke M. Fibrin glues in combination with mesenchymal stem cells to develop a tissue-engineered cartilage substitute. Tissue Eng Part A 2011; 17: 323-335.
12. Jeong CG, Zhang H, Hollister SJ. Three-dimensional polycaprolactone scaffold-conjugated bone morphogenetic protein-2 promotes cartilage regeneration from primary chondrocytes in vitro and in vivo without accelerated endochondral ossification. J Biomed Mater Res A 2012; 100: 2088-2096.
13. Oshima Y, Harwood FL, Coutts RD, Kubo T, Amiel D. Variation of mesenchymal cells in polylactic acid scaffold in an osteochondral repair model. Tissue Eng Part C Methods 2009; 15: 595-604.
14. Badylak SF, Weiss DJ, Caplan A, Macchiarini P. Engineered whole organs and complex tissues. Lancet 2012; 379: 943-952.
15. Nelson CM, Bissell MJ. Of extracellular matrix, scaffolds, and signaling: tissue architecture regulates development, homeostasis, and cancer. Annu Rev Cell Dev Biol 2006; 22: 287-309.
16. D'Onofrio A, Cresce GD, Bolgan I, Magagna P, Piccin C, Auriemma S, et al. Clinical and hemodynamic outcomes after aortic valve replacement with stented and stentless pericardial xenografts: a propensity-matched analysis. J Heart Valve Dis 2011; 20: 319-325; discussion 326.
17. Macchiarini P, Jungebluth P, Go T, Asnaghi MA, Rees LE, Cogan TA, et al. Clinical transplantation of a tissue-engineered airway. Lancet 2008; 372: 2023-2030.
18. Ricchetti ET, Aurora A, Iannotti JP, Derwin KA. Scaffold devices for rotator cuff repair. J Shoulder Elbow Surg 2012; 21: 251-265.
19. Martinello T, Bronzini, I., Volpin, A., Vindigni, V., Maccatrozzo, L., Caporale, G., Bassetto, F., Patruno, M. Successful recellularization of human tendon scaffolds using adipose-derived mesenchymal stem cells and collagen gel. J Tissue Eng Regen Med 2012.
20. Meyer T, Schwarz K, Ulrichs K, Hocht B. A new biocompatible material (Lyoplant) for the therapy of congenital abdominal wall defects: first experimental results in rats. Pediatr Surg Int 2006; 22: 369-374.

21. Armitage S, Seman EI, Keirse MJ. Use of surgisis for treatment of anterior and posterior vaginal prolapse. Obstet Gynecol Int 2012; 2012: 376251.
22. Badylak SF. The extracellular matrix as a biologic scaffold material. Biomaterials 2007; 28: 3587-3593.
23. Tottey S, Johnson SA, Crapo PM, Reing JE, Zhang L, Jiang H, et al. The effect of source animal age upon extracellular matrix scaffold properties. Biomaterials 2012; 32: 128-136.
24. Gilbert TW. Strategies for tissue and organ decellularization. J Cell Biochem 2012; 113: 2217-2222.
25. Gong J, Sagiv O, Cai H, Tsang SH, Del Priore LV. Effects of extracellular matrix and neighboring cells on induction of human embryonic stem cells into retinal or retinal pigment epithelial progenitors. Exp Eye Res 2008; 86: 957-965.
26. Sellaro TL, Ravindra AK, Stolz DB, Badylak SF. Maintenance of hepatic sinusoidal endothelial cell phenotype in vitro using organ-specific extracellular matrix scaffolds. Tissue Eng 2007; 13: 2301-2310.
27. Pei M, Li JT, Shoukry M, Zhang Y. A review of decellularized stem cell matrix: a novel cell expansion system for cartilage tissue engineering. Eur Cell Mater 2011; 22: 333-343; discussion 343.
28. Vorotnikova E, McIntosh D, Dewilde A, Zhang J, Reing JE, Zhang L, et al. Extracellular matrix-derived products modulate endothelial and progenitor cell migration and proliferation in vitro and stimulate regenerative healing in vivo. Matrix Biol 2010; 29: 690-700.
29. Martel-Pelletier J, Boileau C, Pelletier JP, Roughley PJ. Cartilage in normal and osteoarthritis conditions. Best Pract Res Clin Rheumatol 2008; 22: 351-384.
30. Engler AJ, Sen S, Sweeney HL, Discher DE. Matrix elasticity directs stem cell lineage specification. Cell 2006; 126: 677-689.
31. Turner NJ, Yates AJ, Jr., Weber DJ, Qureshi IR, Stolz DB, Gilbert TW, et al. Xenogeneic extracellular matrix as an inductive scaffold for regeneration of a functioning musculotendinous junction. Tissue Eng Part A 2010; 16: 3309-3317.
32. Turner NJ, Badylak JS, Weber DJ, Badylak SF. Biologic Scaffold Remodeling in a Dog Model of Complex Musculoskeletal Injury. J Surg Res 2011.
33. Penolazzi L, Mazzitelli S, Vecchiatini R, Torreggiani E, Lambertini E, Johnson S, et al. Human mesenchymal stem cells seeded on extracellular matrix-scaffold: viability and osteogenic potential. J Cell Physiol 2012; 227: 857-866.
34. Badylak SF. Xenogeneic extracellular matrix as a scaffold for tissue reconstruction. Transpl Immunol 2004; 12: 367-377.
35. Crapo PM, Gilbert TW, Badylak SF. An overview of tissue and whole organ decellularization processes. Biomaterials 2011; 32: 3233-3243.
36. Chun SY, Lim GJ, Kwon TG, Kwak EK, Kim BW, Atala A, et al. Identification and characterization of bioactive factors in bladder submucosa matrix. Biomaterials 2007; 28: 4251-4256.
37. Han E, Chen SS, Klisch SM, Sah RL. Contribution of proteoglycan osmotic swelling pressure to the compressive properties of articular cartilage. Biophys J 2011; 101: 916-924.
38. Keane TJ, Londono R, Turner NJ, Badylak SF. Consequences of ineffective decellularization of biologic scaffolds on the host response. Biomaterials 2012; 33: 1771-1781.
39. Voytik-Harbin SL, Brightman AO, Kraine MR, Waisner B, Badylak SF. Identification of extractable growth factors from small intestinal submucosa. J Cell Biochem 1997; 67: 478-491.
40. Badylak SF, Valentin JE, Ravindra AK, McCabe GP, Stewart-Akers AM. Macrophage phenotype as a determinant of biologic scaffold remodeling. Tissue Eng Part A 2008; 14: 1835-1842.
41. Cole BJ, Farr J, Winalski CS, Hosea T, Richmond J, Mandelbaum B, et al. Outcomes after a single-stage procedure for cell-based cartilage repair: a prospective clinical safety trial with 2-year follow-up. Am J Sports Med 2011; 39: 1170-1179.

42. Chen CC, Liao CH, Wang YH, Hsu YM, Huang SH, Chang CH, et al. Cartilage fragments from osteoarthritic knee promote chondrogenesis of mesenchymal stem cells without exogenous growth factor induction. J Orthop Res 2012; 30: 393-400.
43. Ghanavi P, Kabiri M, Doran MR. The rationale for using microscopic units of a donor matrix in cartilage defect repair. Cell Tissue Res 2012; 347: 643-648.
44. Peretti GM, Campo-Ruiz V, Gonzalez S, Randolph MA, Wei Xu J, Morse KR, et al. Tissue engineered cartilage integration to live and devitalized cartilage: a study by reflectance mode confocal microscopy and standard histology. Connect Tissue Res 2006; 47: 190-199.
45. Elder BD, Eleswarapu SV, Athanasiou KA. Extraction techniques for the decellularization of tissue engineered articular cartilage constructs. Biomaterials 2009; 30: 3749-3756.
46. Yang Q, Peng J, Guo Q, Huang J, Zhang L, Yao J, et al. A cartilage ECM-derived 3-D porous acellular matrix scaffold for in vivo cartilage tissue engineering with PKH26-labeled chondrogenic bone marrow-derived mesenchymal stem cells. Biomaterials 2008; 29: 2378-2387.
47. Yang Z, Shi Y, Wei X, He J, Yang S, Dickson G, et al. Fabrication and repair of cartilage defects with a novel acellular cartilage matrix scaffold. Tissue Eng Part C Methods 2010; 16: 865-876.
48. Schwarz S, Koerber L, Elsaesser AF, Goldberg-Bockhorn E, Seitz AM, Durselen L, et al. Decellularized Cartilage as a Novel Biomatrix for Cartilage Tissue Engineering Applications. Tissue Eng Part A 2012.
49. Lu H, Hoshiba T, Kawazoe N, Koda I, Song M, Chen G. Cultured cell-derived extracellular matrix scaffolds for tissue engineering. Biomaterials 2011; 32: 9658-9666.
50. Lu H, Hoshiba T, Kawazoe N, Chen G. Autologous extracellular matrix scaffolds for tissue engineering. Biomaterials 2011; 32: 2489-2499.
51. Gong YY, Xue JX, Zhang WJ, Zhou GD, Liu W, Cao Y. A sandwich model for engineering cartilage with acellular cartilage sheets and chondrocytes. Biomaterials 2011; 32: 2265-2273.
52. Xue JX, Gong YY, Zhou GD, Liu W, Cao Y, Zhang WJ. Chondrogenic differentiation of bone marrow-derived mesenchymal stem cells induced by acellular cartilage sheets. Biomaterials 2012; 33: 5832-5840.
53. Bank RA, Bayliss MT, Lafeber FP, Maroudas A, Tekoppele JM. Ageing and zonal variation in post-translational modification of collagen in normal human articular cartilage. The age-related increase in non-enzymatic glycation affects biomechanical properties of cartilage. Biochem J 1998; 330 (Pt 1): 345-351.
54. Jia S, Liu L, Pan W, Meng G, Duan C, Zhang L, et al. Oriented cartilage extracellular matrix-derived scaffold for cartilage tissue engineering. J Biosci Bioeng 2012; 113: 647-653.
55. Gerhardt LC, Widdows KL, Erol MM, Nandakumar A, Roqan IS, Ansari T, et al. Neocellularization and neovascularization of nanosized bioactive glass-coated decellularized trabecular bone scaffolds. J Biomed Mater Res A 2012.
56. Yang Q, Peng J, Lu SB, Guo QY, Zhao B, Zhang L, et al. Evaluation of an extracellular matrix-derived acellular biphasic scaffold/cell construct in the repair of a large articular high-load-bearing osteochondral defect in a canine model. Chin Med J (Engl) 2011; 124: 3930-3938.
57. Sadr N, Pippenger BE, Scherberich A, Wendt D, Mantero S, Martin I, et al. Enhancing the biological performance of synthetic polymeric materials by decoration with engineered, decellularized extracellular matrix. Biomaterials 2012; 33: 5085-5093.
58. Kang Y, Kim S, Khademhosseini A, Yang Y. Creation of bony microenvironment with CaP and cell-derived ECM to enhance human bone-marrow MSC behavior and delivery of BMP-2. Biomaterials 2011; 32: 6119-6130.

59. Thibault RA, Scott Baggett L, Mikos AG, Kasper FK. Osteogenic differentiation of mesenchymal stem cells on pregenerated extracellular matrix scaffolds in the absence of osteogenic cell culture supplements. Tissue Eng Part A 2010; 16: 431-440.
60. Benders KEM, Boot W, Cokelaere SM, van Weeren PR, Gawlitta D, Bergman HJ, et al. Multipotent stromal cells outperform chondrocytes on cartilage-derived matrix scaffolds. Under review Biomaterials (2012).
61. Klein TJ, Malda J, Sah RL, Hutmacher DW. Tissue engineering of articular cartilage with biomimetic zones. Tissue Eng Part B Rev 2009; 15: 143-157.
62. Malda J, Benders KE, Klein TJ, de Grauw JC, Kik MJ, Hutmacher DW, et al. Comparative study of depth-dependent characteristics of equine and human osteochondral tissue from the medial and lateral femoral condyles. Osteoarthritis Cartilage 2012; 20: 1147-1151.
63. Klein TJ, Rizzi SC, Reichert JC, Georgi N, Malda J, Schuurman W, et al. Strategies for zonal cartilage repair using hydrogels. Macromol Biosci 2009; 9: 1049-1058.
64. Schuurman W, Khristov V, Pot MW, van Weeren PR, Dhert WJ, Malda J. Bioprinting of hybrid tissue constructs with tailorable mechanical properties. Biofabrication 2011; 3: 021001.
65. Khalil S, Sun W. Bioprinting endothelial cells with alginate for 3D tissue constructs. J Biomech Eng 2009; 131: 111002.
66. Padalino MA, Castellani C, Dedja A, Fedrigo M, Vida VL, Thiene G, et al. Extracellular matrix graft for vascular reconstructive surgery: evidence of autologous regeneration of the neoaorta in a murine model. Eur J Cardiothorac Surg 2012.
67. Geoffrion R, Murphy M, Robert M, Birch C, Ross S, Tang S, et al. Vaginal paravaginal repair with porcine small intestine submucosa: midterm outcomes. Female Pelvic Med Reconstr Surg 2011; 17: 174-179.
68. Yuan H, Fernandes H, Habibovic P, de Boer J, Barradas AM, de Ruiter A, et al. Osteoinductive ceramics as a synthetic alternative to autologous bone grafting. Proc Natl Acad Sci U S A 2010; 107: 13614-13619.
69. Jin CZ, Park SR, Choi BH, Park K, Min BH. In vivo cartilage tissue engineering using a cell-derived extracellular matrix scaffold. Artif Organs 2007; 31: 183-192.
70. Revell CM, Athanasiou KA. Success rates and immunologic responses of autogenic, allogenic, and xenogenic treatments to repair articular cartilage defects. Tissue Eng Part B Rev 2009; 15: 1-15.
71. Guilak F. Biomechanical factors in osteoarthritis. Best Pract Res Clin Rheumatol 2011; 25: 815-823.
72. Kheir E, Stapleton T, Shaw D, Jin Z, Fisher J, Ingham E. Development and characterization of an acellular porcine cartilage bone matrix for use in tissue engineering. J Biomed Mater Res A 2011; 99: 283-294.
73. Badylak SF, Freytes DO, Gilbert TW. Extracellular matrix as a biological scaffold material: Structure and function. Acta Biomater 2009; 5: 1-13.

Chapter 6

Fabrication of decellularized cartilage-derived matrix scaffolds

K.E.M. Benders
R. Levato
J. Malda

Submitted to Journal of Visualized Experiments

ABSTRACT

Osteochondral defects lack sufficient intrinsic repair capacity to regenerate functionally sound bone and cartilage tissue. To this extent cartilage research focuses on the development of regenerative scaffolds. This paper describes the development of scaffolds that are derived completely from natural cartilage extracellular matrix. Potential applications include: i) producing allografts for cartilage repair, ii) scaffolds for osteochondral tissue engineering, iii) *in vitro* models to study tissue formation. By decellularizing this tissue the donor cells are removed, but the natural bioactive cues are thought to be retained. The main advantage of using such a natural scaffold over a synthetically produced scaffold is that no further functionalization of polymers is required in order to drive osteochondral tissue regeneration. The cartilage-derived matrix scaffolds can be used for both bone and cartilage tissue regeneration in *in vivo* and *in vitro* settings.

INTRODUCTION

Traumatic events causing articular cartilage defects in the knee can lead to discomfort, and may have a large impact on the lives of the young and active population[1-3]. Moreover, cartilage damage at a young age may lead to a more rapid onset of osteoarthritis later in life[4]. Currently, the only salvage therapy for generalized osteoarthritis of the knee is joint replacement surgery. As cartilage is a hypocellular, aneural and avascular tissue its regenerative capacity is severely limited. Therefore, regenerative medicine approaches are sought after to aid and stimulate the regenerative capacity of the native tissue. To this purpose scaffolds are designed and used as either a cell-carrier or as an inductive material that incites differentiation and regeneration of tissue by the body's native cells[5].

Decellularized scaffolds have been widely researched within several subfields within regenerative medicine[6]. It has had some successes for example in aiding regeneration of skin[7], abdominal structures[8], and tendons[9]. The advantage of using decellularized scaffolds is their natural origin and their capacity to retain bioactive cues that both attract and induce cell differentiation into the appropriate lineage required for tissue repair[6, 10]. Moreover, as the extracellular matrix (ECM) is a natural biomaterial, and in the case of decellularization, potentially devoid of cellular or genetic content that could cause undesired immune responses, issues regarding biocompatibility and biodegradability are overcome.

Cartilage-derived matrix (CDM) scaffolds have shown great chondrogenic potential in *in vitro* experiments when seeded with mesenchymal stromal cells[11]. Also, these scaffolds have shown the potential to form bone tissue through endochondral ossification on ectopic locations in *in vivo* settings[12]. As CDM scaffolds guide the formation of both bone and cartilage tissue these scaffolds may hold potential for osteochondral defect repair next to cartilage repair only.

This paper describes a protocol adapted from Yang *et al.* (2010)[13] for the production of decellularized CDM scaffolds. These scaffolds are rich in collagen type II, devoid of cells and do not contain any glycosaminoglycans after decellularization. Both *in vitro* and *in vivo* experiments on (osteo-)chondral defect repair can be conducted using these scaffolds.

PROTOCOL

This protocol describes the fabrication of scaffolds from decellularized cartilage, which can be used for applications as *in vitro* tissue culture platforms or for *in vivo* implantation in regenerative medicine strategies. The enzymatic treatment steps must be performed in the described chronological order.

1. Harvesting of articular cartilage from donor (cadaveric) joints.

1.1) Ahead of the harvesting step, prepare the cartilage washing solution, consisting of sterile phosphate-buffered saline (PBS), supplemented with 100U/mL penicillin, 10 mg/mL streptomycin and 1% v/v Fungizone (Amphotericin B). Shake vigorously to ensure homogeneous mixing.

1.2) Perform an arthrotomy on the harvested knee joint, and inspect the cartilage for any macroscopic damage. Note that this step does not have to be performed in a sterile environment.

1.2.1) If the articular cartilage does not have a glossy and smooth appearance or if evident blistering, clefts or defects are present, the sample should be discarded. To prevent the cartilage from drying out, regularly drip some of the PBS and antibiotics solution on the cartilage.

1.3) Use a scalpel to remove the cartilage from the subchondral bone, at this time the size of the cartilage slices does not matter. Make sure to cut all the way down to the subchondral bone to also remove the deep zone of the cartilage (Figure 1).

1.4) After removing the cartilage slices from the joint soak them in previously prepared washing solution (Figure 2A).

1.5) Submerge the washed cartilage slices in liquid nitrogen for 5 minutes to snap-freeze them. Afterwards, take the cartilage slices from the liquid nitrogen and put them into 50 ml tubes.

1.6) Lyophilize the cartilage slices for 24 hours in a freeze-dryer (Figure 2B).

1.7) After lyophilization the cartilage slices can be stored in a dry place until further use.

2. Creating decellularized cartilage particles

2.1) The cartilage slices can be ground either manually or by any milling machine.

2.1.1) When grinding the cartilage slices by hand use a mortar and pestle and submerse the lyophilized cartilage slices in liquid nitrogen and grind for 45 minutes until the slices are pulverized (Figure 2C-D).

2.1.2) When grinding automatically, snap-freeze the cartilage slices in liquid nitrogen and mill the cartilage until the slices are pulverized.

2.2) The cartilage particles can be sieved in order to select a specific range of sizes, depending on the chosen application.

2.2.1) After selecting the fraction of particles having the desired size for the scaffold, such particles can be stored until further use in a dry place.

3. Enzymatic decellularization – trypsin 0.25%-EDTA

3.1) Prepare the digestion solution, consisting of trypsin-EDTA 0.25% with 5ml penicillin/streptomycin and 5ml fungizone in a 1L stock solution. This solution does not have to be sterile and must be stored at 4°C.

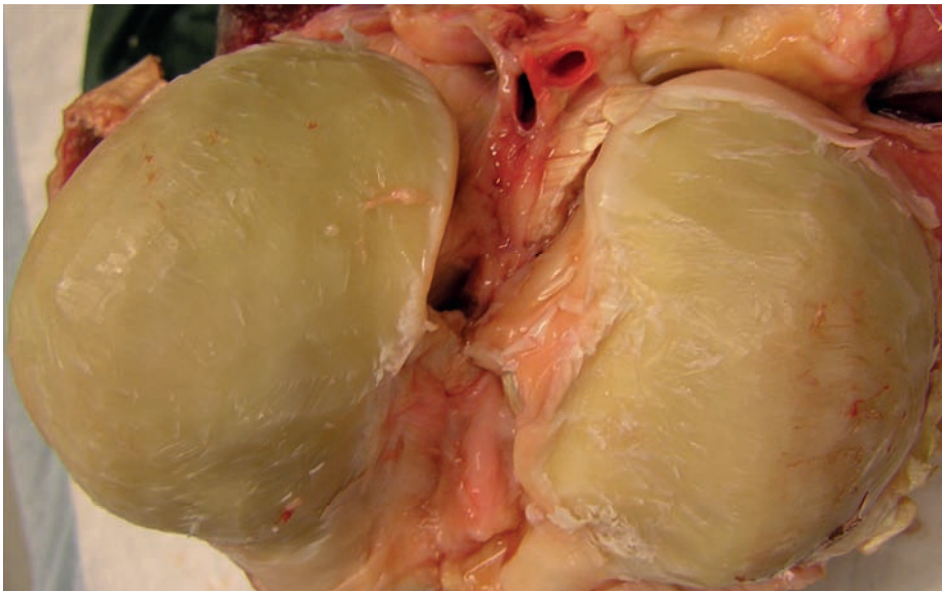

Figure 1: Equine knee after removing full-thickness cartilage. The cartilage is removed from the condyles using a scalpel and is removed until the calcified cartilage layer is reached that cannot be cut using a scalpel.

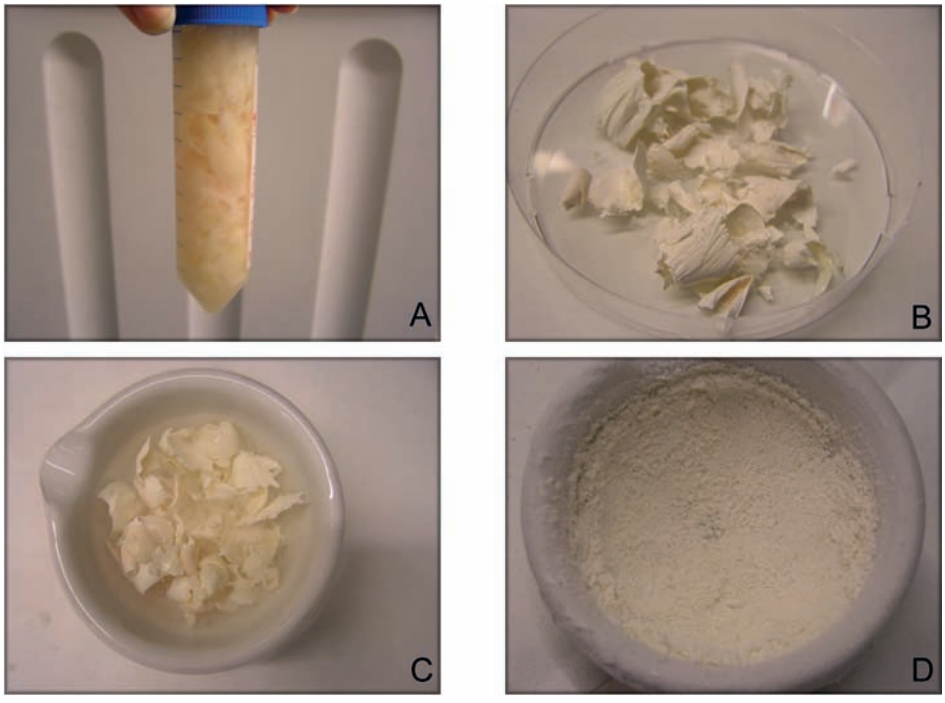

Figure 2: Sequential steps in creating decellularized cartilage-derived matrix particles. (A) Cartilage slices that have been removed from the condyles are washed in an antibiotic-infused solution. (B) Lyophilized cartilage slices, note their white and paper-like appearance. (C) Snap-freezing of the lyophilized cartilage. (D) Pulverized cartilage particles after hand-milling using a mortar and pestle, note that this step can also involve automatic milling. Adapted from Benders *et al.* Cartilage (2014).

3.2) Put the cartilage particles in a 50ml tube ensuring that 30ml of the trypsin-EDTA 0.25% solution can be added to fill up the tube.

3.3) Shake the solution to make sure that all of the cartilage particles that need to be re-hydrated are fully soaked by the enzymatic solution.

3.4) Leave this enzymatic solution with the cartilage particles in a 37°C incubator under vigorous agitation for 24 hours in total.

- 3.4.1) The total trypsin-EDTA 0.25% incubation should last 24 hours, however the trypsin solution must be refreshed every 4 hours.
- 3.4.2) To refresh the trypsin-EDTA 0.25% solution centrifuge the solution for 20 minutes at 4000rpm, to cause sedimentation of the particles.
- 3.4.3) Remove the supernatant. Note that the supernatant will become clearer with every trypsin incubation period.
- 3.4.4) Add a fresh 30ml of trypsin 0.25%/EDTA, make sure to stir the cartilage particles through the solution before leaving it under vigorous agitation at 37°C again for 4 hours.
- 3.4.5) In total refresh the trypsin 0.25% solution 6 times in 24 hours.

3.5) After the final trypsin 0.25% step make sure to remove the supernatant after centrifuging and wash the particles in a PBS and penicillin/streptomycin and fungizone solution twice. Centrifuge the particles for 20 minutes at 4000rpm between each of the washes.

4. Enzymatic decellularization – nuclease treatment

4.1) Prepare a 10mM Tris-HCl solution at pH 7.5 in demi-water.

4.2) Add 50U/ml deoxyribonuclease and 1U/ml ribonuclease A to the Tris-HCl buffer, to obtain the nuclease solution.

4.3) Add 30ml of the nuclease solution to the cartilage particles and stir the particles through the solution making sure that the particles are homogeneously suspended and that no large clumps are unexposed to the solution.

4.4.) Place the 50ml tubes with the nuclease solution and cartilage particles on a continuous roller plate for 4 hours in a 37°C incubator.

4.5) After 4 hours centrifuge the cartilage particles for 20 minutes at 4000rpm, take off the supernatant.

4.6) To wash the samples, add 30ml of 10mM Tris-HCl solution without the deoxyribonuclease and ribonuclease A to the cartilage particles. Stir well. Leave on a roller bench for 20 hours at room temperature.

5. Detergent decellularization – Triton solution

5.1) Centrifuge the cartilage suspended in Tris-HCl for 20 minutes at 4000 rpm, then remove the supernatant.

5.2) Make a 1% Triton-X-100 (v/v) solution in PBS. This solution does not have to be sterile.

5.3) Add 30ml of the 1% Triton-X-100 solution to the cartilage particles. Stir mildly to avoid foaming of the solution.

5.4) Leave the cartilage particles in the Triton solution on a rollerplate at room temperature for 24 hours.

5.5) Remove the Triton solution by centrifugation for 20 minutes at 4000 rpm. Keep the cartilage pellet and discard the supernatant.

5.6) To remove all of the remnants of the decellularization solutions, wash the cartilage particles in 6 cycles of 8 hours in PBS supplemented with penicillin/streptomycin and fungizone. This washing takes place on a roller plate at room temperature.

5.6.1) Make sure that after each PBS wash the cartilage-PBS mixture is centrifuged for 20 minutes at 4000rpm before discarding the supernatant.

5.7) After finishing the 6 PBS washes the remaining cartilage particles are decellularized and can be stored before use at -80°C.

6. Creating the scaffolds from the decellularized particles

6.1) If the particles have been stored frozen, these need to be thawed in warm water before creating the scaffolds.

6.2) Use a small ladle to put the cartilage particles into a cylindrical mold, for example, a plastic vial (TAAB) of 8mm diameter and 2cm height.

6.2.1) When placing the cartilage particles into the plastic mold make sure that all the air-bubbles are pressed out to ensure that there will not be any cavities in the scaffold.

6.2.2) The use of a metal mold will more easily lead to cracks in the scaffold as it is more diffcult to take the scaffolds out later on.

6.3) Freeze the molds with cartilage particles for 10 minutes at -20°C.

6.4) Lyophilize the cartilage scaffolds within their molds for 24 hours in a freeze dryer (Figure 3).

6.5) After lyophilization take the scaffold out of the mold and cross-link them using an UV-light at a 30cm distance overnight.

6.6) In order to use the scaffolds for *in vitro* cell culture or for *in vivo* implantation, they must be sterilized. To this extend, use ethylene oxide gas sterilization.

7. Characterizing decellularized scaffolds – histological stainings

7.1) To ensure complete decellularization and to visualize the remaining natural characters of the cartilage several stainings should be performed before using the scaffolds in any experiment.

7.2) Cut the scaffolds in thin slices of approximately 3mm.

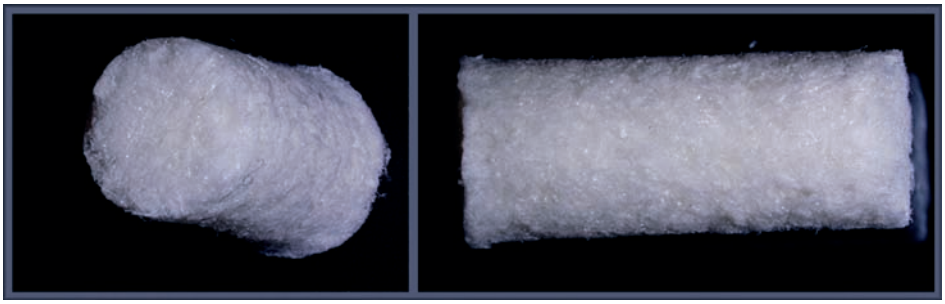

Figure 3: The final product, a decellularized cartilage-derived matrix scaffold. This scaffold is 2cm high and has a diameter of 8mm. The scaffold as a clear porous structure that can be observed from all sides of the scaffold. Note that no large holes are present at the surface of the scaffold as all of the air bubbles were removed prior to lyophilization. Adapted from Benders *et al.* Cartilage (2014).

7.3) Embed the scaffolds in a drop of 4% w/v alginate and cross-link using formalin containing 20mM $CaCl_2$.

7.3.1) Alginate is required to facilitate scaffold handling and ensure that the scaffold without any cells can go through the paraffin embedding process without getting lost during the washing steps.

7.3.2) If the scaffolds are tested by histological analysis after being seeded with cells and cultured, alginate embedding can be skipped as the composition of the scaffold will be resistant enough due to the neo-ECM incorporated into the scaffold.

7.3.3) In case of using alginate to process samples for paraffin embedding make sure to wash off the alginate using citric acid prior to rehydration of the paraffin sections.

7.4) Process the samples for paraffin embedding and sectioning with a microtome, process using a graded ethanol series and collect the obtained slices on microscopy slides.

7.5) Perform the following stainings to characterize the scaffold

- H&E to ensure decellularization
- Safranin-O to visualize residual glycosaminoglycan content
- Picrosirius red to visualize collagen alignment
- Collagen type I immunohistochemistry to differentiate between collagen content
- Collagen type II immunohistochemistry to differentiate between collagen content

8. Characterizing decellularized scaffolds – quantitative analyses

8.1) Obtain papain digests of the scaffolds.

8.2) Perform an assay to measure DNA content of the scaffolds (for example Picogreen) to ensure complete decellularization of the scaffold. Express the amount of DNA per weight of the scaffold.

8.3) Perform a dimethylmethylene blue assay to quantify the remainder of the glycosaminoglycans within the scaffold. Express the amount in GAG per DNA.

9. Seeding of decellularized scaffolds

9.1) Use fully sterilized scaffolds and cut these into 3mm thick slices.

9.2) To seed the scaffolds use chondrocytes that have not been expanded past the P1 passage to reduce the number of already dedifferentiated chondrocytes. Other cell types can be used. In case mesenchymal stromal cells are used, they must be checked for their multi-lineage differentiation ability.

9.3) Prior to seeding the scaffolds, pre-soaking is required due to their dehydrated state.

9.3.1) Put the scaffolds in separate wells of a 6-well plate.

9.3.2) Pipet 1ml of the medium in which the scaffolds will be cultured on the top side of the scaffold and let it soak for 30 min.

9.4) The total number of cells seeded on the scaffold will be 3×10^6 on scaffolds of 8mm diameter and 3mm in height. The cells have to be seeded in 100ml per scaffold. In order to ensure adequate cell attachment this has to be done in two steps.

9.4.1) Pipet 50ml of cell suspension on the top of the pre-soaked scaffold. Incubate the scaffold for 1 hour at 37°C.

9.4.2) Carefully flip over the scaffold and pipet the remaining 50ml of cell suspension on this side of the scaffold and incubate for 1 hour at 37°C.

9.4.3) After incubation add 3ml of medium to the wells, handle the culture plate gently, to avoid shaking of the culture media that might lead to detachment of the cells.

9.5) Culture the scaffolds for the period that is required in the experiment and change the medium 2-3 times a week. Perform medium refreshing always slowly and gently, pipetting as far away from the scaffold as possible.

9.6) After culture, cut the scaffolds in half to process them for both histology and biochemical analyses.

REPRESENTATIVE RESULTS

Decellularization of CDM scaffolds must always be confirmed using histological stainings, and an additional DNA quantification to measure the amount of DNA remnants. Insufficient decellularization might lead to undesired immunological responses that influence the results in *in vivo* settings[14-16]. Full decellularization using this protocol will lead to the production of a scaffold that is rich in collagen type II, has no cells and no proteoglycans (Figure 4).

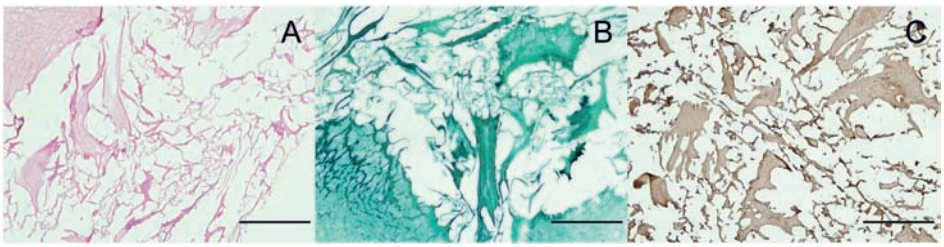

Figure 4: Histological characterization of the scaffold. (A) H&E staining that shows particles of different sizes and the absence of cells. (B) Safranin-O staining that shows that no proteoglycans have been retained in the decellularization process. (C) Collagen type II immunolocalization showing that ll of the decellularized particles are rich in collagen type II. All scale bars represent 500μm. Adapted from Benders *et al.* Cartilage (2014).

The scaffold must display a macroscopically, homogeneous porosity. Air bubbles will lead to easily detectable large holes in the scaffold and should, therefore, be prevented (Figure 3). These large holes in the scaffold may have a detrimental impact on the mechanical properties and lead to inhomogeneous cell attachment upon seeding. Successful production of the scaffold also involves a freeze-drying step lasting at least 24 hours; this will lead to a scaffold that has a white appearance (Figure 3). In case of insuffcient lyophilization the scaffolds will have a yellowish aspect and no clear pores can be observed.

Previous research has shown that matrix production by chondrocytes on this scaffold is unsatisfactory, especially when compared to the abundant matrix deposition by mesenchymal stromal cells[11]. As cartilage-like tissue is deposited on the scaffold, this new matrix is generally first deposited in the periphery of the scaffold before invading the rest of the scaffolds. This can often clearly be seen on the histological slices in which a cell-rich periphery is often seen rather than a cell-rich center (Figure 5). However, this effect may be reduced using perfusion bioreactors for cell seeding and to enhance nutrient exchange. As matrix deposition occurs, the scaffolds will also assume a more glossy appearance, and become more mechanically consistent, and less brittle. As such, they can be easily cut using a scalpel without falling apart completely. The properties of the newly formed matrix can be evaluated using both histological stainings, as well as quantitative assays. As no GAGs are left after the decellularization process, all of the GAGs that can be quantitatively measured will be a product of neosynthesis.

DISCUSSION

The extracellular matrix of articular cartilage is very dense and quite resilient to different enzymatic treatments. The multi-step decellularization protocol described in this paper addresses such resistance and successfully generates decellularized matrices. To achieve that, the process spans over several days. Many decellularization processes have been proposed

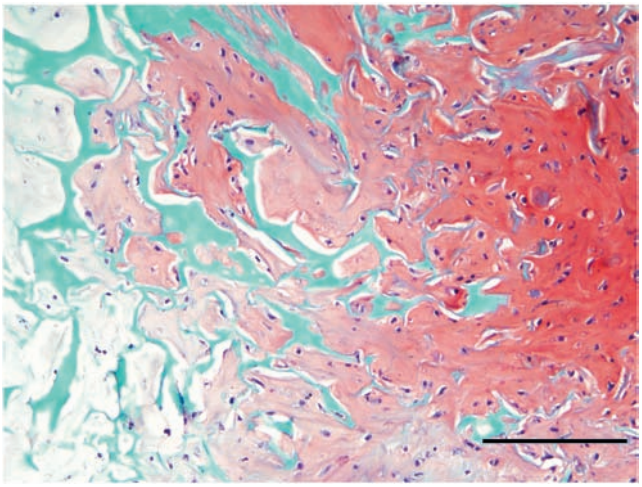

Figure 5: Neo-matrix formation on the scaffold after 6 weeks of culture using mesenchymal stromal cells. The newly formed matrix is rich in proteoglycans as can be observed on this Safranin-O staining. The periphery of this scaffold is on the right side of this image. Cell density is higher at the periphery, as well as the amount of matrix deposition. Scale bar represents 500μm.

for different types of tissues[17], and this paper describes a protocol suitable for the decellularization of cartilage. In this protocol it is, however, necessary to follow the enzymatic treatment with the detergent steps in order to remove all cells. The amount of DNA is diminished critically in the first few steps involving the treatment with trypsin and leaving out these steps will not result in proper decellularization[11].

It should be noted that this protocol is based on the decellularization of equine cartilage tissue. The activity of enzyme solutions used, were found sufficient for the adequate removal of the equine chondrocytes. However, despite the conservation of the matrix composition across species, the protocol may have to be adjusted for decellularization of cartilage from other animals due to the differences in the amount of naturally residing chondrocytes[18]. For example, cartilage of smaller animals is known to have higher cell content, and may, therefore, require a more aggressive decellularization process. A particular reason for choosing equine cartilage to create decellularized scaffolds is that equine and human cartilage show clear resemblance in thickness, cell density and biochemical make-up[19].

To ensure a reproducible product, several assessment criteria may be important to determine whether complete decellularization has been achieved. In this protocol, we use both H&E stainings, as well as biochemical quantification to evaluate the residual amount of DNA in the end product. Others have also proposed to determine the size of the remaining DNA, with a maximum of 200bp in length for quality control[20]. Regardless, alterations to the protocol must always be followed-up with histological evaluation and quantitative

assays to determine the effect on decellularization, as well as the remaining extracellular matrix products.

The main limitation of this protocol is, that the thorough decellularization involving the exposure to trypsin leads to extensive loss of GAGs. These extracellular matrix components are important in retaining the water in articular cartilage and, therefore, play a significant role in providing the tissue its biomechanical resilience[4]. Protocols that aim to reduce the loss of GAGs throughout the decellularization process, will affect the thoroughness of the decellularization process.

The scaffolds produced using this decellularization protocol provide an off-the-shelf solution and can be implanted without the necessity of cell seeding before implantation. However, when applied as a treatment for (osteo-)chondral defects, the biomechanical properties will have to be enhanced to diminish the chance of indentation of the construct in the early phases of articular loading. In the future, the retention of GAGs, preserving collagen fiber orientation or even using other biomaterials to reinforce these scaffolds might prove necessary to allow for a smoothly regenerated articular surface. Consequently, these scaffolds may play a role in the regeneration of osteochondral defects in the future.

REFERENCES

1. Dunlop DD, Semanik P, Song J, Manheim LM, Shih V, Chang RW. Risk factors for functional decline in older adults with arthritis. Arthritis Rheum 2005; 52: 1274-1282.
2. Fitzpatrick K, Tokish JM. A military perspective to articular cartilage defects. J Knee Surg; 24: 159-166.
3. Flanigan DC, Harris JD, Trinh TQ, Siston RA, Brophy RH. Prevalence of chondral defects in athletes' knees: a systematic review. Med Sci Sports Exerc; 42: 1795-1801.
4. Martel-Pelletier J, Boileau C, Pelletier JP, Roughley PJ. Cartilage in normal and osteoarthritis conditions. Best Pract Res Clin Rheumatol 2008; 22: 351-384.
5. Vinatier C, Bouffi C, Merceron C, Gordeladze J, Brondello JM, Jorgensen C, et al. Cartilage tissue engineering: towards a biomaterial-assisted mesenchymal stem cell therapy. Curr Stem Cell Res Ther 2009; 4: 318-329.
6. Badylak SF, Weiss DJ, Caplan A, Macchiarini P. Engineered whole organs and complex tissues. Lancet 2012; 379: 943-952.
7. Vashi C. Clinical Outcomes for Breast Cancer Patients Undergoing Mastectomy and Reconstruction with Use of DermACELL, a Sterile, Room Temperature Acellular Dermal Matrix. Plast Surg Int 2014; 2014: 704323.
8. Satterwhite TS, Miri S, Chung C, Spain DA, Lorenz HP, Lee GK. Abdominal wall reconstruction with dual layer cross-linked porcine dermal xenograft: the "Pork Sandwich" herniorraphy. J Plast Reconstr Aesthet Surg 2012; 65: 333-341.
9. Martinello T, Bronzini I, Volpin A, Vindigni V, Maccatrozzo L, Caporale G, et al. Successful recellularization of human tendon scaffolds using adipose-derived mesenchymal stem cells and collagen gel. J Tissue Eng Regen Med 2014; 8: 612-619.
10. Benders KE, van Weeren PR, Badylak SF, Saris DB, Dhert WJ, Malda J. Extracellular matrix scaffolds for cartilage and bone regeneration. Trends Biotechnol 2013; 31: 169-176.
11. Benders KE, Boot W, Cokelaere SM, Van Weeren PR, Gawlitta D, Bergman HJ, et al. Multipotent Stromal Cells Outperform Chondrocytes on Cartilage-Derived Matrix Scaffolds. Cartilage 2014; 5: 221-230.
12. Gawlitta D, Benders KE, Visser J, van der Sar AS, Kempen DH, Theyse LF, et al. Decellularized cartilage-derived matrix as substrate for endochondral bone regeneration. Tissue Eng Part A 2015; 21: 694-703.
13. Yang Z, Shi Y, Wei X, He J, Yang S, Dickson G, et al. Fabrication and repair of cartilage defects with a novel acellular cartilage matrix scaffold. Tissue Eng Part C Methods 2010; 16: 865-876.
14. Meyer SR, Nagendran, J., Desai, L.S., Rayat, G.R., Churchill, T.A., Anderson, C.C., Rajotte, R.V., Lakey, J.R., Ross, D.B. Decellularization reduces the immune response to aortic valve allografts in the rat. J Thorac Cardiovasc Surg 2005; 130: 469-476.
15. Brown BN, Valentin, J.E., Stewart-Akers, A.M., McCabe, G.P., Badylak, S.F. Macrophage phenotype and remodeling outcomes in response to biologic scaffolds with and without a cellular component. Biomaterials 2009; 30: 1482-1491.
16. Keane TJ, Londono, R., Turner, N.J., Badylak, S.F. Consequences of ineffective decellularization of biologic scaffolds on the host response. Biomaterials 2012; 33: 1771-1781.
17. Crapo PM, Gilbert, T.W., Badylak, S.F. An overview of tissue and whole organ decellularization. Biomaterials 2011; 32: 3233-3243.

18. Malda J, de Grauw, J.C., Benders, K.E.M., Kik, M.J., van de Lest, C.H., Creemers, L.B., Dhert, W.J.A., van Weeren, P.R. Of mice, men and elephants: the relation between articular cartilage thickness and body mass. Plos One 2013; 8.
19. Malda J, Benders KE, Klein TJ, de Grauw JC, Kik MJ, Hutmacher DW, et al. Comparative study of depth-dependent characteristics of equine and human osteochondral tissue from the medial and lateral femoral condyles. Osteoarthritis Cartilage; 20: 1147-1151.
20. Londono R, Badylak, S.F. Biologic scaffolds for regenerative medicine: mechanisms of in vivo remodeling. Ann Biomed Eng 2015; 43: 577-592.

Chapter 7

Multipotent stromal cells outperform chondrocytes on cartilage-derived matrix scaffolds

K.E.M. Benders
W. Boot
S.M. Cokelaere
P.R. van Weeren
D. Gawiltta
H.J. Bergman
D.B.F. Saris
W.J.A. Dhert
J. Malda

Cartilage. 2014 Oct;5(4):221-30.

ABSTRACT

Objective: Although extracellular matrix (ECM)-derived scaffolds have been extensively studied and applied in a number of clinical applications, the use of ECM as a biomaterial for (osteo-)chondral regeneration is less extensively explored. This study aimed at evaluating the chondrogenic potential of cells seeded on cartilage derived matrix (CDM) scaffolds *in vitro*.

Design: Scaffolds were generated from decellularized equine articular cartilage and seeded with either chondrocytes or multipotent stromal cells (MSCs). After 2, 4, and 6 weeks of *in vitro* culture, CDM constructs were analyzed both histologically (H&E, Safranin-O, collagen types I and II) and biochemically (glycosaminoglycan (GAG) and DNA content).

Results: After 4 weeks, both cell types demonstrated chondrogenic differentiation, however, the MSCs significantly outperformed chondrocytes in producing new GAG-containing cartilaginous matrix.

Conclusion: These promising *in vitro* results underscore the potency of CDM scaffolds in (osteo-)chondral defect repair.

INTRODUCTION

The young and active population is often affected by traumatic injuries to the knee leading to cartilage or osteochondral defects[3-5]. When untreated, cartilage defects develop into osteoarthritis (OA), which strongly affects the patient's quality of life due to increased discomfort or pain as well as a strong decline in mobility[6]. The ultimate salvage treatment option for OA is artificial knee replacement, which is not an appropriate option for young and active patients due to the relatively short lifespan of artificial joint replacements.

Ideally, to prevent the onset and progression of osteoarthritis, the body would have to initiate cartilage healing itself. However, the regeneration and repair of cartilage are hampered by insufficient nutrient supply and hypocellularity[7]. To compensate for the incapacity of the body to heal cartilage defects, new techniques to guide articular cartilage regeneration are sought after.

A promising approach for cartilage reconstruction is tissue engineering, which utilizes scaffolds to aid in the delivery of cells and/or growth factors. Additionally, these scaffolds can serve as a mechanically stable platform for the deposition of newly formed extracellular matrix (ECM)[8]. Structural and biological cues, such as growth factors can be incorporated in biomaterials to stimulate the deposition of neo-tissue and/or to tailor the construct's properties for specific tissue requirements. Through interactions between the resident cells and the surrounding ECM, chemotactic stimuli and specific gene expression result in constant remodelling of the tissue[9]. Hence, the tissue-specific ECM drives cellular differentiation and differential functional adaptation[10], therefore it seems logical to explore the application of ECM as a biomaterial for tissue engineering applications. Additional advantages of natural ECM-based scaffolds are their biodegradable nature and the potential to be applied cross-species, as ECM proteins are highly conserved across species[9, 11]. ECM-derived biomaterials are often decellularized to allow for optimal host incorporation and to prevent or modulate possible immunogenic responses after implantation[10, 12, 13]. Indeed, these materials have already been pursued and were found effective in many different fields of reconstructive and regenerative medicine[12, 14-17]. For cartilage tissue, relatively more vigourous decellularization protocols are needed due to the dense nature of the cartilage matrix. This typically results in lower GAG content and loss of biomechanical resilience of the cartilage-derived matrix (CDM)[18]. Nevertheless, scaffolds have been generated from decellularized cartilage matrix particles through lyophilization[19, 20] and, when inoculated with MSCs, hyaline cartilage formation was observed in a orthotopic rabbit model[21]. However, despite this luring prospect of ECM-based scaffolds[2], the number of studies that report on the use of decellularized CDM to drive chondrogenic differentiation and eventually cartilage repair[20-25] is limited. We therefore aimed at further exploring the potential of this approach by producing and characterizing CDM scaffolds and evaluating the *in vitro* chondrogenic potential of chondrocytes or multipotent stromal cells (MSCs) when seeded on CDM scaffolds.

METHODS

Scaffold production

The CDM scaffolds were produced according to a protocol adapted from Yang *et al.*[21] Briefly, full-thickness cartilage from the medial and lateral femoral condyles of the stifle (knee) joint of an equine donor was dissected using a scalpel, and washed in phosphate buffered saline (PBS) (supplemented with penicillin, streptomycin and fungizone (Invitrogen)). Next, the cartilage particles were snap-frozen in liquid nitrogen and lyophilized for 24 hours (Fig 1A). Thereafter, the lyophilized tissue was ground for approximately 40 minutes under liquid nitrogen to obtain fine cartilage particles (Fig 1B). Subsequently, the particles underwent 6 cycles of 0.25% trypsin-EDTA (Invitrogen) treatment in 24 hours at 37°C under vigorous agitation. Next, the tissue was washed in PBS and treated with a nuclease solution of 50U/ml deoxyribonuclease (Sigma) and 1U/ml ribonuclease A (Sigma) in 10mM Tris-HCl, pH 7.5, at 37°C under vigorous agitation. After 4 hours, the nuclease solution was removed and replaced by 10mM hypotonic Tris-HCl for 20 hours on a roller plate at room temperature. Subsequently, the tissue was immersed in 1% (v/v) Triton X-100 in PBS for 24 hours on a roller plate at room temperature. To remove all remnants of the enzymatic treatments, the tissue was washed thoroughly in PBS in 6 cycles over the course of 48 hours. The supernatants of all described steps were stored at -20°C. After the decellularization process, the resulting matrix particles were inserted into 8mm Ø cylindrical molds and lyophilized for 24 hours (Fig 1C). To allow cross-linking, the scaffolds were subjected to UV-light overnight. Prior to cell seeding, the scaffolds were sterilized using ethylene oxide gas. A number of scaffolds were sputter-coated (Cressingdon) with a thin gold layer to study them with a scanning electron microscope (Fig 1D) (SEM; Zeiss).

Equine chondrocyte and equine multipotent stromal cell isolation

Full-thickness equine chondrocytes were obtained from macroscopically healthy cartilage of the load-bearing sites of the medial and lateral femoral condyles of skeletally mature donors (n=3, aged 3-10 years). Cartilage was obtained under aseptic conditions and digested overnight using 0.15% type II collagenase (Worthington Biochemical Corp) at 37˚C. Next, the cell suspension was filtered, and washed thoroughly in PBS. Cells were resuspended in chondrocyte expansion medium consisting of DMEM (Dulbecco's Modified Eagle Medium 41965, Invitrogen), 10% heat-inactivated fetal bovine serum (Biowhittaker), 100 units/ml penicillin and 100µg/ml streptomycin (Invitrogen), and 10ng/ml FGF-2 (R&D Systems). The cells were expanded in a monolayer culture with a cell seeding density of 5.0×10^3 cells/cm^2 until confluency was reached (approximately 10-14 days, ~3-4 population doublings).

Equine sternal bone marrow aspirate was obtained from healthy, living donors (n=3, ages 3-10 years), with approval of the local animal ethical committee. The mononuclear fraction (MNF) was isolated from the bone marrow aspirate by centrifuging on Ficoll-Paque. The

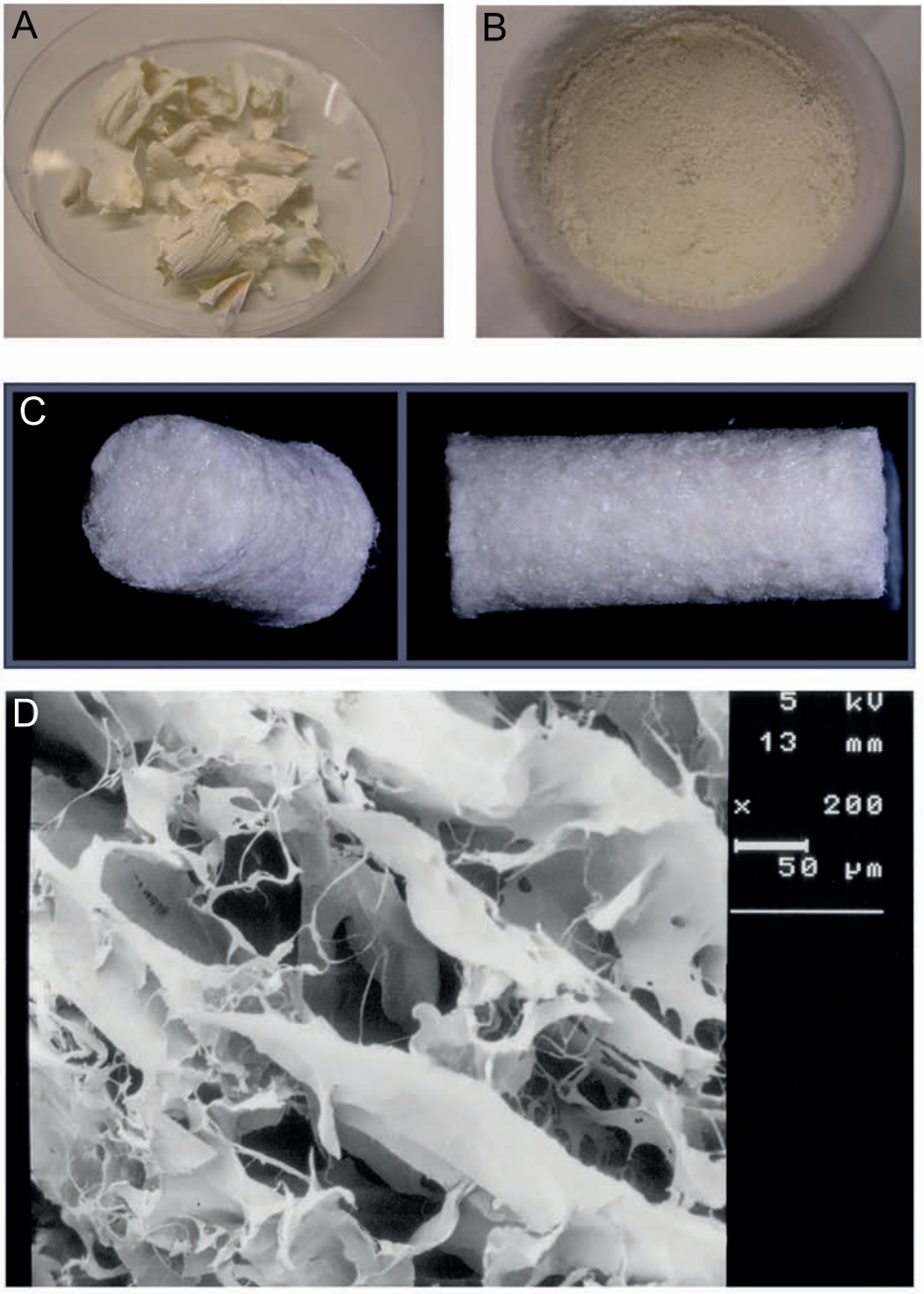

Figure 1: The production of the scaffolds starts with lyophilized cartilage shrapnels (A) that were ground into small particles (B) that are subjected to several enzymatic treatments. The produced scaffolds are porous (C), as was confirmed by scanning electron microscopy (D). The scale bar represents 50µm.

MNF was resuspended in MSC expansion medium containing a-MEM (22561, Invitrogen) complemented with 10% heat-inactivated fetal bovine serum, 0.2mM L-ascorbic acid 2-phosphate (Sigma), 100 units/ml penicillin and 100µg/ml streptomycin, and 1ng/ml FGF-2. Cells were expanded in a monolayer culture with an initial cell density of 2.5×10^5 cells/cm^2. The cells were expanded to subconfluence before passaging.

To ensure that the cells isolated from the sternal bone marrow aspirate were MSCs, the multilineage potential was confirmed by differentiating the equine MSCs into the adipogenic, osteogenic, and chondrogenic lineages, as previously described[26]. In brief, the MSCs were cultured in three different media. Osteogenic and adipogenic differentiation was stimulated in monolayer cultures once confluency was obtained. Osteogenic differentiation was stimulated in a-MEM, supplemented with 10% heat-inactivated FBS, 0.2mM L-ascorbic acid-2-phosphate, 100U/ml penicillin, 100µg/ml streptomycin, 10mM b-glycerophosphate (G9891, Sigma), and 10nM dexamethasone (Sigma). Adipogenic medium consisted of a-MEM, supplemented with 10% inactivated FBS, 100U/ml penicillin, 100µg/ml streptomycin, 1µM dexamethasone, 0.5mM IBMX (3-Isobutyl-1-methylxanthine, Sigma), 0.2mM indomethacin (Sigma), and 1.72µM insulin (Sigma). Chondrogenic differentiation was evaluated in a pellet culture of MSCs in chondrogenic MSC differentiation medium. Pellets were made by centrifuging 250,000 cells in a 15mL tube. Chondrogenic MSC differentiation medium contained DMEM (31966, Invitrogen) supplemented with 0.2mM L-ascorbic acid 2-phosphate, 1x ITS+ premix (BD Biosciences, USA), 0.1µM dexamethasone, 100 units/ml penicillin and 100µg/ml streptomycin, and 10ng/ml TGFb-2 (R&D Systems).

Osteogenic differentiation was evaluated through alkaline phosphatase (ALP) activity of the differentiated MSCs. The monolayer was permeabilized with 0.2% Triton X-100 in tris buffered saline (TBS). The presence of ALP was determined using the Fuchsin-Substrate-Chromogen kit (Dako). Adipogenic differentiation was confirmed by an Oil-red O staining (Sigma). The monolayer was fixed in formalin, washed in distilled water, washed with 60% isopropanol and stained with Oil-red O for 10-20 minutes at room temperature. Chondrogenic differentiation was confirmed by the presence of glycosaminoglycans (GAGs) (Safranin-O staining) and collagen type II (immunohistochemistry), as described below.

Scaffold seeding and culturing

Prior to cell seeding, the scaffolds were cut into discs of approximately 3mm thickness. These discs were pre-soaked in DMEM (Invitrogen) for 1 hour. Next, 3.0×10^6 cells, either chondrocytes (P1) or MSCs (P1), were seeded onto the scaffolds (n=6 per donor). For this, 1.5×10^6 cells were seeded on the top of the scaffold and after 60 min, the scaffold was turned and 1.5×10^6 cells were seeded on the bottom in order to improve cell seeding efficiency.

Scaffolds seeded with expanded chondrocytes were cultured for 2, 4 and 6 weeks (n=3 per donor) in chondrogenic differentiation medium (DMEM (41965, Invitrogen) supplemented with 0.2mM L-ascorbic acid 2-phosphate, 0.5% human serum albumin (SeraCare

Life Sciences), 1% ITS-X (Invitrogen) 100 units/ml penicillin and 100µg/ml streptomycin, 25mM 4-(2-hydroxyethyl)-1-piperazineethanesulfonic acid (HEPES) (Invitrogen) and 5ng/ml TGFb-2).

The MSC-seeded scaffolds were first cultured for 1 week in MSC expansion medium and subsequently differentiated for either 4 and 6 (n=3 per donor) weeks in MSC chondrogenic differentiation medium.

Histology

Samples were cut in half and dehydrated through a graded ethanol series, cleared in xylene and embedded in paraffin. The paraffin embedded samples were sectioned into 5µm slices and stained with hematoxylin and eosin for cell detection, and a triple stain of hematoxylin, fast green, and Safranin-O to identify GAG deposition (all from Sigma). The stained sections were examined using a light microscope (Olympus BX51) and representative images were taken from sections of the centre of the constructs.

Immunohistochemistry

Paraffin-embedded sections were deparaffinized through a graded ethanol series and washed in PBS with 0.1% Tween 20 for 5 minutes prior to immunolocalization of collagen types I and II. Antigen retrieval steps involved exposure to hyaluronidase for 30 minutes (Sigma, 10mg/ml in PBS), and to pronase for 30 minutes (Roche, 1mg/ml in PBS), both at 37°C. Next, the sections were blocked with 5% bovine serum albumin in PBS for 30 minutes at room temperature, and incubated overnight at 4°C with antibodies either against collagen type I (1:50; I-8H5, Calbiochem) or type II (1:100; II-6B3II, Developmental Studies Hybridoma Bank). Then, the samples were incubated with a biotinylated anti-mouse antibody (1:200; GE Healthcare) and streptavidin/peroxidase (1:400; Beckman Coulter), or a secondary anti-mouse antibody conjugated with peroxidase (Dako), respectively, all for 60 minutes at room temperature. Antibody binding in all of the sections was visualized using 3,3'-diaminobenzidine solution (Sigma) for up to 10 minutes. Nuclei were counterstained with Mayer's hematoxylin.

GAG and DNA quantification

The remaining half of each of the samples was digested overnight in papain solution (0.01M cysteine, 250µg/ml papain, 0.2M NaH_2PO_4 and 0.01M EDTA) at 60°C. After reaction with dimethylmethylene blue (DMMB) (Sigma), GAG content was measured spectrophotometrically in a microplate reader (Biorad) by determining the ratio of absorbances at 540 and 595nm. GAG content per scaffold was quantified using a chondroitin sulphate (Sigma) standard.

DNA content was quantified on the papain digests using a Picogreen DNA assay (Invitrogen) according to the manufacturer's instructions.

Statistical analysis

To compare the GAG per DNA of chondrocyte- and MSC-seeded CDM scaffolds two-tailed unpaired Student's *t*-tests were performed. Significance was set at $p<0.05$.

RESULTS

Scaffold characterization

The produced CDM scaffolds had a diameter of 8mm and were approximately 2-3mm in height. Scanning electron microscopy demonstrated that the scaffolds were highly porous and contained randomly aligned extracellular matrix particles (Fig 1D). Successful decellularization was confirmed, as no cells were observed in HE-stained sections (Fig 2A). Moreover, the scaffolds did not contain any residual GAGs, as was demonstrated by the Safranin-O staining and confirmed by the quantitative DMMB analysis (Fig 2C and 5). Quantitative DMMB analysis revealed that the majority of GAGs were lost in the decellularization process during the first enzymatic treatment steps (trypsin) (Fig 2E). In contrast to the loss of GAGs, the scaffolds did show intense staining for collagen type II (Fig 2B), whilst no staining for collagen type I was observed (Fig 2D).

In vitro tissue formation: chondrocyte-seeded CDM scaffolds

CDM scaffolds seeded with equine chondrocytes were differentiated for 2, 4 and 6 weeks. During the culture period, limited matrix deposition was observed Nevertheless, after 4 weeks of culture, the chondrocytes were dispersed throughout the entire volume of the scaffolds (Fig 3A). The newly formed matrix did show positive staining for collagen type II (Fig 3B), as well as some positive staining for collagen type I in the pericellular matrix (Fig 3D), as was demonstrated by immunolocalization. However, Safranin-O staining revealed that hardly any GAGs were deposited (Fig 3C). The chondrocyte-seeded constructs degraded during the culture period (2-4 weeks). After 6 weeks of culture the scaffold was fully disintegrated and samples could not be further analyzed.

In vitro tissue formation: MSC-seeded CDM scaffolds

CDM scaffolds with MSCs were cultured for 4 and 6 weeks in chondrogenic differentiation medium. After 4 and 6 weeks of culture, cells were observed throughout the scaffold structure (Fig 4A and E, respectively) and the deposited matrix stained more intensely for GAGs (Fig 4C and G, respectively) than the matrix in the corresponding chondrocyte-seeded CDM constructs (Fig 3C). After culture the MSC-seeded tissue constructs were stable upon handling and had macroscopically a cartilage-like appearance. In addition, the produced matrix showed intense staining for collagen type II both after 4 (Fig 4B) and 6

weeks (Fig 4F). However, at both time points staining for collagen type I was noted at the periphery of the constructs (Fig 4D and H).

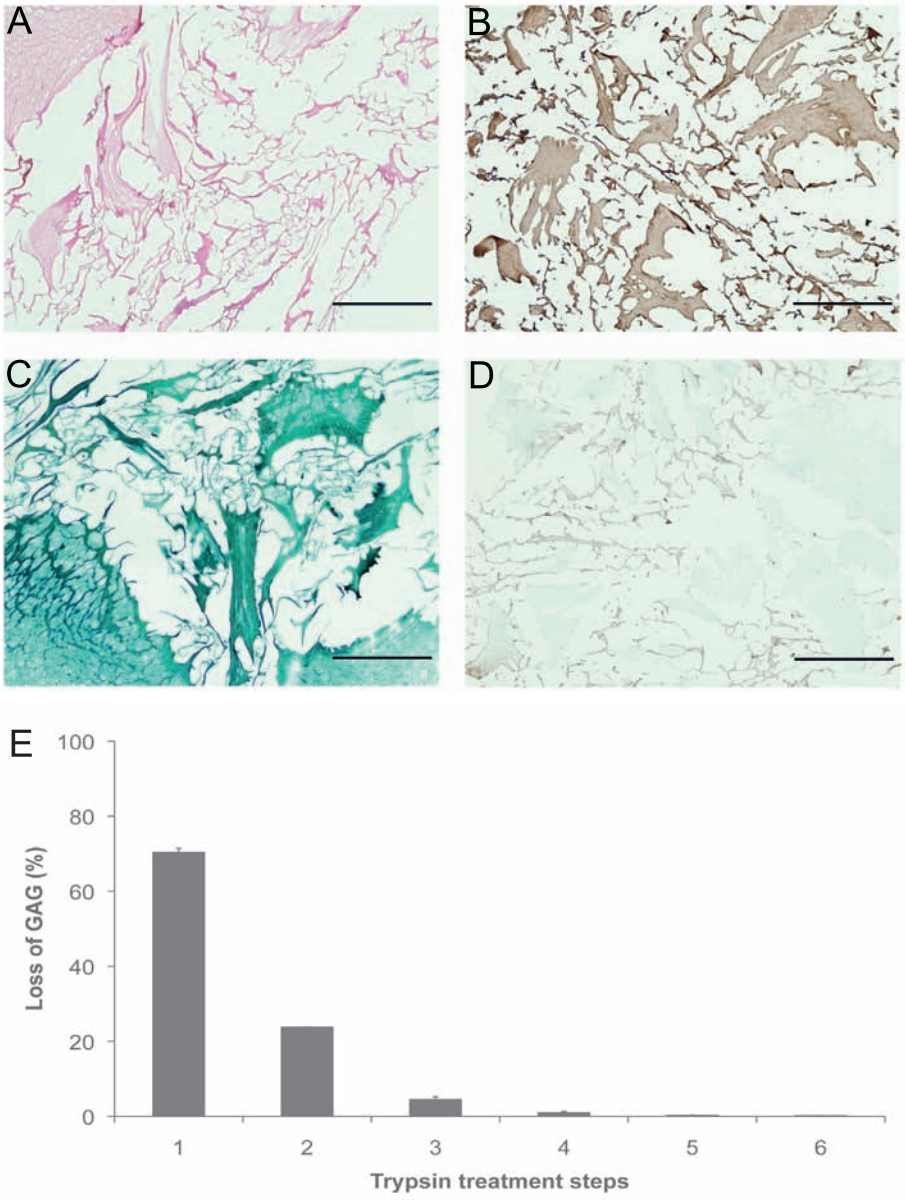

Figure 2: The CDM scaffold is porous with no remaining cells (A, H&E staining), no GAGs (C, Safranin-O staining) and no collagen type I (D). All scaffold material was positive for collagen type II (B). Scale bars represent 500μm.
During the decellularization process the majority of GAGs was lost during the first trypsin treatment steps as confirmed by quantitative GAG analysis (E), error bars indicate 95% confidence intervals.

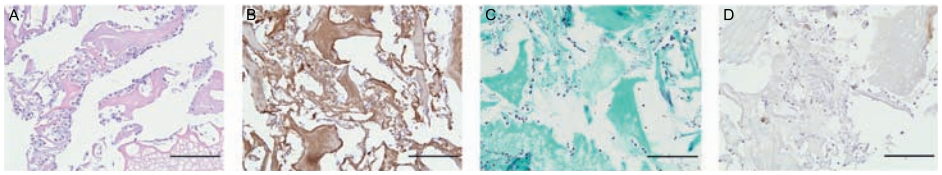

Figure 3: Chondrocyte-seeded scaffolds after 4 weeks of culture, showing cells on remaining scaffold particles (A, H&E staining), with collagen type II positive matrix (stains brown in B), which hardly contains GAGs (stains red in C). In the pericellular matrix, some staining for collagen type I was noted (stains brown in D). Scale bars represent 200μm, S = scaffold, arrows indicate cells.

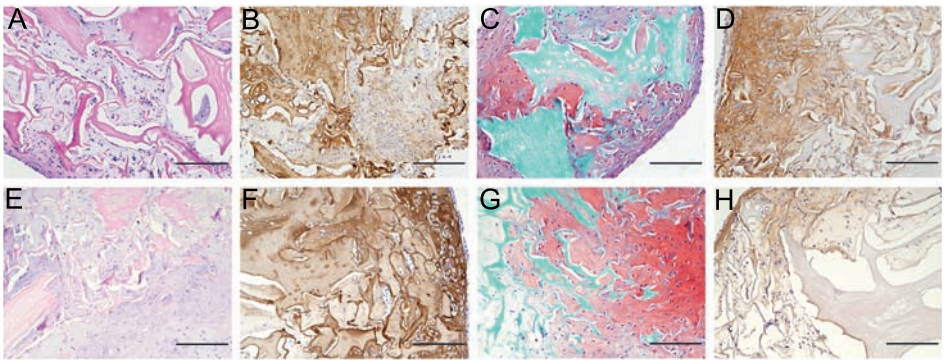

Figure 4: MSC-seeded scaffolds after 4 weeks of culture (top row) and 6 weeks of culture (bottom row). Abundant cartilage matrix production was already noted after 4 weeks and was further increased at 6 weeks of culture (A and E, H&E staining). The newly formed matrix was positive for GAG (C and G, Saf-O stains GAGs red), collagen type II (brown in B and F) and was in the periphery also positive for collagen type I (brown in D and H). Scale bars represent 200μm, S = scaffold.

GAG and DNA analysis

Quantitative GAG and DNA analyses demonstrated an increase in GAG per DNA after culturing both chondrocytes and MSCs, confirming the histological findings (Fig 5). However, a significant difference was observed between the chondrocyte-seeded group and MSC-seeded group after 4 weeks of culture (p=0.002), with the latter showing more GAG/DNA.

DISCUSSION

This study aimed to evaluate the chondrogenic potential of chondrocytes and MSCs that were seeded CDM scaffolds that can ultimately be applied to osteochondral defect repair. Previous studies in other fields of regenerative medicine, including reconstructive skin surgery, heart valve replacement, and bladder repair have shown great regenerative potential of ECM-based materials[9-12, 14-17, 24, 27]. Whilst the treatment of cartilage defects remains

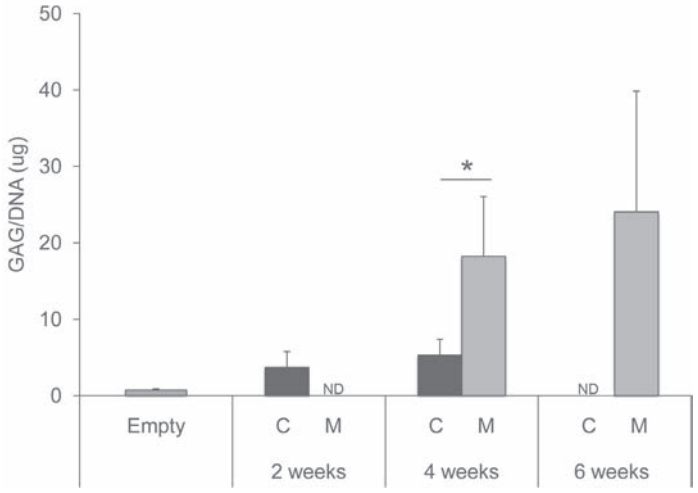

Figure 5: Quantitative analysis of GAG production expressed as GAG/DNA. The amount of GAG/DNA increased for both the chondrocyte-seeded (C) and MSC-seeded (M) conditions compared to the empty scaffolds, but significantly more in the MSC-seeded condition after 4 weeks of culture (*p=0.002). ND=not determined at that time-point. Error bars indicate 95% confidence intervals.

a significant clinical challenge, approaches based on ECM-derived scaffolds have thus far not been extensively studied for this application[2].

Our results demonstrate that porous scaffold structures can be generated from decellularized cartilage matrix. Moreover, the outcomes underscore the chondrogenic potential of CDM scaffolds when seeded with MSCs. In contrast, we showed that chondrocyte-seeded constructs do not result in the production of abundant new cartilaginous matrix. Previous studies, however, performed with chondrocytes (passage 1) from other donors, but expanded under the exact same conditions, confirmed the capacity of these cells to form abundant cartilaginous matrix formation in pellet cultures[1]. While chondrocytes are the resident cells of the cartilage tissue and are clinically applied in regenerative approaches for cartilage repair (*e.g.* via autologous chondrocyte implantation[28]), our results thus question the presumption that they are efficacious in producing matrix when seeded on scaffolds that potentially resemble their collagen-rich natural habitat. Although some differences in GAG deposition and collagen production have been observed between chondrocytes and MSCs on ECM-based scaffolds[29], MSCs performed substantially better on CDM scaffolds.

MSCs are generally known to have a higher proliferative potential and higher capability to retain their differential capacity than chondrocytes[30] and it has been suggested that MSCs intrinsically secrete a higher number of matrix anabolic agents after expansion[30], enhancing their capacity to form new cartilage matrix. Nevertheless, the observed difference is likely also related to the specific composition of the collagen type II rich CDM scaffolds. Chondrocytes are indeed known to produce catabolic factors, such as MMP1, MMP3

and MMP13 in response to exposure to collagen type II fragments[31, 32]. Also, these cells release increased levels of catabolic agents in response to exposure to cartilage ECM components[30]. This may have led to a disruption of the delicate balance of anabolic and catabolic cues, resulting in the more rapid scaffold degradation and disintegration observed in the current study. Chondrocyte-seeded scaffolds could hence only be evaluated up to 4 weeks of culture, whilst MSC-seeded scaffolds did not disintegrate and formed stable tissue constructs during 6 weeks of *in vitro* culture. The exact mechanisms behind the superior production of cartilage matrix by MSCs on this scaffold have not been addressed yet, as is the generally observed tendency of hypertrophic differentiation by the MSCs. This will be the focus of future investigation.

The major ECM components of native cartilage matrix are collagen type II and GAGs[7]. The decellularization protocol used in this study resulted in a predominantly collagen-based scaffold in which the GAGs were not retained. In order to accomplish full and consistent decellularization of dense tissues such as cartilage, the procedure involves the use of multiple agents. This will inevitably lead to a greater deprivation of ECM and structural integrity than in less dense tissues, such as small intestinal submucosa or urinary bladder walls[9, 10, 33]. For example, the extensive use of the enzyme trypsin, and detergent Triton X-100 have previously been reported to lead to a loss of GAGs[10, 34]. Using these agents leads to effective decellularization, but it also results in extensive GAG loss compared to previously reported decellularization protocols for cartilage[20, 21]. Whereas in the present study these circumstances did not hamper satisfactory matrix formation in the MSC-seeded scaffolds, it remains to be evaluated whether remnants of GAG in the scaffold could contribute to enhanced chondrogenic differentiation.

Besides impacting on cartilage repair, the encouraging *in vitro* results observed for MSC-seeded constructs may also offer opportunities for regenerative approaches to treat osteochondral defects. These defects are in direct contact with the bone marrow and MSCs could repopulate the scaffold *in vivo* through cell homing rather than through cell-delivery. This suggests a possible cell-free, "off-the-shelf" application for this scaffold, which might strongly facilitate therapeutic translation. Nevertheless, the potential catabolic effect of the implanted scaffold on the surrounding cartilage tissue should be carefully assessed, despite the fact that preliminary equine pilot studies have not indicated that such damaging effects on the surrounding tissue would occur[2]. Moreover, MSCs have the ability to differentiate towards the osteogenic lineage, either directly or via the endochondral route[35, 36] and can, therefore, also regenerate the bone phase in an osteochondral defect, thus serving a dual purpose. As stated previously, the challenge will be to restrict hypertrophic differentiation and endochondral ossification to the osteogenic layer. The presence of bioactive and bioinductive cues is considered to be the main contributor to the success of biological ECM scaffolds[2, 9, 21, 33]. The ECM of small intestinal submucosa, for example, is often used as a biological scaffold material and has been characterized extensively[37-40]. This material

has been shown to retain endogenous growth factors that remain bioactive after decellularization and sterilization[41-43]. Also, the presence of collagen and other structural and functional molecules has been proposed as a contributing factor for cell proliferation, migration, and differentiation[33].

The tissue and cells that were used in the present study were all of equine origin, since previous studies have shown that there are clear similarities between equine and human cartilage in both thickness, as well as biochemical composition[44-46]. These similarities make the equine model the large animal model of choice to perform *in vivo* pre-clinical translational research on osteochondral defect repair[47-49]. Moreover, equine patients often develop cartilage or osteochondral lesions due to congenital disorders or traumatic events similar to human patients[50-52]. Hence, the development of a new and ECM-based treatment modality may benefit both veterinary and human patients.

We have demonstrated the excellent chondrogenic differentiation capacity of MSCs in CDM scaffolds. The MSCs outperformed chondrocytes in cartilage matrix production when seeded on this scaffold. In addition, the use of CDM scaffolds surpasses the issues of biodegradability and biocompatibility that may arise with synthetic scaffolds. Also, the natural ECM environment might provide bioactive cues that initiate natural regeneration.

REFERENCES

1. Schuurman W, Harimulyo EB, Gawlitta D, Woodfield TB, Dhert WJ, van Weeren PR, et al. Three-dimensional assembly of tissue-engineered cartilage constructs results in cartilaginous tissue formation without retainment of zonal characteristics. J Tissue Eng Regen Med 2013.
2. Benders KE, van Weeren PR, Badylak SF, Saris DB, Dhert WJ, Malda J. Extracellular matrix scaffolds for cartilage and bone regeneration. Trends Biotechnol 2013; 31: 169-176.
3. Flanigan BD, Harris JD, Trinh TQ, Siston RA, Brophy RH. Prevalence of chondral defects in athletes' knees: a systematic review. Med Sci Sports Exerc 2010; 42: 1795-1801.
4. Fitzpatrick K, Tokish JM. A military perspective to articular cartilage defects. J Knee Surg; 24: 159-166.
5. Hjelle K, Solheim E, Strand T, Muri R, Brittberg M. Articular cartilage defects in 1,000 knee arthroscopies. Arthroscopy 2002; 18: 730-734.
6. Anderson DD, Chubinskaya S, Guilak F, Martin JA, Oegema TR, Olson SA, et al. Post-traumatic osteoarthritis: improved understanding and opportunities for early intervention. J Orthop Res; 29: 802-809.
7. Martel-Pelletier J, Boileau C, Pelletier JP, Roughley PJ. Cartilage in normal and osteoarthritis conditions. Best Pract Res Clin Rheumatol 2008; 22: 351-384.
8. Martin I, Miot S, Barbero A, Jakob M, Wendt D. Osteochondral tissue engineering. J Biomech 2007; 40: 750-765.
9. Gilbert TW. Strategies for tissue and organ decellularization. J Cell Biochem; 113: 2217-2222.
10. Crapo PM, Gilbert TW, Badylak SF. An overview of tissue and whole organ decellularization processes. Biomaterials; 32: 3233-3243.
11. Turner NJ, Yates AJ, Jr., Weber DJ, Qureshi IR, Stolz DB, Gilbert TW, et al. Xenogeneic extracellular matrix as an inductive scaffold for regeneration of a functioning musculotendinous junction. Tissue Eng Part A; 16: 3309-3317.
12. Macchiarini P, Jungebluth P, Go T, Asnaghi MA, Rees LE, Cogan TA, et al. Clinical transplantation of a tissue-engineered airway. Lancet 2008; 372: 2023-2030.
13. Haykal S, Zhou Y, Marcus P, Salna M, Machuca T, Hofer SO, et al. The effect of decellularization of tracheal allografts on leukocyte infiltration and of recellularization on regulatory T cell recruitment. Biomaterials 2013; 34: 5821-5832.
14. Armitage S, Seman EI, Keirse MJ. Use of surgisis for treatment of anterior and posterior vaginal prolapse. Obstet Gynecol Int; 2012: 376251.
15. D'Onofrio A, Cresce GD, Bolgan I, Magagna P, Piccin C, Auriemma S, et al. Clinical and hemodynamic outcomes after aortic valve replacement with stented and stentless pericardial xenografts: a propensity-matched analysis. J Heart Valve Dis; 20: 319-325; discussion 326.
16. Meyer T, Schwarz K, Ulrichs K, Hocht B. A new biocompatible material (Lyoplant) for the therapy of congenital abdominal wall defects: first experimental results in rats. Pediatr Surg Int 2006; 22: 369-374.
17. Vardanian AJ, Clayton JL, Roostaeian J, Shirvanian V, Da Lio A, Lipa JE, et al. Comparison of implant-based immediate breast reconstruction with and without acellular dermal matrix. Plast Reconstr Surg; 128: 403e-410e.
18. Elder BD, Eleswarapu SV, Athanasiou KA. Extraction techniques for the decellularization of tissue engineered articular cartilage constructs. Biomaterials 2009; 30: 3749-3756.

19. Schwarz S, Koerber L, Elsaesser AF, Goldberg-Bockhorn E, Seitz AM, Durselen L, et al. Decellularized cartilage matrix as a novel biomatrix for cartilage tissue-engineering applications. Tissue Eng Part A 2012; 18: 2195-2209.
20. Yang Q, Peng J, Guo Q, Huang J, Zhang L, Yao J, et al. A cartilage ECM-derived 3-D porous acellular matrix scaffold for in vivo cartilage tissue engineering with PKH26-labeled chondrogenic bone marrow-derived mesenchymal stem cells. Biomaterials 2008; 29: 2378-2387.
21. Yang Z, Shi Y, Wei X, He J, Yang S, Dickson G, et al. Fabrication and repair of cartilage defects with a novel acellular cartilage matrix scaffold. Tissue Eng Part C Methods 2010; 16: 865-876.
22. Jin CZ, Choi BH, Park SR, Min BH. Cartilage engineering using cell-derived extracellular matrix scaffold in vitro. J Biomed Mater Res A 2010; 92: 1567-1577.
23. Jin CZ, Park SR, Choi BH, Park K, Min BH. In vivo cartilage tissue engineering using a cell-derived extracellular matrix scaffold. Artif Organs 2007; 31: 183-192.
24. Gong YY, Xue JX, Zhang WJ, Zhou GD, Liu W, Cao Y. A sandwich model for engineering cartilage with acellular cartilage sheets and chondrocytes. Biomaterials; 32: 2265-2273.
25. Jia S, Liu L, Pan W, Meng G, Duan C, Zhang L, et al. Oriented cartilage extracellular matrix-derived scaffold for cartilage tissue engineering. J Biosci Bioeng; 113: 647-653.
26. Pittenger MF, Mackay AM, Beck SC, Jaiswal RK, Douglas R, Mosca JD, et al. Multilineage potential of adult human mesenchymal stem cells. Science 1999; 284: 143-147.
27. Vorotnikova E, McIntosh D, Dewilde A, Zhang J, Reing JE, Zhang L, et al. Extracellular matrix-derived products modulate endothelial and progenitor cell migration and proliferation in vitro and stimulate regenerative healing in vivo. Matrix Biol; 29: 690-700.
28. Brittberg M, Lindahl A, Nilsson A, Ohlsson C, Isaksson O, Peterson L. Treatment of deep cartilage defects in the knee with autologous chondrocyte transplantation. N Engl J Med 1994; 331: 889-895.
29. Giavaresi G, Bondioli E, Melandri D, Giardino R, Tschon M, Torricelli P, et al. Response of human chondrocytes and mesenchymal stromal cells to a decellularized human dermis. BMC Musculoskelet Disord 2013; 14: 12.
30. Polacek M, Bruun JA, Elvenes J, Figenschau Y, Martinez I. The secretory profiles of cultured human articular chondrocytes and mesenchymal stem cells: implications for autologous cell transplantation strategies. Cell Transplant; 20: 1381-1393.
31. Fichter M, Korner U, Schomburg J, Jennings L, Cole AA, Mollenhauer J. Collagen degradation products modulate matrix metalloproteinase expression in cultured articular chondrocytes. J Orthop Res 2006; 24: 63-70.
32. Klatt AR, Paul-Klausch B, Klinger G, Kuhn G, Renno JH, Banerjee M, et al. A critical role for collagen II in cartilage matrix degradation: collagen II induces pro-inflammatory cytokines and MMPs in primary human chondrocytes. J Orthop Res 2009; 27: 65-70.
33. Badylak SF, Freytes DO, Gilbert TW. Extracellular matrix as a biological scaffold material: Structure and function. Acta Biomater 2009; 5: 1-13.
34. Gilbert TW, Sellaro TL, Badylak SF. Decellularization of tissues and organs. Biomaterials 2006; 27: 3675-3683.
35. Pelttari K, Steck E, Richter W. The use of mesenchymal stem cells for chondrogenesis. Injury 2008; 39 Suppl 1: S58-65.
36. Pelttari K, Winter A, Steck E, Goetzke K, Hennig T, Ochs BG, et al. Premature induction of hypertrophy during in vitro chondrogenesis of human mesenchymal stem cells correlates with calcification and vascular invasion after ectopic transplantation in SCID mice. Arthritis Rheum 2006; 54: 3254-3266.

37. Hodde J, Janis A, Ernst D, Zopf D, Sherman D, Johnson C. Effects of sterilization on an extracellular matrix scaffold: part I. Composition and matrix architecture. J Mater Sci Mater Med 2007; 18: 537-543.
38. Hodde J, Janis A, Hiles M. Effects of sterilization on an extracellular matrix scaffold: part II. Bioactivity and matrix interaction. J Mater Sci Mater Med 2007; 18: 545-550.
39. Hodde J, Record R, Tullius R, Badylak S. Fibronectin peptides mediate HMEC adhesion to porcine-derived extracellular matrix. Biomaterials 2002; 23: 1841-1848.
40. Hodde JP, Badylak SF, Brightman AO, Voytik-Harbin SL. Glycosaminoglycan content of small intestinal submucosa: a bioscaffold for tissue replacement. Tissue Eng 1996; 2: 209-217.
41. McDevitt CA, Wildey GM, Cutrone RM. Transforming growth factor-beta1 in a sterilized tissue derived from the pig small intestine submucosa. J Biomed Mater Res A 2003; 67: 637-640.
42. Hodde JP, Record RD, Liang HA, Badylak SF. Vascular endothelial growth factor in porcine-derived extracellular matrix. Endothelium 2001; 8: 11-24.
43. Voytik-Harbin SL, Brightman AO, Kraine MR, Waisner B, Badylak SF. Identification of extractable growth factors from small intestinal submucosa. J Cell Biochem 1997; 67: 478-491.
44. Frisbie DD, Cross MW, McIlwraith CW. A comparative study of articular cartilage thickness in the stifle of animal species used in human pre-clinical studies compared to articular cartilage thickness in the human knee. Vet Comp Orthop Traumatol 2006; 19: 142-146.
45. Shepherd DE, Seedhom BB. Thickness of human articular cartilage in joints of the lower limb. Ann Rheum Dis 1999; 58: 27-34.
46. Malda J, Benders KE, Klein TJ, de Grauw JC, Kik MJ, Hutmacher DW, et al. Comparative study of depth-dependent characteristics of equine and human osteochondral tissue from the medial and lateral femoral condyles. Osteoarthritis Cartilage 2012; 20: 1147-1151.
47. Chu CR, Szczodry M, Bruno S. Animal models for cartilage regeneration and repair. Tissue Eng Part B Rev 2010; 16: 105-115.
48. Hurtig MB, Buschmann MD, Fortier LA, Hoemann CD, Hunziker EB, Jurvelin JS, et al. Preclinical studies for cartilage repair: recommendations from the international cartilage repair society. Cartilage 2011; 2: 137-152.
49. McIlwraith CW, Fortier LA, Frisbie DD, Nixon AJ. Equine models of articular cartilage repair. Cartilage 2011.
50. van Weeren PR. Osteochondrosis. In: Equine Surgery, Auer JA, Stick JA Eds. St. Louis: Saunders 2006:1166-1178.
51. Voute LC, Henson FM, Platt D, Jeffcott LB. Osteochondrosis lesions of the lateral trochlear ridge of the distal femur in four ponies. Vet Rec; 168: 265.
52. Ytrehus B, Carlson CS, Ekman S. Etiology and pathogenesis of osteochondrosis. Vet Pathol 2007; 44: 429-448.

Chapter 8

Decellularized cartilage-derived matrix as substrate for endochondral bone regeneration

D. Gawlitta *
K.E.M. Benders*
J. Visser
A.S. van der Sar
D.H.R. Kempen
L.F. Theyse
J. Malda
W.J.A. Dhert

* Authors contributed equally

Tissue Eng Part A. 2015 Feb;21(3-4):694-703.

ABSTRACT

Following an endochondral approach to bone regeneration, multipotent stromal cells (MSCs) can be cultured on a scaffold to create a cartilaginous callus that is subsequently remodeled into bone. An attractive scaffold material for cartilage regeneration that has recently regained attention is decellularized cartilage-derived matrix (CDM). Since this material has shown potential for cartilage regeneration, we hypothesized that CDM could be a potent material for endochondral bone regeneration. Additionally, as decellularized matrices are known to harbor bioactive cues for tissue formation, we evaluated the need for seeded MSCs in CDM scaffolds.

In the present study ectopic bone formation in rats was evaluated for CDM scaffolds seeded with human MSCs and compared to unseeded controls. The MSC-seeded samples were preconditioned in chondrogenic medium for 37 days. After 8 weeks of subcutaneous implantation, the extent of mineralization was significantly higher in the MSC-seeded constructs versus unseeded controls. The mineralized areas corresponded to bone formation with bone marrow cavities. Also, rat-specific bone formation was confirmed by collagen type I immunohistochemistry. Finally, fluorochrome incorporation at 3 and 6 weeks revealed that the bone formation had an inwardly directed progression.

Taken together, our results show that decellularized CDM is a promising biomaterial for endochondral bone regeneration when combined with MSCs at ectopic locations. Modification of current decellularization protocols may lead to enhanced functionality of CDM scaffolds, potentially offering the prospect of generation of cell-free off-the-shelf bone regenerative substitutes.

INTRODUCTION

Previously, bone regeneration strategies have predominantly relied on biomimicry of the intramembranous pathway of bone formation. However, this approach has not yet resulted in a new treatment modality for the repair of large bone defects in clinical practice. In recent years, following the concept of developmental engineering[1], the attention has shifted towards exploration of the feasibility of bone regeneration following an alternative method: the endochondral approach[1-5]. In the endochondral approach, bone formation starts from a cartilaginous template[6]. Cells residing in this template undergo terminal chondrogenic differentiation. During the hypertrophic stage of differentiation, these cells initiate the mineralization of the cartilaginous matrix that is surrounding them. Before cell death, angiogenic and chemotactic factors are excreted that can attract cells to remodel the mineralized cartilage into bone. As a consequence, blood vessels, osteoblasts and osteoclasts invade the template and replace it with bone tissue[6].

Multipotent stromal cells (MSCs) are ideal candidate cells for bone regeneration through the endochondral route, as they have the capacity for hypertrophic differentiation under currently applied chondrogenic culture conditions[5, 7, 8]. The endochondral approach to bone tissue engineering has proven its feasibility for MSC-containing constructs at ectopic locations in rodents[1-5, 9, 10]. In general, MSCs were chondrogenically stimulated *in vitro* and after subcutaneous implantation, the formation of bone tissue was observed. The formed bone was mineralized and contained bone marrow cavities with hematopoietic cells.

Despite its great promise, several challenges remain in the creation of grafts following this approach. A major obstacle is increasing construct size. Endochondral bone formation *in vivo* is either achieved in small pellet cultures[1, 3, 5] or restricted to the periphery of larger constructs[2]. Choosing a scaffold material that can further stimulate and/or accelerate the endochondral process, could address this limitation. As endochondral bone formation is based on the formation of bone from a cartilaginous template, it may be desirable from a developmental engineering standpoint[1], to increase the construct size by increasing the cartilage volume. So, instead of relying on the creation of a cartilaginous matrix by the MSCs only, a logical step would be to add cartilaginous matrix as a scaffold material.

The use of cartilage as a substitute for bone tissue has been vastly explored in the 50s to 80s of the last century[11-14]. It has been shown that autologous or isogenic cartilage transplantation in rats induced bone formation[12, 14]. This effect was affected by donor age and predominantly observed for tissue obtained from young donor animals[12, 13]. Another important prerequisite for *in vivo* bone formation was the presence of viable cartilage cells[12, 13]. Additionally, despite its potential in auto and isotransplantation, ossification of the cartilage matrix was never seen in xenotransplantation[12]. This property would render clinical application of decellularized xenogenic cartilage-derived matrix limited as a biomaterial for endochondral bone regeneration.

To summarize, recently, the use of decellularized cartilage-derived matrix (CDM) has gained attention and its potential for cartilage regeneration was recognized[15-19]. Moreover, preliminary *in vivo* studies indicated that a CDM scaffold could be effective in regenerating bone and cartilage in an osteochondral defect model[15]. In this previous study, the CDM scaffold was cell-free, and it remains unknown if preseeding of the construct with multipotent stromal cells is a prerequisite for endochondral bone regeneration.

To address the latter, we here investigated the feasibility of decellularized cartilage-derived matrix (CDM) xenografts as a scaffold material for ectopic endochondral bone regeneration. Our main question was whether the unseeded scaffolds could attract host cells and induce endochondral bone regeneration. This would offer the prospect of generating off-the-shelf bone constructs consisting of CDM only. The performance of the unseeded CDM scaffolds was compared to that of CDM seeded with human MSCs.

MATERIALS AND METHODS

Experimental design

An overview of the experimental layout is shown in Table 1. The induction of bone tissue formation was evaluated in subcutaneous dorsal pockets of immunocompromised rats. To test the intrinsic osteoinductivity of the CDM scaffold material, samples were either preconditioned with human MSCs (MSC-seeded) or remained unseeded. Human MSCs were chosen with the eventual application in patients in mind. An equine source was chosen to be able to obtain sufficient amounts of cartilage for CDM preparation and in view of potential translation to both human and equine patients. Moreover, equine cartilage closely resembles human cartilage in both histological and biochemical properties[20].

The MSCs were seeded and expanded prior to chondrogenic differentiation *in vitro*. The samples were implanted for a total of 8 weeks. The number of samples taken for each analysis varied as indicated in the table.

Multipotent Stromal Cell isolation and culture

A bone marrow aspirate was taken from the iliac crest of a 69-year old male human patient receiving a total hip arthroplasty following his informed consent according to a protocol approved by the local Medical Ethics Committee (University Medical Center Utrecht). The cells were separated on Ficoll-paque and the mononuclear fraction was then plated for selection on plastic-adherence, as described previously[8]. The cells were passaged at subconfluency and maintained in expansion medium containing αMEM (Minimum Essential Medium α; Invitrogen), with 10% heat-inactivated fetal bovine serum (BioWhittaker), 0.2mM L-ascorbic acid 2-phosphate (Sigma), 100U/mL penicillin with 100mg/mL

Table 1: Overview of the experimental set-up including the time frame and numbers of samples.

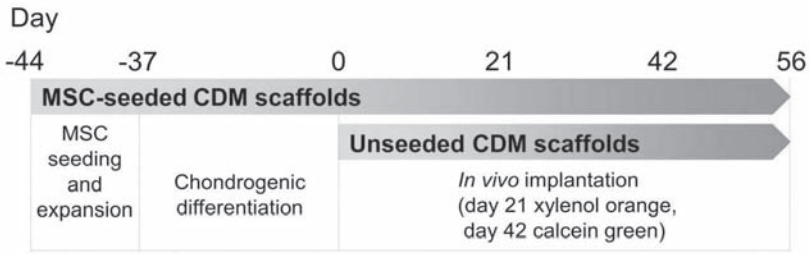

Analysis	N	Day
Histology paraffin	3 seeded 3 unseeded	0
	1 seeded	22*
	7 seeded 6 unseeded	56
Histology MMA	7 seeded 7 unseeded	56
X-ray	14 seeded 13 unseeded	56

* One animal died before the intended end of the experiment at day 22

streptomycin (PenStrep, Invitrogen), and 1ng/mL basic fibroblast growth factor (bFGF, R&D Systems). At passage 4, they were harvested for scaffold seeding.

The potential of the MSCs for multilineage differentiation into adipogenic, osteogenic, and chondrogenic cells was confirmed[8]. Also, FACS analysis was performed for confirmation of the presence of CD73 (BD Pharmagen), CD90 (Biolegend), CD105 (Abcam) and for the absence of CD31 (Serotec), CD34 (BD Pharmagen), and CD45 (BD Pharmagen). Isotype matched controls (Life Science) were also analyzed.

Scaffold preparation

Equine cartilage from 7 donors (age 3-10) was harvested post-mortem from the femoral condyles of the stifle joints after obtaining permission of the owners. The joints were stored at -20°C prior to tissue harvest. The cartilage was removed from the femoral condyles, cut into small pieces with a surgical blade and immersed in PBS supplemented with 10% PenStrep and 10% fungizone (Life Technologies™). Next, the cartilage was subjected to multiple enzymatic and mechanical treatment steps, as described previously[21]. The resulting CDM was transferred into cylindrical molds (3.5mm diameter, 10 mmhigh) and freeze-dried for 24 hours. The scaffolds were cross-linked by UV exposure[22] overnight and sterilized using ethylene-oxide. Before cell seeding, the scaffolds were cut to measure 5mm in height and pre-soaked for one hour in expansion medium without bFGF.

Scaffold seeding and differentiation

The hMSCs were seeded onto the porous scaffolds in two steps. In total, 700,000 cells were suspended in 50µl of expansion medium for each scaffold. In the first round, half of the volume was applied along the mantle of the scaffold cylinder. After one hour, the scaffolds were turned 180°C before pipetting the second half of the suspension onto the scaffolds. On day 7, the medium was changed from expansion to chondrogenic differentiation medium consisting of high glucose Dulbecco's modified Eagle's medium (Invitrogen) with 1% ITS + premix (BD Biosciences), 10^{-7}M dexamethasone (Sigma), 0.2mM L-ascorbic acid 2-phosphate, PenStrep, and 10ng/mL TGFβ2 (R&D Systems). The seeded scaffolds were maintained in 24-wells plates while medium was refreshed twice a week until implantation. Following 37 days in differentiation medium three scaffolds were fixed in formalin for histological analysis.

The two groups of scaffolds that were implanted subcutaneously were either cell-seeded as described above, or unseeded. The unseeded scaffolds were not pre-soaked prior to implantation.

Implantation in immunocompromised rats

The experiment in rats was approved by the local Ethics Committee for Animal Experimentation and in compliance with the Institutional Guidelines on the Use of Laboratory Animals. The experiment was performed on male, athymic nude rats (Hsd:RH-Foxn1^{rnu}, 11 weeks, Harlan, The Netherlands) that were anaesthetized with 2.5% isoflurane and air/oxygen. Subcutaneous pockets were created from 7-10mm dorsal incisions, to each fit one scaffold. Each pocket was created by blunt dissection through the skin incision and filled with one implant. The skin was closed transcutaneously with Vicryl Rapide sutures (Ethicon, Germany). Before and after the operation, the animals received 0.05mg/kg buprenorphin subcutaneously (Temgesic, Schering-Plough/Merck, USA). The rats were housed in pairs at the Central Laboratory Animal Institute of Utrecht University. At week 3 and 6 after implantation, all animals received subcutaneously administered fluorochromes, 100mg/kg xylenol orange (Sigma) and 10mg/kg calcein green (Sigma), respectively. These fluorochromes are known to bind free calcium ions before their incorporation in active mineralization processes, thus indicating sites of active bone formation after the moment of injection[23, 24]. At 8 weeks, the rats were euthanized by CO_2/O_2 inhalation and the scaffolds were explanted and fixed in formalin.

X-ray and fluorescence imaging

While in formalin, the explants were imaged in 2D in a Faxitron® x-ray system with a dose of 22kV for 12 seconds, taking along a femur and tibia of the rats as a positive control. Mineralized areas in the samples were clearly delineated and their brightness was comparable to that of rat bone controls. Using Adobe Photoshop CS5, the total surface area of

the mineralized tissue was quantified and the pixel dimensions were converted to mm^2. To illustrate the total number of samples of the groups that did show mineral content on the x-ray, a ratio was calculated as: ratio of positive x-rays=number of samples with mineral content/ total number of samples in the group.

Additionally, the explants were examined by whole mount fluorescence microscopy using a triple filter (Olympus) for simultaneous detection of the red and green fluorochromes. After image analysis, the explants were further processed and embedded in paraffin or methylmethacrylate (MMA).

Histology and immunohistochemistry on paraffin sections

Explanted samples (n=7 for MSC-seeded CDM, n=6 for unseeded CDM) were decalcified in Luthra solution (0.35M HCl and 2.65M formic acid in distilled water), before dehydration, embedding in paraffin, and sectioning (5µm). For identification of cartilage and bone, a triple stain of Safranin-O, fast green and hematoxylin was used[8].

Besides subcutaneous implants, these rats had also received samples in one critical defect in one of their femora. However, only subcutaneous samples were included in analyses of the present study. One rat died at day 22 after implantation during revision surgery of a loosened internal fixator. Samples retrieved from this animal were not decalcified but fixed in formalin and directly embedded in paraffin. On sections from this animal mineralization could be visualized by a von Kossa staining with Mayer's hematoxylin counterstaining, as well as the presence of tartrate-resistant acid phosphatase (TRAP) in osteoclasts. TRAP is secreted by active osteoclasts that resorb mineralized cartilage or bone in order to be remodeled into new bone. For TRAP staining, sections were deparaffinized and rehydrated, before incubation in 0.2M acetate buffer containing 50mM L-(+)tartaric acid (Sigma) at pH 5.0 for 20 minutes at room temperature. Next, TRAP activity was stained by adding 0.5mg/ml Naphtol AS-MX phosphate and 1.1mg/ml Fast red TR salt (both from Sigma) to this solution and incubating at 37°C for 1-4 hours. Finally, the sections were counterstained with Mayer's hematoxylin.

Immunohistochemical detection of collagen types I, II, and X was performed after deparaffinization and rehydration of the sections. The reactivity of the collagen type I antibodies was extensively tested on rat, human and equine tissues. It was found that the mouse anti-human I-8H5 antibody could recognize both human and equine collagen type I, but not collagen from rat origin. On the other hand, the rabbit anti-rat ABT-123 antibody exclusively detected rat collagen type I and not collagen of equine or human origin.

All sections were blocked to prevent non-specific binding in 5% bovine serum albumin and 0.3% H_2O_2. For collagen type I (human) and type II, antigen retrieval was performed by incubation with 1mg/mL pronase (Sigma) and 10mg/mL hyaluronidase (Sigma) for half an hour each. Retrieval of rat collagen type I was performed by boiling the sections for 10 minutes in 10mM citrate buffer, pH 6.0. Collagen type X antigen was retrieved by incubation at

37°C in 1mg/ml pepsin (Sigma) in 0.5M acetic acid for 2 hours and in 10mg/mL hyaluronidase (Sigma) for half an hour. Next, sections were incubated with the primary antibodies for collagen type I (1:100, monoclonal mouse anti-human, CP17 clone I-8H5, Millipore; and 1:50, polyclonal rabbit anti-rat, ABT123, Millipore), collagen type II (1:100, monoclonal mouse, II-II6B3, DSHB) and collagen type X (1:20, Quartett), all at 4°C overnight. Subsequently, collagen type I (human) and type II sections were incubated with GAM-HRP (1:200, P0447, Dako) at room temperature for an hour. Collagen type I (rat) sections were incubated with goat anti-rabbit biotinylated antibody (1:200, E0432, Dako) and with SA-HRP (1:400, Dako), both for one hour at room temperature. Collagen type X sections were incubated with a biotinylated secondary antibody (1:200, GE Healthcare, RPN1001V) for 1 hour at room temperature, after which they were incubated with SA-HRP (1:400, Dako) for an hour at room temperature. All collagen types were detected by a 10-minute conversion of 3,3'-diaminobenzidine solution (Sigma). Nuclei were counterstained with 50% Mayer's hematoxylin. Isotype control stainings were carried out with a murine IgG1 monoclonal antibody (Dako) at concentrations matching those used for the primary antibodies or by incubation without primary antibody. The stained sections were examined by using a light microscope (Olympus BX51).

To examine the fate of the implanted cells, human mitochondria were stained. Following deparaffinization and rehydration of paraffin sections, the antigen was retrieved by cooking the sections in Tris-EDTA (pH 9, 10mM Tris-HCl, 1mM EDTA), at 95°C for 30 minutes. Then, sections were blocked in 3% H_2O_2, washed and incubated with the primary antibody overnight at 4°C (1:1000, anti-mitochondria, Abcam). The anti-mouse, HRP-labeled Envision+ system (Dako) was used for 30 minutes before the staining was performed with the DAB+ Substrate Chromogen System (1:100, Dako). Section were counterstained with hematoxylin before mounting in depex.

Histology and fluorochrome detection on MMA sections

Undecalcified samples (n=7 for both groups) were dehydrated and embedded in polymethylmethacrylate, MMA. Sections of 20-30µm were generated along the long axis of the cylindrical samples on a saw Microtome system (Leica 4 SP1600, Germany). The axial sections were stained with methylene blue and basic fuchsine and evaluated by light microscopy. In addition, sections were made that remained unstained to evaluate the presence of fluorochromes.

Statistics

The raw data of the 2D quantification of mineralized areas in the Faxitron images were expressed as 'pixel^2'. These data were analyzed with in IBM® SPSS® Statistics, version 20. An independent samples *t*-test was performed, assuming unequal variances, to compare the 2D

projected areas containing mineral in images from CDM samples that were MSC-seeded (n=14) or unseeded (n=13). A $p<0.05$ was considered significant.

RESULTS

In vitro chondrogenesis of hMSCs in CDM scaffolds

The hMSCs spread throughout the CDM scaffold pores and formed matrix containing proteoglycans and collagen type II, the main cartilage matrix components. Cell differentiation and cell density were inhomogeneous, although hMSCs were seeded according to the same protocol into each scaffold, and the cells were able to spread throughout the complete interior of the CDM scaffolds (Figure 1). The cells had also invaded several CDM particles. In general, most deposition of glycosaminoglycans was observed at the circular periphery of the constructs.

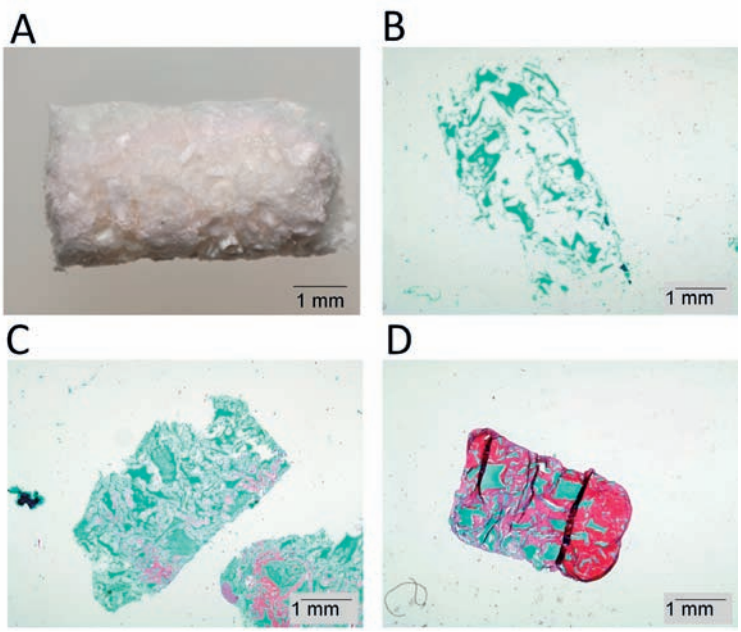

Figure 1: Extent of MSC chondrogenesis in CDM scaffolds demonstrated by safranin-O staining after 37 days of *in vitro* preconditioning. (B-D) Glycosaminoglycans are stained in red while the remaining collagenous tissue is stained green. (A) Macroscopic image of unseeded cylindrical CDM scaffold. (B) Safranin-O-stained paraffin section of an unseeded control scaffold, showing no Safranin-O positive components. (C) Safranin-O-stained paraffin section of human MSC-seeded CDM scaffold that was chondrogenically differentiated for 37 days, containing little glycosaminoglycans (GAGs). (D) Safranin-O-stained paraffin section of human MSC-seeded CDM scaffold showing extensive GAG deposition by the seeded cells. Note that the cells in (C) and (D) have caused sample compaction as compared to the unseeded scaffold in (B).

In vivo ectopic endochondral bone formation in CDM scaffolds

X-ray analysis showed that mineralized tissue was predominantly present in the MSC-seeded samples (Figure 2). Mineralization in the MSC-seeded constructs was evident by x-ray in 13 out of 14 samples, yet the extent of mineralization varied considerably (Figure 2B-D). In contrast, negligible mineralization was present in the unseeded CDM scaffolds. The average size of the mineralized area in MSC-seeded constructs was 4.08 ± 3.75mm^2, while significantly less mineral deposition (0.08 ± 0.17mm^2, p=0.002) was found in the unseeded controls (Figure 2I). Only three of the unseeded control samples contained a small (<0.5mm^2) area that was mineralized under x-ray examination, of which one contained the red fluorochrome. As the originally implanted cylindrical samples had a 2D-projected surface area of 15mm^2, the aforementioned numbers would roughly represent 27.2 ± 25.0% of mineralized area in the MSC-seeded samples and 0.5 ± 1.1% of mineralized area in the unseeded samples.

For the MSC-seeded constructs, it was observed that the red fluorochrome, xylenol orange, was incorporated at the periphery of the newly formed bone tissue at week 3 (Figure 2L-M). Although calcein green was administered 3 weeks after xylenol orange, it was incorporated inwards from the initially delineated area of bone formation at week 6, indicating an inwardly directed progression of mineralization (Figure 2N).

After 8 weeks of implantation, bone formation was evident in the cell-seeded constructs (Figure 3). The circular periphery of the 8-week hMSC-seeded constructs harbored cartilaginous tissue containing glycosaminoglycans and collagen type II (Figure 3A,B). Both scaffold remnants and tissue deposited by the implanted cells stained positive for collagen type II. Besides, neotissue that was negative for human and equine collagen types I and II was identified at the periphery of the construct as well (indicated by B in Figure 3B,C). In Figure 3, the development of bone marrow cavities can be observed morphologically, containing both types of marrow: hematopoietic marrow and fatty bone marrow. Furthermore, morphological evidence and the presence of mineralized cartilage further indicated that new bone had formed via the endochondral pathway (Supplementary Figure 2). However, all samples retrieved after 8 weeks did undergo decalcification in Luthra solution, which did not allow staining of collagen types I (rat) and X, TRAP, or von Kossa.

As mentioned previously, one cell-seeded sample was harvested at day 22. As this sample did not undergo decalcification, it was processed to paraffin to confirm the endochondral process of bone formation. Active matrix remodeling was observed at the circular periphery this MSC-seeded construct, which indicated endochondral bone formation. At the circular periphery of the implant, tissue rich in glycosaminoglycans was present (Figure 4A). Also, a matrix rich in collagen type I of human origin was present between the scaffold particles (Figure 4B). Collagen type II of human and/or equine origin was detected in the newly deposited matrix and in the CDM particles (Figure 4D). Small areas positive for collagen type X of human origin were observed at the circular periphery of the construct, specifically

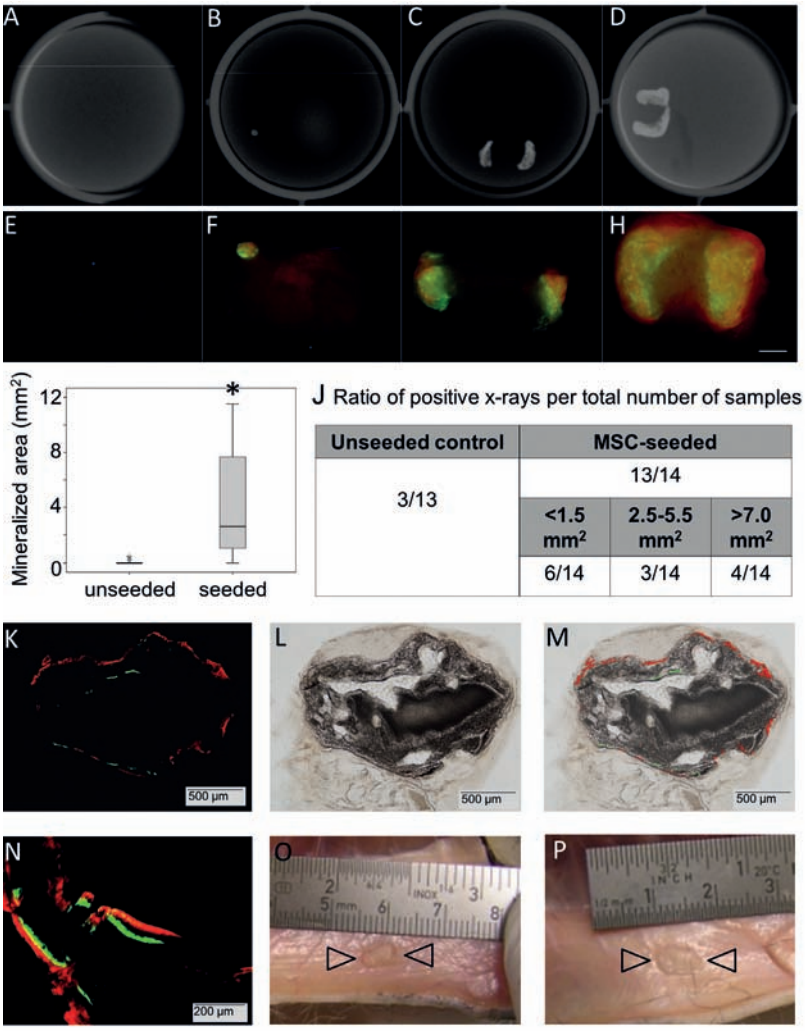

Figure 2: Significantly more bone was formed in MSC-seeded constructs compared to unseeded CDM. (A-D) X-ray representations of an average unseeded (A) control sample and the lowest (B), average (C) and highest (D) mineralized areas in MSC-seeded CDM scaffolds, following an 8-week subcutaneous implantation period. (E-H) Whole-mount fluorescence images of the explants (in A-D, respectively) showing the fluorochrome incorporation in the newly formed bone tissue at 3 (red) and 6 (green) weeks of implantation. (I) The extent of mineralization was measured on x-ray images of all explants and calculated as mm^2 in the 2D representations. Significantly more mineralized tissue formation was observed in the MSC-seeded versus the unseeded samples. Note that the theoretical maximum surface area was $15mm^2$. (J) The ratio of the numbers of samples showing mineral deposition on x-ray over the total number of samples in that respective group is shown for all samples. For the MSC-seeded samples also the number of samples showing lowest ($<1.5mm^2$), average ($2.5\text{-}5.5mm^2$), and highest ($>7.0mm^2$) mineralized areas are included. (K-N) In MSC-seeded samples, fluorochrome incorporation was shown on MMA-sections. The pattern of fluorochrome incorporation in general was that the red (3 week) label was present on the outer periphery of the formed bone, while the green label (6 weeks) was located inward. (O,P) Macroscopic appearance of MSC seeded (O) and unseeded (P) constructs upon explantation.

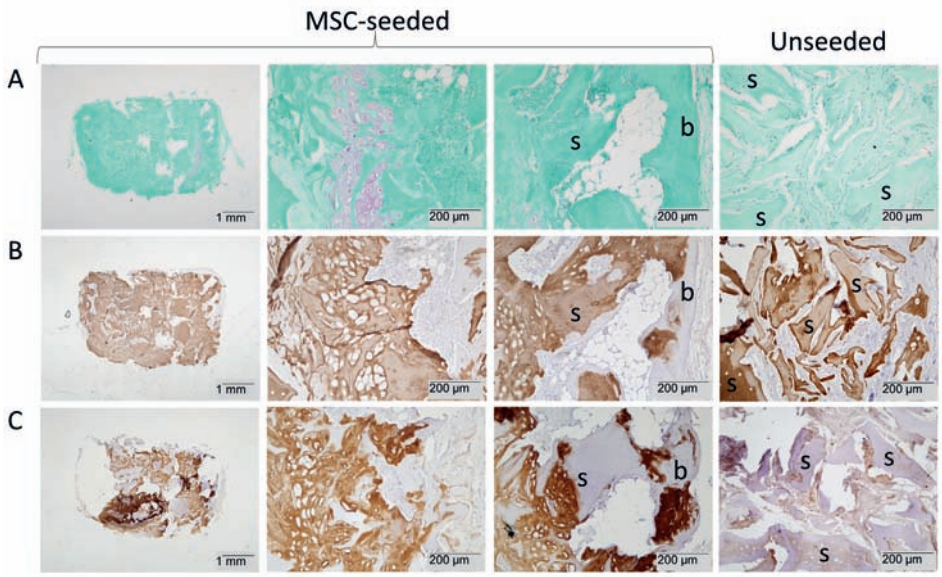

Figure 3: All aspects of endochondral bone formation were apparent after 8 weeks of subcutaneous implantation in MSC-seeded samples only (columns 1-3). Unseeded samples did not show bone formation (column 4). (A) Cartilaginous neotissue was indicated by Safranin-O staining in MSC-seeded constructs. In the lacunae also hypertrophic cells were present. No safranin-O stained tissue was observed in the unseeded constructs. (B) At the sites of bone formation, the cartilaginous collagen type II staining is partly replaced by bone ('b' in image, lightly stained in purple by hematoxylin). Unseeded constructs contained collagen type II only in the scaffold material but not in the fibrous ingrowth. (C) Collagen type I of human and/or equine origin was present in the neotissue, between CDM scaffold remnants (s) in MSC-seeded constructs. The scaffold material did not stain for collagen type I. As the newly formed bone stained negative for human collagen type I, its most likely origin is rat.

indicating hypertrophic differentiation of the implanted human MSCs (Figure 4E). Active remodeling of the hypertrophic cartilage matrix at these sites was shown by a TRAP staining that revealed osteoclast activity (Figure 4F). The areas undergoing remodeling also contained mineral depositions (Figure 4G). In addition, the early onset of the formation of bone marrow cavities was observed already after 22 days (Figure 4C,E). Noteworthy, several small areas of woven bone were visible at the construct periphery, which were not stained by the human and equine collagen antibodies. The patches did however react with a rat-specific antibody for collagen type I, confirming bone formation of rat origin (Figure 4C).

Finally, the predominant presence of bone formation in the MSC-seeded CDM scaffolds, as compared to the unseeded scaffolds, was also observed on the basic fuchsin-stained MMA sections (Figure 5). The newly formed bone was mainly found at the periphery of the CDM constructs and had a woven and trabecular appearance. At the interface between de CDM matrix and newly formed bone, clear signs of endochondral ossification could be observed with mineralization of the cartilaginous matrix. Within the trabecular bone

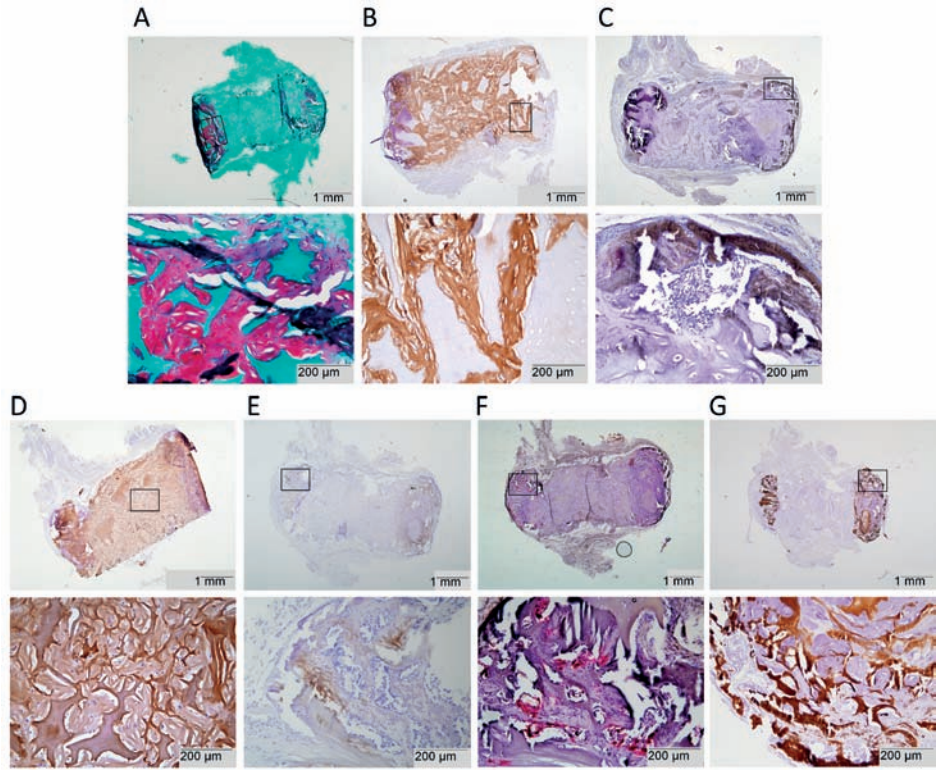

Figure 4: Tissue formation after 22 days of implantation (n=1) on undecalcified paraffin sections. Active remodeling of cartilaginous matrix into host-derived bone by the endochondral route was shown at the circular ends of the cylindrical construct. (A) Safranin-O stained sections showing the presence of proteoglycans in the construct at the circular cylinder ends. (B) Collagen type I was produced in the constructs by the seeded MSCs. As the antibody does not detect collagen type I produced by rat cells, it is assumed that this matrix is deposited by the implanted human cells. (C) Collagen type I of rat origin was produced in the construct periphery where the newly formed bone was laid down. (D) Collagen type II was detected both in the equine scaffold material and in the neotissue in the construct. (E) At the circular cylindrical ends, remnants of collagen type X production are shown. This matrix was produced by the implanted cells as the antibody did not react with rat collagen type X. (F) Active matrix remodeling was revealed by TRAP staining of multinucleated osteoclasts in red. (G) Mineralization of predominantly the CDM scaffold was present at the periphery of the construct.

structure, bone marrow cavities had formed containing both hematopoietic and fatty bone marrow. In contrast to the bone formation in the MSC-seeded scaffold, the resorbed areas of the unseeded scaffolds were replaced by fibrous tissue that also infiltrated the scaffold pores. Only in one construct of the unseeded scaffolds, a very small area of bone formation was observed.

The fate of the implanted human cells was examined by anti-human mitochondrial staining on day 22 and on week 8 after implantation (Supplementary Figure 3, A-D and E-H, respectively). Human cells were detected in the cartilaginous tissue that was deposited by

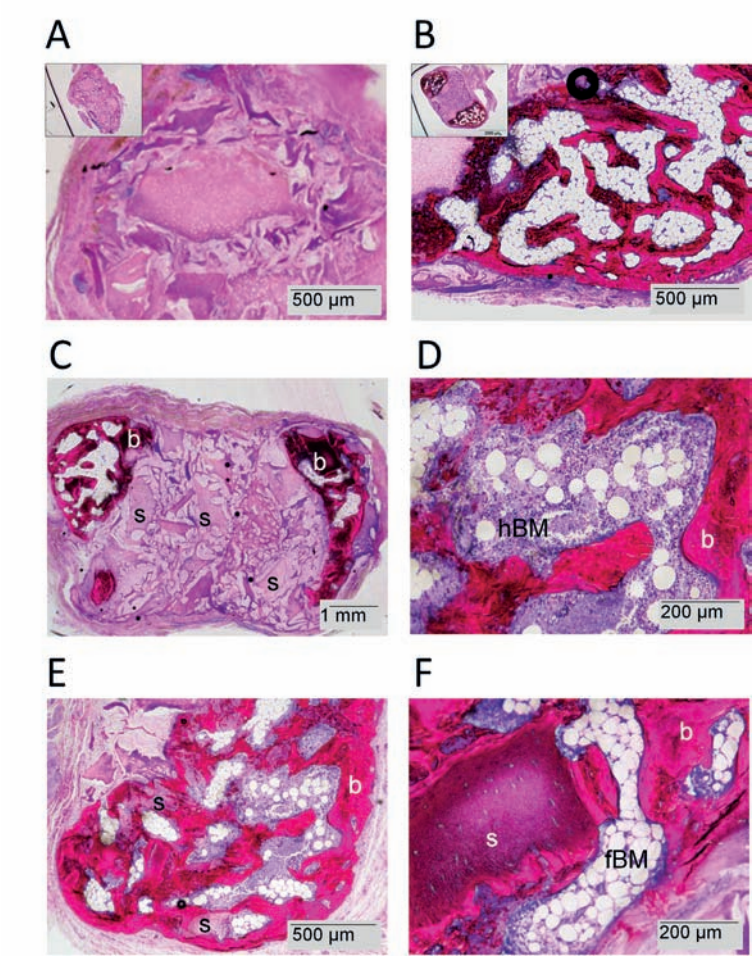

Figure 5: Bone formation (b) was only present on MMA sections from MSC-seeded constructs after 8 weeks of subcutaneous implantation. Loose fibrous tissue was observed among the CDM particles in unseeded control scaffolds (A), while the seeded samples contained areas of bone formation, including bone marrow cavities (B-F). (C) Bone formation was evident at the construct periphery (B) and scaffold remnants were present (s). The marrow cavities contained hematopoietic bone marrow (D, hBM) and also fatty bone marrow (F, fBM). (E) Besides cell-derived matrix, the CDM particles (s) were also mineralized.

the human cells but not in the fibrous infiltrate. Next to the bone marrow, the tissue's cells were a mixture of human (green arrowhead) and rat (open arrowhead) cells. On Safranin-O stained consecutive sections, the tissue appeared to be composed of a mixture of newly formed bone (dashed lines) and other tissue. Overall, human cells were present in areas of bone formation but from our results it was not possible to establish whether they were present in the newly formed bone itself.

DISCUSSION

The concept of developmental engineering[1] suggests that understanding and mimicry of natural processes can assist in improving tissue regeneration. We applied this concept by using current knowledge on endochondral bone development from a cartilaginous tissue template. While most endochondral bone tissue regeneration approaches rely on cartilage tissue engineering to create a cartilage extracellular matrix, we explored the potential of a decellularized cartilaginous scaffold for this purpose. Here we report on the successful ectopic bone regeneration from a material of xenogenic origin containing xenogenic MSCs and their matrix.

Effects of cells and culture methods

The present study showed effective bone regeneration at a subcutaneous location in CDM scaffolds implanted with MSCs. The implanted cells were chondrogenically primed for 37 days before implantation. This preconditioning period did not induce *in vitro* matrix mineralization and was within the previously reported ranges required for induction of ectopic endochondral bone formation from predominantly pellet cultures, varying from two[1] or four[2], to six[10] or seven[5] weeks of *in vitro* preconditioning in chondrogenic media. Induction of hypertrophy during the *in vitro* preconditioning period has had positive effects[1], while *in vitro* mineralization of the matrix had negative effects[3] on the *in vivo* endochondral process. Overall, the induction of hypertrophy by thyroid hormone was not considered crucial for endochondral bone regeneration[1, 2, 5] and therefore omitted in the present study.

During our preconditioning period, the MSCs had started to produce a cartilaginous matrix, rich in glycosaminoglycans. The most intense staining for GAGs following the *in vitro* preconditioning period was observed at the circular periphery of the constructs. This spatial pattern later coincided with the regions of bone formation in the *in vivo* samples. This tendency may indirectly support the assumption that regions of optimal *in vitro* cartilage tissue formation, give rise to *in vivo* bone formation. Moreover, this may explain the variability in the extent of bone formation among the MSC-seeded *in vivo* samples. After all, the applied seeding methods and preconditioning period cannot guarantee homogeneous tissue formation by the MSCs *in vitro* and thus no homogeneity in tissue formation upon implantation.

Inhomogeneous tissue differentiation in the constructs could be caused by nutrient limitations[25]. However, it is expected that if the geometry of the constructs pores would be carefully controlled that still a considerable increase in construct size can be obtained by adding CDM particles to a construct. In addition, flow-perfusion of the *in vitro* culture can also assist in providing sufficient nutrients to the core of the construct[26]. The issue of necrotic core development, which can start as soon as the construct is removed from a flow-

perfusion system, will however still apply to large cartilaginous constructs for endochondral bone formation. Nevertheless, if it would be possible to pinpoint the optimal time window for implantation, dying hypertrophic cells could be implanted that secrete the angiogenic factors. This way, construct size could be increased without core necrosis.

The timing of events in our study was comparable to those observed during endochondral bone from living cartilage implants[13], where the onset was discerned after 3-4 weeks and completion of matrix remodeling into bone by week 8. Further, in line with previous findings[2, 4], new bone in our CDM scaffolds was formed by host cells that had infiltrated the construct. This was shown by the absence of type I collagen of human origin and abundance of rat-derived collagen type I in the newly formed bone tissue. However, immunohistochemical detection did reveal the presence of human cells up to 8 weeks after implantation in areas of newly formed bone tissue (Supplementary Figure 3). It has been suggested previously that implanted MSCs could contribute to bone formation[2, 10] and do not reside in the hematopoietic niche[10] after the hypertrophic cartilage has been replaced by bone. For transplanted cartilage tissue, it was estimated that 1% of bone cells had originated from the implanted chondrocytes[13]. In the present study, the matrix origin has been identified next to the cellular origin. Our data suggest that overall, new bone consists of rat-specific collagen type I.

The implanted cells were still present at 22 days after implantation, both in cartilaginous and bone-like tissues. It has been reported before that these implanted cells actually do contribute to the bone formation and end up encapsulated in the bone matrix[1, 10]. The contribution of these cells is still elusive, whether the hypertrophic chondrocytes transdifferentiate to the osteoblastic lineage or the MSCs become osteoblasts directly, or a mixture of both, remains disputable.

Effects of CDM composition

Although equine age is known to affect GAGs in the cartilage matrix[27], this factor is not expected to have a major impact on our results as our decellularization protocol resulted in negligible amounts of GAG in the CDM scaffolds. In fact, CDM scaffolds do contain mainly type II collagen, and collagen composition of equine cartilage has been shown not to significantly change with age[28].

The CDM scaffolds that were obtained after decellularization in the present study contained negligible remnants of glycosaminoglycans[29]. However, other decellularization protocols may result in as many different scaffold compositions. For example, the GAG content of decellularized cartilage can vary depending on the number of SDS (sodium dodecyl sulfate) cycles involved[30]. Therefore, several decellularized cartilage scaffolds have been developed that do contain GAGs[30, 31], in contrast to the scaffolds evaluated in the present study. Notably, in order to retain GAGs in the scaffolds, concessions have to be made in terms of the level of decellularization[15]. Likewise, all other steps in a decellularization

protocol can affect the performance of the final product. Future studies may therefore focus on elucidation the influence of CDM composition on *in vivo* bone formation.

The exact contribution of the GAG-rich matrix to ectopic bone formation is unclear. Besides the effects of the seeded cells, the matrix may have been important since it was lacking in the unseeded control scaffolds. It is for example likely that the growth-factor retaining potential of the GAG structures[32] played a certain role in for example recruitment of host cells and local stimulation of cellular processes. In a previous study, a reduced GAG content of cartilaginous tissues resulted in a delayed progression of bone formation from articular cartilage implants[13]. In contrast, the removal of GAGs and subsequent inhibition of GAG synthesis did not inhibit bone formation in cartilage that was transplanted to the anterior chamber of the eye[13]. These contradicting results stress the need for future studies into the necessity of GAGs in decellularized cartilage-derived matrix for ectopic endochondral bone regeneration.

Overall, our data indicate that the presence of the MSCs stimulated bone formation. One factor or a combination of the following may have contributed to the onset of endochondral bone formation: (a) component(s) of the decellularized cartilaginous matrix, or the matrix or other factors produced by the MSCs. Future studies may therefore incorporate devitalized preconditioned samples to distinguish the effects of the cells and the matrix or factors they produce.

Further, the simultaneous occurrence of intramembranous bone deposition next to the observed endochondral bone formation cannot be excluded based on our results.

Effects of implantation model

The ectopic implantation model is suitable for screening of the osteoinductive capacity of different construct compositions. Although this environment is challenging for establishing bone formation, MSC-seeded CDM samples successfully regenerated bone tissue. So far, ectopic bone regeneration in devitalized cartilaginous constructs has not been successful[12, 13, 33]. Of course, inclusion of healthy, non-immunocompromised animals in the model could result in a different outcome and will be subject of our future studies.

This study shows that re-vitalizing a CDM matrix with pre-cultured MSCs in chondrogenic medium helps to regain its osteoinductive potential. However, the presence of cells may not be a prerequisite for endochondral bone formation in CDM at orthotopic locations. In previous studies, bone did regenerate from unseeded decellularized cartilage in an osteochondral defect in one instance[15]. As bone marrow-derived MSCs may have access to the scaffold in an osteochondral defect model, an unseeded scaffold will probably behave differently at an orthotopic location or at a site of fracture healing. If indeed unseeded scaffolds could stimulate endochondral bone formation at an orthotopic site, there is a great promise for pursuing clinical application by going towards a cell-free, off-the-shelf solution for bone regeneration at orthotopic sites.

CONCLUSION

Endochondral bone formation at ectopic location is greatly enhanced by the presence of viable chondrogenic MSCs in decellularized CDM scaffolds compared to unseeded control scaffolds.

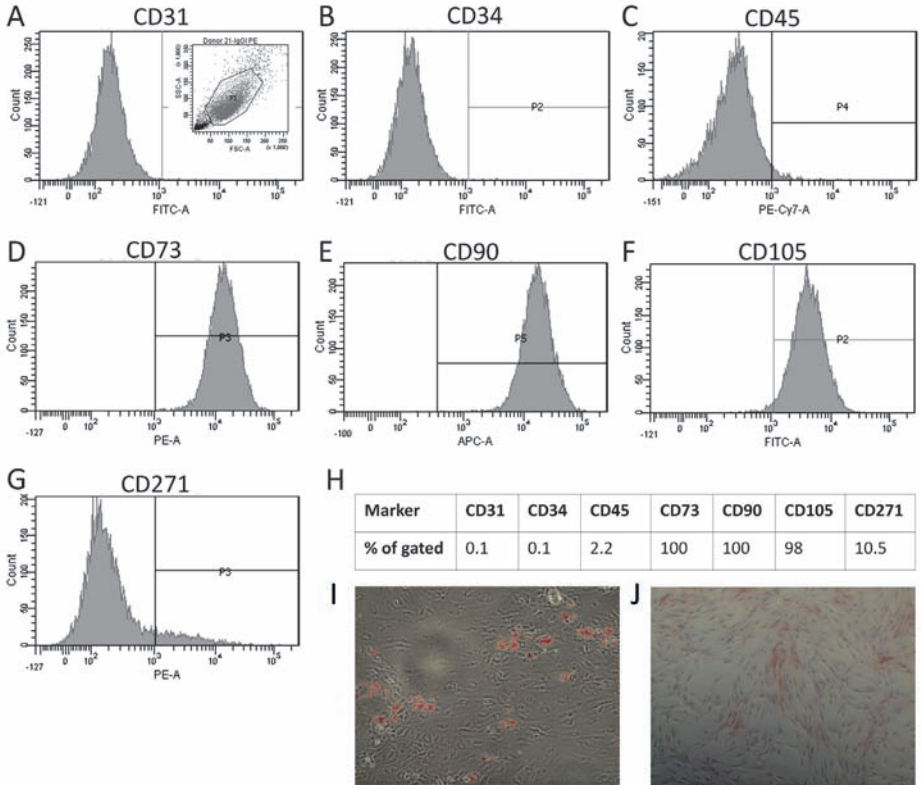

Marker	CD31	CD34	CD45	CD73	CD90	CD105	CD271
% of gated	0.1	0.1	2.2	100	100	98	10.5

Supplementary Figure 1: MSC characterization by expression of surface markers and adipogenic and osteogenic differentiation capacity. The flow cytometry results are shown for CD31 (A), CD34 (B), CD45(C), CD73 (D), CD90 (E), CD105 (F), and CD271 (G). The percentages of positive cells of the gated population (inset in A) are presented in the table (H). Oil red O-stained fat vesicles are demonstrated (I) and ALP activity is stained in red (J).

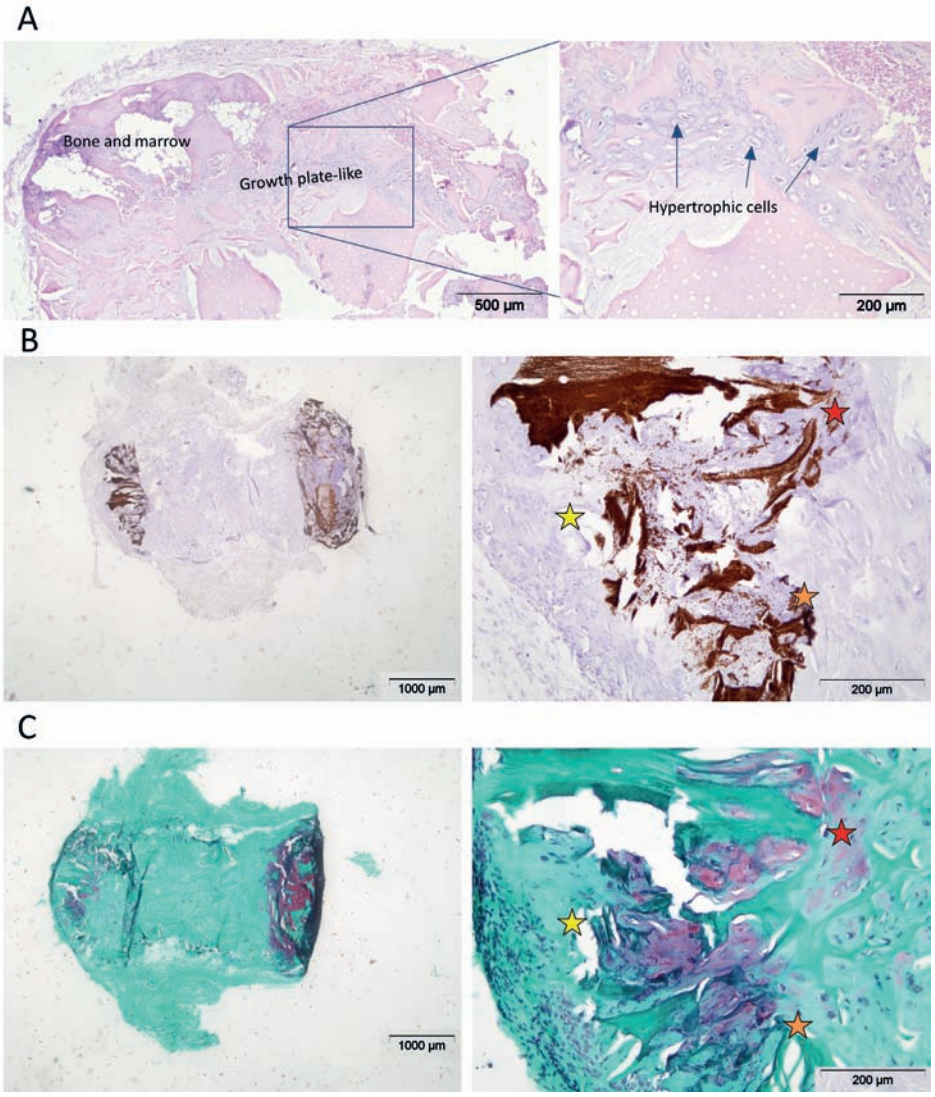

Supplementary Figure 2: Several hallmarks of endochondral bone formation are shown. (A) Hypertrophic chondrogenic cells (arrows) in an MSC-seeded implanted sample after 8 weeks of subcutaneous implantation (hematoxylin/ eosin stained paraffin section). (B) Von Kossa-stained undecalcified paraffin sections of the sample that was retrieved after 3 weeks of subcutaneous implantation. (C) For comparison, consecutive sections were stained with Safranin-O to demonstrate the presence of mineralizing cartilage.

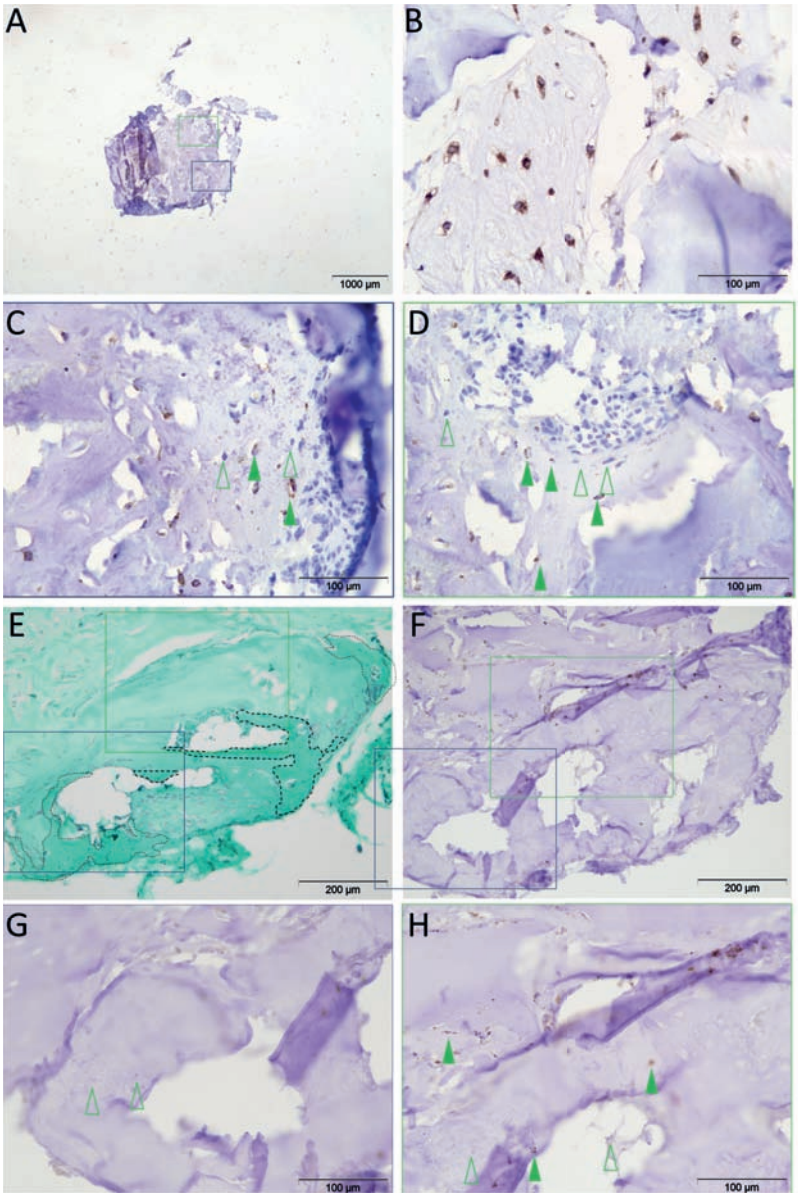

Supplementary Figure 3: Fate of implanted human cells on day 22 (A-D) and 8 weeks (E-H) after implantation. Human cells (brown, green arrowheads) were present in the tissues adjacent to the bone marrow niches (D) along with rat cells (open arrowheads). Also, mixed cell populations were present in mineralizing tissue (C). An *in vitro* cultured control sample shows abundant mitochondrial staining in all cells (B). After 8 weeks human cells are still present in areas where bone is formed (F-H). Newly formed bone (dashed lines in E, safranin-O/fast green staining) is present in these areas as well.

REFERENCES

1. Scotti C, Tonnarelli B, Papadimitropoulos A, Scherberich A, Schaeren S, Schauerte A, et al. Recapitulation of endochondral bone formation using human adult mesenchymal stem cells as a paradigm for developmental engineering. Proc Natl Acad Sci U S A 2010; 107: 7251-7256.
2. Farrell E, Both SK, Odorfer KI, Koevoet W, Kops N, O'Brien FJ, et al. In-vivo generation of bone via endochondral ossification by in-vitro chondrogenic priming of adult human and rat mesenchymal stem cells. BMC Musculoskelet Disord 2011; 12: 31.
3. Farrell E, van der Jagt OP, Koevoet W, Kops N, van Manen CJ, Hellingman CA, et al. Chondrogenic priming of human bone marrow stromal cells: a better route to bone repair? Tissue Eng Part C.Methods 2009; 15: 285.
4. Tortelli F, Tasso R, Loiacono F, Cancedda R. The development of tissue-engineered bone of different origin through endochondral and intramembranous ossification following the implantation of mesenchymal stem cells and osteoblasts in a murine model. Biomaterials 2010; 31: 242-249.
5. Pelttari K, Winter A, Steck E, Goetzke K, Hennig T, Ochs BG, et al. Premature induction of hypertrophy during in vitro chondrogenesis of human mesenchymal stem cells correlates with calcification and vascular invasion after ectopic transplantation in SCID mice. Arthritis Rheum. 2006; 54: 3254.
6. Mackie EJ, Ahmed YA, Tatarczuch L, Chen KS, Mirams M. Endochondral ossification: how cartilage is converted into bone in the developing skeleton. Int.J.Biochem.Cell Biol. 2008; 40: 46.
7. Gawlitta D, Farrell E, Malda J, Creemers LB, Alblas J, Dhert WJ. Modulating endochondral ossification of multipotent stromal cells for bone regeneration. Tissue Eng Part B Rev 2010; 16: 385-395.
8. Gawlitta D, van Rijen MH, Schrijver EJ, Alblas J, Dhert WJ. Hypoxia impedes hypertrophic chondrogenesis of human multipotent stromal cells. Tissue Eng Part A 2012; 18: 1957-1966.
9. Jukes JM, Both SK, Leusink A, Sterk LM, van Blitterswijk CA, de Boer J. Endochondral bone tissue engineering using embryonic stem cells. Proc.Natl.Acad.Sci.U.S.A 2008; 105: 6840.
10. Janicki P, Kasten P, Kleinschmidt K, Luginbuehl R, Richter W. Chondrogenic pre-induction of human mesenchymal stem cells on beta-TCP: enhanced bone quality by endochondral heterotopic bone formation. Acta Biomater 2010; 6: 3292-3301.
11. Gabrielli MF, Okamoto T, Marcantonio E, Barbosa CE. Autogenous transplantation of rib cartilage, preserved in glycerol, to the malar process of rats: a histological study. J Nihon Univ Sch Dent 1986; 28: 87-99.
12. Asch L, Asch G. [Ossification after transplantation of model cartilage in the rat patella]. Arch Anat Histol Embryol 1989; 72: 81-96.
13. Urist MR, Adams T. Cartilage or bone induction by articular cartilage. Observations with radioisotope labelling techniques. J Bone Joint Surg Br 1968; 50: 198-215.
14. Urist MR, Mc LF. Osteogenetic potency and new-bone formation by induction in transplants to the anterior chamber of the eye. J Bone Joint Surg Am 1952; 34-A: 443-476.
15. Benders KE, Weeren PR, Badylak SF, Saris DB, Dhert WJ, Malda J. Extracellular matrix scaffolds for cartilage and bone regeneration. Trends Biotechnol 2013; 31: 169-176.
16. Ye K, Felimban R, Moulton SE, Wallace GG, Di Bella C, Traianedes K, et al. Bioengineering of articular cartilage: past, present and future. Regen Med 2013; 8: 333-349.
17. Schwarz S, Elsaesser AF, Koerber L, Goldberg-Bockhorn E, Seitz AM, Bermueller C, et al. Processed xenogenic cartilage as innovative biomatrix for cartilage tissue engineering: effects on chondrocyte differentiation and function. J Tissue Eng Regen Med 2012.

18. Schwarz S, Koerber L, Elsaesser AF, Goldberg-Bockhorn E, Seitz AM, Durselen L, et al. Decellularized cartilage matrix as a novel biomatrix for cartilage tissue-engineering applications. Tissue Eng Part A 2012; 18: 2195-2209.
19. Elder BD, Eleswarapu SV, Athanasiou KA. Extraction techniques for the decellularization of tissue engineered articular cartilage constructs. Biomaterials 2009; 30: 3749-3756.
20. Malda J, Benders KE, Klein TJ, de Grauw JC, Kik MJ, Hutmacher DW, et al. Comparative study of depth-dependent characteristics of equine and human osteochondral tissue from the medial and lateral femoral condyles. Osteoarthritis Cartilage 2012; 20: 1147-1151.
21. Benders KEM, Boot W, Cokelaere SM, Van Weeren PR, Gawlitta D, Bergman HJ, et al. Multipotent stromal cells outperform chondrocytes on cartilage-derived matrix scaffolds. Cartilage 2014; Epub ahead of print, doi:10.1177/1947603514535245.
22. Yang Z, Shi Y, Wei X, He J, Yang S, Dickson G, et al. Fabrication and repair of cartilage defects with a novel acellular cartilage matrix scaffold. Tissue Eng Part C Methods 2010; 16: 865-876.
23. van Gaalen SM, Kruyt M, Geuze R, de Bruijn J, Alblas J, Dhert W. The use of fluorochrome labels for in vivo bone tissue engineering research. Tissue Eng Part B Rev 2009; 16: 209-217.
24. Pautke C, Vogt S, Tischer T, Wexel G, Deppe H, Milz S, et al. Polychrome labeling of bone with seven different fluorochromes: enhancing fluorochrome discrimination by spectral image analysis. Bone 2005; 37: 441-445.
25. Malda J, Rouwkema J, Martens DE, Le Comte EP, Kooy FK, Tramper J, et al. Oxygen gradients in tissue-engineered PEGT/PBT cartilaginous constructs: measurement and modeling. Biotechnol Bioeng 2004; 86: 9-18.
26. Chen HC, Hu YC. Bioreactors for tissue engineering. Biotechnol Lett 2006; 28: 1415-1423.
27. Platt D, Bird JL, Bayliss MT. Ageing of equine articular cartilage: structure and composition of aggrecan and decorin. Equine Vet J 1998; 30: 43-52.
28. Brama PA, TeKoppele JM, Bank RA, van Weeren PR, Barneveld A. Influence of site and age on biochemical characteristics of the collagen network of equine articular cartilage. Am J Vet Res 1999; 60: 341-345.
29. Benders KEM, Boot W, Cokelaere SM, Van Weeren PR, Gawlitta D, Bergman HJ, et al. Multipotent stromal cells outperform chondrocytes on cartilage-derived matrix scaffolds. Cartilage under review.
30. Kheir E, Stapleton T, Shaw D, Jin Z, Fisher J, Ingham E. Development and characterization of an acellular porcine cartilage bone matrix for use in tissue engineering. J Biomed Mater Res A 2011; 99: 283-294.
31. Yang Q, Peng J, Guo Q, Huang J, Zhang L, Yao J, et al. A cartilage ECM-derived 3-D porous acellular matrix scaffold for in vivo cartilage tissue engineering with PKH26-labeled chondrogenic bone marrow-derived mesenchymal stem cells. Biomaterials 2008; 29: 2378-2387.
32. Gandhi NS, Mancera RL. The structure of glycosaminoglycans and their interactions with proteins. Chem Biol Drug Des 2008; 72: 455-482.
33. Barradas AMC, van Grunsven W, van Blitterswijk CA, de Boer J. Devitalised cartilage matrix as a template for bone formation. In: TERMIS. Galway, Ireland 2010.

Chapter 9

Varying particle sizes has no influence on cartilage matrix production on decellularized cartilage-derived matrix scaffolds

K.E.M. Benders
T.L. Haut Donahue
W. Boot
D.B.F. Saris
P.R. van Weeren
J. Malda

Submitted to Cartilage

ABSTRACT

The use of extracellular matrix (ECM)-derived scaffolds has been extensively studied and applied in a number of tissue-engineering applications, including bladder reconstruction, skin regeneration, and heart valve replacement. Within the field of orthopedic surgery, treatment of (osteo-)chondral defects remains challenging. Current cell-based treatment strategies are both costly and often lead to defect filling with scar tissue rather than the regeneration of the original tissue. Previous studies have shown the potential of decellularized cartilage-derived matrix (CDM) scaffolds in the repair of cartilage defects. The aim of this study was to further investigate these scaffolds and study the influence of varying ECM particle sizes on the biomechanical characteristics and chondrogenic potential of these scaffolds.

To this extent, scaffolds were generated from decellularized equine articular cartilage in different fractions (100:0, 50:50, 0:100) of smaller (<300μm) and larger (>710μm) particles, and seeded with multipotent stromal cells (MSCs). Histological analysis after 4 and 6 weeks of culture revealed the synthesis of collagen and proteoglycan rich matrix in all of the groups. Biochemical analysis revealed no differences in the amount of glycosaminoglycan production between the different scaffold groups. Additional biomechanical testing was performed to further characterize these scaffolds.

We conclude that CDM scaffolds show great potential for the regeneration of cartilage tissue. Moreover, as using different sized particles of CDM does not significantly alter the chondrogenic potential or the biomechanical characteristics of these scaffolds, and hence does not seem to be essential, the production process of these scaffolds may be simplified.

INTRODUCTION

Articular cartilage defects are known to have limited regenerative capacity. Due to pain complaints in the early stages of articular damage, and painful stiff joints after progression of the damage towards osteoarthritis, the quality of life of patients is heavily affected because of a substantial decrease in daily mobility[1]. Long-term functional limitations may in turn lead to generalized health problems as well as psychological issues, burdening society with a steep rise in associated health care costs[2].

The current treatment strategies for cartilage defect repair, such as microfracture and autologous chondrocyte implantation (ACI) are restricted to certain patient groups due to their limited inclusion criteria. Furthermore, these techniques lead to fibro-cartilaginous repair tissue in the case of microfracture, and are time-consuming and expensive in the case of ACI[3]. Other reasons why these novel repair strategies struggle to find their way to global clinical application are the associated costs, regulatory, insurance and logistical issues[4]. Therefore, the quest for novel, and preferably one-stage off-the-shelf regenerative strategies still continues.

Tissue engineering is a potential solution to effectively treat cartilage defects, which, however, relies on finding the perfect combination of biomaterials, bioactive compounds and cells[5]. Biomaterials for cartilage tissue engineering can be of natural origin (*e.g.* collagen or alginate) or synthetic polymer compounds (*e.g.* polycaprolactone or polylactic acid)[6]. Despite the technological advances in the development of artificial scaffolds that mimic the complex nature of native cartilage, as closely as possible, the ultimate scaffold will need to incorporate the majority of the natural bioactive cues that can be found in the extracellular matrix (ECM) of cartilage. To achieve this, the use of native extracellular matrix as the main scaffold compound could be beneficial.

Decellularized extracellular matrices have been extensively studied and have been used successfully for the repair of for example, skin[7], tendon[8], and abdominal wall tissues[9]. They also serve as a platform for tissue engineering purposes in whole-organ bioengineering[10, 11]. Despite this successful application in a range of clinical situations, the use of ECM scaffolds in articular cartilage regeneration has only recently been identified as a possible successful strategy.

Previously, we reported the fabrication of a decellularized cartilage-derived matrix (CDM) scaffold from equine cartilage[12]. In that study, we showed that multipotent stromal cells (MSCs) outperform chondrocytes in forming new cartilage tissue on these scaffolds[12].

Cartilage-derived matrix scaffolds are porous structures in which cells can infiltrate and lay down new cartilage-like matrix. The porosity of the CDM scaffolds is bound to differ with differing particle size. The same holds true for the biomechanical properties of the scaffold. Also, the availability of the bioactive cues that are present in decellularized cartilage matrix[13] likely varies in constructs of differing particle sizes. Intuitively, particle size

will hence affect biological performance of the scaffold and might need to be standardized, but this has never been proven. To assess the need for such standardization, we evaluated CDM scaffolds of various particle size compositions. The hypotheses to be tested were: 1) decellularized CDM scaffolds will show significantly different biomechanical strength, and 2) decellularized CDM scaffolds made from different particle sizes will have significantly different chondrogenic potential.

MATERIALS AND METHODS

Scaffold production

Macroscopically healthy, full-thickness cartilage was harvested post-mortem from equine donors that were euthanized for other reasons than musculoskeletal disease (n=10). The cartilage slices were washed in phosphate buffered saline (PBS) supplemented with penicillin/streptomycin (Invitrogen), snap-frozen in liquid nitrogen and lyophilized for 24 hours. The slices were then milled in liquid nitrogen using an automated mill and sieved into two fractions of particles: a fraction smaller than 710μm and a fraction of particles smaller than 300μm. The two fractions were combined to form different ratios (100:0, 50:50, and 0:100) of the 710μm and 300μm particles.

Next, the different mixtures were decellularized as previously described [12]. Briefly, the cartilage particles underwent enzymatic treatment using 0.25% trypsin-EDTA (Invitrogen) in 6 cycles in 48 hours at 37°C under vigorous agitation. Subsequently, the cartilage slurry was subjected to a nuclease solution (50U/ml deoxyribonucease and 1U/ml ribonuclease A (both from Sigma) in 10mM Tris-HCl, pH 7.5 at 37°C under agitation. After 4 hours, the nuclease solution was removed and replaced by 10mM Tris-HCl for 20 hours on a roller plate at room temperature. Next, the slurry was immersed in 1% (v/v) Triton X-100 in PBS for 24 hours on a roller plate at room temperature. To remove all enzymatic agents and detergents from the remaining cartilage sludge, vigorous PBS washing steps were applied in 6 cycles over the course of 48 hours at room temperature. In order to shape the sludge into CDM scaffolds, the sludge was put into 8mm Ø cylindrical molds and these were lyophilized for 24 hours. For additional cross-linking, the CDM scaffolds were subjected to UV-light overnight. Sterilization of the scaffolds was performed using ethylene oxide gas.

Equine multipotent stromal cell isolation

Sternal bone marrow aspirate of three healthy, living equine donors was obtained with approval of the local animal ethical committee. The bone marrow aspirate was centrifuged on Ficoll-Paque to isolate the mononuclear fraction (MNF). The MNF was resuspended in multipotent stromal cell (MSC) expansion medium (a-MEM (22561, Invitrogen) complemented with 10% heat-inactivated fetal bovine serum, 0.2mM L-ascorbic acid 2-phosphate

(Sigma), 100 units/ml penicillin and 100µg/ml streptomycin (Invitrogen), and 1ng/ml FGF-2 (R&D Systems)). The cells were expanded in a monolayer culture to subconfluence before passaging. All cells were used at P3. To guarantee that the isolated cells were actually MSCs, the multilineage potential was confirmed by differentiating the cells towards the osteogenic, adipogenic and chondrogenic lineage as previously described[14].

Cell seeding and cell culture

The scaffolds were cut into smaller discs of approximately 3mm in height and pre-soaked for approximately 60 minutes in a-MEM. Afterwards, a total of $3{\cdot}10^6$ cells were seeded per scaffold. To ensure cell attachment, $1.5{\cdot}10^6$ cells were seeded on the top of the scaffold and after leaving the scaffolds at 37°C for 60 minutes, the scaffolds were flipped over and another $1.5{\cdot}10^6$ cells were seeded on the other side. Again, the scaffolds were left for 60 minutes at 37°C before the culture medium was added to the culture plate.

All scaffolds were cultured in MSC expansion medium for 6 days. Next, the scaffolds were cultured in chondrogenic MSC differentiation medium (DMEM (31966, Invitrogen), supplemented with 0.2mM L-ascorbic acid 2-phosphate, 1% ITS+ premix (BD Biosciences, USA), 0.1µM dexamethasone (Sigma), 100units/ml penicillin and 100µg/ml streptomycin, and 10ng/ml TGFb-2 (R&D Systems)) for either 4 or 6 weeks. Medium was changed twice every week.

MicroCT analysis

Scaffolds with different ratios (100:0, 50:50, 0:100) of the 710µm and 300µm particles were scanned via micro-computed tomography (Scanco µCT 80, Scanco Medical AG, Brüttisellen, Switzerland) with an isotropic voxel size of 25µm. Using the built-in µCT evaluation software (Scanco Medical AG, Brüttisellen, Switzerland) the total volume versus solid volume was determined as a measure for porosity.

Mechanical indentation analysis on non-seeded samples

Relaxation indentation testing (Mini Bionix 858 MTS Corp, Eden Praire, MN) was performed on both the edge and middle of non-seeded scaffolds with different ratios of particles (100:0, 50:50 and 0:100, n = 4 each group). Specimens were placed perpendicular to the rigid indenter (diameter 1.59mm) on an X-Y stage, so each sample could be positioned for indentation near the edge of the sample and in the middle of the sample. Load and displacement data were recorded during the stress relaxation test while samples were allowed to relax up to 2500 seconds. A Matlab (Mathworks, Natick, MA) routine using a Hertzian contact equation was used to determine both ramp and equilibrium moduli.

Dynamic mechanical analysis on cultured samples

Dynamic mechanical analysis (TA instruments DMA 2980) was performed on two samples of each donor of each group (100:0, 50:50, 0:100) before culture, after 4, and 6 weeks of culture. The compression modulus (unconfined) of the samples was measured using cylindrical structures. A total force of 5N was applied to the surface of the samples over a time period of 10 minutes (rate 0.5N/min). The measured force and displacement during compression were used to determine the stress-strain curve of each sample. The Young's modulus was calculated from the slope of the linear part of the stress-strain curve.

Histology

Samples for histology were dehydrated through a graded ethanol series, cleared in xylene and embedded in paraffin. Paraffin-embedded samples were sectioned into 5μm slices prior to staining. A hematoxylin and eosin staining for cell detection was performed as well as a triple stain of hematoxylin, fast green and Safranin-O for glycosaminoglycan deposition (all from Sigma). A light microscope was used to examine and record the stainings (Olympus BX51).

Immunohistochemistry

Sectioned paraffin-embedded samples were deparaffinized through a graded ethanol series and washed in PBS with 0.1% Tween 20 for 5 minutes. Next, antigen retrieval was applied, first hyaluronidase for 30 minutes (Sigma, 10mg/ml in PBS), and pronase for 30 minutes (Roche, 1mg/ml in PBS), both at 37°C. Subsequently, the sections were blocked with 5% bovine serum albumin in PBS for 30 minutes at room temperature. The samples were incubated with either an antibody against collagen type I (1:50; I-8H5, Calbiochem) or collagen type II (1:100; II-6B3II, Developmental Studies Hybridoma Bank) overnight at 4°C. Then, samples underwent incubation with a biotinylated anti-mouse antibody (1:200; GE Healthcare) and streptavidin/peroxidase (1:400; Beckman Coulter), or a secondary anti-mouse antibody conjugated with peroxidase (Dako), respectively, all for 60 minutes at room temperature. A 3,3'-diaminobenzidine solution (10 minutes, Sigma) was used to visualize antibody binding in all of the sections. A counterstain of Mayer's hematoxylin was used to stain the nuclei.

GAG and DNA quantitative analysis

Samples for biochemical analysis were digested overnight at 60°C using a papain solution (0.01M cysteine, 250μg/ml papain, 0.2M NaH_2PO_4 and 0.01M EDTA). Glycosaminoglycan (GAG) content was measured spectrophotometrically after reaction with dimethylmethylene blue (DMMB) (Sigma) by determining the ratio of absorbances at 540 and 595nm. GAG content was quantified using a standard of chondroitin sulphate (Sigma).

DNA content was quantified on papain-digested samples using a picogreen DNA assay (Invitrogen) according to the manufacturer's instructions.

Statistical analysis

To analyze and compare the different groups a one-way ANOVA with a Tukey's *post-hoc* test was performed using IBM SPSS Statistics 21. Statistical significance was set at $p<0.05$.

RESULTS

MicroCT scanning

The three different compositions of CDM scaffolds were scanned using microCT to obtain images of the scaffolds prior to cell seeding and to visualize the differences in particle size throughout the scaffolds (Figure 1). Visual inspection showed that the 0:100 ratio contained relatively smaller particles compared to the 100:0 ratio.

Figure 1: Micro-CT images of the different scaffolds 100:0 (a), 50:50 (b), 0:100 (c). These images illustrate the differences in particle size between the groups. Scale bar represents 1 millimeter.

Indentation mechanical analysis on non-seeded samples

No significant differences were found in modulus between the 50:50 and 0:100 groups, whilst the ramp and equilibrium moduli in the 100:0 group were significantly lower than in the other two groups (Figure 2). No significant differences were observed between edge and middle modulus in any of the groups.

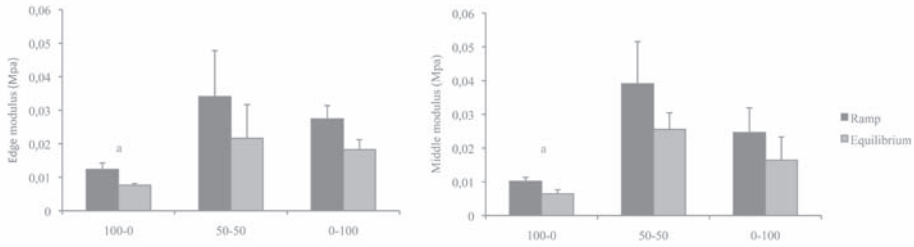

Figure 2: Edge and ramp mechanical indentation moduli. A significant difference (a= $p<0.05$) was found between the 100:0 group and the 50:50 and 0:100 groups.

Histology

To verify full decellularization of the scaffolds and to visualize their composition in terms of proteoglycan, collagen type II, and collagen type I presence, histological stainings were performed. Indeed, the scaffolds appeared to be fully decellularized (data not shown), which was consistent with our previous findings[12]. The CDM scaffolds were predominantly rich in collagen type II, and no positive staining for proteoglycans or collagen type I was observed, confirming previous observations[12].

The cultured scaffolds of the different conditions after both 4 and 6 weeks of culture were also stained for cells, proteoglycans and collagen types I, and II. The H&E staining showed clear ingrowth of the cells into the different scaffolds with the majority of the cells aligning along the outer border of the scaffolds (Figure 3A, E, I). The Safranin-O staining revealed the presence of GAGs in the newly formed tissue. Subjectively, the amount of proteoglycans seemed higher in the 0:100 scaffold group where the red staining was more intense red (Figure 3B, F, J). The amount of proteoglycans was more abundant at the periphery of the scaffold and diminish towards the center. The amount of newly formed proteoglycan containing tissue did seem to increase between 4 and 6 weeks of culture. The collagen immunohistochemical analysis showed that the newly formed tissue was mainly comprised of type I collagen (Figure 3C, G, K), especially at the periphery of the seeded scaffolds. Nonetheless, some patches of collagen type II rich areas could also be found (Figure 3D, H, L).

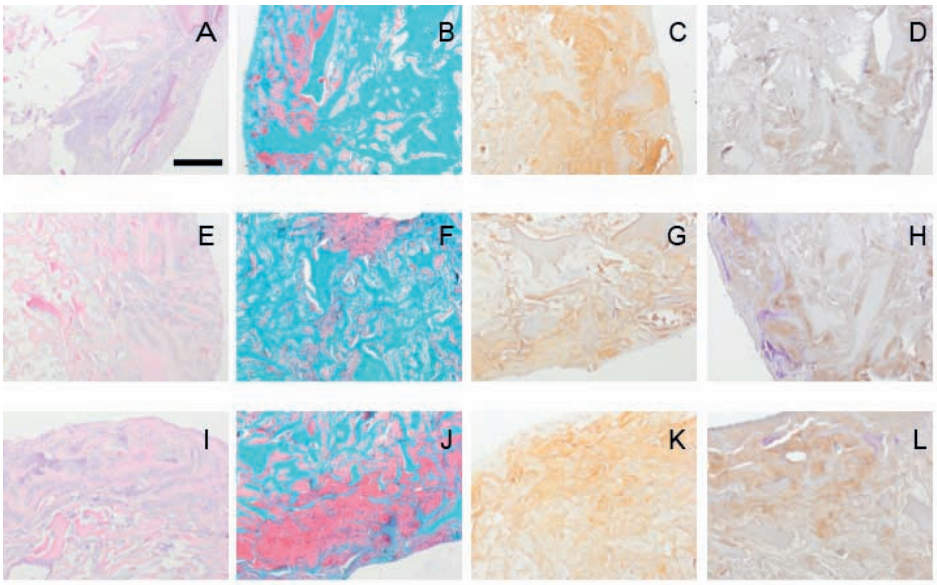

Figure 3: H&E, Safranin-O, collagen type II and collagen type I staining of the different scaffolds after 6 weeks of culture. Images A-D represent 100-0 scaffolds, images E-H represent 50-50 scaffolds, images I-L represent 0-100 scaffolds. Scale bar equals 200μm.

Quantitative glycosaminoglycan and DNA analysis

All scaffolds were GAG-poor with the highest amount of GAGs per scaffold still present in the 100:0 group (2.2μg±0.05), the second highest amount in the 50:50 group (2.0μg±0.04), and the lowest amount in the 0:100 group (0.8μg±1.00). The remnants of DNA were still measurable by the picogreen assay, but were as expected very low. The lowest amount of DNA per scaffold was measured in the group with the smallest particles 0:100 (0.007μg±0.006) when compared to the 50:50 (0.023μg±0.020) and 100:0 groups (0.013μg± 0.015).

To compare the effective GAG production between the different scaffold groups, the amount of GAG per DNA per scaffold was quantified. At both 4 weeks and 6 weeks of culture, no significant differences were found between the different scaffold groups (Figure 4).

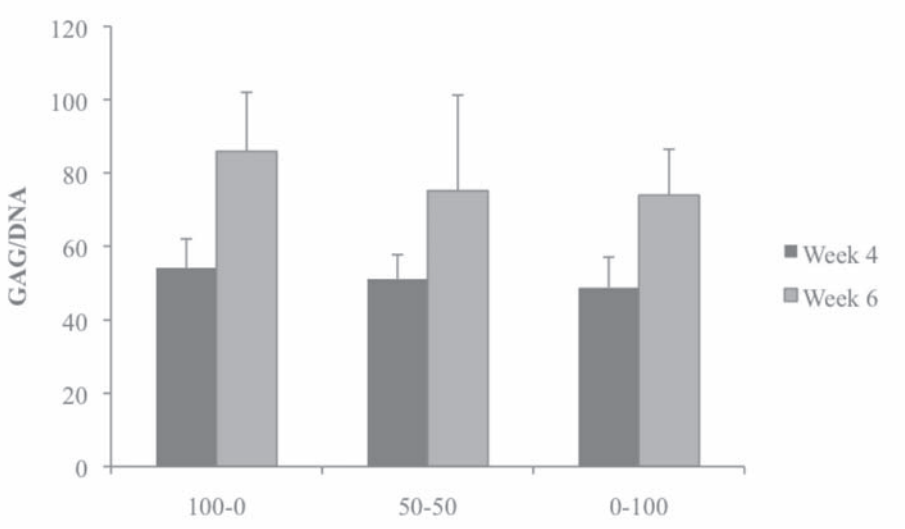

Figure 4: GAG/DNA in μg per μg, at four and six weeks of culture. No significant differences were found in GAG production between the different groups at the different time points.

Young's moduli of the scaffolds

The characterization of the scaffolds prior to cell seeding also involved measuring Young's modulus. A slightly higher, but not significantly different, Young's modulus was found for the 0:100 scaffolds, when compared to 100:0 and 50:50 scaffolds (data not shown). After cell seeding and culture periods of either 4 or 6 weeks no significant differences were observed between the different groups (Figure 5).

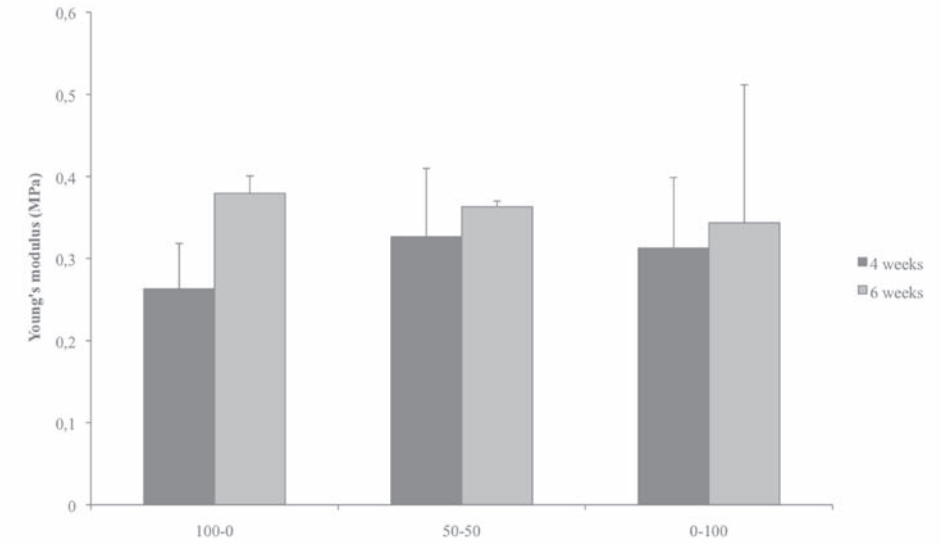

Figure 5: Young's moduli of the different experimental groups after four and six weeks of culture. There were no significant differences between the different scaffold groups.

DISCUSSION

The aims of this study were twofold. The first aim was to investigate the effect of different particle sizes of CDM on the biomechanical characteristics of the decellularized scaffold. The second aim focused at the potential effect of particle size on the chondrogenic potential of multipotent stromal cells that were seeded onto this scaffold. Our previous study already demonstrated a clear differentiation potential of multipotent stromal cells towards the chondrogenic lineage on decellularized CDM scaffolds[12]. Extracellular matrix scaffolds are gaining interest within cartilage tissue engineering. They have potential not only for the repair of cartilage defects, but they may also play a role in the repair of osteochondral defects as multipotent stromal cells seem to differentiate towards the appropriate lineage of the target tissue[13]. However, there is more to cell differentiation and proliferation and suitable constructs for osteochondral repair also require certain biomechanical strength and resilience to cope with the biomechanical shear and compression forces that are present in the joint. By altering the composition of the decellularized CDM scaffolds through the use of different particle sizes we might be able to influence the biomechanical properties of the scaffolds.

Our results, however, show that the alterations in scaffold composition as carried out in this study by using different relative fractions of particle sizes in the <710μm and <300μm ranges did not have significant effects on the biomechanical properties of the scaffolds as measured by mechanical indentation and dynamic compression. The indentation moduli of

the unseeded scaffolds were smaller for the 100:0 samples consisting of the larger particles because this fraction of particle sizes leads to more porous scaffolds, as evidenced by the μCT images. Spatial homogeneity of all scaffolds was confirmed by the similarities between the moduli at the edge and the center of the constructs. This observation provides evidence that scaffold production by freeze drying produces scaffolds with uniform mechanical properties throughout the entire construct. It is interesting to note that, where the CDM scaffolds have a rather poor resistance to compressive forces, the indentation moduli of the non-seeded constructs are smaller than the Young's moduli, meaning that the extracellular matrix that is produced within these scaffolds enhances their biomechanical strength. Still, the values remain far below the elastic compression modulus of natural cartilage, which on the femoral condyles typically ranges between 1-5MPa[15]. The reinforcement of scaffolds for cartilage repair often necessitates a compromise in functionality. This is true for both synthetic and CDM scaffolds, but compared to the latter synthetic scaffolds are considered foreign bodies and do not contain the bioactive cues that are present in natural tissues, which may lead to hampered tissue ingrowth and delayed cell differentiation. Nonetheless, in search for the most appropriate scaffold for cartilage regeneration, and even more challenging osteochondral repair, we will have to focus on enhancing the biomechanical properties of the CDM scaffold. One of the solutions might be combining decellularized CDM with fiber reinforced 3D bioprinted constructs[16-18]. In due time, this technique might even allow for the recreation of the zonal organization of native cartilage tissue[19]. Future applications may involve creating a printable decellularized CDM hydrogel[20] that can be combined with a more biomechanically resistant printable material, or the functionalization of synthetic polymers with CDM particles[21].

The present study showed that the decellularized CDM scaffolds that were employed had good functionality. All scaffolds allowed for the deposition of cartilage-like tissue that was rich in GAGs, as well as collagen type II. There were no significant differences between the different groups. Theoretically, one might expect that multipotent stromal cell differentiation and subsequent chondrogenesis would be highest in the group in which the bioactive cues that are preserved within the ECM are more readily available to the cells. The question then arises whether this availability is dependent on the gradual release of these functional molecules during the process of degradation of the scaffold by the resident cells, or whether these functional molecules act as integrins and require cell-extracellular matrix binding. Until recently, the exact mechanisms behind the bioactive cues in the extracellular matrix remained elusive. However, the (effective) presence of matrix-bound nanovesicles in several commercially available and laboratory-produced scaffolds might provide the answer[22].

These nanovesicles are closely associated with collagen networks and contain nuclease-protected miRNA that is preserved across species and tissue types. These miRNAs are involved in regenerative processes such as 'cellular development, cellular growth and proliferation, cell death and survival, cellular movement, and cell cycle activity'[22]. The high

degree of preservation of the miRNA molecules across species and tissues also broadens the scope towards a xenogenic application of extracellular matrices for cartilage repair strategies.

The variation in particle size that was used in this study had, through its influence on the microstructure of the scaffolds effect on the pore sizes throughout the scaffold. In this study this effect was only semi-quantitatively achieved via microCT scanning and the determination of the exact pore sizes was beyond the scope of this experiment. Nevertheless, pore size is known to have an impact on cell adhesion and cell differentiation and, hence, matrix production. The benefit of having larger pores is that cells will be able to move more freely into the scaffold, leading to a more evenly distributed cell population than with small pore sizes[23]. However, when pores become too large this will inevitably lead to cells 'falling through' the scaffold. Pore size also influences nutrient supply to the seeded cells. Larger pore sizes allow for greater influx of nutrients from the surrounding environment; *in vitro* this would mean the influx of medium, *in vivo* this would involve infiltration of blood from the underlying bone marrow in case of osteochondral defects. A certain amount of nutrient and catabolic factor exchange is required to ensure a balance in matrix production[24]. In the current experiment, the histological analysis showed highest cell density at the periphery of the scaffold but also infiltration into the center of the scaffold, suggesting pore size was sufficiently large to allow for cell adhesion throughout the scaffold. The higher abundance of cells in the periphery can most likely be attributed to the larger availability of nutrients in this area due to the submersion of the scaffolds in nutrient-rich medium.

Chondrocytes tend to retain their phenotype better and lay down more cartilage-like tissue in collagen matrices containing smaller pores[24, 25]. Chondrocytes also thrive in a hypoxic environment, as cartilage is an avascular tissue in nature[26]. By reducing the pore size the amount of oxygen that will be delivered to the cells will diminish, possibly creating a more favorable anabolic environment for chondrocytes, or chondrogenically differentiated multipotent stromal cells. Smaller pore size also drives chondrocytes to grow into 3D microstructures as they have less surface area to form a monolayer on[24], again mimicking a more natural environment for matrix deposition. As no significant differences in GAG/DNA or other parameters indicating chondrogenic functionality were found in this experiment, it can be concluded that the particle size range as used for the scaffolds used in this study did not contain a pore size that negatively influenced chondrogenic capacity. This relatively large margin in particle size can be considered advantageous in generating CDM scaffolds as the bioactivity of these scaffolds seems, at least within the range investigated in this study, to be independent on particle size, especially since control over pore size will be difficult in generating CDM scaffolds. This vastly simplifies the production process. In addition, the observation may open up the possibility to use different sized particles to functionalize other scaffold materials. When further pursuing the development of these

CDM scaffolds as potential tools for cartilage defect repair, future experiments will need to focus on improving the biomechanical characteristics of these scaffolds.

CONCLUSIONS

Decellularized cartilage-derived matrix scaffolds have shown to promote cartilage matrix deposition when seeded with multipotent stromal cells. Using different fractions of different particle sizes to create the scaffold did not alter the biomechanical characteristics of the scaffolds, nor did it influence the cartilage-matrix production. This relative independence of functionality of particle size greatly facilitates production and hence the practical applicability of these potentially very interesting scaffolds.

REFERENCES:

1. Heir S, Nerhus, T. K., Rotterud, J. H., Loken, S., Ekeland, A., Engebretsen, L., Aroen, A. Focal cartilage defects in the knee impair quality of life as much as severe osteoarthritis: a comparison of knee injury and osteoarthritis outcome score in 4 patient categories scheduled for knee surgery. Am J Sports Med 2010; 38: 231-237.
2. Dunlop DD, Semanik, P., Song, J., Manheim, L. M., Shih, V., Chang, R. W. Risk factors for functional decline in older adults with arthritis. Arthritis Rheum 2005; 52: 1274-1282.
3. de Windt TS, Sorel, J. C., Vonk, L. A., Kip, M. M., Ijzerman, M. J., Saris, D. B. Early health economic modelling of single-stage cartilage repair. Guiding implementation of technologies in regenerative medicine. J Tissue Eng Regen Med 2016.
4. Farr J, Gomoll AH. 2016 barriers to cartilage restoration. J Clin Orthop Trauma 2016; 7: 183-186.
5. Vinatier C, Mrugala D, Jorgensen C, Guicheux J, Noel D. Cartilage engineering: a crucial combination of cells, biomaterials and biofactors. Trends Biotechnol 2009; 27: 307-314.
6. Ye K, Felimban, R., Moulton, S. E., Wallace, G. G., Di Bella, C., Traianedes, K., Choong, P. F., Myers, D. E. Bioengineering of articular cartilage: past, present and future. Regen Med 2013; 8: 333-349.
7. Vashi C. Clinical Outcomes for Breast Cancer Patients Undergoing Mastectomy and Reconstruction with Use of DermACELL, a Sterile, Room Temperature Acellular Dermal Matrix. Plast Surg Int 2014; 2014: 704323.
8. Martinello T, Bronzini, I., Volpin, A., Vindigni, V., Maccatrozzo, L., Caporale, G., Bassetto, F., Patruno, M. Successful recellularization of human tendon scaffolds using adipose-derived mesenchymal stem cells and collagen gel. J Tissue Eng Regen Med 2014; 8: 612-619.
9. Satterwhite TS, Miri, S., Chung, C., Spain, D. A., Lorenz, H. P., Lee, G. K. Abdominal wall reconstruction with dual layer cross-linked porcine dermal xenograft: the "Pork Sandwich" herniorraphy. J Plast Reconstr Aesthet Surg 2012; 65: 333-341.
10. Peloso A, Dhal, A., Zambon, J. P., Li, P., Orlando, G., Atala, A., Soker, S. Current achievements and future perspectives in whole-organ bioengineering. Stem Cell Res Ther 2015; 6: 107.
11. Badylak SF, Weiss DJ, Caplan A, Macchiarini P. Engineered whole organs and complex tissues. Lancet 2012; 379: 943-952.
12. Benders KEM, Boot, W., Cokelaere, S. M., Van Weeren, P. R., Gawlitta, D., Bergman, H. J., Saris, D. B., Dhert, W. J., Malda, J. Multipotent Stromal Cells Outperform Chondrocytes on Cartilage-Derived Matrix Scaffolds. Cartilage 2014; 5: 221-230.
13. Benders KE, van Weeren PR, Badylak SF, Saris DB, Dhert WJ, Malda J. Extracellular matrix scaffolds for cartilage and bone regeneration. Trends Biotechnol 2013; 31: 169-176.
14. Pittenger MF, Mackay, A. M., Beck, S. C., Jaiswal, R. K., Douglas, R., Mosca, J. D., Moorman, M. A., Simonetti, D. W., Craig, S., Marshak, D. R. Multilineage potential of adult human mesenchymal stem cells. Science 1999; 284: 143-147.
15. Shepherd DE, Seedhom BB. The 'instantaneous' compressive modulus of human articular cartilage in joints of the lower limb. Rheumatology (Oxford) 1999; 38: 124-132.
16. Visser J, Melchels, F. P., Jeon, J. E., van Bussel, E. M., Kimpton, L. S., Byrne, H. M., Dhert, W. J., Dalton, P. D., Hutmacher, D. W., Malda, J. Reinforcement of hydrogels using three-dimensionally printed microfibres. Nat Commun 2015; 6: 6933.
17. Visser J, Peters, B., Burger, T. J., Boomstra, J., Dhert, W. J., Melchels, F. P., Malda, J. Biofabrication of multi-material anatomically shaped tissue constructs. Biofabrication 2013; 5: 035007.
18. Jeong CG, Atala A. 3D Printing and Biofabrication for Load Bearing Tissue Engineering. Adv Exp Med Biol 2015; 881: 3-14.

19. Malda J, Benders, K. E., Klein, T. J., de Grauw, J. C., Kik, M. J., Hutmacher, D. W., Saris, D. B., van Weeren, P. R., Dhert, W. J. Comparative study of depth-dependent characteristics of equine and human osteochondral tissue from the medial and lateral femoral condyles. Osteoarthritis Cartilage 2012; 20: 1147-1151.
20. Pati F. J, J., Ha, D.H., Won Kim, S., Rhie, J.W., Shim, J.H., Kim, D.H., Cho, D.W. Printing three-dimensional tissue analogues with decellularized extracellular matrix bioink. Nat Commun 2014; 2.
21. Visser J, Gawlitta, D., Benders, K. E., Toma, S. M., Pouran, B., van Weeren, P. R., Dhert, W. J., Malda, J. Endochondral bone formation in gelatin methacrylamide hydrogel with embedded cartilage-derived matrix particles. Biomaterials 2015; 37: 174-182.
22. Huleihel L, Hussey, G. S., Naranjo, J. D., Zhang, L., Dziki, J. L., Turner, N. J., Stolz, D. B., Badylak, S. F. Matrix-bound nanovesicles within ECM bioscaffolds. Sci Adv 2016; 2: e1600502.
23. Li WJ, Jiang YJ, Tuan RS. Cell-nanofiber-based cartilage tissue engineering using improved cell seeding, growth factor, and bioreactor technologies. Tissue Eng Part A 2008; 14: 639-648.
24. Nava MM, Draghi L, Giordano C, Pietrabissa R. The effect of scaffold pore size in cartilage tissue engineering. J Appl Biomater Funct Mater 2016; 14: e223-229.
25. O'Brien FJ, Harley BA, Yannas IV, Gibson LJ. The effect of pore size on cell adhesion in collagen-GAG scaffolds. Biomaterials 2005; 26: 433-441.
26. Thoms BL, Dudek KA, Lafont JE, Murphy CL. Hypoxia promotes the production and inhibits the destruction of human articular cartilage. Arthritis Rheum 2013; 65: 1302-1312.

Chapter 10

Cartilage-derived matrix scaffolds for osteochondral repair: an equine pilot study

K.E.M. Benders
W. Boot
S.M. Cokelaere
P.R. van Weeren
J. Malda

ABSTRACT

Decellularized cartilage-derived matrix (CDM) scaffolds have shown great promise in the regeneration of cartilage tissue in *in vitro* settings. Also, the generation of bone tissue through the endochondral pathway has been demonstrated *in vivo* at ectopic implantation sites. By combining the regeneration of cartilage and bone tissue using a decellularized CDM scaffold a new step towards the repair of osteochondral defects could be made. To this extent, this equine pilot study (n=1) was designed.

Osteochondral defects were created on the lateral trochlear ridge of the stifle joint, and either filled with a CDM scaffold or with an already clinically applied TruFit plug (Smith and Nephew) as a control. After 8 weeks, macroscopic and microscopic evaluation on the formation of cartilage and bone tissue within the defects was performed. The CDM scaffold showed osteochondral defect filling and distinct cartilage-like and bone-like phases could be identified. The TruFit plug showed only limited filling of the osteochondral defect and clear remnants of the scaffold could still be observed when compared to the CDM scaffold.

This pilot study showed favorable results regarding the implantation of a CDM scaffold in an osteochondral defect in the equine stifle joint. Especially when compared to the TruFit plug, abundant neo-tissue with a distinct cartilage and bone phase could be identified. This study will therefore be, the foundation for a large equine *in vivo* study in the future.

INTRODUCTION

Extracellular matrix (ECM) scaffolds are gaining interest within the field of cartilage tissue engineering. Previously, they have been successfully used within regenerative medicine, in for example engineering of cardiovascular tissues, skin, and tendons[1]. The use of decellularized ECM as a scaffold material overcomes the restraints on biodegradability, biocompatibility and bioactivity that are present when synthetic materials are used to create scaffolds. Moreover, decellularized ECM is thought to naturally retain bioactive cues, such as growth factors, peptides and other functional molecules that initiate, drive, and regulate tissue regeneration[2].

Cartilage tissue harvested from cadaveric donors can be decellularized and used to create scaffolds[3]. Previously, decellularized cartilage-derived matrix (CDM) scaffolds were successfully generated and their ability to facilitate abundant cartilage extracellular matrix production by mesenchymal stromal cells was demonstrated *in vitro*[4, 5]. Interestingly, these scaffolds can potentially be applied to regenerate both the cartilage and the underlying bone. Evolutionary, bone tissue is generated through the intramembranous ossification pathway, but also through endochondral bone formation[6]. This latter pathway is of particular interest for osteochondral repair by CDM scaffolds as the scaffold can provide the cartilage template that is required for endochondral ossification. Moreover, decellularized tissue of other origins than the target tissue have proven to be beneficial in driving regeneration of completely different tissues[7]. The regeneration of osteochondral defects might not require scaffolds to be pre-cultured prior to implantation as mesenchymal stromal cells (MSCs) from the subchondral bone could be used as an adequate cell source to drive regeneration, a technique that is based on current microfracture techniques[8].

In order to translate *in vitro* work to the bed-side, preclinical animal studies must first be performed to evaluate the performance of these scaffolds in an *in vivo* setting. Small animal studies are often harder to extrapolate towards the human application due to differences in size, skeletal immaturity, and biochemical differences in cartilage composition[9]. The equine model has become increasingly popular as equine and human cartilage is similar in composition and thickness[10, 11]. Also, the equine population suffers from naturally occurring cartilage defects and can, therefore, also be considered a target population rather than simply a pre-clinical model[12].

Therefore, this pilot study aims at evaluating osteochondral repair by implanting a cell-free decellularized cartilage-derived matrix scaffold in an osteochondral defect in the stifle joint of a horse. It is performed as a work-up towards a larger study in which the potential of CDM scaffolds in a highly challenging orthotopic location will be tested. We hypothesize that the host's mesenchymal stromal population from the subchondral bone will populate this scaffold. Our second hypothesis is that both cartilage and bone tissue will be formed in their respective natural environments in the defect.

MATERIALS AND METHODS

Animal

This was a pilot study that involved one healthy mature Dutch Warmblood horse of 490kg, age 6 years. Prior to surgery no lameness was observed, nor was there any radiological indication of joint disease. During the study the horse was housed in an individual box and fed a standard maintenance ration of concentrate with hay and water. The study protocol was approved by the ethical and animal welfare committee of Utrecht University. To reduce the use of experimental animals, this horse was also destined to be sacrificed for educational purposes after 8 weeks.

Scaffold production

Full-thickness cartilage from the medial and lateral femoral condyles of the stifle (knee) joints of equine donors (n=5, ages 3-10 years) that were euthanized for reasons other than joint disease, was dissected using a scalpel. The full-thickness cartilage slices were washed in phosphate-buffered saline (PBS) supplemented with penicillin, streptomycin, and fungizone (Invitrogen, Carlsbad, CA). Next, the cartilage slices were snap-frozen in liquid nitrogen and lyophilized for 24 hours. After lyophilization the cartilage slices were snap-frozen using liquid nitrogen and ground using a pestle and mortar for approximately 40 minutes to obtain fine cartilage particles. Subsequently, these particles underwent the first enzymatic treatments using (0.25% trypsin-ethylene-diamine tetraacetic acid (trypsin-EDTA; Invitrogen, Carlsbad, CA). The particles were immersed in this solution for 24 hours in 6 cycles of 4 hours at 37°C under vigorous agitation. Next, the trypsin-EDTA was removed by washing the particles in PBS, before treatment with a nuclease solution of 50U/mL deoxyribonuclease (Sigma, St. Louis, MO) and 1U/mL ribonuclease A (Sigma, St. Louis, MO) in 10mM Tris-HCl, pH 7.5 at 37°C under vigorous agitation. After 4 hours, the nuclease solution was removed and replaced by 10mM hypotonic Tris-HCl for 20 hours on a roller plate at room temperature. To remove all of the remnant enzymatic solutions, the tissue was thoroughly washed using PBS in 6 cycles over the course of 48 hours. After the last PBS washes the decellularization process was finished (Figure 1). The cartilage particles were scooped into cylindrical molds of 11mm diameter and 10mm deep, and lyophilized for 24 hours. To allow for final cross-linking, the scaffolds were after lyophilization subjected to ultra violet light overnight. Before i*n vivo* implantation the scaffolds were sterilized using ethylene oxide gas.

Experimental design

A defect of 11mm diameter and 10mm depth was surgically created through a mini-arthrotomy on the proximal lateral 1/3 of the trochlear ridge of the stifle joint in both knees. The defect in the right stifle joint was filled with the decellularized CDM scaffold. The left stifle joint was filled with a commercially available TruFit plug (Smith and Nephew), as a control.

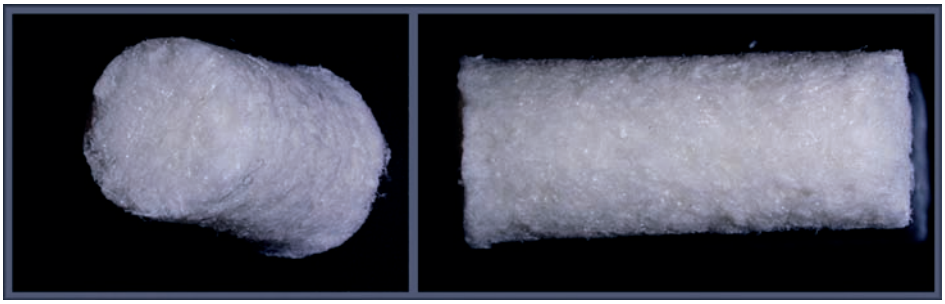

Figure 1: Decellularized cartilage-derived matrix scaffolds for osteochondral implantation. Adapted from *Benders et al., (2014), Cartilage 5(4): 221-230*[4].

Surgical procedure

After general anesthesia the horses were positioned in dorsal recumbence. The stifle joint was opened through a mini-arthrotomy approach between the patellar ligaments. The osteochondral defect was created on the proximal 1/3 of the lateral trochlear ridge using pre-designed hollow punches. Next the defects were flushed using a saline solution. The scaffold and the TruFit plug were implanted press-fit into the created osteochondral defects. The CDM scaffold was covered with fibrin glue to ensure that it would stay in place. The arthrotomy wounds were closed in four layers (joint capsule, deep fascia, superficial fascia, and skin).

Post-operative care and rehabilitation

The horses received post-operative pain medication in the form of metacam for five days post-surgery. The rehabilitation protocol was adapted from Frisbie *et al.*[13] and ensured a gradual increase in mobility in 8 weeks (Table 1). The horse was subjected to daily monitoring of clinical parameters (temperature, heart rate, and respiratory rate). Radiographs of the femoropatellar joints were taken before and after surgery to check for radiographic abnormalities before and after surgery.

Table 1: Rehabilitation protocol

Time point	Activity
Week 1	Boxrest
Week 2	Handwalk 5 min/day
Week 3	Handwalk 10 min/day
Week 4	Handwalk 15 min/day
Week 5	Handwalk 20 min/day
Week 6	Treadmill trot 2 min/day
Week 7	Treadmill trot 5 min/day
Week 8	Treadmill trot 5 min/day

Euthanasia and sample harvesting

After 8 weeks the horse was euthanized by a combination of detomidine (0,01 mg/kg, Vetoquinol), ketamine (2mg/kg, Vetoquinol), midazolam (0,1 mg/kg, Actavis), and pentobarbital (50mg/kg, AST Farma). The femoropatellar joint was opened and blocks of tissue were sawed out of the joint and fixed in 10% formalin until further histological evaluation.

Histological processing

The formalin fixed samples were decalcified using ethylene diamine tetraacetic acid (EDTA) and dehydrated through a graded ethanol series, cleared in xylene and embedded in paraffin. The paraffin embedded samples were sectioned into 5µm sections. To assess tissue ingrowth the sections were stained with hematoxylin and eosin. To evaluate GAG deposition, sections were stained with a triple stain of hematoxylin, fast green and Safranin-O, and for collagen orientation by a picrosirius Red stain (all from Sigma).

Immunohistochemical localization of collagen type II and collagen type I was performed on the paraffin-embedded sections. The sections were deparaffinized through a graded ethanol series and washed in PBS with 0.1% Tween 20 for 5 minutes prior to this immunolocalization. The antigen retrieval steps involved exposure to hyaluronidase for 30 minutes (Sigma; 10mg/mL in PBS), and to pronase for 30 minutes (Roche, Basel, Switzerland; 1 mg/mL in PBS), both at 37°C. Next, the sections were blocked with 5% bovine serum albumin in PBS for 30 minutes at room temperature, and incubated overnight at 4°C with antibodies against either collagen type II (1:100; II-6B3II, Developmental Studies Hybridoma Bank), or collagen type I (1:50; I-8H5, Calbiochem, Darmstadt, Germany). Afterwards, the samples were incubated with a biotinylated anti-mouse antibody (1:200; GE Healthcare, Fairfield, CT) and streptavidin/peroxidase (Dako, Glostrup, Denmark), respectively, all for 60 minutes at room temperature. Antibody binding in all of the sections was visualized using 3,3'-diaminobenzidine solution (Sigma, St. Louis, MO) for up to 10 minutes. A counterstain using Mayer's hematoxylin was used to visualize the nuclei.

All the stained sections were examined using a light microscope (Olympus BX51) and representative images were taken from sections in the center of the constructs.

RESULTS

Post-operative course

After surgery, the horse initially presented with lameness of both legs. However, at the end of the study period no lameness was observed. No wound infection, rise in temperature or any abnormal joint effusion was observed. The rehabilitation period elapsed completely uneventful. The rehabilitation protocol did not seem to be too cumbersome for the horse.

Macroscopic evaluation

A clear indentation was seen at the site of CDM scaffold implantation. However, a cartilage-like layer could clearly be identified and be distinguished from the underlying bone layer. Bone bruising seemed apparent with accompanying bloody infiltration of the tissue. Also, at the site of implantation into the bone part a glossy cartilage-like appearance was still visible (Figure 2). In comparison, the defect that was filled with the TruFit plug showed slightly less indentation at the cartilage surface. The cartilage layer however showed clear cracks and had a more yellowish color. Also, remnants of the TruFit plug could still be observed (Figure 2).

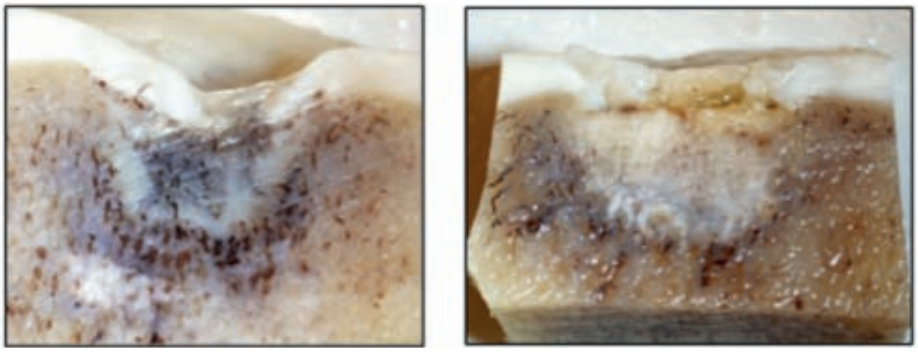

Figure 2: Macroscopic image of the osteochondral defect after implantation of a CDM scaffold (left) after 8 weeks of *in vivo* evaluation, and the osteochondral defect after implantation of the TruFit plug (right).

Histological evaluation

The hematoxylin and eosin, and Safranin-O staining revealed filling of the CDM-treated defect with a cartilage-like tissue in the upper layer and a bone-like tissue in the bony part of the osteochondral defect (Fig 3). There was clearly visible indentation at the cartilage surface with some cleft formation when compared to the healthy articular surface, however the defect was fully filled with tissue. The integration within the bone phase was excellent (Fig 3B); also within the cartilage phase tissue integration at the margins was evident. There was intense staining for proteoglycans within the repair tissue as well as in the previously healthy surrounding tissue. Also, the repair tissue was rich in collagen type II at the articular surface (Fig 3C), as well as some remnants of the CDM scaffold within the bony phase. The orientation of collagen was, however, disorganized as conformed by a picrosirius red staining (Fig 3D). Bone density at the defect site seems to be slightly increased when compared to the surrounding subchondral bone.

In comparison to the CDM scaffold, the TruFit plug (Fig 4) performed rather poorly in terms of osteochondral tissue regeneration. The cartilage layer showed evident tears and was only partly filled up with a neo-tissue that does not resemble native or fibrous cartilage tissue. The bone part did integrate with the surrounding bone. However, the bone tissue did not replace the osseous phase of the scaffold as was seen in the CDM scaffold.

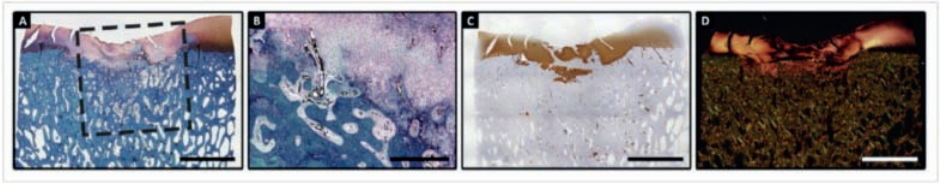

Figure 3: Histological stainings of the osteochondral defect repair. A) Safranin-O staining revealing successful integration within the bone phase and GAG-rich cartilage tissue with good tissue integration at the margins of the defect. The square represents the area of the created osteochondral defect. B) Safranin-O staining showing the cartilage-bone interface within the defect. C) Collagen type II immunolocalization shows that the neo-cartilage tissue is positive for collagen type II, as well as the remnants of the CDM scaffolds within the subchondral bone phase. D) Polarized picrosirius red staining that shows the disorganized collagen orientation within the cartilage repair tissue. Scale bars represent 500 μm. Image from *Vindas Bolaños, RA et al. Osteoarthritis and Cartilage (2016) doi: 10.1016/j.joca.2016.08.005 [14].*

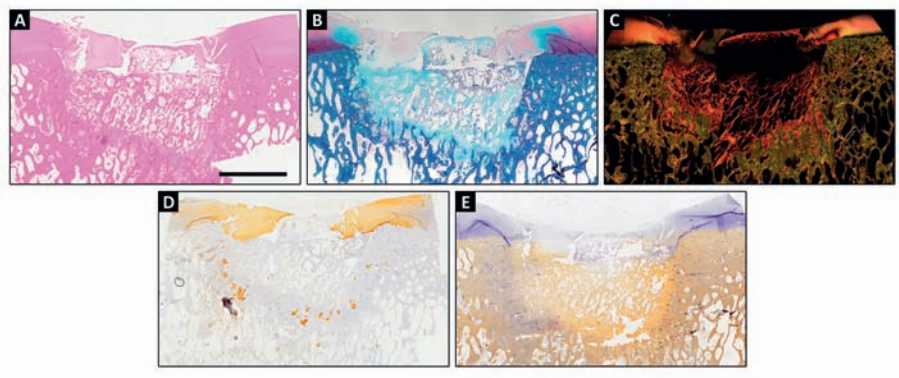

Figure 4: Histological stainings of TruFit implantation at 8 weeks. A) H&E staining showing evident cartilage fibrillation, as well as the presence of areas with no tissue filling. B) Safranin O staining shows proteoglycan-rich cartilage at the edges of the defect, in contrast to the 'cartilage-layer' filled by the TruFit. C) Picrosirius Red staining reveals unorganized collagen fibrils and a lack of collagen in the center of the articular surface. D) Collagen type II shows some collagen type II at the surface, but also a lack of collagen similar to the Picrosirius Red staining. E) Collagen type I immunohistochemistry shows that the bone part is in fact rich in collagen type I similar to the surrounding bone.

DISCUSSION

Osteochondral defects occur in the young and active human population, as well as in the equine population. The natural regeneration of this tissue involves defect filling with scar tissue at best. This leads to painful joints, swelling, and impairment in mobility, leading to significant rise in socio-economic costs[15]. For the equine population, problems arising from osteochondral defects often arise in sports horses. The development of a new technique that addresses the biphasic repair of osteochondral defects would, therefore, benefit both the human and the equine population.

The decellularized CDM scaffold has been developed previously and has shown promising results in *in vitro* settings[4]. Also, the implantation of these scaffolds in a small animal model underscored its potential for cartilage and bone tissue engineering[5]. However, to extrapolate these results towards the human clinic, a large animal pilot study would have to be performed, as a work-up to a larger *in vivo* equine study. In particular the equine model has gained interest in the last few years as a large animal model to study joint regeneration and repair[11]. Therefore, this pilot study was performed to evaluate the performance of the decellularized CDM scaffold in osteochondral defect repair in a large animal model.

Our first hypothesis involved the ability of this scaffold to be invaded with the host's own cells to regenerate the osteochondral tissue. The scaffold was implanted without preseeding with mesenchymal stromal cells, chondrocytes or osteocytes. This means that any tissue that was formed within this critical size osteochondral defect has been produced by the resident cells in the surrounding osteochondral tissue, or was driven by the MSCs that reside in the bone marrow of long bones. Although chondrocytes may have the ability to migrate from the surrounding cartilage edges and are the resident cells of natural hyaline cartilage, MSCs are most likely responsible for the abundant extracellular matrix deposition in the defect as they have the potential to differentiate to both the osteogenic and the chondrogenic lineage[16]. Moreover, previous *in vitro* studies have already shown that MSCs outperform chondrocytes on these CDM scaffolds in terms of cartilage-like tissue formation[4]. It seems that this scaffold can be considered as a carrier of biologically active cues and as an anchoring site for the extracellular matrix that is produced by the host's own cells. This is beneficial and it highlights the possibility for CDM scaffolds to act as a cell-free and off-the-shelf product that does not involve any cell therapy.

Our second hypothesis involved the development of both bone and cartilage tissue at their respective sites within the osteochondral defect. Previously, scaffolds considered in regenerating osteochondral tissue have often been biphasic to take into account the different natural prerequisites to cartilage and bone regeneration[17]. These scaffolds are often composed of a ceramic bone phase that is topped off with either natural or synthetic polymers for the cartilage layer[17]. The TruFit plug for example, that was used in this pilot is made of the synthetic materials poly d,l-lactide-co-glycolide (PLG) copolymer, polyglycolide acid (PGA) and the ceramic calcium sulfate. These biphasic scaffolds suggest that bone and cartilage require two different scaffold materials to drive regeneration. However, the embryonic development of bone involves two pathways, the intramembranous and the endochondral pathway[6]. Especially the latter is of interest when regenerating osteochondral tissues as it involves a cartilage template from which bone tissue develops and growths. Building upon this principle, the use of cartilage extracellular matrix as a biomaterial for both cartilage and bone regeneration might not seem too farfetched. Indeed, the use of this decellularized CDM scaffold showed distinct layers of regenerated cartilage and regenerated bone. This newly formed bone tissue integrated excellently with the surrounding bone tissue, and

also the neo-cartilage tissue showed integration at the margins of the defect. It is striking that the neocartilage layer did not seem to be invaded by calcifications that would lead to bony overgrowth into the cartilage layer. These findings might question the need to create biphasic scaffolds when considering osteochondral repair. Especially the rather poor tissue regeneration and tissue integration that was seen at 8 weeks post-implantation of the TruFit plug suggests slight superiority of the natural scaffold in this case. It is important to note that tissue integration has always been an issue regarding the TruFit scaffold as bone cysts have been observed in patients treated with this scaffold for osteochondral defect repair[18].

Despite the development of adequate bone and cartilage tissue within the defect, a clear indentation at the top of the defect could still be observed. Also, there was still cleft formation present after 8 weeks of implantation. The biomechanical forces that the neo-tissue is exposed to in an equine model are extensive. This expresses the need for a biomechanically strong scaffold that can overcome these loads in this biomechanically challenging environment. The clefts that could be seen at 8 weeks of implantation could also be a result of large biomechanical shear forces. Whether these clefts and indentation are the end-stage of the cartilage regeneration using a CDM scaffold or whether this is just the initial repair that will improve over time will have to be studied in a long-term follow-up study. The termination at 8 weeks was a relatively early time-point considering the long-term equine studies that have been done in for example the evaluation of autologous chondrocyte implantation[13], in which further maturing of the tissue was observed over time.

The promising results of this pilot study are clear, as tissue regeneration seems evident and a clear distinction between the two tissue types was seen. Until now it remains unclear how the cartilage and bone neo-tissues will further develop in long-term studies. Also, to ensure that these positive results are not only a reflection of the intrinsic regenerative capacity of this horse a long-term study with a larger sample size is undoubtedly required.

CONCLUSION

This short-term equine pilot study has shown promising results of a decellularized cartilage-derived matrix scaffold for osteochondral repair. Both cartilage and bone neo-tissues were formed after 8 weeks of implantation and integration with the surrounding healthy tissue was observed. These results form the foundation for a larger and long-term equine follow-up study to further evaluate the potential of CDM scaffolds for osteochondral defect repair.

REFERENCES

1. Badylak SF. The extracellular matrix as a biologic scaffold material. Biomaterials 2007; 28: 3587-3593.
2. Badylak SF, Freytes, D.O., Gilbert, T.W. Reprint of: Extracellular matrix as a biological scaffold material: Structure and function Biomaterials 2015; 23: S17-S26.
3. Benders KE, van Weeren PR, Badylak SF, Saris DB, Dhert WJ, Malda J. Extracellular matrix scaffolds for cartilage and bone regeneration. Trends Biotechnol; 31: 169-176.
4. Benders KE, Boot W, Cokelaere SM, Van Weeren PR, Gawlitta D, Bergman HJ, et al. Multipotent Stromal Cells Outperform Chondrocytes on Cartilage-Derived Matrix Scaffolds. Cartilage; 5: 221-230.
5. Gawlitta D, Benders, K.E., Visser, J., van der Sar, A.S., Kempen, D.H., Theyse, L.F., Malda, J., Dhert, W.J. . Decellularized cartilage-derived matrix as substrate for endochondral bone regeneration. Tissue Eng Part A 2015; 21: 694-703.
6. Berendsen AD, Olsen BR. Bone development. Bone 2015; 80: 14-18.
7. Londono R, Badylak, S.F. Biologic Scaffolds for Regenerative Medicine: Mechanisms of In vivo Remodeling. Ann Biomed Eng 2015; 43: 577.
8. Steadman JR, Rodkey WG, Briggs KK. Microfracture to treat full-thickness chondral defects: surgical technique, rehabilitation, and outcomes. J Knee Surg 2002; 15: 170-176.
9. Chu CR, Szczodry M, Bruno S. Animal models for cartilage regeneration and repair. Tissue Eng Part B Rev; 16: 105-115.
10. Malda J, Benders KE, Klein TJ, de Grauw JC, Kik MJ, Hutmacher DW, et al. Comparative study of depth-dependent characteristics of equine and human osteochondral tissue from the medial and lateral femoral condyles. Osteoarthritis Cartilage; 20: 1147-1151.
11. McIlwraith CW, Fortier LA, Frisbie DD, Nixon AJ. Equine Models of Articular Cartilage Repair. Cartilage; 2: 317-326.
12. Olstad K, Ekman S, Carlson CS. An Update on the Pathogenesis of Osteochondrosis. Vet Pathol; 52: 785-802.
13. Frisbie DD, Bowman, S. M., Colhoun, H. A., DiCarlo, E. F., Kawcak, C. E., McIlwraith, C. W. . Evaluation of autologous chondrocyte transplantation via a collagen membrane in equine articular defects: results at 12 and 18 months. Osteoarthritis Cartilage 2008; 16: 667-679.
14. Vindas Bolanos RA, Cokelaere, S. M., Estrada McDermott, J. M., Benders, K. E. M., Gbureck, U., Plomp, S. G., Weinans, H., Groll, J., van Weeren, P. R., Malda, J. The use of cartilage decellularized matrix scaffold for the repair of osteochondral defects: the importance of long-term studies in a large animal model. Osteoarthritis Cartilage 2016; 20.
15. Dunlop DD, Semanik P, Song J, Manheim LM, Shih V, Chang RW. Risk factors for functional decline in older adults with arthritis. Arthritis Rheum 2005; 52: 1274-1282.
16. Pittenger MF, Mackay AM, Beck SC, Jaiswal RK, Douglas R, Mosca JD, et al. Multilineage potential of adult human mesenchymal stem cells. Science 1999; 284: 143-147.
17. Li X, Ding, J., Wang, J., Zhuang, X., Chen, X. Biomimetic biphasic scaffolds for osteochondral defect repair. Regen Biomater 2015; 2: 221-228.
18. Verhaegen J, Clockaerts, S., Van Osch, G.J.V.M., Somville, J., Verdonk, P., Mertens, P. TruFit plug for repair of osteochondral defects - where is the evidence? Systematic review of literature. Cartilage 2015; 6: 12-19.

Chapter 11

General discussion

THE COMPOSITIONAL MAKE-UP OF CARTILAGE

At a first glance, articular cartilage may seem a relatively simple tissue as it is a highly hydrated tissue that contains only a few cells and a dense matrix that predominantly consists of collagen and proteoglycans. However, when taking a closer look at the uncalcified cartilage tissue, three distinct zonal layers can be distinguished[1, 2]. The superficial zone in the top layer (10-20%) has collagen fibers that are aligned horizontally, a relatively high number of cells with flattened morphology, and a relatively low amount of proteoglycans. These attributes allow for the cartilage to resist the continuous shear forces that are present at the articular surface. The middle zone (the next 40-60%) of cartilage can be considered an intermediate zone between the cartilage resisting shear forces in the top layer and the deeper layer that transmits the compressive forces from the articular surface towards the bone. To resist these intense compressive forces, the deep layer (last 30-40%) has perpendicularly aligned collagen fibers, and a high proteoglycan content to retain water molecules. This layer is well integrated with the subchondral bone through the calcified cartilage layer.

These zonal characteristics of articular cartilage are preserved across species. Evident similarities were described in this thesis between equine and human articular cartilage in terms of the zonal distribution of proteoglycans and DNA as a measure of cell density. As expected, collagen content was similar across the different zones as the zonal differences are based upon collagen fiber orientation rather than the amount of collagen.

Cartilage or osteochondral tissue engineering aims at recreating the native tissue with its natural biochemical properties and functionalities. Many attempts have been made at creating cartilage neo-tissue that employs these zonal differences from the start[2]. However, *in vitro* recreation of the different characteristics in the different zonal layers has proven to be quite challenging. Possible attempts have aimed at creating scaffolds of different biomaterials[3], recreating collagen fiber alignment[4, 5] or even using different cell sources per zonal layer[6-8]. However, as Isaac Newton already posed in his *Philosophia Naturalis Principia Mathematica* (1687): "Nature is pleased with simplicity", and we may be overcomplicating our attempts to completely mimic the adult composition of articular cartilage. This seems even truer when taking into account the initial homogeneity of neonatal articular cartilage. The adult heterogeneous composition throughout the joint only develops in the first two years post-partum in sheep[9] and horses[10]. These studies showed that prenatal cartilage is similar at different sites within the same joint. Only after exposure to biomechanical loading, do biochemical differences in composition become evident. As biomechanical loading cannot be fully imitated in *in vitro* settings, we might have to consider 'immature' cartilage to be sufficient as an initial cartilage blueprint that will be further developed and functionalized as it is exposed to naturally occurring mechanical stimuli. Moreover, when aiming for *in vivo* regeneration, the initial repair tissue will only mature when it is exposed to the appropriate mechanical stimuli.

THE IMPORTANCE OF THE FOUNDATION: OSTEOCHONDRAL DEFECT REPAIR

Despite our attempts at keeping it simple, the underlying bone should also be taken in account as it is rarely spared in traumatic injuries. Bone bruising occurs directly after trauma. But over timee damage to the cartilage progresses, subchondral cysts may develop, making the overlying cartilaginous structures more prone to secondary injuries[11]. These deeper lesions must be addressed by resurfacing these defects as indentation of the overlying cartilage tissue will otherwise persist[12]. Moreover, inappropriate healing of cartilage defects by current therapies, such as autologous chondrocyte implantation (ACI) and microfracture can result in the formation of destructive subchondral cysts[13]. The presence of these cysts often leads to the recurrence of previous symptoms in patients, and is an indicator of failure of previous treatment.

The repair of osteochondral defects thus requires the regeneration of two very different tissue types. While the cartilage lacks intrinsic vascular nutrient supply, is elastic and contains a matrix that is fully organic, the bone is relatively inelastic, has a matrix that is both organic and inorganic and nutrients are supplied through a vascular system. The development of these distinct tissues requires specific boundary conditions. Many approaches for osteochondral defect repair have aimed at the creation of multilayered or biphasic scaffolds[14, 15]. These provide separate environments that are favorable to either cartilage or bone regeneration. One of the advantages of using osteochondral scaffolds is that they are implanted into the cell-rich bone phase. This in turn leads to infiltration of the scaffold with multipotent stromal cells (MSCs) that naturally reside in the bone marrow. MSCs are known for their ability to differentiate towards both the chondrogenic lineage and the osteogenic lineage[16] and would, therefore, be an excellent cell source for this regenerative approach. As was described in this thesis, MSCs do indeed produce abundant cartilage matrix on the scaffolds that we have created for osteochondral defect repair *in vitro*. Moreover, when these scaffolds are seeded with MSCs that are primed to induce chondrocyte hypertrophy, they also form bone tissue *in vivo* as was also described in this thesis. As MSCs are readily available to invade scaffolds from the bone marrow that is present in osteochondral defects these scaffolds can be implanted as cell-free off-the-shelf products. This will make the handling more easy and it will lead to a dramatic drop in costs compared to the expensive cell transplantation alternatives[17].

The fact that osteochondral defect repair requires the regeneration of two different tissue types seems challenging. However, when considering the natural development of bone, the endochondral ossification pathway may provide us with a solution. During the early development of bone, cartilage tissue is used as a template from which long bones grow by gradual ossification of cartilage[18]. If our regenerative strategies allow for the formation of an adequate cartilage template, stimulated by bioactive factors from the healthy bone

surrounding the defect, endochondral ossification in the bone phase of the osteochondral defect may be triggered. In fact, the decellularized cartilage-derived matrix scaffold allowed for bone regeneration in the bone phase as was shown in our *in vivo* experiments.

In regenerating osteochondral tissue, care should be taken to prevent intra-lesional osteophytes and upward migration of the subchondral bone plate. This phenomenon may occur when there is no clear cartilage-bone interface. Osteophytes and a migrated bone plate will lead to a failure of the regenerative strategy, and to further cartilage degeneration[19]. Unfortunately, the etiology of these bony changes is not yet known and preventive measures are thus difficult to discern. Any novel regenerative strategy will, however, have to be studied *in vivo* with adequate long-term follow-up to prevent theses complications from being missed in (pre-)clinical trials.

THE EQUINE MODEL FOR OSTEOCHONDRAL DEFECT REPAIR

Innovative approaches, in their translation from the bench to the bedside, have to be thoroughly tested and re-tested in both *in vitro* and *in vivo* settings before human clinical application. The Food and Drug Administration (FDA) has issued a draft guidance that describes the necessity of using animal models to pre-clinically prove the safety and efficacy of new treatment modalities[20]. This underscores the need of appropriate animal models in osteochondral defect repair. The 'ideal' pre-human model would allow for direct extrapolation towards the human clinic whilst considering the high variability in biological repair response between patients. Also, the appropriate animal for osteochondral repair would allow for sequential, noninvasive monitoring and entail large enough subjects that could undergo kinematic studies for gait analysis. It would also involve animals that can be trained to follow rehabilitation regimes, and most importantly have comparable cartilage characteristics in terms of thickness, and biochemical properties. As all of these prerequisites can never be reached in a single animal model, it is safe to say that the 'ideal' pre-human model does not exist.

Small animal models (rodents and rabbits) have generally been the first choice in analyzing preliminary outcomes regarding novel therapies[20, 21]. The main advantages regarding small animal models involve their easy housing, lower costs and their relatively easy handling. However, the extrapolation of results to the human application should be done with care, as distinct differences in cartilage maturity, thickness [20, 22], and cell density exist. Nevertheless, these animals should be considered for proof of concept studies, and testing of foreign body responses of new (cell-laden) biomaterials[20].

According to the FDA guidelines, approval of new medical devices needs to involve extensive testing in large animal models after the proof of concept studies[20]. Initial pilot testing in larger animals would have to be followed up with pivotal studies of at least 6

months or longer to draw any final conclusions on the efficacy and safety of the new device. To live up to these guidelines, larger animal models that are often used for articular cartilage regeneration are the canine, caprine or porcine model. The downside to these models is that the joints are anatomically different and the cartilage is relatively thin[21]. Therefore, this thesis focuses on a different large animal model: the equine model. This model has gained increasing interest over the past few years due to the increasing body of evidence that equine cartilage and human cartilage are greatly alike[20, 23]. As described in this thesis, they are not only alike in cartilage thickness, but also the zonal characteristics of this tissue are similar. In addition, (traumatic) osteochondral defects also occur in the equine population. Therefore, the development of successful osteochondral repair strategies might benefit both patient groups.

The need for long-term large animal studies that involve multiple subjects is important. Promising results from pilot studies will need to be confirmed in a larger number of subjects in order to correct for the variability in biological repair response. Long-term complications must also be examined. For example, previous studies have already proven that failure of repair tissue at twelve months is commonly due to insufficient strength of the collagen networks[24, 25]. After the initial promising results of the pilot study described in this thesis, a larger follow-up study was required to further study the efficacy of the CDM scaffold. Despite some differences in study set-up, the CDM scaffolds showed rather poor osteochondral defect repair in a larger long-term study that has recently been published[26]. The major factors that may have accounted for the differences in performance of the CDM scaffolds are the location of implantation and the rehabilitation protocol. Firstly, the scaffold was implanted on the medial trochlear ridge rather than the lateral trochlear ridge as was done in the pilot study. This may have led to differences in biomechanical loading. Secondly, as a result of the less conservative rehabilitation protocol than in the pilot study, biomechanical loading may have been too extensive in the follow-up study. The neo-tissue may not have matured sufficiently to be a match for the loading that it was exposed to in early walking, trotting and even cantering of the horses. Nevertheless, the failure of the repair tissue may also be the result of an insufficiently matured collagen network, and insufficient amounts of proteoglycans that can be retained within this collagen network. This in turn will have had an effect in reducing the biomechanical strength of the regenerated tissue. To evaluate the differences between the results from the pilot study and the long-term study, future large animal studies involving this scaffold may have to include interval monitoring through second-look arthroscopies[27] or imaging techniques.

An improvement to the equine model, as a large animal model for osteochondral defect repair, would be to introduce subacute or chronic osteochondral defects. Human patients rarely present themselves at the orthopedic surgery clinic with an acute osteochondral defect[28]. These are often chronic or subacute at best as initial management of traumatic injuries to the knee often involves conservative treatment. Moreover, symptoms from traumatic

cartilage injury may not prompt patients to seek medical advice initially, but the late-onset complaints of degeneration might lead to a doctor's consultation. As osteochondral defects are left untreated in the initial stages, they will have had an impact on joint homeostasis, matrix degradation, and other catabolic effects influencing the regenerative effect of tissue engineering approaches[28]. Therefore, positive results from equine studies that use acute osteochondral defects may be an overestimation of the truth, as the catabolic effects might still be relatively low. Thus, the need for human clinical trials will always remain.

DECELLULARIZED TISSUES FOR TISSUE REGENERATION – BACK TO NATURE'S TEMPLATE

Natural ECM can be used as scaffold material for many tissue engineering purposes[31-33]. Scaffolds that are produced from decellularized cartilage matrix have also shown potential for osteochondral defect repair, as described in the second part of this thesis. As presented in the studies in this thesis, decellularized cartilage matrix scaffolds can also regenerate bone, which is a distinctly different tissue than the source material. Moreover, xenogeneic implantation is possible and leads to infiltration with host's cells and subsequent host species-specific matrix deposition.

Multiple extracellular matrices derived from other sources than the target tissue are already used in clinical settings, for example human dermal tissue is applied in breast and tendon reconstruction and human pericardium is used for regenerative applications in ophthalmology, dentistry and neurosurgery[34, 35]. Besides cross-tissue application, cross-species implantation has also found its application in the human clinic. More specifically, porcine, bovine and equine products are already available for a multitude of regenerative strategies[34]. Currently, no clinical evidence exists that allogeneic or xenogeneic decellularized matrix implantation results in abundant inflammatory host responses that result in the rejection of these implants[35]. This is mostly based upon the idea that ECM scaffolds are decellularized and therefore devoid of donor cells. A mild inflammatory host response will undoubtedly occur, however, these are mainly macrophage-based responses that are considered to play an important role in the regenerative process[36, 37]. The magnitude of this remodeling process is dependent on the ratio between the pro-inflammatory M1 macrophages and the more constructive M2 macrophages. The latter of the two tends to be the more dominant macrophage present in response to ECM scaffolds[35, 36]. The degeneration of ECM scaffolds by the macrophages will in turn release the retained growth factors and other bioactive molecules. These growth factors, as well as the collagens, the main components of any ECM, are preserved across species and are therefore believed to still exert their function even when implanted in different species[35]. This may greatly benefit osteochondral tissue engineering as healthy cartilage from human donors is less

abundantly available than healthy cartilage from another donor species, such as horses, and might therefore serve as an adequate xenogeneic source for scaffold production. Moreover, as the cartilage characteristics of humans and horses are similar, this source animal might even be more promising. Xenogeneic implantation of equine decellularized CDM scaffolds have already shown the ability to form both bone and cartilage tissue in subcutaneous pockets in rats, as was described in Chapter 8.

Until recently the success of ECM scaffolds has been ascribed to the elusive 'bioactive factors' that seem to be retained in the matrix despite decellularization processes. These are relatively undefined factors and could for example involve growth factors, functional peptides, or any other ECM component. Extracellular vesicles have been demonstrated to play a role in tissue homeostasis, and are considered facilitative in tissue development[38]. Their presence has been affirmed in synovial fluids and they seem to derive from different cell types[38]. They are mainly free-floating or budding from different cells within the ECM. Recently, a matrix-bound equivalent to these free-floating extracellular vesicles has been identified that may explain the bioactivity of ECM scaffolds. These matrix-bound nanovesicles have been found in multiple commercially available decellularized ECM products, as well as laboratory decellularized urinary bladder and small intestine matrices[39]. The matrix-bound nanovesicles tend to encapsulate and protect miRNA from the decellularization processes, and they are closely associated with the collagen network of the different ECMs. The identified miRNAs that are encapsulated in the nanovesicles are conserved across species, and were also found in ECM products regardless of their tissue origin[39]. Moreover, the miRNAs that have already been identified seem to be associated with tissue homeostasis and cell proliferation[39]. These findings are the first step in elucidating the factors that make ECM scaffolds succesfull in driving tissue regeneration. As articular cartilage is also composed of an ECM that is rich in collagen, the presence of matrix-bound nanovesicles may well give CDM scaffolds the biofunctionality that leads to the abundant matrix formation both *in vitro* and *in vivo,* as presented in this thesis.

The use of natural biomaterials is not a novelty within the field of cartilage tissue engineering. Even the use of scaffolds that have been made from extracellular matrix (ECM) products, such as hyaluronic acid or collagen, is not entirely new. One of the widely clinically used collagen-based scaffolds is MaioRegen[29]. This biomimetic scaffold is actually composed of collagen type I, and hydroxyapatite and can be used as an off-the-shelf product that does not require cell seeding upon implantation. This relatively new product does not yet have long-term follow-up results, and the 1 and 3 year results are inconclusive[29, 30]. Especially filling of the bone phase of the defect seems in some cases insufficient[30]. The main difference, however, between the decellularized CDM scaffolds described in this thesis and scaffolds that are made from natural products is that the latter lack the presence of bioactive nanovesicles that may give the scaffold its additional biofunctionality.

FUTURE PERSPECTIVES AND CONCLUDING REMARKS

The research described in this thesis supports the use of decellularized CDM scaffolds for the repair of osteochondral defects. However, it also reflects the challenges we are continuously facing in osteochondral tissue engineering. Clinical application of any scaffold would require not only the ability to produce abundant amounts of appropriate cartilage and bone matrix but also requires the appropriate biomechanical properties. Moreover, initial promising results in large animal pilot studies should be followed up in larger studies with longer follow-up. As such, one can conclude that the use of ECM scaffolds for osteochondral repair is still in its infancy compared to the application of ECM scaffolds in other fields.

Cartilage-derived matrix scaffolds, as presented in this thesis, lack biomechanical strength upon implantation and fail to mature enough *in vivo* to overcome this issue. Several enhancements to the present scaffold design are required to tackle this issue. By taking a closer look at the natural architecture of cartilage tissue, and more specifically at the collagen fibers that have their specific depth-dependent alignment, we might be able to use this to our advantage to introduce extra strength to these scaffolds. Through unidirectional freezing of ECM, structural alignment of ECM particles may mimic the naturally occurring collagen alignment, and this has proven to enhance biomechanical properties[40]. Recently, an attempt to decellularize porcine cartilage without losing the intrinsic collagen fiber orientation has been successful[41]. By leaving this network intact, the biomechanical resistance of the scaffolds increases rapidly. Moreover, these scaffolds have been successfully seeded with chondrocytes isolated from the different zonal layers and might therefore enhance the ability of the neo-tissue to quickly mature *in vivo[42]*.

Another option is to use reinforcement with polymer fibers to enhance the strength of the constructs. This concept has proven to greatly enhance the stiffness of hydrogels[43], and might do the same for CDM scaffolds. Another option would be to coat a printable hydrogel or polymer with CDM particles, so that the nanovesicles can still act as the bioactive components but in a sturdier construction. Other options, such as mixing CDM particles through hydrogels[44], and creating hydrogels out of decellularized matrices, have also recently been described[45].

A possible solution for osteochondral defect repair would be to use a xenogeneic decellularized and cell-free osteochondral graft. This might limit bony overgrowth, as the infiltrated cells are forced to stop their matrix deposition at the cartilage interface that is naturally present in this type of ECM scaffold. However, current attempts have not yet led to successful regeneration of both tissues *in vivo*[46]. Decellularization of osteochondral grafts may prove difficult as cartilage has a much more dense matrix and thus involves more aggressive decellularization than bone. More aggressive decellularization techniques will inevitably also alter the ECM and thereby reduce its bioactivity and biomechanical resilience[34].

In conclusion, the use of cartilage-derived matrix scaffolds for osteochondral defect repair is still in the phase of early development and many adjustments may have to be made for this solution to be successful for human application. However, by creating cartilage-derived matrix scaffolds, we respect nature's template for this complex tissue and open up a new possibility in osteochondral defect tissue regeneration. It may be especially beneficial to patients suffering from osteochondral defects, as these cell-free scaffolds will be more readily available to a broader patient population than current regenerative cell therapies.

REFERENCES

1. Hayes AJ, Hall, A., Brown, L., Tubo, R., Caterson, B. Macromolecular organization and in vitro growth characteristics of scaffold-free neocartilage grafts. J Histochem Cytochem 2007; 55: 853-866.
2. Klein TJ, Rizzi, S.C., Reichert, J.C., Georgi, N., Malda, J., Schuurman, W., Crawford, R.W., Hutmacher, D.W. Strategies for zonal cartilage repair using hydrogels. Marcomol Biosci 2009; 10: 1049-1058.
3. Camarero-Espinosa S, Rothen-Rutishauser, B., Weder, C., Foster, E.J. Directed cell growth in multi-zonal scaffolds for cartilage tissue engineering. Biomaterials 2016; 74: 42-52.
4. McCullen SD, Autefage, H., Callanan, A., Gentleman, E., Stevens, M.M. Anisotropic fibrous scaffolds for articular cartilage regeneration. Tissue Eng Part A 2012; 18: 2073-2083.
5. Woodfield TB, van Blitterswijk, C.A., De Wijn, J., Sims, T.J., Hollander, A.P., Riesle, J. Polymer scaffolds fabricated with pore-size gradients as a model for studying the zonal organization within tissue-engineered cartilage constructs. Tissue Eng 2005; 11: 1297-1311.
6. Kim TK, Sharma, B., Williams, C.G., Ruffner, M.A., Malik, A., McFarland, E.G., Elisseeff, J.H. Experimental model for cartilage tissue engineering to regenerate the zonal organization of articular cartilage. Osteoarthritis Cartilage 2003; 11: 653-664.
7. Klein TJ, Schumacher, B.L., Schmidt, T.A., Li, K.W., Voegtline, M.S., Masuca, K., Thonar, E.J.M.A., Sah, R.L. Tissue engineering of stratified articular cartilage from chondrocyte subpopulations. Osteoarthritis Cartilage 2003; 11: 595-602.
8. Ng KW, Ateshian, G.A., Hung, C.T. Zonal chondrocytes seeded in a layered agarose hydrogel create engineered cartilage with depth-dependent cellular and mechanical inhomogeneity. Tissue Eng Part A 2009; 15: 2315-2324.
9. Little CB, Ghosh, P. Variation in proteoglycan metabolism by articular chondrocytes in different joint regions is determined by post-natal mechanical loading. Osteoarthritis Cartilage 1997; 5: 49-62.
10. Brama PA, Tekoppele, J.M., Bank, R.A., Barneveld, A., van Weeren, P.R. Functional adaptation of equine articular cartilage: the formation of regional biochemical characteristics up to age one year. Equine Vet J 2000; 32: 217-221.
11. Durr H, Martin, H., Pellengahr, C., Schlemmer, M., Maier, M., Jansson, V. The cause of subchondral cysts in osteoarthrosis: A finite element analysis. Acta Orthopaedica Scandinavica 2004; 75: 554-558.
12. Berruto M, Delcogliano, M., de Caro, F., Carimati, G., Uboldi, F., Ferrua, P., Ziveri, G., de Biase C.F. Treatment of large knee osteochondral lesions with a biomimetic scaffold: Results of a multicenter study of 49 patients at 2 year follow-up. Am J Sport Med 2014; 42: 1607-1617.
13. Gao L, Orth, P., Goebel, L.K., Cucchiarini, M., Madry, H. A novel algorithm for a precise analysis of subchondral bone alterations. Sci Rep 2016; 6.
14. Atesok K, Doral, M.N., Karlsson, J., Egol, K.A., Jazrawi, L.M., Coelho, P.G., Martinez, A., Matsumoto, T., Owens, B.D., Ochi, M., Hurwitz, S.R., Atala, A., Fu, F.H., Lu, H.H., Rodeo, S.A. Multilayer scaffolds in orthopaedic tissue engineering. Knee Surg Sports Traumatol Arthrosc 2016; 24: 2365-2373.
15. Levingstone TJ, Thompson, E., Matsiko, A., Schepens, A., Gleeson, J.P., O'Brien, F.J. Multi-layered collagen-based scaffolds for osteochondral defect repair in rabbits. Acta Biomat 2016; 32: 149-160.
16. Pittenger MF, Mackay AM, Beck SC, Jaiswal RK, Douglas R, Mosca JD, et al. Multilineage potential of adult human mesenchymal stem cells. Science 1999; 284: 143-147.
17. Elvidge J, Bullement, A., Hatswell, A.J. Cost effectiveness of characterised chondrocyte implantation for treatment of cartilage defects of the knee in the UK. Pharmacoeconomics 2016; 34: 1145-1159.
18. Berendsen AD, Olsen, B.R. Bone development. Bone 2015; 80: 14-18.
19. Orth P, Cucciarini, M., Kohn, D., Madry, H. Alterations of the subchondral bone in osteochondral repair - translational data and clinical evidence. Eur Cell Mat 2013; 25: 299-316.

20. Hurtig MB, Buschmann, M.D., Fortier, L.A., Hoemann, C.D., Hunziker, E.B., Jurvelin, J.S., Mainil-Varlet, O., McIlwraith C.W., Sah, R.L., Whiteside, R.A. Preclinical studies for cartilage repair: recommendations from the international cartilage repair society. Cartilage 2011; 2: 137-152.
21. Chu CR, Szczodry, M., Bruno, S. Animal models for cartilage regeneration and repair. Tissue Eng Part B Rev 2010; 16: 105-115.
22. Frisbie DD, Cross, M.W., McIlwraith C.W. A comparative study of articular cartilage thickness in the stifle of animal species used in human pre-clincal studies compared to articular cartilage thickness in the human knee. Vet Comp Orthop Traum 2006; 19: 142-146.
23. McIlwraith CW, Fortier, L.A., Frisbie, D.D., Nixon, A.J. Equine models of articular cartilage repair. Cartilage 2011; 2: 317-326.
24. Shapiro F, Koide, S., Glimcher, M.J. Cell origin and differentiation in the repair of full-thickness defects of articular cartilage. J Bone Joint Surg Am 1993; 75: 532-553.
25. Howard RD, McIlwraith, C.W., Trotter, G.W., Powers, B.E., McFadden, P.R., Harwood, F.L., Amiel, D. Long-term fate and effects of exercise on sternal cartilage autografts used for repair of large osteochondral defects in horses. Am J Vet Res 1994; 55: 1158-1167.
26. Vindas Bolanos RA, Cokelaere, S.M., Estrada McDermott, J.M., Benders, K.E., Gbureck, U., Plomp, S.G., Weinans, H., Groll, J., van Weeren, P.R., Malda, J. The use of cartilage decellularized matrix scaffold for the repair of osteochondral defects: the importance of long-term studies in a large animal model. Osteoarthritis Cartilage 2016.
27. Frisbie DD, Bowman, S.M., Colhoun, H.A., DiCarlo, E.F., Kawcak, C.E., McIlwraith, C.W. Evaluation of autologous chondrocyte transplantation via collagen membrane in equine articular defects - results at 12 and 18 months. Osteoarthritis Cartilage 2008; 16: 667-679.
28. Saris DB, Dhert, W.J., Verbout, A.J. Joint homeostasis. The discrepancy between old and fresh defects in cartilage repair. J Bone Joint Surg Br 2003; 85: 1067-1076.
29. Delcogliano M, de Caro, F., Scaravella, E., Ziveri, G., de Biase, C.F., Marotta, D., Marenghi, P., Delcogliano A. Use of innovative biomimetic scaffold in the treatment for large osteochondral lesions of the knee. Knee Surg Sports Traumatol Arthrosc 2014; 22: 1260-1269.
30. Christensen BB, Foldager, C.B., Jensen, J., Jensen, N.C., Lind, M. Poor osteochondral repair by biomimetic collagen scaffold: 1- to 3-year clinical and radiological follow-up. Knee Surg Sports Traumatol Arthrosc 2016; 24: 2380-2387.
31. Badylak SF, Freytes, D.O., Gilbert, T.W. Reprint of: Extracellular matrix as a biological scaffold material: Structure and function. Acta Biomat 2015; 23: S17-26.
32. Faulk DM, Johnson, S. A., Zhang, L., Badylak, S.F. Role of extracellular matrix in whole organ engineering. J Cell Physiol 2014; 229: 984-989.
33. Meng F, Modo, M., Badylak, S.F. Biologic scaffold for CNS repair. Regen Med 2014; 2014: 3.
34. Crapo PM, Gilbert, T.W., Badylak, S.F. An overview of tissue and whole organ decellularization processes. Biomaterials 2011; 32: 3233-3243.
35. Keane TJ, Badylak, S.F. The host response to allogeneic and xenogeneic biological scaffold materials. J Tissue Eng Regen Med 2015; 9: 504-511.
36. Valentin JE, Stewart-Akers, A.M., Gilbert, T.W., Badylak, S.F. Macrophage participation in the degradation and remodeling of extracellular matrix scaffolds. Tissue Eng Part A 2009; 15: 1687-1694.
37. Aamodt JM, Grainger, D.W. Extracellular matrix-based biomaterial scaffolds and the host response. Biomaterials 2016; 86: 68-82.
38. Malda J, Boere, J., van de Lest, C.H.A., van Weeren, P.R., van Wauben, M.C.H. Extracellular vesicles - new tool for joint repair and regeneration. Nat Rev Rheum 2016; 12: 243-249.

39. Huleihel L, Hussey, G.S., Naranjo, J.D., Zhang, L., Dziki, J.L., Turner, N.J., Stolz, D.B., Badylak, S.F. Matrix-bound nanovesicles within ECM bioscaffolds. Sci Adv 2016; 10.
40. Rowland CR, Colucci, L.A., Guilak F. Fabrication of anatomically-shaped cartilage constructs using decellularized cartilage-derived matrix scaffolds. Biomaterials 2016; 91: 57-72.
41. Luo L, Eswaramoorthy, R., Mulhall, K.J., Kelly, D.J. Decellularization of porcine articular cartilage explants and their subsequent repopulation with human chondroprogenitor cells. J Mech Beh Biomed Mat 2016; 55: 21-31.
42. Luo L, Chu, J.Y.J., Eswaramoorthy, R., Mulhall, K.J., Kelly, D.J. Engineering tissues that mimic the zonal nature of articular cartilage using decellularized cartilage explants seeded with adult stem cells. ACS Biomater Sci Eng 2016.
43. Visser J, Melchels, F.P., Jeon J.E., van Bussel, E.M., Kimpton, L.S., Byrne, H.M., Dhert, W.J., Dalton, P.D., Hutmacher, D.W., Malda, J. Reinforcement of hydrogels using three-dimensionally printed microfibres. Nature Communications 2015; 6.
44. Visser J, Gawlitta, D., Benders, K.E., Toma, S.M., Pouran, B., van Weeren, P.R., Dhert, W.J., Malda, J. Endochondral bone formation in gelatin methacrylamide hydrogel with embedded cartilage-derived matrix particles. Biomaterials 2015; 37: 174-182.
45. Visser J, Levett, P.A., te Moller, N.C., Besems, J., Boere, K.W., van Rijen, M.H., de Grauw, J.C., Dhert W.J., van Weeren, P.R., Malda, J. Crosslinkable hydrogels derived from cartilage, meniscus and tendon tissu. Tissue Eng Part A 2015; 21: 1195-1206.
46. Novak T, Gilliland, K.F., Xu, X., Worke, L., Ciesielski, A., Breur, G., Neu, C.P. In vivo cellular infiltration and remodeling in a decellularized ovine osteochondral allograft. Tissue Eng Part A 2016; 22: 1274-1285.

SUMMARY

The work in this thesis describes the development of decellularized cartilage-derived matrix (CDM) scaffolds for the repair of osteochondral defects. The first part of this thesis focuses on the compositional differences throughout the layers of articular cartilage tissue, and compares these observed differences between a wide range of species and in closer detail between humans and horses. These studies demonstrate the resemblance in biochemical and histological make-up of cartilage of human and equine tissue. This was the foundation for the studies in the second part of this thesis, where equine tissue was used to further study osteochondral defect repair with decellularized CDM scaffolds. These scaffolds showed great promise for osteochondral repair both *in vitro* and in small and large animal (pilot) studies.

In **Chapter 2** we describe the depth-dependent similarities between human and equine cartilage tissue. Cartilage thickness and cell density show similar trends between these two species across the different layers within cartilage. Also, the biochemical make-up, in terms of glycosaminoglycans, DNA content and collagen content was the same. The similarities between these two species is useful as the equine model has gained great interest within the field of cartilage tissue engineering to evaluate novel tissue engineering techniques.

To put the findings of the first chapter into a broader perspective, **Chapter 3** shows the differences and similarities in cartilage thickness and cell density across 58 different mammals. A negative allometric relationship to body mass was found. Moreover, cellular density seems to decreases with increasing body mass, but gross biochemical composition is remarkably constant. However, this seems to be compensated by the joint congruence, posture and activity pattern of larger mammals.

The biochemical parameters that are described in the first two chapters have all been determined using destructive biochemical assays. However, analyzing cartilage components whilst preserving the sample may have additional benefits as these samples may also be used for other analyses. Therefore, **Chapter 4** describes a nondestructive imaging technique that may be used to determine glycosaminoglycan content in cartilage tissue. Interestingly, this technique is influenced by the use of formalin fixation. The use of this technique is thus most easily applicable to fresh (frozen) samples.

The second part of this thesis focuses on the development of decellularized CDM scaffolds. **Chapter 5** provides the rationale for using CDM scaffolds for cartilage tissue engineering. It also gives an overview of the different decellularization techniques that can be applied in cartilage decellularization.

Chapter 6 describes the process of developing CDM scaffolds in closer detail. The decellularization process involves multiple enzymatic treatments as well as washing steps with detergents. This extensive protocol allows for full decellularization and the production of multiple scaffolds that can be used as an off-the-shelf product.

The first *in vitro* results using CDM scaffolds show great promise in **Chapter 7**. The CDM scaffolds were seeded with the resident cells of articular cartilage, chondrocytes, but also with multipotent stromal cells (MSCs) that are known to be able to differentiate towards the chondrogenic lineage. Interestingly, MSCs outperformed the chondrocytes in terms of matrix deposition and overall glycosaminoglycan and DNA content. These results suggest that pre-seeding the CDM scaffold with chondrocytes is not beneficial for cartilage tissue regeneration. Moreover, as MSCs reside in the bone marrow and can be attracted to the site of implantation, the cell-free application of CDM scaffolds seems possible.

The abundant cartilage matrix formation that occurs when seeding the CDM scaffold with MSCs may provide a platform for endochondral bone formation. **Chapter 8** describes the potential of CDM scaffolds in endochondral bone regeneration at ectopic locations in a rat model. As bone formation seems possible on these scaffolds, their use may even be extrapolated further towards osteochondral defect repair that requires both bone and cartilage tissue regeneration.

Chapter 9 focuses on the development of CDM scaffolds using different particle sizes. Interestingly, altering particle sizes does not influence the chondrogenic potential of the scaffold. Moreover, also the biomechanical properties remain the same when changing particle size. These findings may simplify the process of creating CDM scaffolds as no control needs to be exerted on the size of the decellularized particles.

In **Chapter 10**, the work in this thesis is concluded with the first equine pilot study in which a CDM scaffold and a commercially available scaffold are implanted in osteochondral defects in the stifle (knee) joint of a horse. After 8 weeks of implantation, clear cartilage and bone was formed in the defect filled with the CDM scaffold. It outperformed the commercial scaffold in terms of matrix formation and glycosaminoglycan deposition within the cartilage layer. The results of this pilot study are the foundation for a larger and long-term equine follow-up study to further evaluate the potential of CDM scaffolds for osteochondral defect repair.

NEDERLANDSE SAMENVATTING

Dit proefschrift beschrijft de ontwikkeling van gedecellulariseerde kraakbeenimplantaten voor de behandeling van osteochondrale defecten. In het eerste deel van dit proefschrift komen de verschillen in de van nature gelaagde opbouw van kraakbeenweefsel aan de orde. Deze verschillen zijn onderzocht in een grote groep zoogdieren en worden in detail besproken voor humaan en paardenkraakbeen. De studies beschreven in dit proefschrift laten zien dat er een grote overeenkomst is tussen humaan en paardenkraakbeen wanneer wordt gekeken naar de biochemische en histologische opbouw van het weefsel. Deze overeenkomsten vormen de rationale voor het tweede deel van het proefschrift. Daarin wordt paardenweefsel gebruikt voor de regeneratie van osteochondrale defecten. De implantaten die hiervan gemaakt zijn hebben zowel bij in-vitro- als bij in-vivo-experimenten tot veelbelovende resultaten geleid.

In hoofdstuk 2 worden de overeenkomsten tussen humaan en paardenkraakbeen beschreven. Als gekeken wordt naar de verschillende lagen die in kraakbeen voorkomen, is er sprake van een duidelijke overeenkomst in weefseldikte en celdichtheid tussen paarden en mensen. Ook de biochemische opbouw, die bestaat uit glycosaminoglycanen, DNA en collageen, is hetzelfde tussen deze twee soorten. Deze gelijkenis zorgt ervoor dat bij het onderzoek naar de regeneratie van osteochondrale defecten het paard als diermodel in opmars is.

Hoofdstuk 3 plaatst de resultaten uit het voorgaande hoofdstuk in een breder kader. De dikte en de celdichtheid van het kraakbeenweefsel zijn gemeten in 58 verschillende zoogdieren. Hieruit blijkt dat er een negatieve allometrische relatie is tussen lichaamsmassa en kraakbeendikte. Daarnaast lijkt de celdichtheid af te nemen naarmate het lichaamsgewicht van het zoogdier toeneemt, ondanks het feit dat de biochemische opbouw van glycosaminoglycanen en collageen constant blijft. Het kraakbeen lijkt zijn functionaliteit te behouden omdat de vorm van het gewricht, de houding van het dier en het activiteitenpatroon veranderen bij toename van het lichaamsgewicht.

De hoeveelheid glycosaminoglycanen in de verschillende lagen van het kraakbeen, beschreven in de eerste twee hoofdstukken, wordt vaak gemeten met behulp van destructieve biochemische analyses. Echter, het meten van deze kraakbeencomponenten zonder het specimen op te hoeven lossen kan ervoor zorgen dat de specimens voor meerdere analyses gebruikt kunnen worden. Hoofdstuk 4 beschrijft een nieuwe niet-destructieve beeldvormende techniek waarmee de hoeveelheid glycosaminoglycanen in het kraakbeen gemeten wordt. Gebleken is dat formalinefixatie deze techniek beïnvloedt en dat deze techniek het beste toegepast kan worden op verse monsters.

Het tweede deel van dit proefschrift beschrijft de ontwikkeling van gedecellulariseerde kraakbeenimplantaten. Hoofdstuk 5 laat zien waarom dit soort implantaten relevant is voor

de regeneratie van osteochondrale defecten. Het geeft ook een overzicht van de verschillende technieken die gebruikt kunnen worden om kraakbeen te decellulariseren.

Hoofdstuk 6 geeft een gedetailleerde beschrijving van het decellularisatieproces in de ontwikkeling van de kraakbeenimplantaten die in dit proefschrift worden gebruikt. Dit proces bevat meerdere enzymatische behandelingen en wasstappen. Dit uitgebreide protocol zorgt voor volledige decellularisatie van kraakbeen en beschrijft de productie van meerdere implantaten die als een off-the-shelf product kunnen worden gebruikt.

De eerste in-vitro-experimenten waarin de gedecellulariseerde kraakbeenimplantaten worden gebruikt worden beschreven in hoofdstuk 7. De implantaten werden gezaaid met chondrocyten (de natuurlijk aanwezige cellen in kraakbeen) en multipotente stromale cellen (MSC's) die zichzelf kunnen differentiëren naar kraakbeen- en botcellen. Het is met name interessant dat de MSC's nieuw kraakbeenmatrix vormden met daarin een grotere hoeveelheid glycosaminoglycanen en DNA. Deze resultaten suggereren dan ook dat het voorzaaien van de implantaten met chondrocyten niet bijdraagt aan kraakbeenregeneratie. Bovendien zijn MSC's al te vinden in osteochondrale defecten aangezien deze cellen in het beenmerg aanwezig zijn. Bij plaatsing van het implantaat in het osteochondrale defect zullen de MSC's zich hechten aan het implantaat. Hierdoor zou het ontwikkelde implantaat een celvrije toepassing binnen osteochondrale defectregeneratie kunnen zijn.

De grote hoeveelheid nieuwe matrix die gevormd wordt als de gedecellulariseerde implantaten worden gezaaid met MSC's kan ook een basis vormen voor botregeneratie via de enchondrale route (botvorming vanuit bestaand kraakbeenweefsel). Hoofdstuk 8 beschrijft deze potentiële toepassing. Enchondrale botvorming werd onderzocht in ectopische locaties in een rattenmodel. Botvorming via de enchondrale route bleek in deze studie eveneens mogelijk. De regeneratie van osteochondrale defecten vereist nieuwvorming van bot en kraakbeen, dus met deze studie komt die toepassing weer een stap dichterbij.

In hoofdstuk 9 werd het effect van implantaten die gemaakt zijn van partikels van verschillende groottes geëvalueerd. Hieruit bleek dat de grootte van de partikels geen invloed had op de mate waarin nieuw kraakbeenweefsel werd gevormd. Ook die biomechanische eigenschappen van de implantaten veranderden niet. Dit zou mogelijk het productieproces van de implantaten kunnen versimpelen, omdat met deze parameter dan geen rekening gehouden hoeft te worden.

In hoofdstuk 10, het laatste hoofdstuk van dit proefschrift, wordt de eerste pilotstudie beschreven waarin een gedecellulariseerd implantaat werd geïmplanteerd in een paard. Daarnaast werd het ontwikkelde implantaat vergeleken met een implantaat dat reeds klinisch wordt toegepast. Na acht weken werd duidelijke regeneratie van bot- en kraakbeenweefsel gezien in het defect in de paardenknie. De resultaten van deze studie vormen de basis voor een vervolgstudie in paarden om de potentie van gedecellulariseerde kraakbeenimplantaten verder te kunnen onderzoeken.

DANKWOORD

Geen proefschrift komt er zonder de hulp van anderen, zo ook dit proefschrift niet. Er zijn teveel mensen om te bedanken ten aanzien van dit proefschrift en mijn persoonlijke ontwikkeling tijdens het schrijven hiervan. Desalniettemin wil ik hieronder een selectie nader toelichten.

Prof. Dr. Malda, beste Jos,
Ik weet niet waar ik moet beginnen of eindigen, but here it goes. Dank voor het warme welkom in je onderzoeksgroep. Dank voor de les "hoe-hou-ik-een-pipet-vast". Dank voor het vertrouwen dat je hebt gehad in dit project en in mij. Dank voor de tripjes naar buitenlandse laboratoria. Dank voor mijn tijd in Australië, inclusief smerige Australische bessen en vogels. Dank voor de deur die altijd openstond. Dank voor de snelle respons op al mijn geschreven stukken of nieuwe grafieken. Dank voor je hulp in die vreselijke Diergeneeskunde snijzaal. Dank voor de vele congressen. Dank voor alle introducties aan buitenlandse kraakbeen-grootheden. Dank voor de etentjes bij je thuis. Dank voor het tripje naar de SEH na die scalpel in mijn vinger. Dank voor de ritjes naar paardenklinieken. Dank voor een kijkje in de wereld van patentaanvragen. Dank voor het werk op die ene buitenplaats bij Paard. Dank voor die gele en blauwe notitieboekjes van je waarin de 'megalomane ideeënwereld van Jos Malda' beschreven staat. Dank voor de ruimte die je gaf aan mijn eigen invulling van dit proefschrift. Dank voor de 'goede woordjes' die je voor me hebt gedaan. Dank voor het mogelijk maken van de laatste twee maanden die ik nog nodig had, ondanks dat we er misschien allebei op sommige momenten even niet meer in geloofden. Af is af… dankjewel, dankjewel, dankjewel.

Prof. dr. Saris, beste Daan,
Ik zal de dag waarop ik je voor het eerst vroeg of ik onderzoek bij je zou mogen doen nooit vergeten. Ik stond namelijk binnen vijf minuten weer buiten… Onderzoek in het lab kon zeker, klinisch onderzoek niet. Dank voor je duidelijkheid wanneer dat nodig was en de kans om deel uit te maken van Orthopedisch Utrecht.

Prof. dr. Dhert, beste Wouter,
Hier is het dan, vanaf mijn eerste paper die je face-to-face met je vulpen voor me na hebt gekeken, tot dit proefschrift. Het is af! Iets meer dan een jaar geleden zei je tijdens een promotie-receptie: "Ik gun jou ook zo'n mooie dag". Die woorden hebben me zeker gedurende de laatste lootjes geholpen om dit boek af te maken. Dank voor je steun, de kansen die je me gaf om dit onderzoek uit te kunnen voeren en je tomeloze vriendelijkheid.

Prof. dr. van Weeren, beste René,
Je mag dan officiëel geen promotor heten, maar als co-auteur op bijna al mijn publicaties en als mede-bedenker van menig nieuw experiment, beschouw ik je wel als onderdeel van mijn promotiecommissie. Dank voor het openstellen van de afdeling Paard voor een niet-dierenarts. Ik heb erg veel aan je kritische blik ten aanzien van mijn experimenten gehad en nog meer aan je schrijftalent. Ik hoop dat je nog vele mensen zult inspireren, en vergeet niet: *"la vie est trop courte pour boire du mauvais vin"*.

Prof. dr. Hutmacher, dear Dietmar,
Thank your for the Australian adventure that started at IHBI in Brisbane. It was the beginning of this thesis, and made all of this possible. I admire how you manage to clear your very busy schedule for research meetings and little dinner gatherings. I hope to see you again in the future.

Dr. Klein, dear Travis,
My supervisor-from-down-under. Thank you for making me feel welcome in Brisbane and showing me how to work that insanely difficult microCT. It has always been great running into you at research events. Thanks for everything, still cannot believe that you used to say D'Oh…

Alexandre Suerman Commissie van het UMC Utrecht,
Dank voor het vertrouwen in mijn onderzoeksvoorstel en het bijpassende rugzakje. Ook veel dank aan Lucette Teurlings voor de altijd weer inspirerende masterclasses waar het vaak ook 'even bijkomen' was. Dank voor je stimulerende woorden en enthousiasme waarmee je ons aan de intervisie zette, out of the box leerde denken en liet schermen en lacrosse spelen.

Dank aan de Su(p)erman buddies, ik had het beloofd… Heel veel dank voor de toptijd.

Mijn paranimfen,
Anika Tsuchida, sestra. We've come a long way en het is niet meer dan logisch dat jij naast mij staat tijdens mijn verdediging. Terwijl ik dit over jou schrijf sta jij aan de andere kant van de muur Japanse rijst te koken en een berg groente te snijden. Velen hadden niet gedacht dat wij het zo lang in hetzelfde huis uit zouden houden. Maar wat is er fijner dan thuiskomen in een huis waar je jezelf kunt zijn, keihard kunt lachen, de ugly cry mag uitoefenen en mooie plannen voor de toekomst kunt maken. Het heeft geen zin om al onze mooie herinneringen hier op te noemen want dat zijn er teveel. Ook als we straks onze eigen weg gaan hoop ik dat er altijd plek is voor mij op een W-tripje.

Lidewij Ochtman, mijn Antonius-buddy, mijn fellow ortho-chickie, mijn serial whatsapp connectie, mijn bench-press spotter, mijn trotse mede-netflixer, maar boven al mijn goede vriendin. Ik zou me niet voor kunnen stellen hoe saai het zou zijn zonder jouw bijna dagelijkse quote-updates. Dank dat je er bent.

Anne Spaans, opleidingsmaatje. De eerste dag dat ik met angstige ogen aan kwam op de poli Orthopedie heb je me met die gierende lach uitgelachen. Geeft niet… wist ik veel dat we vrienden zouden worden en dat ik die lach nu kan waarderen. Je bent in deze laatste fase de stok achter de deur geweest. Ik ben blij met onze vriendschap en het feit dat je me soms ook gewoon de waarheid zegt. Hopelijk zullen in de toekomst de noodzaak tot koffie-drink-momentjes afnemen, maar blijven we ze wel gewoon doen voor de gezelligheid. Please, wanneer mag ik weer appel-boterkoek?

Dino Colo, DC. Wat zorg jij toch altijd voor leven in de brouwerij en wat moet ik toch altijd vreselijk lachen als we elkaar zien. Met jou weet je nooit wat er komt, behalve dat het weer een 'pareltje' gaat worden. Om maar wat te noemen: surprise Stockholm, Bossche Bol in je gezicht en wa-wa-wa-waar kommen ju-ju-ju-jullie dan vandaan? Ik kijk uit naar onze eerste operaties samen, met Coldplay aan, de omgeving mag zijn borst wel nat maken. En als je geluk hebt dan draaien we, vooruit, ook al haat ik het… "Another one…"

Anjo Nieuwoudt, they say that when you've been friends for seven years you are like family. We didn't need seven years, we needed seven seconds. You are my person…you will always be my person. Enough said.

Mijn collega-onderzoekers,
Wouter Schuurman, als eerste genoemd! Deze 'sterke vrouw' heeft het ook gered. Dank dat ik je opvolger mocht zijn. Michiel Beekhuizen, Mbeki, je bent een fantastische collega en ik hoop dat we het koffie drinken nog jaren vol zullen houden. Joris Bekkers, vaderfiguur in het lab, vaderfiguur in de opleiding. Michiel Jansen, Djens, topgozer. Ruth Geuze, dank dat jij er ALTIJD in hebt gelooft en dat jij het altijd al zeker wist. Tommy de Windt, die pokke-muggen zou ik zo nog een keer voor je overwinnen. Tom Schlösser, gelukkig ben ik mijn zusje niet. Loek Loozen, als er iemand sterk genoeg is om orthopeed te worden… Jetze Visser, fijn die Friese nuchterheid. Peter Levett, you and Libby are the funniest Australians on bikes. Debby Gawlitta, ik kan geen piña colada kauwgom meer zien zonder aan jou te denken. Michiel Croes, jij was de dependance van de Asian Room. Anita Krouwels, sterke surf-chick, je bent altijd goed gezelschap. Linda Kock, hoezo hebben we nog steeds geen biertjes gedronken? Mechteld Lehr, dank voor je interesse in zowel het onderzoek als de mens erachter.

Laura Creemers, Jacqueline Alblas en Lucienne Vonk, dank voor jullie scherpe blik tijdens research meetings.

De collega's bij afdeling Paard: Everaldo, Janneke, Janny en Harold dank voor jullie hulp. In het bijzonder Annemiek Oomen, zo ver weg nu maar zeker je dromen achterna. We hebben het goed gehad. Stefan Cokelaere, een Vlaamsch en een Hollandsch boekje! Het is gelukt!!!

Sylvia, Irene, Antoinette, Andrea, Simone, Mariska, Brenda, hartelijk dank voor jullie ondersteuning en gesprekken in de wandelgangen.

My international collaborators, thank you for your input and the work we have done together: Wayne McIlwraith and Tammy Donahue at Colorado State University, and Jeremy Mao and Chang Hun Lee at Columbia University.

Senior Girls Borrelclub,
Michelle Poldervaart, het spijt me dat ik hem ooit Fanfare heb genoemd…Knap hoe jij dit werk met je gezin combineert. Petje af. Hsiao-yin Yang, yeeeeeeeeesssss I finished it too!!! Thank you for your everlasting kindness, and thank you for the best Asian baby pictures ever. Rhandy Eman, ik zal nooit vergeten dat we een bureau moesten delen, wat hebben we mooie W Barcelona herinneringen en ik ben blij dat je ook nog steeds bij de senior girls bent.

Fiona Wegman (en Jordi, en Jip, en Lola). Lieve Fi, je mag dan de dag dat ik onderzoeker werd bij jullie danwel vergeten zijn of nooit opgemerkt hebben, maar dat doet niets af aan de vriendschap die daarna is ontstaan. Als ik iets wil doen wat anderen een beetje 'vreemd' zouden vinden weet ik altijd wie ik moet bellen. We hebben die bucketlist en we gaan hem afvinken!

Dank ook aan Jordi die altijd klaar staat als er iets gefixt moet worden en lieve Jip en Lola, altijd welkom…zeker bij de Sinterklaasintocht.

Willemijn Boot, Bootje. Dit proefschrift is voor een deel ook een beetje van jou. Er zitten onmeunig veel uren werk van jou in. De avondmaaltijden in het UMCU, de vroege ochtenden in de paardenkliniek en de ritjes naar Lienden waren allemaal een stuk zwaarder geweest zonder jou. Je was mijn topstudent en ik ben blij dat je daarna mijn collega werd. Ik ben trots op ons werk.

Mattie van Rijen, je was mijn steun en toeverlaat op het lab. Degene die mijn verhoudingen WEL altijd kon uitrekenen. En inmiddels veel meer dan dat. Ik koester onze vriendschap

en ben blij dat ik ook Marcha erbij heb gekregen ;-). De Brabantse gezelligheid in de Nederlandse zon of in de sneeuw. Ik kan niet meer zonder. Marcha, dank voor jouw altijd heerlijk eerlijke mening en dank dat ik die van mij altijd mag uitspreken. Dat is ons clubje!

Mijn buddies Eugène Diekman en Joep Hufman, we zien elkaar te weinig, maar eten met jullie is altijd een oplaadmoment.

Linda van Wagenberg en Jojanneke Kuhlmann, mijn SUMMA-vriendinnetjes. Alle drie dokter, jullie al specialist maar ik kom achter jullie aangerend! Laten we elkaar nooit uit het oog verliezen.

Dank aan Action de la Frette, Soprano Moliere, Amadeus, Colorado, Sam, Balero, Tadano, Wallstreet, Co, Edwin en Stefan.

Cambridgelaan 205: Lauranne Cox and Antonis Voutsinos…The book about cartridges is here!

Mijn Chirurgie collega's in het St. Antonius Ziekenhuis in Nieuwegein, met speciale vermelding het traumatologie-team en mijn opleiders. En uiteraard de volgende personen: Ernst Steller, David Roks, Xiaoye Zhu, Young-kon Lambeck, Janity Pawiroredjo, Valerie Monpellier en Olga Arguedas Flores.

De OLVG-clan. Hier heb ik voor het eerst geleerd wat Orthopedie echt is. Ik kijk uit naar mijn laatste jaren bij jullie.

De UMC Orthopeden en collega's, dank voor de mogelijkheid om dit proefschrift af te maken. Dank ook voor jullie wetenschappelijke vorming buiten dit schrijven om. Ik heb veel geleerd en ben niet meer bang voor wervels!

De traumachirurgie in het UMC Utrecht. Dank voor het warme bad waarin ik terecht ben gekomen tijdens mijn stage bij jullie. Nooit, nooit, nooit zal ik de single-port traumalaparotomie vergeten en het woord "precies" is voor altijd besmet. Siegrid de Meer, mijn Duo Penotti helft!!! Wat was het mooi! Time flies when you are having fun…

Mijn gezellige Indo-familie. Dank voor jullie interesse in wat ik doe. En dank voor de liefde die in overmaat aanwezig is tijdens onze verjaardagen.

Mijn peet-familie: Dennis en Aimée, Christian en Josephine, Daniëlle (Bami) en Rishi, en uiteraard Oom Tom en Tante Christine, zonder jullie had ik misschien nog steeds niet

gelopen ;-). Ik kijk er steeds weer naar uit om jullie te zien. Ik kijk er ook naar uit om jullie tijdens mijn promotie vooraan te zien zitten! Heel veel liefs!

Arjan Markus, potjandorie mij is niks gevraagd maar….vooruit je mag met haar trouwen.

Astrid en Ingeborg, Bas en Borg. Mijn lieve, lieve kleine grote zusjes, de terror-tweeling die nooit naar me luisterden als ik ze voorlas. De vriendinnen met wie ik Linda, Roos en Jessica moest playbacken. De partners in crime voor verrassingen voor papa en mama. Maar tegenwoordig twee zelfstandige vrouwen op wie ik alleen maar trots kan zijn. Ik ben trots op wat jullie allemaal voor elkaar hebben gebokst. We hebben nog minimaal 60 jaar samen te gaan en ik kijk er naar uit!

Lieve papa en mama, het is gelukt, het boek is af. Wat ik hier ook opschrijf, het beschrijft niet wat jullie voor mij betekenen. Jullie hebben er voor gezorgd dat ik vandaag hier sta en mag zijn wie ik ben. Ik ben trots dat ik er eentje ben van Benders-Oei. Waar ik ook ben geweest of waar ik nog naar toe ga: het mooiste aan weggaan is nog altijd het thuiskomen. Ik hou van jullie.

CURRICULUM VITAE

Kim Eva Maria Benders was born in Nieuwegein, The Netherlands, on the 12th of October 1984. She graduated from high school in 2003 (Tweetalig VWO, Anna van Rijn College, Nieuwegein).

After high school she decided to go to the Liberal Arts University College Utrecht (UCU). During her studies at UCU, she studied at the University of California, Berkeley for 6 months. In 2006, she obtained her Bachelor of Science with Honors. From 2006-2012 she studied at the University Medical Center in Utrecht and obtained her medical degree in 2010 (Selective Utrecht Medical MASter). During her study, she participated in several research projects at the Department of Paediatric Surgery and the Department of Orthopedic Surgery. Also, she fulfilled a research internship at the Institute of Health and Biomedical Innovation in Brisbane, Australia under supervision of Prof. Dr. D.W. Hutmacher and Dr. T.J. Klein. This research internship resulted in a research proposal that was awarded the Alexandre Suerman Stipendium, which allowed her to start her PhD at the Department of Orthopedic Surgery, under the supervision of Prof. dr. W.J.A. Dhert, Prof. dr. D.B.F. Saris and Prof. dr. J. Malda. This research is the focus of this thesis.

In December 2012 she started her clinical training at the Department of General Surgery at the Sint Antonius Ziekenhuis in Nieuwegein (under supervision of dr. P.M.N.Y.H Go). Afterwards she started her orthopedic training in the Onze Lieve Vrouwe Gasthuis in Amsterdam (under supervision of dr. R.W. Poolman), followed up by her academic clinical training in the University Medical Center Utrecht (under supervision of Prof. dr. D.B.F. Saris). She will finish her orthopedic training in 2019.

Cartilage and osteochondral defects lead to painful joints and limited mobility. These defects often occur after sports injuries and thus mostly affect the young and active population. In contrast to other human tissues, cartilage is not capable to initiate its own repair. This will inevitably lead to further degeneration of the joint.

Osteochondral damage is not limited to the human population. Horses are equally affected by similar defects. Interestingly, the histological and biochemical composition of human and equine (horse) cartilage tissue show great similarities. The development of a novel treatment strategy could therefore benefit both populations.

This thesis decribes the development of a natural scaffold for osteochondral defect repair. Natural cartilage tissue can be decellularized and used to create a new scaffold that can be implanted into the defect. These scaffolds have been evaluated in *in vitro* and *in vivo* settings and have shown great potential in repairing the natural tissue.